SCALABLE FABRICATION OF MIXED-MATRIX MEMBRANES FOR GAS SEPARATIONS: POLYMER-MODIFICATION-ENABLED IN-SITU METAL-ORGANIC FRAMEWORK FORMATION

A Dissertation

by

SUNG HWAN PARK

Submitted to the Office of Graduate and Professional Studies of
Texas A&M University
in partial fulfillment of the requirements for the degree of

DOCTOR OF PHILOSOPHY

Chair of Committee,	Hae-Kwon Jeong
Committee Members,	Faruque Hasan
	Benjamin Wilhite
	Hongcai Joe Zhou
Head of Department,	Arul Jayaraman

May 2021

Major Subject: Chemical Engineering

ABSTRACT

Mixed-matrix membranes (MMMs) combining the advantages of polymer and inorganic membranes have been intensively studied for gas separations by incorporating molecular sieves such as zeolite, silica, and metal-organic framework (MOF) to a polymer matrix. Despite the potential, there have been no commercial applications of MMMs due to the several challenging MMM processing issues. One of the major challenges is the difficulty of controlling defects of a thin selective layer and microstructure of polymer/filler upon the single-step MMM spinning at the same time. We investigated a new paradigm of scalable MMM fabrication, named polymer-modification-enabled *in-situ* metal-organic framework formation (PMMOF) by decoupling polymer membrane fabrication and filler incorporation. PMMOF involves four steps, hydrolysis, ion-exchange, ligand treatment, and imidization, enabling *in-situ* formation of metal-organic framework (MOF) fillers inside polymers. The first MMMs by PMMOF were demonstrated by in-situ forming zeolitic-imidazole framework-8 (ZIF-8) fillers up to 32.9 vol% in the 6FDA-DAM polymer. The binary C_3H_6/C_3H_8 separation performance of the MMMs showed much higher separation factors than conventionally-prepared 6FDA-DAM/ZIF-8 MMMs at similar filler loadings, satisfying the commercial C_3H_6/C_3H_8 separation performance criteria. For the more in-depth study of PMMOF, the actual reaction conditions synthesizing MOF crystals in a polymer free volume was investigated using the phase transformation of ZIF-7. In addition, the C_3H_6/C_3H_8 separation performance of MMMs by PMMOF was further improved by combining PMMOF with linker-doping strategy. Despite these successes, there were several remaining issues for PMMOF. Among them, most importantly, as the filler contents increased, the permeability of MMM decreased continuously despite the higher separation factors compared with those of MMMs

prepared by conventional blending methods. To address this issue, cross-linked polyimides (i.e., 6FDA-DAM:DABA (3:2)) were used with different cross-linking degrees. It was found that the inherent rigidity of polymer as well as the swelling of the polymer followed by chain rearrangement were critical to prevent the severe permeation reduction. Finally, the first MMM module containing multi-stranded mixed-matrix hollow fiber membranes with submicron-thick selective skin layers was demonstrated by transforming a preformed module with PI-coated polyethersulfone hollow fibers using the PMMOF.

ACKNOWLEDGEMENTS

I would like to thank to Load for giving me this opportunity and for giving me the strength and blessing with loving family and friends that is here to encourage me.

I would like to thank the committee chair, Dr. Jeong and committee members, Dr. Zhou, Dr. Hasan, and Dr. Wilhite for their guidance and support throughout the course of this research.

Thanks also go to my friends and colleagues and the department faculty and staffs for making my time at Texas A&M University a worthwhile experience. I would like to express my special thanks to members at Vision mission church and pastor Hong I Lim.

Last but not least, thank my loving family. I will never forget parents and parents-in-law's physical and mental supports. I sincerely appreciate my wife's devotion, patience, and encouragement. It is my greatest pleasure to have my lovely children Daniel Junsung, and Joshua Junwon during this time. Without my family's support, this work would not have been possible.

CONTRIBUTORS AND FUNDING SOURCES

Contributors

This work was supported by a dissertation committee consisting of Professor Hae-Kwon Jeong [advisor] and Professor Faruque Hasan and Professor Benjamin Wilhite of the Department of Chemical Engineering and Professor Hongcai Joe Zhou of Department of Chemistry. I would like to thank Dr. Micah Green and Xiaofei Zhao and Dr. Mustafa Akbulut in Chemical Engineering at Texas A&M University for the use of TGA (Chapter III, IV, and V) and oxygen plasma (Chapter III), respectively. I am grateful to Prof. Young Moo Lee at Hanyang University for kindly providing PIM-1 (Chapter VI). All other work conducted for the dissertation was completed by the student independently.

Funding Sources

Graduate study was supported by in parts from the National Science Foundation (CBET-1510530 and CBET-1929596), the Qatar National Research Fund (NPRP 8-001-2-001 and NPRP 12S-0209-190064), the National Science Foundation supported the FE-SEM acquisition under grant DBI-0116835, the VP for Research Office, and the Texas A&M Engineering Experimental Station.

TABLE OF CONTENTS

Page

Page

Page

LIST OF FIGURES

Page

Page

Page

Page

Page

Page

LIST OF TABLES

CHAPTER I

INTRODUCTION AND OVERVIEW

The attention to membrane-based gas separation is growing fast since it is one of the most promising technologies to replace current energy-intensive and high-cost distillation-based gas separation processes.[2] Polymeric membranes have been dominantly used for commercial applications for divers gas separations due to the cheap material cost and high processability (Figure 1.1a). Nevertheless, there are fundamental limitations of gas separation performances of polymer membranes known as a trade-off between permeability related to productivity and selectivity relevant to efficiency. Robeson[3] systematically defined the upper-bound curves of polymer membranes using the freeman theory based on the transition state theory for diffusion and the thermodynamic relationship for solubility.[4] Besides, the chemical/thermal stability of polymer membranes is poor. Those membranes are often plasticized under a high pressures of condensable gases such as CO_2, CH_4, C_3H_6, C_3H_8, and etc, which could result in unfavorable gas separation performances.[5] Consequently, chemically/thermally robust inorganic membranes with well-defined crystal structures such as zeolites have been intensively studied (Figure 1.1b). Due to the size-fitting molecular sieving effects, some of inorganic membranes show impressive separation performances that are far beyond those of polymer membranes and without the restriction imposed on the relationship between permeability and selectivity.[6-7] However, a large-scale fabrication of polycrystalline inorganic membranes is impeded by their high membrane processing cost due to the difficulty of controlling microstructure such as grain boundaries and their fragile mechanical properties.[8-9] To overcome the issues of polymeric and inorganic membranes, polymer/inorganic filler mixed-matrix membranes (MMMs) have been studied as a

potential breakthrough (Figure 1.1c). By incorporating highly selective inorganic molecular sieve fillers in a cheap and processible polymer matrix MMMs simultaneously balance the processability and gas separation performance which could surpasses the upper bound curves of polymer membranes.

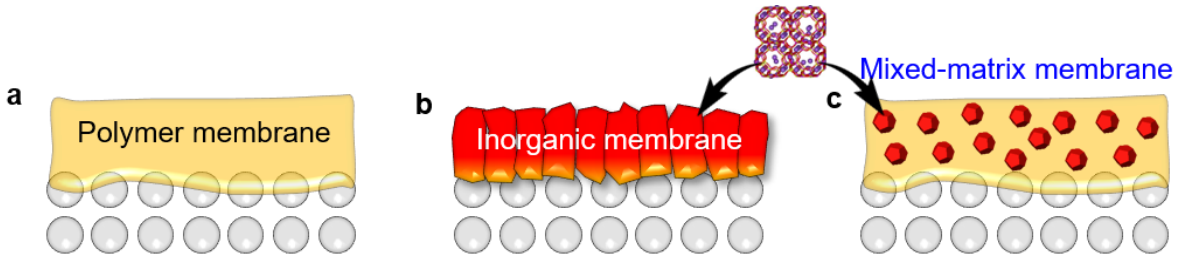

Figure 1.1. Illustration of gas separation membranes.

Nonetheless, there have been several challenges for MMMs based gas separations. The contact between organic phase and inorganic filler is a critical factor for MMM processing. The hydrophilic surface of inorganic fillers often establishes an unsatisfactory compatibility with the hydrophobic nature of polymer. As a result, a defective sieve-in-a-cage morphology that act as a by-pass of gas molecule transports is formed.[10] In addition, due to the strong interactions between fillers, those fillers are agglomerated. As such, mesoporous spaces are formed within the agglomerations, which may allow gas molecules to circumvent molecular sieves.[11] The particle agglomeration phenomenon becomes deteriorated, as the size of filler decreases that is necessary to fabricate ultrathin MMM thickness. Regarding these primary drawbacks of MMMs, many researchers have strived to improve polymer/filler interactions and filler distributions to achieve scalable and high performance MMMs by using scientific approaches.

There have been many noticeable review papers summarizing the current developments of MMMs for gas separations from the scientific perspectives. In order to overcome these challenges, Dong et al.[12] systematically presented the major challenges of MMMs and they pointed out the important scientific approaches. The principle of proper matching between polymers and fillers was suggested with regard to enhancing the compatibility and potential large-scale production. The MMM studies introducing tertiary components as a compatibilizer displayed positive effects on the interfacial interactions and separation performances of MMMs, demonstrating their potential applications for large-scale MMM fabrications.[13] Furthermore, it has been investigated in detail that MMMs containing noble inorganic fillers that provide strong interactions with polymers and effective molecular sieving properties. Gao et al.[14] published a review aiming to demonstrate the progress of the properties and application of MXene/polymer membranes. Guan et al.[15] epitomized the modification of ZIF-based MMMs for CO_2 separation. Lin et al.[16] focused on the filler/matrix interfacial morphology of MOF-based MMMs. In addition, the mathematical modeling studies based on the interactions and interfacial morphologies of MMMs suggested potential applications and future directions of MMMs for gas separations.[17]

However, to date, there have been few commercial applicated MMMs for gas separations.[18] It is likely due to the fundamental engineering challenges of the current MMM processes. Although the aforementioned progress of MMM based on the scientific point of view demonstrated the potential applicability for large-scale MMM fabrications, there might be considerable gaps between the potential and the practical applications.

CHAPTER II

BACKGROUNDS

2.1. Chronological progress of MMM

The chronological progress of MMM is important to understand the current and future directions of MMM developments. The timeline of significant findings of MMM is represented in Figure 2.1. The origin of MMM for gas separation is incorporating minerals in a polymeric rubber to measure CO_2 sorption and permeation in 1912 by Steinitzer.[19] After about half centuries later, the first porous zeolite filler (i.e., mordenite) containing MMMs using polydimethylsiloxane (PDMS) as a continuous polymer phase were reported for O_2/N_2 separation in 1971 by Christen et al.[20] Followed by the publication of the silicon rubber/zeolite 5A MMM firstly demonstrated the molecular sieving effect of the immobilized fillers in 1974 by Kemp et al.[21] The authors described the gas transport phenomenon by dual-mode model and reestablished transition-state and steady-state gas permeation models. In 1988, the term 'mixed-matrix membrane' firstly put forward by Kulprathipanja et al.[22] in their patent demonstrating improved O_2/N_2 separation performance taking advantage of a cellulose acetate (CA)/silicalite-1 MMM. Also, they suggested the potential applicability of diverse polymers (polycarbonates (PC), polyamides (PA), polysulfone (PSf), and CA) and fillers (zeolites, silicalites, activated carbons, and ion-exchange resins) combinations to form MMMs.

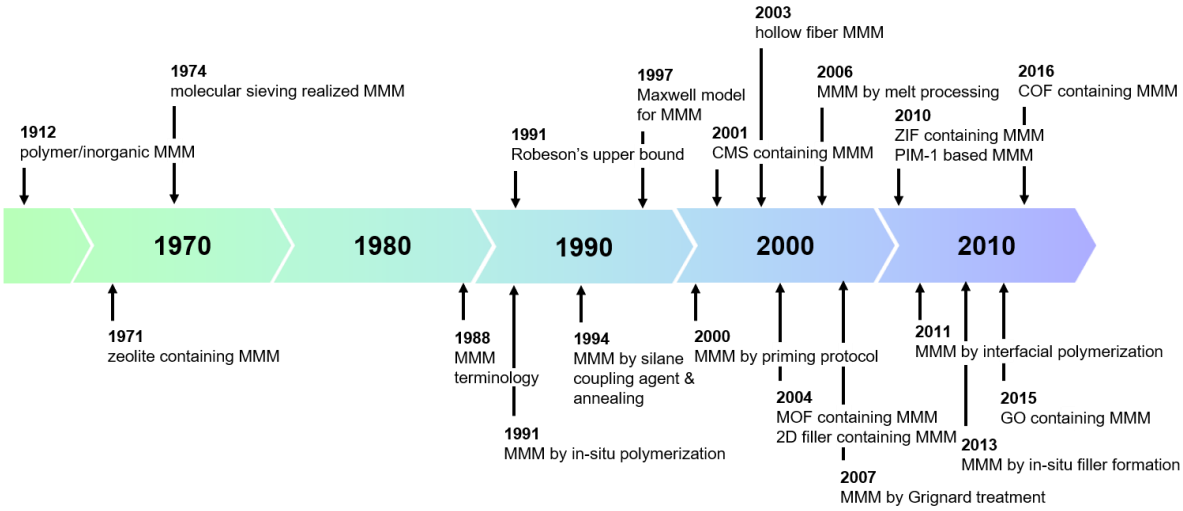

Figure 2.1. Timeline of MMM developments.

The limitations of polymeric membranes indicating the direction toward MMM separation performance improvements were established in 1991.[23] It was revised in 2008 by including more advanced polymer membranes such as thermally-rearranged (TR) polymers and polymers of intrinsic microporosity (PIMs).[24] In the same year (1991), although there had been reports for MMM prepared by blending fillers with a PDMS polymer, Jia et al.[25] demonstrated in-situ polymerization of PDMS-based MMMs by crosslinking the cast film containing silicalite particles. It was one of the pioneers of in-situ MMM formation. It allows homogeneous filler dispersion, efficiently suppressing interfacial void formations and scalable MMM processing in current MMM developments. In 1994, Duval and Mulder et al.[26] proposed a noticeable advancement to improve the interfacial structure of zeolite/glassy polymer MMMs by using silane coupling agents and thermal annealing process. Bouma and Drioli et al.[27] applied Maxwell model which was originally designed for dielectrics to estimate gas separation performance of MMMs in 1997. This strong tool is widely accepted even in the current MMM community. In

2000, Mahajan and Koros[28] proposed the interfacial defect issues of MMMs more scientifically based on the three-component interactions of filler-solvent-polymer system. Based on the principle, they achieved 40 % of high loading PVAc/ zeolite 4A MMMs without interfacial voids using the priming protocol. A year later (2001), carbon molecular sieve (CMS) containing MMM was firstly introduced by Corbin et al.[29] With increasing attention to MMMs for gas separations, the first mixed-matrix hollow fiber membranes prepared by a dry/wet phase inversion approach emerged in 2003 by Ekiner et al.[30] In 2004, there were the foremost reports of MMMs incorporating two types of fillers attracting considerable interest in the current MMM researches. One is metal-organic framework (MOF)-based MMM by Yehia and Musselman et al.[31] and the other is 2-dimensional layered porous material-based MMM by Jeong and Tsapatsis et al.[32] As an effort to improve the adhesion between polymer and filler without using coupling agents, the MMMs were prepared by the melt processing in 2006 by Takahashi and Paul.[33] Another strategy to improve the interfacial adhesion of MMM without silane coupling agents is Grignard treatment by increasing the external surface roughness of inorganic particles reported by Shu and Koros et al.[34] in 2007.

For the last decade, there have been noteworthy findings and breakthroughs for MMMs. Zeolitic-imidazole framework (ZIF), which is a sub-class of MOF, was firstly used as fillers of MMMs ,ZIF-8 and ZIF-90-based MMMs by Ordoñez and Musselman et al.[35] , Bae and Jones et al,[36] respectively in 2010. Those chemically/thermally stable ZIF fillers[37] represented effective molecular sieving effects for gas separations as well as good adhesions with polymer matrix resulted from the presence of organic linkers. Starting from those reports, ZIF containing MMMs have been enthusiastically studied to date. In the same year, the first PIM-based MMM was developed by Ahn and Guiver et al.[38] In recent MMM studies, the highly permeable PIMs are

intensively used by matching with diverse molecular sieve materials to achieve higher performances. In 2011, for the first time Yu and Wang et al.[39] successfully demonstrated the applicability of MMM with sub-micron thickness prepared by interfacial polymerization for gas separations. In 2013, a novel strategy to fabricate MMM of the one-pot in-situ growth of MOF filler in a polymer solution was introduced by Seoane and Coronas et al.[40] In 2015, the MMM containing 2D graphene, which is evaluated as a next-generation MMM material in many review articles,[41-48] was firstly reported by Li and Wu.[49] Another promising 2D porous material covalent organic framework (COF) containing MMMs was studied by Kang and Zhao in 2016.[50]

2.2. Type of MMMs

A modulation of gas separation membranes is essential for commercial applications. A membrane module is the smallest unit into which membranes are packed. Based on the types of membrane modules, the efficiency of gas separation can be varied. In general, there are two types of membranes, one is a flat sheet membrane and the other is a tubular-type membrane. Modules of flat sheet MMMs can be designed as plate-frame module MMMs (PF-MMMs) and spiral-wound module MMMs (SW-MMMs) (Figure 2.2a). MMMs in hollow fiber forms (i.e., mixed-matrix hollow fiber membrane (MMHFM)) is the common geometry of tubular-type MMMs and its modulated form is hollow-fiber module MMMs (HF-MMMs) (Figure 2.2b). From an engineering view, cost of module fabrication and maintenance, packing density, surface-area-to-volume ratio, and application area are the main criteria to consider for commercial products of MMM modules. The advantages and disadvantages of membrane modules are well summarized by Mubashir and Fong et al.[51] as shown in Table 2.1.

Table 2.1. Comparison of different membrane modules for gas separation.[51] Copyright 2018, Wiley.

Property	Membrane geometry		
	PF-MMM	SW-MMM	HF-MMM
Manufacturing cost (USD m^{-2})	100 - 200	30 - 100	5 - 20
Packing density	Low	Low	High
Pressure drop	Low	High	Low
Suitability for high pressure	Yes	Yes	Yes
Surface area per unit volume	Low	High	High
Space required	Large	Large	Small

2.2.1. Flat sheet type MMMs

PF-MMMs have been used for decades due to its easy MMM fabrication processes, low pressure drops and low operation energy.[51] Multiple types of fillers have been embedded into various polymeric matrix to form PF-MMMs for different gas separation system, such as carbon natubes/PI for CO_2/CH_4,[52] ZIF-8/PEBAX for CO_2/N_2,[53] organoclay/PSF for O_2/N_2,[54] ZIF-8/6FDA-DAM for C_3H_6/C_3H_8 [1] and so on.[55-56] By combining these inorganic fillers, the as-synthesized MMMs exhibit improved property and gas separation performance. For example, asymmetric PF-MMMs containing low loading of nano-sized ZIF-8 (up to 1 wt%) fillers and PSf were synthesized by a dry/wet phase inversion approach.[57] Compared to the neat polymeric membrane, the PF-MMMs showed an enhanced CO_2 permeability and CO_2/CH_4 selectivity.[57] For the MMMs at a 0.5 wt% ZIF-8 filler loading, the permeability of CO2 increased by 37 %

(from 21.27 GPU to 29.22 GPU) and at the same time, the CO_2/CH_4 selectivity was enhanced by 19 % (from 19.43 to 23.16).[57] The significant improvement in thermal and mechanical stability were observed even at a 0.25 wt% ZIF-8 loading.[57]

SW-MMMs are consisted of two flat sheet MMMs. These two MMMs are separated by a spacer and a hollow is placed in the center to collect permeated gas molecules. Compared to PF-MMMs, SW-MMMs shows a higher packing density, higher pressure drop, lower cost and higher surface area per volume (Table 2.1). Both SW-MMMs and PF-MMMs need large operation space. Another disadvantage of SW-MMMs is that they are hard to clean which means the maintenance of SW-MMMs will be complicated.

2.2.2. Tubular type MMMs

Hf-MMMs have the highest packing density and surface-area-to-volume ratio, and the lowest manufacturing cost in comparison to PF-MMMs and SW-MMMs, making HF-MMM to be attractive for commercial applications among the MMM modules. Despite the advantages, HF-MMMs often have relatively low pressure tolerance and those are more difficult to repair among the MMM modules.[51] More importantly, hollow fiber membrane fabrication processes are more complicated and challenging than that of flat sheet membranes due to their unique geometry. There have been several research works showing the promising gas separation performance of lab-scale HF-MMMs. Zahri at al.[58] reported HF-MMMs containing graphene oxide and polysulfone for CO_2 separation. With a 0.25% GO loading, the CO2 permeability of HF-MMMs reached 74.47 GPU as well as a 44.4 CO_2/N_2 selectivity. Liu et al.[59] embedded Y-fum-fcu-MOF into 6FDA-DAM to fabricate HF-MMMs for the removal of CO_2 and H_2S from natural gas. Nevertheless, the majority of reported MMMs were flat sheet forms rather than hollow fiber

forms, likely due to the difficulty of controlling skin layer defects and polymer/filler microstructures of MMHFMs by the current fabrication processes.[43, 60-61]

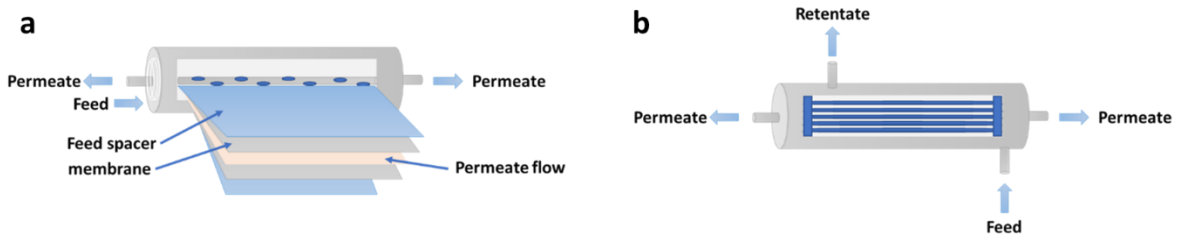

Figure 2.2. Illustration of (a) SW-MMM and (b) HF-MMM.

2.3. MMM fabrication strategies

2.3.1. Solution processing

Solution processing is the most classical and widely used blending-based method for MMM fabrications due to the simplicity. This method was mainly used for flat sheet membranes on a lab-scale despite a few reports of MMHFMs. In general, the procedures of solution processing involve (1) preparing a polymer/filler dope solution by blending, (2) casting the solution into a desirable form, (3) solidifying the MMM by evaporating solvent, and (4) drying the film.[16, 62-63]

As shown in Figure 2.3, there are three different routes to prepare the filler suspended mixed-matrix dope solutions commonly. First, the mixed-matrix dope solution can be prepared by adding fillers in a polymer solution, which is prepared by dissolving a polymer completely in a proper solvent (route a, Figure 2.3a). After homogeneously dispersing inorganic fillers in a solvent, a polymer is dissolved in the filler suspension (route b, Figure 2.3b). A polymer solution

and a filler suspension are prepared separately and then the two solutions are blended (route c, Figure 2.3c). In this process, the selection of proper solvent is of critical importance to achieving successful fabrications of MMMs. Therefore, the following factors might be primarily considered; solubility of a certain polymer, volatility, boiling point, and interaction with fillers. In particular, the importance of solvent interacted with fillers was emphasized by Koros et al.[28, 64] based on the three-component interaction theory. The balanced solvent-filler interactions enable to prevent agglomerations as well as sedimentations of particles along with improved adhesion of fillers with a polymer.[64-65] Based on the theory, the priming protocol was proposed to enhance the wettability of fillers by the polymer solution by dissolving some portion of polymers in a filler suspension in the route c.[28] In addition, the homogenization of fillers in the suspension was able to be accomplished with an aid of outer forces such as a high shear mixing or an ultra-sonication. Nevertheless, the too strong homogenization may result in a disintegration or an Ostwald ripening of fillers.[66] As such, the appropriate manners of filler dispersion are required.

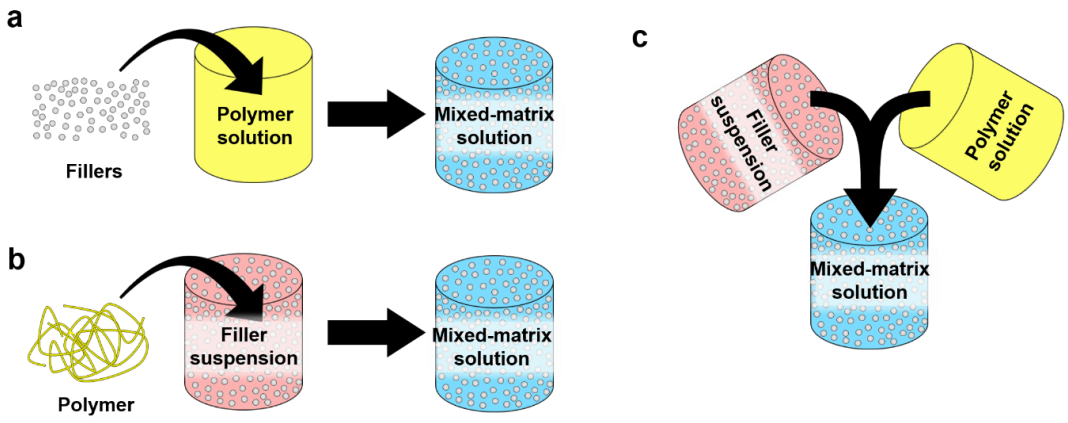

Figure 2.3. Illustration of different routes for mixed-matrix dope solution preparations.

The thickness and uniformity of MMMs using the solution processing varies from several micrometers to a few nanometers depending on casting methods and its parameters. There are four representative MMM casting methods: solution-casting, knife-casting, spin-coating, and dip-coating. In Table 2.2, the MMM casting techniques are compared. The casting methods of MMMs are analogous to those of polymer membranes. The well-described explanations of each casting method also can be found in the previous review papers associated with polymer membranes.[67] Solution-casting (or drop-casting) has been widely used since it is one of the classical and simple casting methods among the solution processing (Figure 2.4a).[68-70] The procedure of the solution-casting method is as follows; (1) dropping a mixed-matrix dope solution onto the casting mold (i.e., ring or plate), (2) spreading out the liquid solution, which fills the casting mold evenly, (3) evaporating the solvent, forming the solidified MMMs. In this process, it is desirable to dilute the dope solution with the solvent to decrease viscosity and well spread out, nevertheless, which may increase the solvent evaporation time and sedimentation of the fillers. When the solution-casting is performed on a porous substrate, a very thin gutter layer may be needed to prevent the penetration of the diluted dope solution into the porous layer. The thickness of the MMM can be controlled by the solution concentration (i.e., [polymer + filler]/[polymer + filler + solvent]), the mold size, and solvent density. However, it is not easy to get an ultra-thin (< 1 μm) and uniform thickness without defects using this method. On the other hand, knife-casting (or Doctor blade or tape-casting) provides more uniform thicknesses by the mechanical slipping of dope solution through the gap between a substrate and a casting knife (Figure 2.4b). As a mean to get thinner and more uniform MMMs, spin-coating can be applied. It spreads the dope solution through the centrifugal force by spinning the substrate (Figure 2.4c). The spinning rate as well as the dope solution concentration are the major parameters to control

the thickness of MMM.[71] Another advantage of the spin coating in comparison to others is that the process is time-saving since solvent evaporation occurs upon the spinning. Although the solution processing is simple and inexpensive, however, they are mostly discontinuous processes, which could impede the fast and large-scale MMM fabrications. While knife-casting can be used to fabricate spiral wound type membranes, otherwise, dip-coating (Figure 2.4d) is almost the sole strategy enabling continuous MMHFM fabrications among the solution process based approached. Nevertheless, among the reports introducing dip coating to fabricate MMMs, most of they are related to flat sheet membranes rather than hollow fibers.[72] More detailed discussion about the MMHFM taking advantage of dip-coating is presented in Section 3. To control the thickness of MMM during the dip-coating process, the deposition rate, drenched time along with the number of dipping cycles should be taken into consideration.[73] Besides the above mentioned solution process methods, there are uncommon methodologies involving solution processing such as spray coating[74] and slot die coating.[75]

Table 2.2. Comparisons of different casting techniques.

Casting method	Thickness	Uniformity	Time	Simplicity	Continuity
Solution-casting	Moderate	Low	Slow	Very high	Low
Knife-casting	Moderate	High	Moderate	Very High	Moderate
Spin-coating	Very thin	High	Fast	High	Low
Dip-coating	Thin	Moderate	Fast	High	High

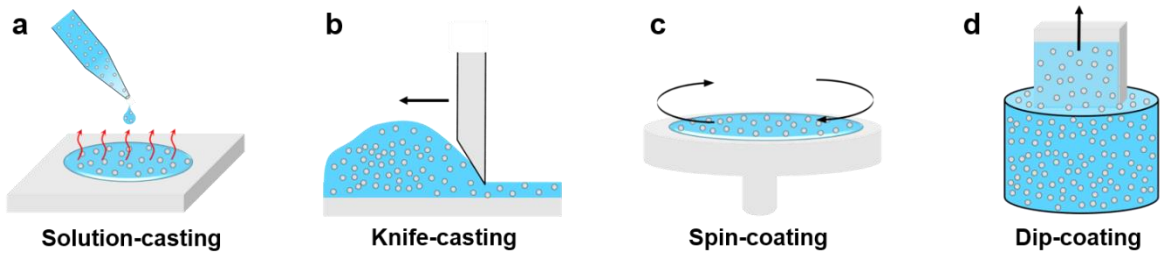

Figure 2.4. Illustration of MMM fabrication methods using solution processing.

Furthermore, solvent evaporation affects significantly on forming a uniform and defect-free MMMs during solution processing. Rapid solvent evaporation leads to wrinkling, surface unevenness, and pin-holes.[76] The humidity, atmospheric condition, and temperature also contribute considerably to the solidification of polymers. In light of these, the control of solvent evaporation rate is an essential factor in fabricating MMMs. The solvents can be classified into two main categories based on their volatility. For example, dichloromethane (DCM), chloroform, and tetrahydrofuran (THF) are the common volatile solvents and N,N- dimethylacetamide (DMAc), N,N- Dimethylformamide (DMF), and 1-Methyl-2-pyrrolidone (NMP) are the common non-volatile solvents for MMM fabrications.[77] Casting dope solutions in a solvent saturated chamber is an beneficial means to slow down the evaporation rates of volatile solvents and to maintain low humidity.[78] For the non-volatile solvents, MMMs have been fabricated under heating and/or vacuum along with a gradual increase in temperature.[79]

2.3.2. Melt processing

Compared to solution processing, melt processing is faster, easier to be continuous, and especially more economic and environmentally friendly due to the absence of toxic organic

solvent and the cost saving of solvent recycling. There are four steps covered in the melt processing for MMM fabrications. (1) Solid polymers are transformed into liquids by melting with increasing temperature. (2) Molten liquid polymer is blended with fillers under gravity or external pressure using extruder, internal mixer, and two-roll mill. (3) The homogeneously dispersed fillers containing polymer liquid is cast into molds with desired shapes. (4) By cooling, the cast liquid is solidified to MMMs.[80] The micropores of membranes fabricated by melt processing can be generated by cold-stretching[81-82] and salt-leaching.[83]

There have been a few reports using melt processing for MMMs of gas separations. Razzaz et al.[84] incorporated nano-sized zeolite 5A into low-density polyethylene (LLDPE)/polyethylene (LDPE) to form MMHFMs by continuous melt extrusions. The process was carried out via a twin-screw extruder combined with a calendaring system, as shown in Figure 2.5. With the zeolite 5A loading up to 20 wt%, the gas separation performance of the MMHFMs was enhanced compared to that of neat polymer membranes. Covarrubias et al.[85] also showed the significantly increased gas separation performances of polyethylene (PE)/porous layered aluminophosphate (ALPO) MMMs prepared by melt compounding. The ALPO swollen by cetyltrimethylammonium (CTA) formed the intercalated structure, resulting in that it provided an effective gas transport pathway and reduced PE crystal sizes. Nevertheless, Kathuria et al.[86] pointed out the limitations of melt compounding for the fabrication of MMMs. For the case of poly(L-lactic acid) (PLLA)/water saturated HKUST-1 MMMs, the crystal structure of the HKUST-1 fillers was changed and the PLLA polymer was degraded by the high temperature upon the melt extrusion. Likewise, the chemical modification of graphene incorporated in MMMs was damaged during melt processing.[87] Furthermore, melt processing is only applicable to semi-crystalline thermoplastic polymer-based MMMs. Since the crystalline phase of these

polymers is mostly impermeable to gas molecules, MMMs prepared by melt processing are more promising to use as gas barrier membranes rather than gas separation membranes.[88]

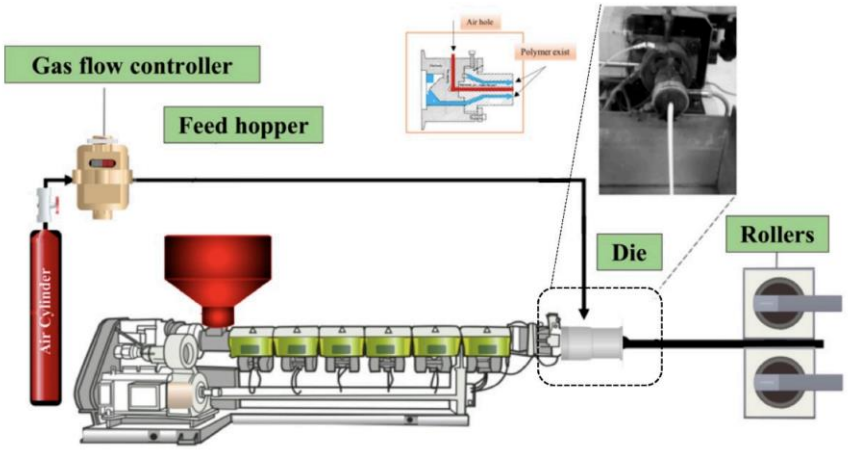

Figure 2.5. Schematic representation of the extrusion set-up to produce hollow fiber mixed matrix foamed membranes.[84] Copyright 2018, Multidisciplinary Digital Publishing Institute.

For the developments of gas barrier MMMs by melt processing, diverse non-porous fillers such as clay,[89-90] silica,[91] graphene,[92-95] and layered silicate[96-97] were incorporated into semi-crystalline polymers. Especially, these fillers with 2D sheet-like morphology enabled to largely increase tortuosity of gas molecule diffusion pathway due to their high aspect-ratio, effectively improving the gas barrier properties of MMMs.[89-90, 92-94, 97] Thereby, the distribution (i.e., exfoliation and intercalation) is of critical importance for the successful improvements of gas barrier efficiency. For example, Adak et al.[89] prepared polyurethane/nanoclay MMMs as gas barriers through melt extrusion using two different mixing approaches: direct mixing and master-batch mixing where nanoclays are formally dispersed in a solvent. Compared to the direct mixing where nanoclays were agglomerated, the master-batch mixing enabling to exfoliate

nanoclays showed the improved gas barrier properties ~ 30 % due to the increase in the tortuosity of gas diffusion pathways. In these regards, to prevent filler agglomerations, the optimal loading of fillers in MMMs was commonly less than 5 wt%.[89-91, 94, 98]

2.3.3. Phase inversion

For the commercial applications of gas separation membranes, it is critical to achieving a selective skin layer to be as thin as possible from several microns up a few nanometers without defects for high gas production. To provide enough mechanical stability, the thin skin layer should be supported by a relatively thick porous support layer (i.e., > ~ 100 μm) to withstand the transmembrane pressure that is the driving force of gas transfer across membranes with negligible mass transport resistances. In these regards, an asymmetric structure is the desirable form of commercial gas separation membranes. Phase inversion process is an effective mean to form asymmetric structures of polymeric materials. As such, it has been widely used to fabricate commercial polymeric membranes. Based on the successful fabrications of polymer membranes, the phase inversion technique has been moved on to MMMs. Diverse asymmetric MMMs have been fabricated by phase inversion process.[45]

The key of phase inversion process is the choice of polymer/solvent/non-solvent system whose compositions can be elaborated by a ternary phase diagram.[99] The cast or spun dope solution is immersed into a non-solvent coagulation bath and transformed to the solid membrane via liquid (solvent)-liquid (non-solvent) demixing process. The morphologies of membranes are determined by ratios and rates of demixing process. A sponge-like membrane morphology is formed when the demxing rate is slow by the low miscibility of solvent with the non-solvent. Otherwise, a finger-like morphology shows up. On the other hand, for MMMs, the demixing

process can be affected by dispersed fillers in dope solutions. For example, the hydrophilic HSSZ-13 zeolite dispersed in the mixed-matrix dope solution accelerated locally the rates of demixing with water, resulting in that the low polymer concentration around the zeolite led to the formation of interfacial voids.[100]

There are several challenges of commercially available MMM fabrications using phase inversion. Due to the presence of fillers in a dope solution, the defects on membrane skin layers can be generated by not only the pinholes of skin layer but also the polymer/filler interfacial voids and filler agglomerations. Considering the manufacturing costs of MMMs, the support layer can be replaced with an inexpensive polymer, representing that fillers are only present at the skin layer. As such, MMHFMs typically consist of a dual-layer asymmetric structure (i.e., a shell of a mixed matrix having a thin skin layer and a core of a porous support layer made of inexpensive polymer).[101] Due to the different phase inversion conditions of shell and core layers, the formation of a defect-free skin layer is more challenge upon a dual-layer spinning process compared to that of single-layer spinning. Furthermore, the high filler loadings in MMMs are limited by the MMM processing factors. For MMHFMs, the high filler contents in a mixed-matrix dope solution may increase the viscosity and decrease the elasticity, reducing the spinnability of dope solutions.[101]

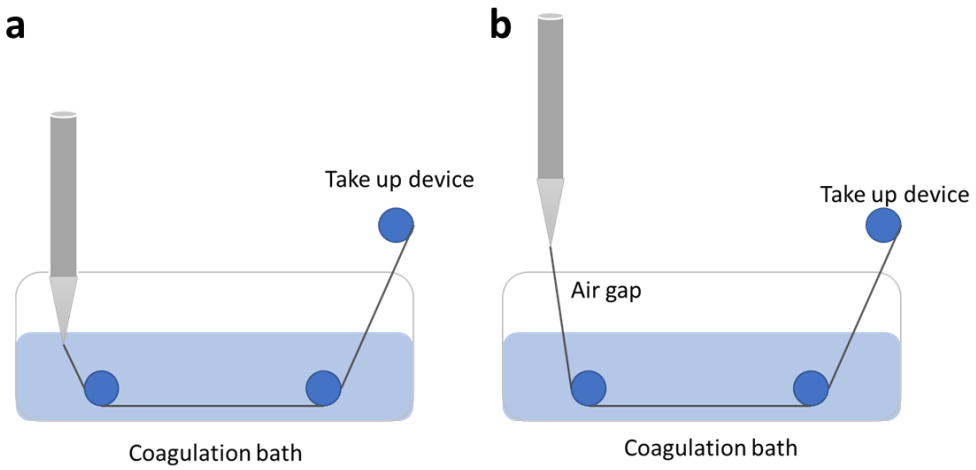

Figure 2.6. Illustration of hollow fiber membrane spinning: (a) wet-spinning and (b) dry-wet spinning.

2.3.3.1. Wet-spinning

The outer layer of wet spun asymmetric MMHFMs solidifies immediately when get in contact with the coagulant bath without any air gap (Figure 2.6a). With the increase of air gap, more defects may be generated because of large elongation and gravitational stress.[102] Dual-layer PES/P84 asymmetric MMHFMs containing PES–zeolite beta was fabricated through wet spinning process.[103] The outer of the wet spun MMHFMs contained less defects compared to the MMHFMs spun at 1.5 cm air gap. At the same time, the presence of PES–zeolite beta plays a positive role in both pure and mixed gas separation tests.

2.3.3.2. Dry-wet spinning

In the process of dry-wet spinning, the nascent filaments need to pass through the air gap when the solvent evaporation occurs at the same time (Figure 2.6b). Also, the phase inversion happens at the interface between dope and bore. A larger air gap means a longer time for

evaporation of volatile components in air which will result in the increase polymer concentration of the outer layer of spun dope solutions, leading a less pinhole formation on the shell side of MMHFMs. In order to investigate the influence of incorporation of inorganic particles to the phase inversion process, MIL-53 based asymmetric MMHFMs were fabricated and performed gas separation tests.[104] The asymmetric MMHFMs containing MIL-53 particles were formed by dry-wet spinning process. MIL-53 grouped with EtOH as a non-solvent showed significant effect on the phase inversion. With 5 wt% MIL-53 loading, the asymmetric MMHFM demonstrated increased gas separation performance. The permeability of CO_2 and O_2 increased 129 % and 138 % respectively in comparison to the neat Ultem hollow fiber membrane while the selectivity of O_2/N_2 and CO_2/CH_4 remained constant.

2.3.4. In-situ approach

Recently, the in-situ bottom-up approaches have attracted many MMM researchers' interests as promising strategies to overcome the issues of MMMs (i.e., polymer/filler adhesion and filler dispersion). Their flexibility and scalability provide great potential for the development of advanced MMMs for gas separations. The in-situ approach can be mainly categorized as in-situ polymerization and in-situ filler formation.[105] For in-situ polymerization methods, polymer precursors (i.e., monomers, oligomers, solvent, and/or additives including crosslinker or polymerization initiator) are blended with filler particles and then sequent polymerization occurs via in-situ manner. The in-situ polymerization is distinguished into in-situ crosslinking, post-synthetic polymerization, and interfacial polymerization. In stark contrast, the in-situ filler formation methods involve the growth of filler crystals either inside the cast dope solutions or inside the solidified polymer membranes.

2.3.4.1. In-situ crosslinking

Despite the recent attention on the in-situ polymerization, the conventional in-situ crosslinking-based MMM fabrications has been used since the early 1990s.[106-107] One of the primary applications of the in-situ crosslinking was that the precursors of silicone rubber blended with silicalite-1 zeolite fillers followed by in-situ crosslinking upon the film formation.[25] Taking the advantages of the in-situ polymerization approach and the flexibility of polymer chains, the filler loading was reached up to 70 wt% without defects. The as-synthesized MMMs established the improved permeability for He, H_2, CO_2, and O_2 along with selectivity from 2.14 and 11.6 to 2.92 and 17.1 for O_2/N_2 and CO_2/N_2 separations, respectively. As a more recent study, Ma et al.[107] prepared poly(PEGMA-co-PEGDMA)/UiO-66 type MOF MMMs by in-situ crosslinking PEG containing monomers, poly(ethylene glycol) methacrylate (PEGMA) and poly-(ethylene glycol) dimethacrylate (PEGDMA) (Figure 2.7). The CO_2/CH_4 separation performance of *in-situ* crosslinked membranes was enhanced by incorporating filler loading up to 35 wt%.

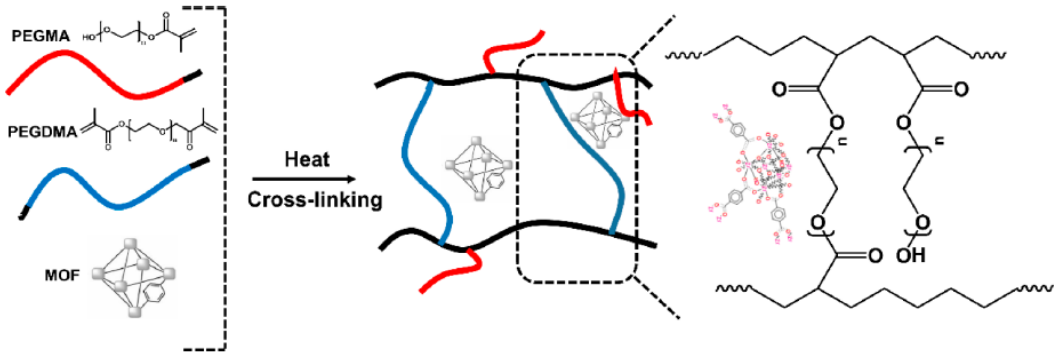

Figure 2.7. Schematic Illustration of the synthetic approach for the preparation of MMM-based on cross-linked poly[(ethylene glycol) methacrylate] and MOF.[107] Copyright 2018, American Chemical Society.

2.3.4.2. Post-synthetic polymerization

The post-synthetic polymerization (PSP) (also known as grafting-from approach), which is in-situ polymerization from a solid surface,[67] seems to resemble with the in-situ crosslinking since both methods employ in-situ polymerization by crosslinking of small molecules blended with fillers. However, the key difference of the PSP from the in-situ crosslinking is the functional groups on the surface of fillers, which are polymerizable by strong covalent bonds with oligomers.[105] The functionalization of filler surface enables copolymerization of monomers and fillers. Due to the interconnection of oligomer and filler by chemical bonds, the MMMs fabricated by the PSP method displayed significantly enhanced particle dispersion and adhesion between polymer and fillers compared to that of in-situ crosslinking.[108-110]

A novel strategy to fabricate MMMs made of covalently linked fillers and a polymer by the photoinduced PSP was successfully demonstrated by Feng and Wang et al.[111] As a first step, UiO-66-NH_2 fillers were functionalized with vinyl functional groups, which are polymerizable (Figure 2.8a). The subsequent in-situ copolymerization of vinyl functionalized UiO-66-NH_2 fillers and butyl methacrylate monomers was performed by the irradiation of UV-light (Figure 2.8a). The enhanced interaction between MOF fillers and polymer chains enabled the formation of crack-free MMMs with the uniform filler distribution. Another example of the PSP using vinyl group induced polymerization for MMM fabrications was reported by Molavi and Shojaei et al.[108] They synthesized the MMMs by in-situ copolymerization of vinyl functionalized UiO-66 and methyl methacrylate (MMA) monomers, achieving the high degree of grafting between PMMA and UiO-66. The high degree of grafting provided the stronger interfacial adhesion and the more uniform filler distribution compared to that of counterpart MMMs prepared without

polymer-filler grafts. As a result, the grafted PMMA/UiO-66 MMMs showed the highest gas selectivity among the tested MMMs.

Applying the PSP to glassy polymers with high fractional free-volumes is a great interest to achieve high gas separation performances with the improved microstructure of MMMs. Cadmium (Cd)-based MOF fillers that were made of 6FDA, as an organic ligand, were introduced to the in-situ copolymerization of 6FDA and ODA monomers, resulting in the grafted 6FDA-ODA/Cd-6FDA MMMs (Figure 2.8b).[109] The polymer/filler interfaces of MMMs were significantly enhanced by the formed bonds between the COO^- group of Cd-6FDA filler surface and the NH_2 group of ODA monomer at the end of 6FDA-ODA polymer chain. As such, the resulting in-situ polymerized MMMs showed improved polymer/filler interface morphology, exhibiting 4 times higher CO_2/N_2 and CO_2/CH_4 selectivity than those of other MMMs by blending. In addition, Tien-Binh and Kaliaguine et al.[110] grafted UiO-66-NH_2 fillers with a monomer of PIM-1 (i.e., DCTB), fabricating UiO-66 grafted PIM-1 MMMs via the PSP. The MMMs consisting of 20 wt% UiO-66-NH_2 crosslinked with PIM-1 enabled to increase the CO_2 separation performance ~ 250 % and revealed the considerably intensified anti-aging effects compared to those of MMMs prepared by blending. The strong interactions between homogeneously dispersed UiO-66-NH2 fillers and PIM-1 matrix enabled to significantly suppress the physical aging of PIM-1.

Recently, the attention to ionic liquid (IL) has been grown due to the non-volatility, the favorable solubility for various large molecules, and the high sorption capacity for polar vapor/gas molecules such as H_2O and CO_2.[112] Yao and Dong et al.[113] adopted IL as a polymerizable grafting agent between UiO-66 and polyurethane oligomer to synthesis MMMs via PSP (Figure 2.8c). The modification of UiO-66 with IL provided covalent bonds with the

isocyanate terminal groups of polyurethane oligomers. The filler loading of 50 wt% in the grafted MMMs enabled to increase CO_2 permeance by ~ 600 % and CO_2/N_2 separation factor ~ 500 %.

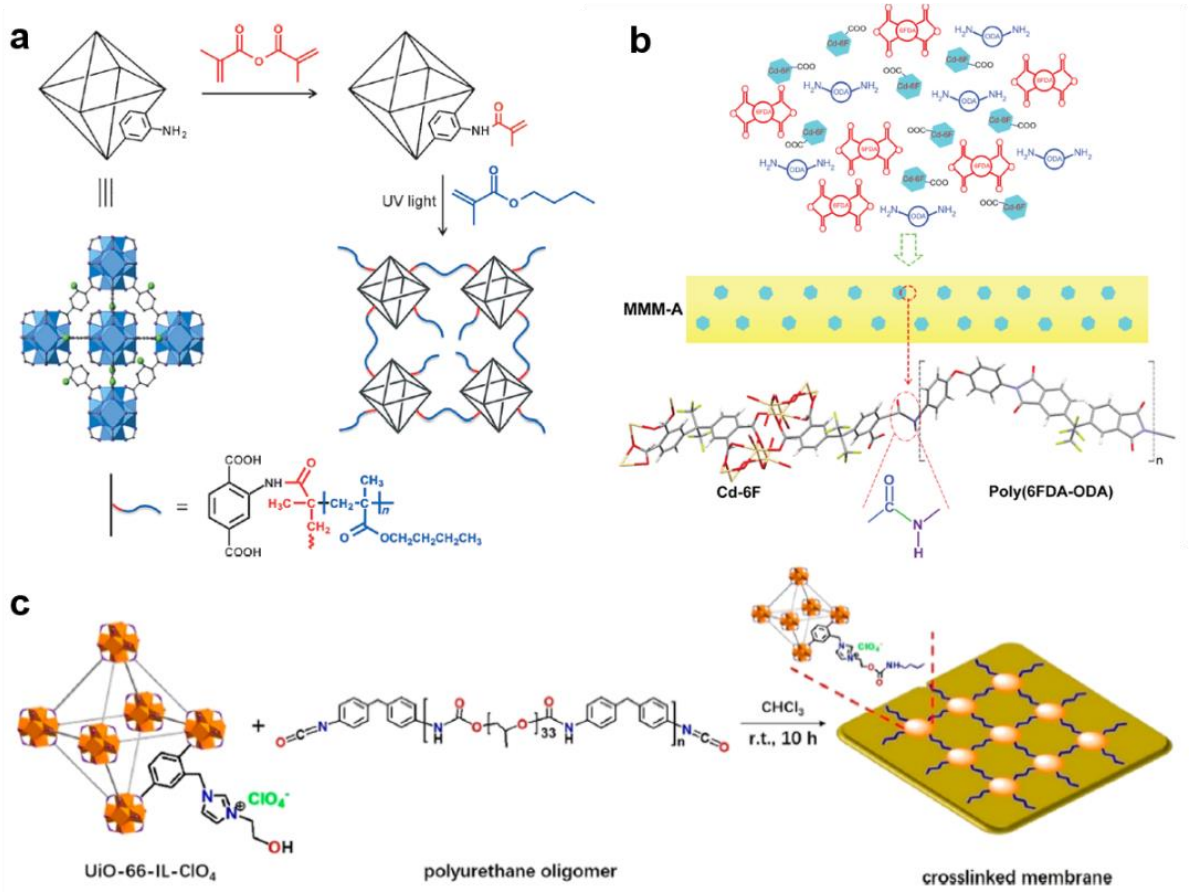

Figure 2.8. (a) Post-synthetic modification of UiO-66-NH_2 with methacrylic anhydride and subsequent polymerization with butyl methacrylate by irradiation with UV light.[111] Copyright 2015, Wiley. (b) Diagram of designed interaction between Cd-6FDA and 6FDA-ODA in the grafted MMM.[109] Copyright 2014, American Chemical Society. (c) Chemically cross-linked membrane-based on UiO-66-IL-ClO_4 nanoparticles and the polyurethane oligomer.[113] Copyright 2017, American Chemical Society.

2.3.4.3. Interfacial polymerization

Interfacial polymerization (IP) is another promising MMM fabrication strategy to commercialize MMMs. IP is applied to synthesize an ultrathin polymer layer at the interface of two separated phases (i.e., aqueous and organic phases) rapidly.[114] Thin film composite (TFC) membranes are polymer membranes prepared by IP. Besides, thin film nanocomposite (TFN) membranes are MMMs fabricated by incorporating fillers during the synthesis of IP. These membranes show a thickness of less than a few hundred nanometers in general and are supported by porous substrates, which is normally prepared by phase-inversion methods.[115] Although IP is one of the highly scalable techniques for MMM fabrications, currently, its applications are mostly liquid separations rather than gas separations. This is likely due to the agglomeration derived defects on the ultrathin layers.[115] Nonetheless, there have been a few reports claiming that TFNs were used as gas separation membranes.[39, 116-118]

The restriction of pinhole formation during IP with the presence of fillers is of critical importance for the utilization of TFNs as gas separation membranes. Wong and Goh et al.[117] fabricated the TFN of PEO-based polyamide containing carbon nanotube (CNT) functionalized with polymethyl methacrylate (PMMA) by grafting for CO_2 separations by using IP. The dispersion and adhesion of CNT fillers were enhanced by the grafted PMMA. However, the TFNs showed uncovered areas with polyamide, sacrificing the gas selectivity. On the other hand, the polyamide/carbide-derived-carbon (CDC) TFNs prepared by IP for gas separations were reported by Awad and Aljundi.[118] Forming the layer-by-layer structure of polyamide film by multi-cycles of IP, the CO_2/CH_4 selectivity of polyamide/CDC TFNs increased from ~20 to ~24 resulting from the sealing of pinholes. However, as a consequence, the increase in membrane thickness compromised the CO_2 permeance by ~ 43 %.

Besides from the carbon-based TFN studies, there were TFNs for gas separations combining ZIF-based fillers, which enabled the integrity of polyamide layers. Sánchez-Laínez and Coronas et al.[119] demonstrated the applicability of TFNs by IP for gas separations using ZIF-8 as a filler. The synthesized TFN was ~ 50 ~ 100 nm in thickness and it contained ZIF-8 of 30 nm in size with filler loadings of 0.2 ~ 0.8 % w/v (Figure 2.9). It was pointed out that the amount of ZIF-8 required to fabricate TFNs was substantially reduced by using IP comparing with that of MMMs using other fabrication strategies. The TFN showed the increased H_2/CO_2 selectivity and the decreased H_2 permeance compared to those of the TFC, indicating the integrity of the polyamide layer in the TFN. Nevertheless, due to the filler agglomeration, the optimal ZIF-8 loading was relatively small (i.e., 0.4 w/v). To enhance the compatibility and dispersion of fillers, Yu and Liu et al.[116] fabricated TFNs via IP using amine-functionalized ZIF-8 fillers. The amine-functional groups on ZIF-8 fillers formed covalent bonds and hydrogen bonds with the organic phase monomers and the aqueous phase monomers, respectively. As a result, the optimal filler loading of TFN was ~ 1.0 w/v, showing 228 % and 106 % increase in CO_2 permeance and CO_2/N_2 selectivity, respectively, in comparison with that of the corresponding TFC.

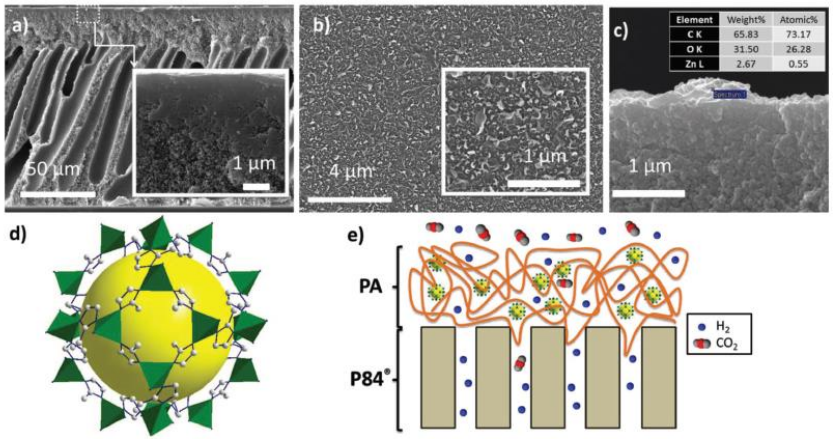

Figure 2.9. SEM characterization of TFCs & TFNs prepared on polyimide P84® supports. (a) Image of the cross-section of a TFC with an inset at higher magnification. (b) Image of the surface of the TFC with a zoom as inset. (c) EDX analysis of a TFN containing a 0.8 % w/v of ZIF-8. Schematic representations of (d) ZIF-8 and (e) the TFN membrane.[119] Copyright 2018, Wiley.

2.3.4.4. In-situ filler formation in solution

One of the first attempts to fabricate MMMs using in-situ filler formation was the in-situ synthesis of silica through the sol-gel process of silica precursors (e.g., tetraethyl orthosilicate (TEOS)) in a polymer solution.[120-121] After years, Seoane and Coronas et al.[40] fabricated MOF-based MMMs by using the in-situ formation of MIL-68 (Al) fillers in a PSf solution. The in-situ MOF formation in the polymer solution was accomplished by developing the new synthesis method of MIL-68 (Al) in THF solvent, which was also used as a solvent of PSf. The loading of MOF fillers in the resulting MMMs was estimated by the yield of MIL-68 (Al) particle in the same synthesis conditions of the in-situ filler formation. The in-situ MIL-68 (Al) formation enabled to effectively prevent particle agglomeration, achieving a uniformly distributed fillers in the polymer at the filler loading of 8 wt%. Due to the uniform filler distribution as well as the enhanced polymer/filler interaction, the H_2/CH_4 and CO_2/CH_4 selectivities were increased with the increase in filler loadings. In stark contrast, the PSf/MIL-68 (Al) MMMs prepared by the conventional blending methods exhibited severe particle agglomeration, resulting in a decrease in the gas selectivity compared to that of the neat polymer membrane.

Unlike the Seoane and Coronas et al.'s work,[40] of which in-situ filler formation was conducted in the bulk polymer solution before film casting, recently, Matrimid®/UiO-66 MMMs

were prepared by the in-situ filler formation inside the cast polymer solution (Figure 2.10).[122] This straightforward MMM fabrication strategy provided the synthesis of UiO-66 and the film formation simultaneously by using the dope solution prepared through dissolving a polymer in the MOF precursor solution. It is important to note that the one-step approach significantly reduced the MMM preparation procedures compared to other MMM fabrication strategies, making it favorable for a large-scale MMM production. In addition, the resulting MMMs showed the improved interfacial interaction and filler distribution compared to the MMMs prepared by the conventional blending methods at the lower filler loading of ~ 2 wt%. Unfortunately, at the higher filler loading of ~ 11 wt%, it was inevitable to form the severe particle agglomeration. As such, despite the separation performance improvement compared to that of neat polymer membranes, the CO_2/N_2 selectivity of MMMs prepared by the in-situ filler formation was lower than that of MMM prepared by the blending method from the filler loading of above 6 wt%.

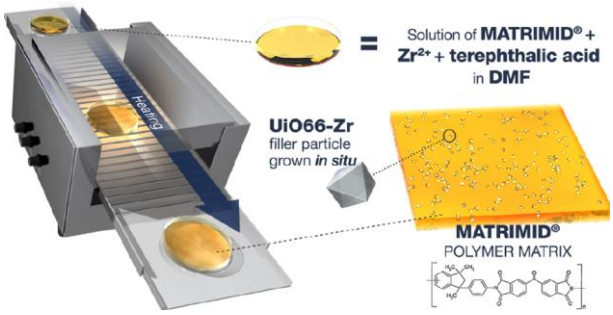

Figure 2.10. Schematic illustration of Matrimid®/UiO-66 MMMs fabrication via in-situ synthesis of UiO-66 in the polymer solution while simultaneous solvent evaporation by heating.[122] Copyright 2018, American Chemical Society.

2.3.4.5. In-situ filler formation in solid

Although the in-situ filler formation in polymer solutions demonstrated their potential by the improving filler distribution, polymer/filler interfacial interaction, and scalability, the applications of these approaches were limited in a low filler loading (< 10 wt%).[122] It is possible to explain that since the polymer solution may provide enough mobility to rearrange the in-situ formed crystals, in order to minimize the surface energy, the in-situ formed crystals that are originally distributed at the molecular level tend to agglomerate. Hence, as the concentration of in-situ formed fillers increases in a solution, the distance between in-situ formed fillers decreases, undermining the distribution of in-situ formed fillers. In these regards, recently, the in-situ filler formations in a solid polymer membrane have been reported. These approaches generated more uniform filler distribution even at the higher filler loading (> 25 wt%) through fixing position of the in-situ formed fillers.[123-125]

Ma and Tan et al.[123] proposed a new concept of MMM fabrication using the in-situ filler formatting in a crosslinked polymer matrix. The cross-linkable precursors of PEO-based polymer and the precursors of ZIF-8 (i.e., $Zn(NO_3)_2 \cdot 6H_2O$ and 2-methylimidazole) were blended without solvents (Figure 2.11). After the polymerization, the ZIF-8 fillers were in-situ formed in the crosslinked polymer upon the polymer swelling in water at room temperature. However, the in-situ formed ZIF-8 fillers were partially agglomerated, even though those MMMs showed the much uniform filler distribution compared to that of MMMs prepared by the in-situ filler formation in a solution. To prevent the agglomerations potentially occurred by the random distribution of ZIF-8 precursors, the polymer membrane containing ZIF-8 precursor was thermally treated at the temperature above the melting point of the polymer. The in-situ formed ZIF-8 fillers from the rearranged ZIF-8 precursors by the thermal treatment were uniformly distributed with the high compatibility with the polymer, achieving ZIF-8 loading up to 60 wt%.

It is noted that the size of in-situ formed ZIF-8 increased by the thermal treatment and it was continuously increased with the increase in the concentration of ZIF-8 precursors (i.e., from ~ 100 nm to ~ 800 nm in size). The resulting MMMs showed considerable CO_2 permeability enhancements.

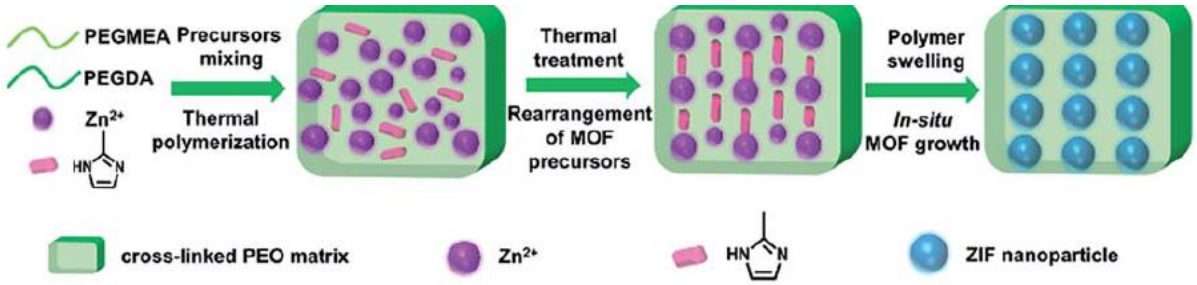

Figure 2.11. Schematic illustrations of the preparation of ZIF-based mixed matrix membranes using the in-situ growth approach. Copyright 2019, The Royal Society of Chemistry.

CHAPTER III

HIGHLY PROPYLENE-SELECTIVE MIXED-MATRIX MEMBRANES BY IN-SITU MOF FORMATION USING A POLYMER-MODIFICATION STRATEGY

3.1. Introduction

Membrane-based gas separation has attracted tremendous research interests as a cost and energy-efficient alternative to conventional gas separation technologies such as cryogenic distillation. C_3H_6/C_3H_8 separation,[126-127] in particular, is one of the most challenging separations due to the very similar physical and chemical properties of the two gas molecules. It has been shown that membrane-based separation or distillation-membrane hybrid system can significantly save the annual utility cost for C_3H_6/C_3H_8 separation by 32–66 % or 18–47 %, respectively.[128] In addition, the same study found that the cost saving efficiency largely depends on membrane materials and the processing of the materials into membranes.[128] Polymer membranes have been extensively studied and commercially successful primarily due to the low cost of polymers and their cost-effective processing. However, polymer membranes suffer from their performance limitations, known as upper bounds, making polymeric membranes less attractive for C_3H_6/C_3H_8 separation.[129] On the other hand, polycrystalline molecular sieve membranes such as ZIF-8 membranes showed high C_3H_6/C_3H_8 separation performances.[130-131] Nevertheless, there have been no polycrystalline molecular sieve gas separation membranes commercialized due to their prohibitively high cost stemming mainly from difficulty of large scale fabrication.[132] In these

*Modified and reprinted with permission from "Highly propylene-selective mixed-matrix membranes by in-situ MOF formation Using a polymer-modification strategy" by Sunghwan Park, Mohamad Rezi Abdul Hamid, and Hae-Kwon Jeong, *ACS applied materials & interfaces*, 2019, 11 (29), 25949-25957, Copyright 2019 American Chemical Society

regards, mixed-matrix membranes (MMMs) combining the advantages of polymer membranes and inorganic molecular sieve membranes by incorporating inorganic molecular sieve particles within a polymer matrix have been intensively investigated for the past two decades.[60, 61]

There have been many MMMs reported,[61, 133-134] showing improved gas separation performances comparing with those of polymer membranes upon the addition of selective molecular sieves such as zeolites, carbon molecular sieves, and metal-organic frameworks (MOFs), ordered mesoporous materials, layered silicates, covalent organic framework, and etc. Zeolitic-imidazole framework-8 (ZIF-8) is among the most actively investigated molecular sieve filler for MMMs for gas separations, in particular, C_3H_6/C_3H_8 separation[1, 135-140] due to its well-fitted effective aperture size of 4.0–4.2 Å (cf. van der Waals diameters of C_3H_6 and C_3H_8 are 4.03 Å and 4.16 Å, respectively).[141] Koros et al.[1] fabricated MMMs based on 6FDA-DAM polyimide by blending ZIF-8 nanoparticles up to 48 wt% and showed 258 % enhancement in C_3H_6 permeability and 150 % increase in C_3H_6/C_3H_8 ideal selectivity. Later, the same group extended their earlier work and successfully demonstrated the first C_3H_6-selective 6FDA-DAM/ZIF-8 mixed-matrix hollow fiber membranes (MMHFMs) with 30 wt% of ZIF-8 loading,[142] which is a major step towards the large-scale applications of MMMs. It is worthy of mentioning here that the improved C_3H_6/C_3H_8 separation performance of 6FDA-DAM/ZIF-8 MMHFMs was only possible after post treatment of the MMHFMs with polydimethylsiloxane (PDMS) and/or polyaramid. Even though there have been a few reports on ZIF-8 based MMMs in the form of hollow fiber membranes (HFMs) for separations of other gases,[143] to the best of our knowledge, the 6FDA-DAM/ZIF-8 MMHFM by the Koros group[142] is the only MMHFM, despite the presence of additional polymer coatings, that showed improved C_3H_6/C_3H_8 separation. This rarity of scalable MMHFMs attests to significant challenges of conventional MMM processing. Among major challenges are interfacial

void formation between polymer and inorganic particles and particle agglomerations to list a few.[60-61] Though many of these challenges have been addressed in the case of relatively simple planar MMMs, these are daunting challenges when it comes to HFM fabrications due to the complicated variables and conditions of fiber spinning processes.[142 144] These issues are expected to become even more pronounced at higher sieve loadings, limiting the concentration of incorporated filler particles.[142] The sizes of inorganic fillers investigated were normally greater than 100 nm in order to avoid particle agglomerations, rendering it fundamentally challenging to fabricate ultra-thin MMM selective skin layers on hollow fibers (ca. $\leq$ 500 nm).[142] It is, therefore, highly desirable to develop new processing methods for scalable production of defect-free MMMs and eventually asymmetric MMHFMs with sub-micron selective skin layers.

Very recently, our group reported a new strategy to grow ZIF-8 layers on polymer substrates based on a polymer modification strategy, namely polymer-modification-enabled *in-situ* metal-organic framework formation (PMMOF).[145] First, Kapton® polyimide (poly-oxydiphenylene-pyromellitimide) films were hydrolyzed and doped the hydrolyzed films with Zn ions through ion exchange. Upon treating the ion-exchanged polymer substrates in a ligand solution solvothermally, ZIF-8 layers were formed on the modified polymer substrates. Interestingly, a few ZIF-8 agglomerates of ~ 300 nm in size were found inside the polymer substrates. We envisioned that, by controlling diffusion and reaction rates, this polymer-modification method would enable to be applied to form MMM by *in-situ* growth of MOF (ZIF) mostly inside polymers at the entire membrane thick range uniformly. There are several advantages of *in-situ* growing molecular sieve fillers inside polymers for MMMs: 1) potential elimination of interfacial voids, 2) formation of monodispersed fillers, 3) well dispersion of fillers, and 4) potentially higher molecular sieve loadings.[146] More importantly, the *in-situ* MOF formation in polymer enables decoupling of

polymer HFM processing step (i.e., spinning) from MOF incorporation step. It is quite challenging to spin filler-containing polymer dopes into asymmetric MMHFMs with defect-free ultra-thin MMM selective skin layers. By decoupling HFM and MMM formation processes, it is expected possible to facilely transform low-cost off-the-shelf polymer HFMs and their modules to high-value asymmetric MMHFMs and their modules without disturbing current optimized polymer HFM spinning/module formation processes. The first *in-situ* grown UIO-66 containing MMMs by simply dissolving a polymer and MOF precursors all together followed by thermal curing has been reported by Marti et al. [122] This approach is, however, not compatible with current polymer processing technologies and the resulting membranes showed significant particle agglomeration, resulting in the lower gas separation performance than those of conventionally prepared MMMs.[122]

In this work, we report the preparation of high-quality planar MMMs and asymmetric MMHFMs with ultrathin selective skin layers using polymer-modification-enabled *in-situ* metal-organic framework formation (PMMOF). Each polymer modification step upon PMMOF and the resulting MMMs based on *in-situ* growing of ZIF-8 inside polymer were fully characterized. The C_3H_6/C_3H_8 gas separation performances of the MMMs by PMMOF were measured and compared with those of MMMs by conventional physical blending methods. General applicability of the PMMOF concept was demonstrated by preparing MMMs containing ZIF-67 and HKUST-1. Lastly, as a proof-of-concept, we presented fabrication of asymmetric MMHFMs with sub-micron thick selective skin layers by PMMOF. To the best of our knowledge, the asymmetric MMHFMs presented here exhibit the thinnest skin layers among reported MMHFMs.

3.2. Experimental

3.2.1. Materials

Commercial polyimide-based polymer, 6FDA-DAM (4,4-(Hexafluoroisopropylidene) diphthalic anhydride 2,4,6-trimethyl-1,3-phenylenediamine, Mw: 148k, PDI: 2.14) was used. 6FDA-DAM was purchased from Akron Polymer Systems Inc. Polyethersulfone (PES) ultrafiltration hollow fiber membranes were purchased from Spectrum Laboratories. To dissolve polymers, N,N-dimethylformamide (DMF) (C_3H_7NO, > 99.8 %, Alfa Aesar), and N-methyl-2-pyrrolidone (NMP) (C_5H_9NO, ≥ 99 %, Sigma-Aldrich) were used as solvents. For the PMMOF process, sodium formate (HCOONa, ≥ 99 %), zinc nitrate hexahydrate ($Zn(NO_3)_2 \cdot 6H_2O$, 98 %), cobalt(II) nitrate hexahydrate ($Co(NO_3)_2 \cdot 6H_2O$, 98 %), copper(II) nitrate trihydrate ($Cu(NO_3)_2 \cdot 3H_2O$, ≥ 99%), and 2-methylimidazole (Hmim) ($C_4H_6N_2$, 99 %) were obtained from Sigma-Aldrich. As other reagents, 1,3,5-benzene tricarboxylic acid (H_3BTC) ($C_9H_6O_6$, 98 %, Alfa Aesar), methanol (CH_3OH, > 99.8 %, Alfa Aesar), ethanol (C_2H_5OH, 94–96 %, Alfa Aesar), and hexane (C_6H_{14}, ≥ 98.5 %, VWR International) were used. All chemicals were used as-received without further purification.

3.2.2. Preparation of polymer films

Thin polymer films were coated on porous α-alumina supports (diameter of 2.2 cm) by using a drop-casting method with the uniform film thickness of 8.0 ± 1.5 μm. Preparation of α-alumina supports is described elsewhere.[131] In a typical procedure for 6FDA-DAM films, 2 wt% of a polymer dope solution was prepared by dissolving 0.25 g of polymer powder in 12.25 g of DMF by stirring using a magnetic bar until the solution became homogeneous. 2.4 ml of the polymer dope solution was dropped on the polished side of an α-alumina support using a micropipette, fully covering the support surface. Immediately after, the sample was placed in a vacuum oven

pre-heated at 150 ^{o}C and baked at the same temperature for 24 h under vacuum to evaporate DMF. The sample was naturally cooled down to room temperature in the vacuum oven.

3.2.3. Fabrication of mixed-matrix membranes

To hydrolyze a polyimide-based polymer film coated on an α-alumina support, an aqueous sodium formate solution was prepared by dissolving 100 mmol of sodium formate in 30 ml of deionized (DI) water. A supported polyimide film prepared above was vertically placed using a custom-made Teflon holder in a Teflon-lined autoclave containing the sodium formate solution. The autoclave was then heated at 120 ^{o}C for 5 h. After cooling down the autoclave at room temperature for 2 h, the hydrolyzed polymer film (i.e., PAA(polyamic acid)-Na salt film) was removed and rinsed in 80 ml of DI water overnight in a lab shaker to completely remove physically absorbed Na ions and formate ions. Na ions in the hydrolyzed polymer were then exchanged with Zn ions (Cu ions for HKUST-1 or Co ions for ZIF-67) by vertically immersing the film into a metal ion solution. The metal ion solution was prepared by dissolving 16 mmol of zinc nitrate hexahydrate (copper(II) nitrate trihydrate for HKUST-1 or cobalt(II) nitrate hexahydrate for ZIF-67) in 40 ml of water at room temperature for an hour. After the ion-exchange step, the zinc containing sample (i.e., PAA-Zn salt film) was quickly rinsed in 80 ml of methanol for 10 sec and then positioned vertically in a Teflon-lined autoclave containing an organic ligand solution. The ligand solution was prepared by dissolving 28.4 mmol of 2-methylimidazole (9.47 mmol of 1,3,5-benzene tricarboxylic acid for HKUST-1) in 30 ml of methanol. The zinc containing film was then treated in the ligand solution at 40 ^{o}C for 2 h, followed by 2 h of cooling to room temperature. The resulting ZIF-8 containing film was washed in fresh methanol overnight. To minimize surface tension during solvent evaporation,[147] the

sample was subjected to solvent exchange in methanol and in hexane for 30 min each. The sample was then dried at room temperature for 1 h and then at 60 ^{o}C for over 2 h. Lastly, the sample was thermally imidized at 250 ^{o}C for 4 h in a convection oven.

3.2.4. Polymer coating on hollow fibers

6FDA-DAM coating on PES hollow fibers was performed by dip-coating method at a glove bag saturated with ethyl acetate. The polymer dope solution was prepared by ethyl acetate solvent with the polymer concentration of 4 wt%. After immersing PES hollow fibers in the prepared polymer dope solution, immediately, the hollow fibers dipped in the polymer solution were taken out and dried in the glove bag vertically for 7 h. The resulting 6FDA-DAM coated PEH hollow fibers were further dried at 60 ^{o}C overnight under convection.

3.2.5. Polymer swelling experiments

A polymer swelling experiment was conducted by soaking a free-standing polymer in water for 1 h and in methanol for 2 h at room temperature. Weight of the swollen polymer was measured after carefully blotting the surface using Kimwipes.

3.2.6. Plasma etching experiments

A plasma etching of MMMs were performed by PDC-32G (Harrick Plasma) under vacuum for 10 min intervals. The air flow rate was adjusted to the maximum intensity of plasma.

3.2.7. Characterizations

Scanning electron microscope (SEM) images were collected using a JEOL JSM-7500F at acceleration voltage of 5 keV and working distance of 15 mm after freeze fracturing samples in liquid nitrogen. Transmission electron microscope (TEM) was conducted by JEOL JEM-2010 TEM at an operation voltage of 200 keV. Thin TEM specimens were prepared by microtoming epoxy-sealed membrane samples. X-ray photoelectron spectroscopy (XPS) was performed by an Omicron ESCA+ with Mg X-ray source at 300W. Crystallinities and phases of samples were determined by X-ray diffraction (XRD) patterns using a Miniflex II (Rigaku) with Cu-Kα radiation (λ = 1.5406 Å) in the 2 θ range of 5 – 40 º. Attenuated total reflectance Fourier transform infrared (ATR-FTIR) spectra were collected by Nicolet iS5 spectrophotometer equipped with iD7 ATR (Thermo Scientific) at a resolution of 2 cm^{-1} with 16 scans in the span of 4000 – 400 cm^{-1}. Thermogravimetric analysis (TGA) using a Q50 (TA instruments) was conducted from 25 ºC to 800 ºC at the heating rate of 10 ºC min^{-1} under air flow of 60 cm^3 min^{-1}. Before conducting TGA, each sample was dried at 100 ºC for 12 h under vacuum to remove any absorbed water.

3.2.8. Gas permeation measurements

Gas permeation properties of pristine polyimide membranes as well as MMMs were measured using the Wicke-Kallenbach technique at room temperature under atmospheric pressure. A feed gas mixture was provided at 20 cm^3 min^{-1} while the permeate side was swept using argon at 20 cm^3 min^{-1}. Steady-states were declared after 12 h of operation when difference in the measured propylene permeance of a sample was less than 1 % in an hour interval.

Composition of the permeated gases was determined by gas chromatography (GC 7890A, Agilent) equipped with a flame ionized detector (FID) and a HP-plot Q column.

3.3. Results and discussion

3.3.1. Polymer modification enabled *in-situ* metal-organic framework formation (PMMOF)

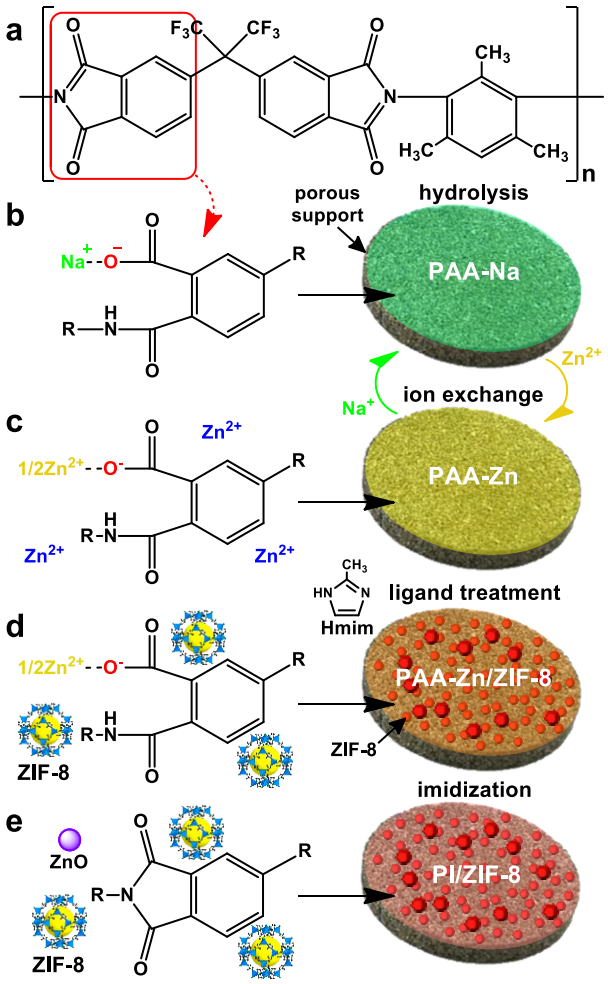

Figure 3.1. Schematic of PMMOF using 6FDA-DAM. (a) pristine PI, (b) PAA-Na, (c) PAA-Zn, (d) PAA-Zn/ZIF-8, and (e) PI/ZIF-8.

The key concept of PMMOF is to enlarge and modify polymer free volumes where MOF precursors can be accommodated, thereby providing ideal environments inside polymer for *in-situ* growth of MOFs. As illustrated in Figure 3. 1, the first step of the process is hydrolysis of a polyimide by cleaving heterocyclic imide rings in a base solution (i.e., deimidization). This deimidization step turns a polyimide (PI) into a poly(amic acid) sodium salt (PAA-Na) (Figure 3. 1b). The subsequent step is exchange of Na ions with Zn ions, forming poly(amic acid) zinc salt (PAA-Zn) (Figure 3. 1c). Solvothermal treatment of the PAA-Zn in an organic ligand, 2-methylimidazole, solution leads to *in-situ* formation of ZIF-8 in the PAA-Zn (PAA-Zn/ZIF-8) (Figure 3. 1d). Finally, the PAA-Zn containing ZIF-8 is thermally imidized, resulting in a PI/ZIF-8 composite film (Figure 3. 1e).

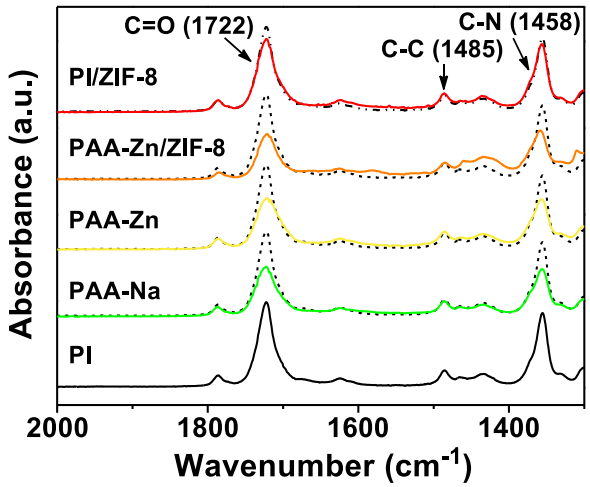

Figure 3.2. ATR-IR spectra of samples at each PMMOF step. The overlapped dotted lines are the ATR-IR spectra of 6FDA-DAM for the comparison.

The hydrolysis step, where a polyimide (PI) is partially transformed to a poly(amic acid) (PAA), is essential to the success of PMMOF. To show the importance of the hydrolysis, two different PIs, Matrimid and 6FDA-DAM, were tested with and without hydrolysis. Without hydrolysis, no ZIF-8 were formed in the Matrimid while there were very little ZIF-8 appeared in the 6FDA-DAM. In a stark contrast, substantial amounts of ZIF-8 were found in the hydrolyzed PIs, indicating the critical role of the hydrolysis. It is surmised that when imide rings are open by the hydrolysis, polymer backbone chains become more flexible,[148] thereby enlarging polymer free volumes[149] as well as making polymer hydrophilic.[150] Consequently, Zn ions can easily diffuse inside, eventually leading to formation of ZIF-8 inside polymer. It is clear that under the same hydrolysis condition, 6FDA-DAM is more amenable to form ZIF-8 than Matrimid likely due to the fact that it has inherently larger free volume. Furthermore, 6FDA-DAM is known for its excellent gas separation performance and in particular for its C_3H_6/C_3H_8 separation property match with ZIF-8 in MMMs.[151] Based on these, 6FDA-DAM was chosen as a model polyimide.

It was found possible to control the degree of deimidization of 6FDA-DAM by simply changing the hydrolysis time in sodium formate at a fixed temperature of 120 ºC. Upon hydrolysis, as presented in Figure 3. 2, it was observed slight shifts in the ATR-IR peaks at 1356-1361 cm^{-1} and 1720-1724 cm^{-1} assigned to the C-N stretching and the symmetric C=O stretching in the imide rings, respectively. Also, the relative intensities of those peaks decreased comparing with that of the C-C stretching in the aromatic rings at a wavenumber of 1485 cm^{-1} (Figure 3. 2). To quantify imidization, the degree of imidization (DI) was commonly used as an indicator and calculated as below:[152-154]

$$\text{DI}\ (\%) = \frac{(A_{1358}/A_{1485})_{specimen}}{(A_{1358}/A_{1485})_{standard}} \times 100 \qquad (2.1)$$

where *A* is the intensity of IR absorbance and the subscripts are the wavenumbers of the assigned IR peaks. A pristine 6FDA-DAM film was used as a standard, assuming 100% imidization. Conversely, the degree of deimidiziation (DD) was calculated by using the following equation:

$$\text{DD}\ (\%) = \left[1 - \frac{(A_{1358}/A_{1485})_{specimen}}{(A_{1358}/A_{1485})_{standard}}\right] \times 100 \qquad (2.2)$$

The DD was linearly augmented with an increase in the hydrolysis time. As the DD increased, PAA-Na formation was promoted, consequently increasing the uptake of Zn ions, thereby enhancing formation of ZIF-8. However, too high DD can damage and eventually disintegrated polymer films. It was found that when the DD was greater than ~ 50 %, there formed undesirable micro-voids which are detrimental to gas separations (Figure 3. 3). For these reasons, an optimized hydrolysis time was set to 5 h with the DD of 35.3 ± 4.6 %.

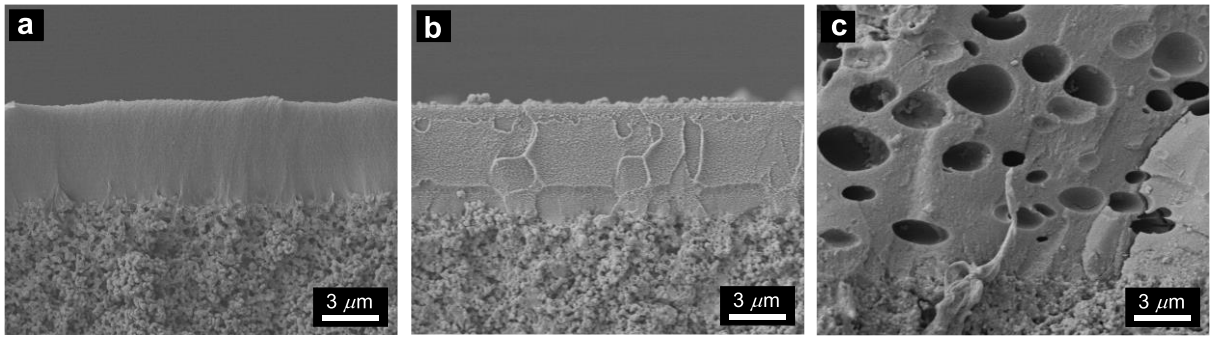

Figure 3.3. Cross-sectional SEM images of (a) PI, (b) PI/ZIF-8 hydrolyzed for 5 h, and (c) PI/ZIF-8 with hydrolyzed for 8 h.

Table 3.1. At% of elements for PAA-Na and PAA-Zn samples measured by XPS.

Unit: at %	Carbon	Oxygen	Nitrogen	Fluorine	Sodium	Zinc
PAA-Na	71.20	18.36	3.98	5.84	0.62	0.00
Unwashed PAA-Zn	71.97	19.84	3.83	3.10	0.00	1.27
Washed PAA-Zn	75.54	17.17	2.99	3.13	0.00	0.29

Upon ion exchange, ionically coordinated monovalent Na ions in PAA-Na are replaced with divalent Zn ions forming PAA-Zn. To confirm complete exchange of the Na ion coordinated to the polymer, an elemental analysis using XPS was performed. The amounts of Na in the PAA-Na and Zn in the PAA-Zn were estimated ~ 0.62 at% and ~ 1.27 at%, respectively (Table 3.1). The ratio of Na to Zn was ~ 0.5:1, which is much lower than the expected stoichiometric ratio of Na to Zn of 2:1, indicating the presence of excess Zn ions in the PAA-Zn. To verify the presence of excess Zn ions, the narrow scan of the XPS spectra of Zn $2p_{3/2}$ in an as-prepared PAA-Zn was compared to that of the PAA-Zn extensively washed in methanol. Excess Zn ions that are not coordinated are expected to be removed by extensive washing. The Zn $2p_{3/2}$ peak of the as-prepared PAA-Zn was deconvoluted into three peaks at 1023.0 eV, 1022.1 eV, and 1021.3 eV, which were assigned to Zn ion coordinated to water (Zn-water), Zn ion coordinated to polymer (Zn-polymer), and free Zn ion (Zn^{2+}), respectively (Figure 3. 4a).[155-156] In contrast, the deconvoluted Zn $2p_{3/2}$ peaks of the extensively washed sample showed only two peaks, Zn-polymer and Zn^{2+}, indicating that Zn-water ions were completely washed out by methanol (Figure 3. 4b). In addition, the intensity of the Zn^{2+} comparing with that of the Zn-polymer substantially decreased upon washing, confirming that the excessive Zn ions were present in the forms of free ions as well as ions coordinated with water. The atomic percentage of Zn in the PAA-Zn after washing displayed a noticeably lower value of 0.29 at% compared to that of the unwashed PAA-Zn (1.27 at%). For the PAA-Zn sample with excessive Zn ions removed, the Na-to-Zn ratio was close to the stoichiometric ratio of 2:1, confirming that coordinated Na ions were replaced by Zn ions upon the ion-exchange.

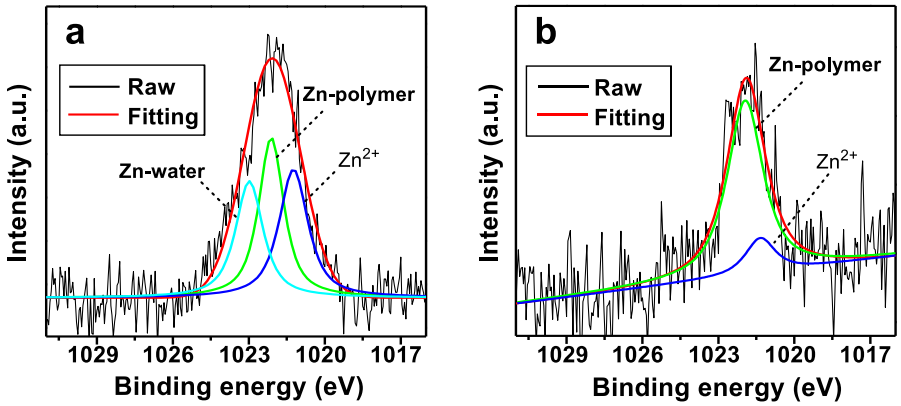

Figure 3.4. Zn $2p_{3/2}$ XPS spectra and curve fits of PAA-Zn: unwashed PAA-Zn (b) and washed PAA-Zn (c).

We attempted to find out which one(s) of the three zinc sources (i.e., Zn-water, Zn-polymer, and free Zn^{2+}) was responsible for the *in-situ* formation of ZIF-8 inside polymer. If Zn-polymer are a primary zinc source for ZIF-8 formation, even after extensive washing right after ion exchange, the sample is expected to contain ZIF-8 crystals once PMMOF is completed. As seen in Figure 3. 5, however, the washed PI/ZIF-8 sample (i.e., washed after ion exchange) only showed broad amorphous polymer peaks while the unwashed PI/ZIF-8 presented ZIF-8 peaks. This result strongly suggests that Zn ions that were not coordinated with polymer were responsible for ZIF-8 formation. This is ascribed to the fact that Zn-polymer is not as mobile due to their strong electrostatic interactions with the carboxylate anions in polymer via multiple bonds (i.e., one Zn ion interacts with two car boxylate anions). These multiple coordinations might create crosslinking-like states in PAA.[157-159]

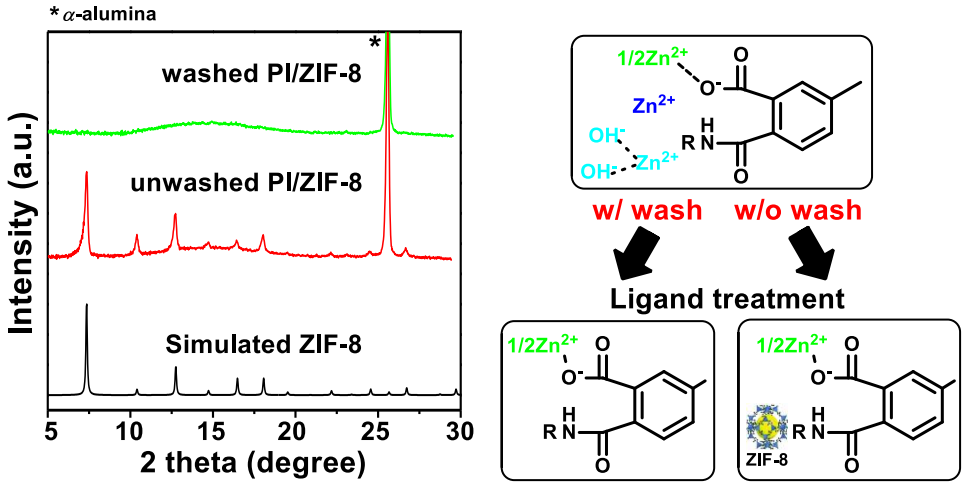

Figure 3.5. XRD patterns of PI/ZIF-8 washed and unwashed after ion exchange.

As seen in Figures 2.6a and b, the cross-sectional SEM images of PI/ZIF-8 revealed densely packed ~ 100 nm sized fillers that were uniformly dispersed without interfacial voids inside polymer and large clusters bonded on the top surface. Despite the formation of ZIF-8 upon the ligand (i.e., Hmim) treatment confirmed by XRD diffraction patterns, it should be clarified that those fillers inside polymer were ZIF-8 by demonstrating the location of the diffraction patterns coming from ZIF-8. First, the absence of ZIF-8 in the α-alumina support was verified by dissolving the polymer from the PI/ZIF-8 in 80 ^{o}C NMP for one day and confirming a negligible amount of ZIF-8 in the support. The surface-bound clusters were easily removed by gently wiping the surface with a diluted acid solution (i.e., 0.1 M HNO_3), since the clusters were ZIF-8, which is very sensitive to acid.[160] As exhibited in Figure 3. 6c, even though the ZIF-8 on the surface were entirely eliminated by the surface acid treatment, the characteristic peaks of ZIF-8 were almost maintained (Figure 3. 6c). This confirms that most of ZIF-8 were grown inside polymer as fillers during the ligand treatment, thereby forming high quality MMMs.

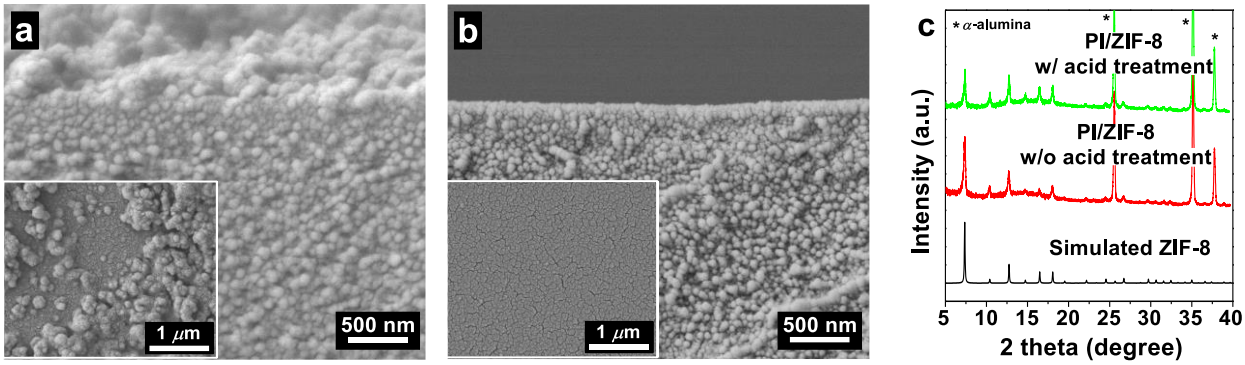

Figure 3.6. (a-b) SEM images of cross-section view and top view (inserted at left bottom) of PI/ZIF-8 (a) and surface treated PI/ZIF-8 by acid (b). (c) XRD patterns of PI/ZIF-8 w/ and w/o surface acid treatment.

For MMMs containing ZIF-8 to perform stably and to recover an original gas separation performance of PI, the deimidized PI (i.e., PAA) needs to be imidized. Nevertheless, the very stable coordination bond between zinc cations and carboxylate anions is expected to hamper complete imidization.[161] Previous studies[154, 161] showed that Zn ions coordinated polymer (PAA-Zn), in particular, exhibited a lower DI (Equation 1) than PAA as well as PAAs coordinated with other metal ions. Kim et al.[154] found that a relatively high imidization temperature (≥ 250 °C) was required in order to disengage coordinated Zn ions from chelate complexes and to form imide groups. As shown in the TGA weight loss and its derivative curve in Figure 3. 7, the imidization started from ~ 150 °C with the maximum rate at ~ 250 °C. The DI was attained at 88.0 ± 5.0 % by conducting the thermal imidization at 250 °C for 4 h (Figure 3. 2). While detached Zn ions during the imidization were possibly transformed into ZnO, it was not observed in this study likely due to the very small amount.[162] In addition, the (110) peak intensity of the PAA-Zn/ZIF-8 gradually decreased over several weeks as shown in Figure 3. 8a. The acidic components of PAA presumably

degraded ZIF-8 since ZIF-8 is known unstable in an acid condition.[160] The acidic components of PAA were generated probably by some carboxylic acid groups formed during PMMOF. This observation is consistent with the previous study of a ZIF-8 containing MMM with a benzoic acid containing polymer (i.e., 6FDA-DAM/DABA).[163] Upon imidization, however, the (110) peak intensity of the PI/ZIF-8 remained unchanged during the same time span (Figure 3. 8b), strongly indicating importance of post-imidization in stabilizing the membranes.

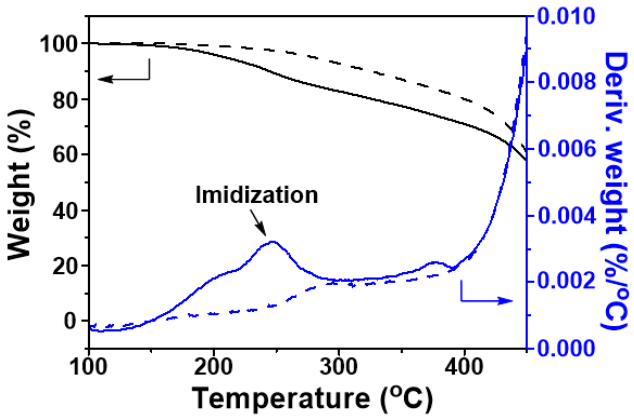

Figure 3.7. TGA curves and the corresponding derivative curves. Solid lines indicate before imidization (PAA-Zn/ZIF-8) and dashed lines are after imidization (PI/ZIF-8).

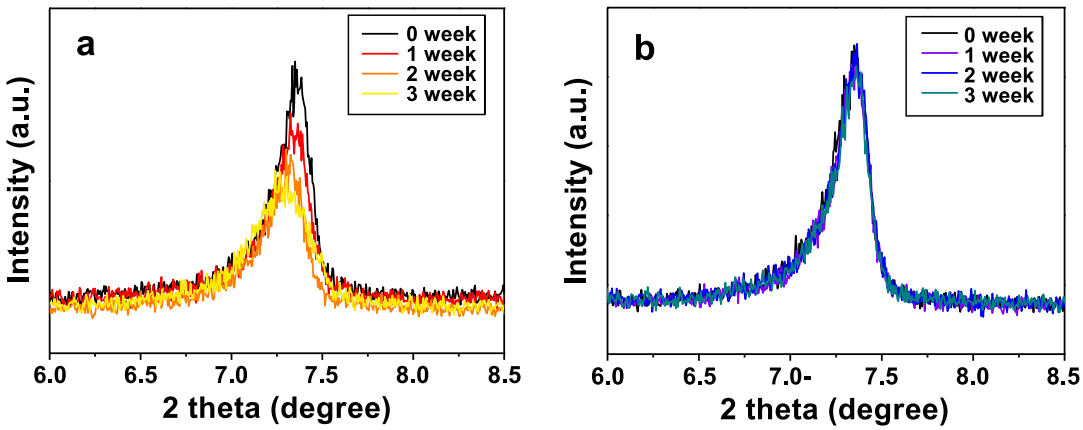

Figure 3.8. Time-dependent evolution of the (110) XRD peak. (a) PAA-Zn/ZIF-8 (before imidization) and (b) PI/ZIF-8 (after imidization).

3.3.2. Structure control and characterization of MMMs by PMMOF

The distribution of *in-situ* formed ZIF-8 fillers is influenced by the diffusion of organic linkers (i.e., Hmim) into a polymer matrix. The diffusion of Hmim through polymer can be controlled by the type of solvents: size of solvents and affinity of solvents with polymer. To characterize the distribution of ZIF-8, an oxygen plasma etching was conducted. The XRD peaks of two PI/ZIF-8 samples, one Hmim-treated in methanol (named PI/ZIF-8_MeOH) and the other in ethanol (named PI/ZIF-8_EtOH), were taken as a function of oxygen plasma etching time. Figure 3. 9 presents the relative (110) peak intensities of the samples normalized by those of the as-prepared samples. The linear decrease of the (110) peak intensity likely indicates the uniform distribution of ZIF-8 fillers in polymer. For the PI/ZIF-8_MeOH, there observed a quite linear decline of the relative (110) peak intensity (Figure 3. 9). On the other hand, in the case of the PI/ZIF-8_EtOH, the relative (110) intensity was sharply dropped for 20 min of initial oxygen plasma etching. The precipitous decrease of the (110) intensity of the PI/ZIF-8_EtOH was possibly due to the relatively high concentration of ZIF-8 near the surface of the sample. It should be mentioned that both samples showed comparable changes in their (110) peak intensities after the removal of surface bonded ZIF-8 by the acid treatment, indicating that the sharp decrease upon the etching is not owing to the decomposition of surface grown ZIF-8. Since ethanol is bulkier and less polar compared to methanol, the diffusion of Hmim in ethanol inside polymer is restrained as compared with that in methanol, thereby forming more ZIF-8 near the surface.

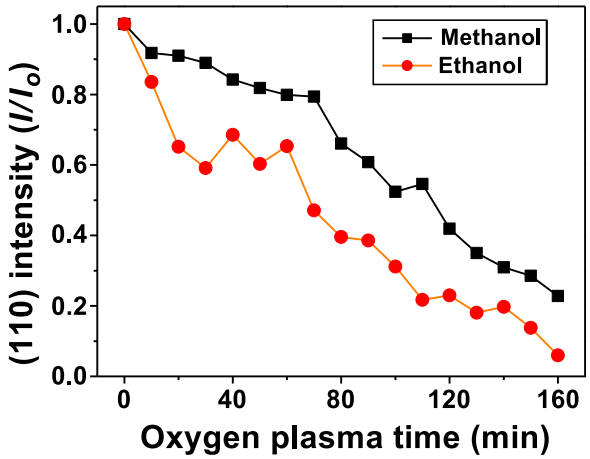

Figure 3.9. Normalized crystal peak intensity of the (110) plane of PI/ZIF-8 films treated in methanol and ethanol-based linker solutions as a function of oxygen plasma etching time.

The shape and size of ZIF-8 fillers within a polymer was confirmed by the TEM images of PI/ZIF-8 samples. As shown in Figure 3b, the morphology of the *in-situ* grown individual ZIF-8 crystals was an anisotropic rod-like structure with a high aspect ratio. Those individual ZIF-8 nanoparticles were agglomerated, forming ZIF-8 clusters ~ 100 nm in size (Figure 3. 10). This size was consistent with the observation by SEM (Figure 3. 6a) and significantly smaller than that of ZIF-8 formed on the surface. It is noteworthy that rod-shaped ZIF-8 have been reported in few previous work.[135] Interestingly, the (110) peak intensity of XRD patterns was notably decreased relative to the (112) peak intensity after removing the surface grown ZIF-8 (Figure 3. 6c). To quantify, crystallographic preferred orientation (CPO) was determined by taking the ratio of the (112)/(110) of the samples normalized by that of a randomly oriented sample.[164] The estimated CPO(112)/(110) of the PI/ZIF-8 after removing surface grown ZIF-8 (~ 2.85) was 1.65 times greater than that of the PI/ZIF-8 with the surface grown ZIF-8 (~ 1.73). There were similar observations that an anisotropic shaped ZIF-8 showed a relatively high CPO(112)/(110).[135] The

previous study by Yang et al.[135] showed the shape of ZIF-8 was controllable by using a shape-inducing agent, cetyltrimethylammonium bromide (CTAB), which adsorbed preferentially onto certain surface facets of ZIF-8, thereby decreasing the crystal growth of those facets. Anisotropic nano-rod- and interpenetrated twin-shaped ZIF-8 crystals showed relatively low (110) peak intensity, resulting in the higher CPO(112)/(110) than that of other shapes,[135] consistent with our observation. The differences in the shape and size of ZIF-8 crystals formed inside polymer and at the interface are probably because the growth of ZIF-8 inside polymer occurs in confined spaces while the interfacial growth of ZIF-8 happens in unconfined spaces.

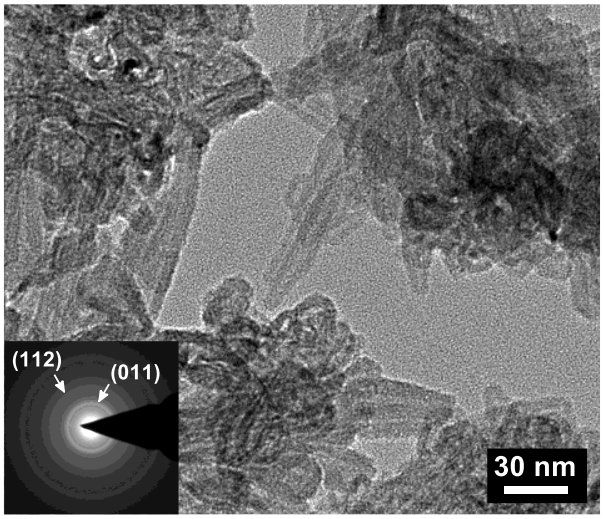

Figure 3.10. TEM image of *in-situ* grown ZIF-8 fillers in PI/ZIF-8 and its selected-area electron diffraction (SAED) pattern in left bottom.

The concentration of *in-situ* grown ZIF-8 in a polymer was controlled by varying the concentration of zinc in an ion exchange solution since the excess Zn ions are the main source for ZIF-8 fillers forming in a polymer as mentioned earlier. It is noted that the concentration of Zn-

polymer is expected independent of the concentration of a zinc solution, rather depending on the DD. The zinc content in the solution was varied at 8, 16, 24, 32, and 40 mmol in 40 ml water and the zinc concentration was denoted as Zn(mmol). As the zinc concentration increased, TGA analysis presented in Figure 3. 11 showed an increase in ZnO residues upon thermal oxidization, indicating that the concentration of ZIF-8 increased.

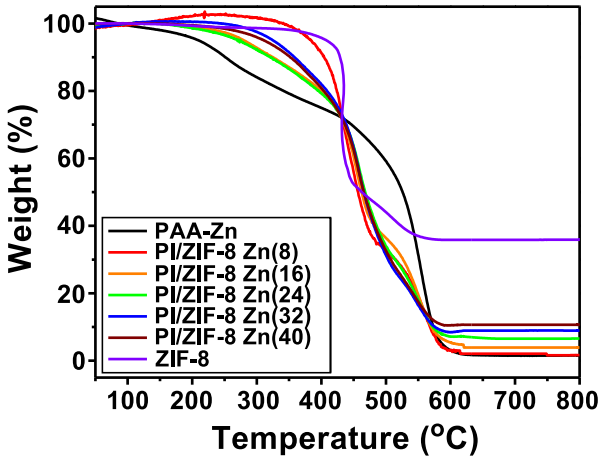

Figure 3.11. TGA thermogram of PAA-Zn, ZIF-8, and PI/ZIF-8 with different zinc concentrations.

The amount of ZIF-8 *in-situ* grown in a polymer was determined using TGA measurement by thermally oxidizing PI/ZIF-8 samples under air flow (Table 3.2). The resulting residues are assumed to ZnO since organic components including polymer and linkers of ZIF-8 are almost completely decomposed at the final temperature of 800 °C.[1, 165-166]. There are two possible sources generating ZnO upon the thermal oxidization: ZnO (I) from ZIF-8 and ZnO (II) resulting from the oxidization of remaining free and coordinated Zn ions. Also, ZnO (III) formed by the Zn ions detached from polymer coordination bonds during the imidization can already exist in a polymer. To clarify the quantity of ZnO (I), the amount of residue of PI/ZIF-8 was subtracted from that of

washed PAA-Zn consist of ZnO (II). Moreover, it should be mentioned that the ZIF-8 on the polymer surface, which does not give influence upon gas transport, was removed by the surface acid treatment. The quantity of ZIF-8 inside polymer, hence, was calculated by dividing the amount of ZnO (I) by that of pure ZIF-8, as follow:

$$ZIF\text{-}8\ wt\%\ in\ PI/ZIF\text{-}8 = \frac{W_{ZnO\ from\ PI/ZIF\text{-}8} - W_{ZnO\ from\ PAA\text{-}Zn}}{W_{ZnO\ from\ pure\ ZIF\text{-}8}} \times 100(\%) \quad (2.3)$$

where W is a residual weight percentage of thermal decomposition. High ZIF-8 content in a polymer matrix can be obtained due to the expanded volume of polymer upon the hydrolysis, consequently increasing the uptake of metal and ligand sources during PMMOF. The bulk volume of PAA-Zn increased 7.7 ± 2.0 % and 14.3 ± 1.9 % when swollen in water and in methanol, respectively.

Table 3.2. Weight and volume percentages of ZIF-8 in PMMOFed MMMs.

Sample	Weight percentage (wt %)	Volume percentage (vol%)
PAA-Zn(8)	4.2	5.9
PAA-Zn(16)	9.2	12.8
PAA-Zn(24)	15.9	21.4
PAA-Zn(32)	20.3	26.8
PAA-Zn(40)	25.5	32.9

3.3.3. C_3H_6/C_3H_8 separation performance of MMMs by PMMOF

The C_3H_6/C_3H_8 separation performances of the PI/ZIF-8 MMMs prepared by PMMOF (PMMOFed MMMs) were investigated and compared with conventional MMM counterparts prepared by blending ZIF-8 fillers with polymer. The conventional MMMs exhibited an increase in C_3H_6/C_3H_8 separation factor as well as C_3H_6 permeability as the ZIF-8 loading in polymer

increased (Figure 3. 12a and Table 3.3).[1] The PMMOFed MMMs, surprisingly, showed a slight decrease in the C_3H_6 permeability with a more dramatic increase in the C_3H_6/C_3H_8 separation factor of up to 38.0 ± 7.1 (Figure 3. 12a and Table 3.3). The C_3H_6 permeability remained unchanged at the ZIF-8 loading increasing up to ~13 vol% and then decreased as the ZIF-8 loading further increased. The decreasing permeability as increasing ZIF-8 loading is ascribed possibly to the decrease in the permeability of the continuous polymer phase with increasing ZIF-8 loading. This is likely due to a decrease in the polymer free volume (i.e., densification), leading to a decrease in the permeability of the PMMOFed MMMs with increasing ZIF-8 loading. It is not unreasonable to assume that the *in-situ* growth of ZIF-8 in the polymer free volume enlarged by hydrolysis and swelling might decrease the polymer free volume (Figure 3. 12b).

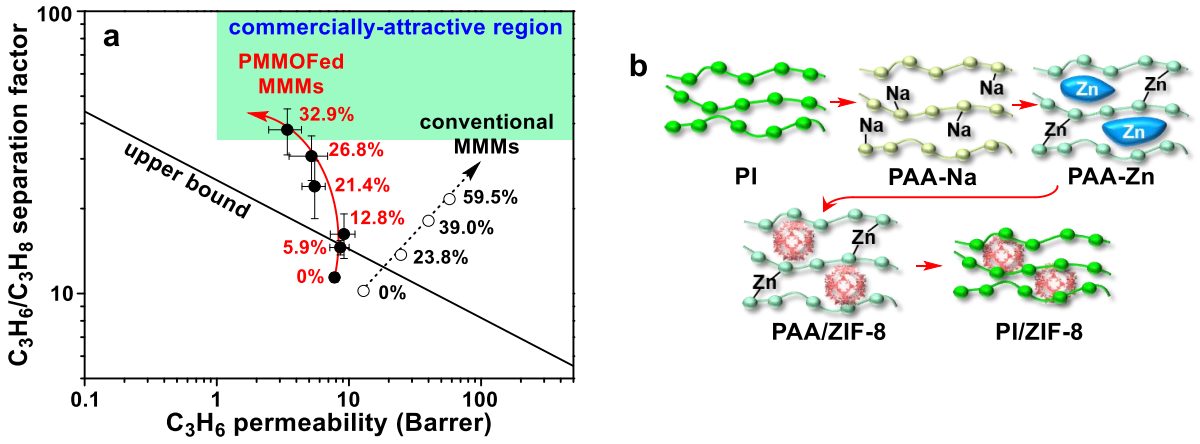

Figure 3.12. (a) Gas transport results of 6FDA-DAM and PMMOFed MMMs for C_3H_6/C_3H_8 separation. C_3H_6 permeability versus C_3H_6/C_3H_8 separation factor plot with the C_3H_6/C_3H_8 upper bond curve.[129] The closed circles are the experimental data of PMMOFed MMMs and the open circles are the literature data of conventional filler blending based MMMs.[1] The arrows direct the

increase of ZIF-8 concentration and the annotated percentage is the volume percentage of ZIF-8 in MMMs. (b) Illustration of ZIF-8 formation in a free volume by steps.

Table 3.3. Summary of C_3H_6/C_3H_8 separation results of PMMOFed MMMs and the 6FDA-DAM polymer membrane.

	C_3H_6 permeability (Barrer)	C_3H_6/C_3H_8 separation factor
PI	7.79 ± 0.24	11.40 ± 0.44
PI/ZIF-8 Zn(8)	8.60 ± 1.44	14.55 ± 0.85
PI/ZIF-8 Zn(16)	9.17 ± 1.95	16.22 ± 2.91
PI/ZIF-8 Zn(24)	5.51 ± 1.10	23.95 ± 5.54
PI/ZIF-8 Zn(32)	5.21 ± 1.69	30.67 ± 5.52
PI/ZIF-8 Zn(40)	3.42 ± 0.95	38.04 ± 7.07

To qualitatively estimate the densification effect of the polymer, the C_3H_6 and C_3H_8 permeabilities of the polymer in the corresponding PMMOFed MMMs were evaluated using Maxwell equation.[167] While both of the C_3H_6 permeability and the C_3H_6/C_3H_8 separation factor of ideal MMMs were continuously enhanced with increasing ZIF-8 loading as observed in conventional MMMs, the predicted C_3H_6/C_3H_8 separation of polymer phases showed a decreasing trend in the C_3H_6 permeability and an increasing trend in the C_3H_6/C_3H_8 separation factor, following the polymeric upper bound (Figure 3. 13). The estimated C_3H_6/C_3H_8 separation performance of the polymer slightly outperforms the upper bound likely due to the uncertainty of Maxwell model at high ZIF-8 loadings: Maxwell model is valid at loadings less than 20 vol%.[60, 167]

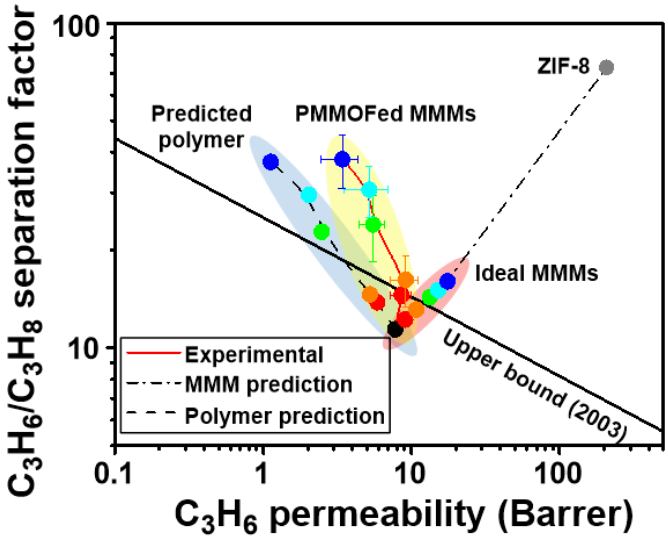

Figure 3.13. C_3H_6/C_3H_8 separation performance of PMMOFed MMMs, ideal MMMs, and predicted polymers based on PMMOFed MMMs with the upper bound curve.[129] The same color represents the same zinc concentration; red for Zn(8), orange for Zn(16), green for Zn(24), cyan for Zn(32), blue for Zn(40).

The PMMOFed PI/ZIF-8 MMMs represented much higher C_3H_6/C_3H_8 separation factor than that of the conventionally prepared PI/ZIF-8 MMMs even at the lower ZIF-8 concentration (Figure 3. 12a). These higher C_3H_6/C_3H_8 separation factor and moderate C_3H_6 permeability marginally satisfied the commercially-attractive region in the Robeson plot at the ZIF-8 concentration of 32.9 vol%.[129, 168] Furthermore, to the best of our knowledge, the PMMOFed MMMs show the highest C_3H_6/C_3H_8 mixed-gas separation factor among the reported polymer-based MMMs. Despite the compromise in the permeability, the exceptionally high separation factor of the PMMOFed MMMs as compared to conventional MMMs is likely due to not only better adhesion and enhanced distribution of ZIF-8 in a polymer matrix but also densification of polymer matrix induced by the *in-situ* growth of ZIF-8 fillers in polymer free volume.

3.3.4. General applicability of PMMOF

General applicability of PMMOF was tested using other MOFs including ZIF-67 and HKUST-1. As shown in Figure 3. 14, depending on the type of MOFs, the colors of the MMMs by PMMOF were varied; white for PI/ZIF-8, violet for PI/ZIF-67, and turquoise for PI/HKUST-1 MMMs. The crystal phases of the *in-situ* grown MOFs inside polymers well-matched with the corresponding simulated patterns, supporting the general applicability of PMMOF (Figure 3. 14). PMMOF is, therefore, expected to enable facile formation of a myriad number of MOF/polymer composite films/membranes by combining various MOFs and polyimide-based-polymers. This makes a stark contrast in that conventionally prepared MOF/polymer composite films have been limited to certain MOFs and polymer combinations often due to the poor compatibility between certain polymers and MOFs.[169] Not only are MOF-polymer composite films prepared by PMMOF very useful for separation applications, but also polymer composites with a various kind of MOFs with different functionalities can also be applied in the diverse areas such as gas/liquid adsorption,[170] capacitive sensors,[171] and proton exchange membranes for fuel cell.[172]

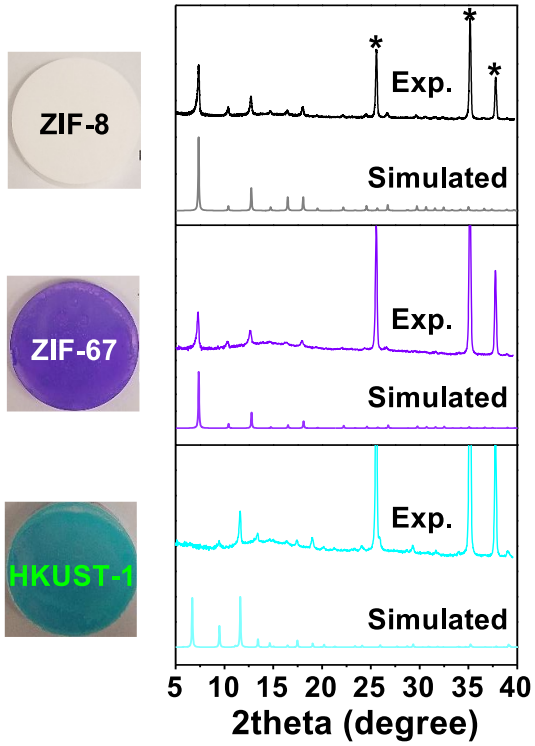

Figure 3.14. Photographs of PMMOFed MMMs ZIF-8, ZIF-67, and HKUST-1. The corresponding XRD patterns.

3.3.5. Scalability of MMMs by PMMOF

Finally, even though this work mainly focused on flat membranes supported on porous α-alumina disks, as a proof-of-concept, we attempted to demonstrate the scalability of MMMs by PMMOF using off-the-shelf porous PES (polyethersulfone) ultrafiltration HFMs coated with submicron thick 6FDA-DAM skin layers (Figure 3. 15). The 6FDA-DAM HFMs with ~ 750 nm thick skin layers were then transformed into 6FDA-DAM/ZIF-8 MMHFMs with the same thickness (Figure 3. 15). It is noted that this finding is of great significance for large-scale applications of MMMs since one can transform low-cost ultrafiltration HFMs and their modules

into high-value gas separation HFMs and their modules. The C_3H_6/C_3H_8 separation performances of the MMHFMs were encouraging with C_3H_6 permeance of 2.17 GPU and C_3H_6/C_3H_8 separation factor of ~ 20, which is triple as high as that of 6FDA-DAM-coated HFM. To the best of our knowledge, the MMHFMs by PMMOF exhibit one of the highest C_3H_6/C_3H_8 separation performances among MMHFMs without additional defect plugging steps.

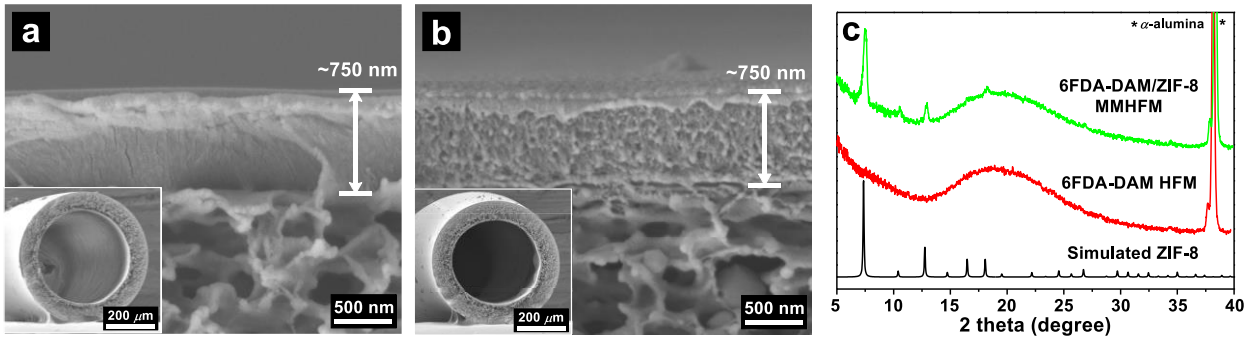

Figure 3.15. SEM images of (a) 6FDA-DAM HFM and (b) 6FDA-DAM/ZIF-8 MMHFM formed by PMMOF and (c) corresponding XRD diffraction patterns.

3.4. Conclusion

In summary, we demonstrated *in-situ* formation of ZIF-8 fillers inside polymers by a new potentially scalable MMM fabrication process, namely PMMOF. The first step of PMMOF, hydrolysis of 6FDA-DAM polyimide, enlarged the polymer free volume, making spaces to grow ZIF-8. The ZIF-8 were grown mostly inside polymer by physically absorbed excessive Zn ion sources. Moreover, the *in-situ* grown ZIF-8 clusters made of rod-like shaped individual nanocrystals ~100 nm in size were uniformly dispersed inside the polymers. By varying the zinc concentration in an exchange solution, the ZIF-8 concentration increased up to 32.9 vol%. The resulting 6FDA-DAM/ZIF-8 MMMs showed much higher C_3H_6/C_3H_8 separation factor than the

conventionally prepared 6FDA-DAM/ZIF-8 MMMs. This significant enhancement is attributed to the better adhesion, the better dispersion, and the densification of polymer. Therefore, the 6FDA-DAM/ZIF-8 MMMs enabled not only to potentially overcome the current challenging processing issues of MMM formation but also to exhibit superior C_3H_6/C_3H_8 separation performances. PMMOF was found potentially general, applicable to other MOFs. Finally, we successfully demonstrated scalability of PMMOF by transforming low-cost off-the-shelf ultrafiltration HFMs into asymmetric MMHFMs with ultrathin selective skin layers, the thinnest among reported. PMMOF reported here is expected to bring MMMs close to their commercial applications by lowering the cost of MMMs and their modules due to its decoupling of MMM formation from fiber spinning process.

CHAPTER IV

POLYIMIDE/ZIF-7 MIXED-MATRIX MEMBRANES: UNDERSTANDING IN-SITU CONFINED FORMATION OF ZIF-7 PHASES INSIDE POLYMER AND THEIR EFFECTS ON GAS SEPARATIONS

4.1. Introduction

Metal-organic frameworks (MOFs) consist of metal nodes ligated by organic bridging ligands with unique features of uniform pore structures, large surface areas, chemical and thermal stability, and tunable properties.[173-174] Due to these unique features, MOFs have attracted extensive attention for diverse applications including drug delivery, optics, catalysis, gas separation, and etc.[175-178] In particular, the well-defined molecular scale pores and the tunable properties of MOFs make them an ideal membrane material for gas separations.[179] Of particular interest is their potential as functional fillers in mixed-matrix membranes (MMMs), which could overcome limitations of polymeric membranes by taking advantages of both polymers and molecular sieving fillers.[61] Despite their promises and successes in literatures,[180] MMMs have never been commercialized for industrial-scale applications. This is primarily due to the several challenging issues in the conventional blending-based MMM fabrication methods, including poor interfacial adhesion between MOF and polymer, agglomeration of MOF fillers, limited filler loadings, and difficulty in forming MOF nanoparticles (smaller than 100 nm).[181] Even after addressing the above-

*Modified and reprinted with permission from "Polyimide/ZIF-7 Mixed-Matrix Membranes: Understanding in-situ Confined Formation of ZIF-7 Phases inside Polymer and Their Effects on Gas Separations" by Sunghwan Park, Kie Yong Cho, and Hae-Kwon Jeong, *Journal of Materials Chemistry A*, 2020, 8, 11210-11217, Copyright 2020, Royal Society of Chemistry

mentioned issues, conventional blending-based methods are hardly scalable since it is tremendously challenging to spin dope solutions containing fillers into commercially viable hollow fibers with sub-micron thick selective skin composite layers.[61, 142]

Recently, we developed and reported polymer-modification-enabled *in-situ* metal-organic framework formation (PMMOF).[124] PMMOF enables MOF nanoparticles to *in-situ* form inside polymers, effectively suppressing several issues that conventional blending-based MMMs face. Moreover, since PMMOF decouples the filler incorporating step and the MMM fabrication step, PMMOF is expected to be applied directly to large-scale commercially available polymer membranes, thereby enabling a simple upgrade of relatively cheap polymer membranes to more valuable MMMs. Properties of MMMs are greatly influenced by microstructures (i.e., phase, size, shape, etc.) of fillers, which often affect microstructures of composites (i.e, interface, distribution of fillers, etc.). Filler microstructures are determined by the synthesis reaction conditions (e.g., precursor concentration, precursor diffusion, chemical interactions, etc.).[182-183] Since the actual conditions for *in-situ* MOF formation by PMMOF are expected quite different from those for MOF synthesis in a bulk solution, the investigations for the actual synthesis conditions are very important, yet quite challenging because of the nature of *in-situ* synthesis in confined spaces.

Zeolitic-imidazole framework-7 (ZIF-7, $Zn(bIm)_2$) consists of zinc tetrahedrally coordinated with benzimidazole forming six-membered rings with a sodalite (SOD) topology.[174] ZIF-7 has been considered as one of the most important ZIFs reported because of its unique gate opening phenomenon, intrinsic hydrophobic and thermally-stable properties, and excellent molecular sieving effects for mostly hydrogen over other light

gases.[174, 184-185] Moreover, ZIF-7 undergoes phase transformation with three different crystal phases:[186] a symmetric structure with a large-pore structure (ZIF-7-I), a distorted structure of Phase I with a narrow-pore structure (ZIF-7-II), which is transformed from Phase I when guest molecules such as DMF, water, and CO_2 are removed, and a layered structure with a nonporous structure (ZIF-7-III), which is induced by hydrolysis of Phase I or II. While transformation between Phases I and II is reversible, transformation of Phase I or II to Phase III is irreversible. It is noteworthy to mention that formation of the three crystal phases of ZIF-7 is governed by synthesis parameters including precursor concentration, solvents, and post-treatments.[187] As such, the aforementioned unique features of ZIF-7 give a unique opportunity to investigate how the actual reaction conditions in PMMOF differ from those in solution precipitation.

There are a few reports on ZIF-7-based MMMs prepared by a conventional physical blending method. Li *et al.*[188] prepared poly(ether-block-amide)1657 (Pebax®1657)/ZIF-7 MMMs and showed their promising separation performances for CO_2/N_2 and CO_2/CH_4 mixtures despite a decrease in CO_2 permeation. Also, Yang *et al.*[189] successfully incorporated ZIF-7 nanoparticles of < 50 nm in size in polybenzimidazole (PBI) up to 50 wt%. The resulting MMMs showed considerable performance improvement in H_2/CO_2 separation at the temperature up to 180 ^oC. They attributed the significantly enhanced H_2 permeability to the enlarged polymer free volume as ZIF-7 loading increased. Recently, enhanced gas separations were observed in MMMs with functionalized ZIF-7.[190-191]

Here, we take systematic approaches to understand *in-situ* growth of ZIF-7 inside a polymer thin-film by PMMOF. 6FDA-DAM/ZIF-7 MMMs are fabricated by PMMOF and the crystal phase of *in-situ* formed ZIF-7 is compared with that of ZIF-7 precipitated in a bulk solution. A

crystal phase diagram for solution-precipitated ZIF-7 is constructed by varying important synthesis parameters in solutions. Based on the ZIF-7 phase diagram, the reaction condition of each ZIF-7 crystal phase is determined during PMMOF, which eventually leads to form 6FDA-DAM/ZIF-7 MMMs with three different ZIF-7 crystal phases. Lastly, the gas separation properties of the resulting MMMs are examined under both single and mixed gas conditions to investigate tunable gas separation performances of MMMs with different ZIF-7 crystal phases.

4.2. Experimental

4.2.1. Materials

6FDA-DAM (Mw: 148k, PDI: 2.14) was purchased from Akron Polymer Systems Inc. Sodium formate (HCOONa, ≥ 99 %, Sigma Aldrich), zinc nitrate hexahydrate ($Zn(NO_3)_2 \cdot 6H_2O$, 98 %, Sigma Aldrich), and benzimidazole (HbIm) ($C_7H_6N_2$, ≥ 98 %, Sigma Aldrich) were used for ZIF-7 synthesis. Ethanol (C_2H_5OH, 94–96 %, Alfa Aesar) and N,N-dimethylformamide (DMF) (C_3H_7NO, > 99.8 %, Alfa Aesar) were used as solvents. Methanol (CH_3OH, > 99.8 %, Alfa Aesar) was used for washing. All chemicals were used as received.

4.2.2. ZIF-7 particle synthesis

A crystal phase diagram of ZIF-7 was constructed based on solvothermal synthesis of ZIF-7 particles in a bulk solution. Both metal and linker precursor solutions were prepared by varying precursor compositions ranging between 0.1 – 100 mmol of zinc nitrate hexahydrate and 0.1 – 75 mmol of benzimidazole in ethanol/DMF co-solvents (30 ml, 99/1

v/v). A metal and a linker solution were mixed and the precursor mixture solution was placed in a Teflon-lined stainless-steel autoclave. The synthesis was carried out at 100 ºC for 2 h without stirring. The resulting ZIF-7 powder was decanted after centrifugation with 8000 RPM for 20 min. The powder sample was then purified by re-dispersing in methanol under sonication followed by centrifugation. This purification step was repeated two more times. The acquired ZIF-7 powder was dried at 60 ºC for overnight before characterizations.

4.2.3. Fabrications of 6FDA-DAM/ZIF-7 MMMs by PMMOF

A 2 wt% 6FDA-DAM solution in DMF was prepared as a stock polymer solution and used for polymer thin films on porous α-alumina substrates. 2.4 ml of the polymer solution was slowly dropped onto the polished side of a home-made α-alumina disk. Porous α-alumina disks (22 mm in diameter, 2 mm in thickness, and 46 % porosity with an average pore diameter of ~ 200 nm) were prepared by following a previously reported recipe.[131] Thereafter, the sample was immediately placed into a vacuum oven and then dried at 150 ºC for 24 h under vacuum. For hydrolysis, the 6FDF-DAM coated α-alumina disk was vertically loaded on a custom-made Teflon holder and placed in a Teflon-lined autoclave containing a sodium formate solution (100 mmol of sodium formate in 30 ml of D.I. water). The hydrolysis reaction was performed at 120 ºC for 5 h, followed by natural cooling to room temperature. The hydrolyzed polymer thin film was then washed with D.I. water for overnight using a lab shaker to remove physically absorbed sodium and formate ions. A Zn ion exchange step was carried out by immersing the hydrolyzed polymer film into an ion exchange solution (10, 25, or 50 mmol of zinc nitrate hexahydrate in 30 ml of D.I. water) at room temperature for 3 h followed by a simple rinsing with ethanol. The ligand treatment

was performed by immersing the Zn ion adsorbed film into the benzimidazole solution (25 mmol of HbIm in 30 ml of ethanol/DMF, 99/1 v/v) in a Teflon-lined autoclave at 100 ºC for 2 h without stirring. After slow cooling the reactor to room temperature, the resulting film was washed with methanol for overnight. Lastly, the imidization reaction was conducted by heating at 220 ºC for 3 h in a pre-heated convection oven.

4.2.4. Characterizations

Scanning electron microscope (SEM) measurements were conducted using a JEOL JSM-7500F at an acceleration voltage of 5 keV with 15 mm working distance. Transmission electron microscope (TEM, JEOL JEM-2010) was operated at a voltage of 200 keV. X-ray diffraction (XRD, Rigaku Miniflex II) was performed in the 2 θ range of 5 – 40 º with Cu-Kα radiation (λ =1.5406 Å). Fourier transform infrared spectra (FT-IR) were taken using a Nicolet iS5 spectrometer (Thermo Scientific) equipped with attenuated total reflectance (ATR, iD7) accessory. X-ray photoelectron spectroscopy (XPS) measurements were conducted by an Omicron ESCA+ with Mg X-ray source at 300W. Thermogravimetric analysis (TGA, Q50 TA instruments) were carried out under air at the temperature ranging from 25 ºC to 800 ºC with a heating rate of 10 ºC min^{-1}.

4.2.5. Gas permeation measurements

Gas permeation tests were performed using the Wicke-Kallenbach technique at room temperature under atmospheric pressure. For single gases of H_2, CO_2, N_2, and CH_4, a feed gas was provided at 20 cm^3 min^{-1} while the permeate side was swept by argon gas with the flow rate

of 20 cm^3 min^{-1}. Similarly, for equal-molar binary gas mixtures of H_2/CO_2, H_2/CH_4, and CO_2/N_2, the total feed flow rate was kept at 20 ml min^{-1}. The composition of the permeated gases was determined using a gas analyzer (QGA, Hiden Analytical).

4.3. Results and discussion

4.3.1. Fabrication and characterization of PI/ZIF-7 MMMs by PMMOF

6FDA-DAM/ZIF-7 MMMs were fabricated using our polymer-modification-enabled *in-situ* metal-organic framework formation (PMMOF) process reported recently.[192] A 6FDA-DAM polyimide (PI) thin film was prepared on an α-alumina disk by a drop-casting method, resulting in a PI film with a thickness of 7.9 ± 2.0 μm. As represented in Chapter 3, ZIF-7 was *in-situ* formed inside the PI thin film by PMMOF which consists of four steps: hydrolysis, ion-exchange, ligand treatment, and imidization. The XRD patterns of the PI/ZIF-7 MMM match with the simulated pattern of ZIF-7-I, which has a symmetric large-pore structure (Figure 4.1a).[186] The cross-sectional SEM image of the PI/ZIF-7-I exhibits a grainy surface, which may or may not be ZIF-7, compared with the relatively smooth cross-section of the PI (Figure 4.1b). Also, relatively large clusters were found on the top surface of the PI/ZIF-7-I (Figure 4.1b). The cross-sectional TEM image of the sample in the inset of Figure 4.1b shows poorly defined ZIF-7-I crystals of less than 100 nm in size. Based on these observations, it was concluded that ZIF-7-I nanoparticles less than 100 nm in size were formed mostly inside the PI film by PMMOF.

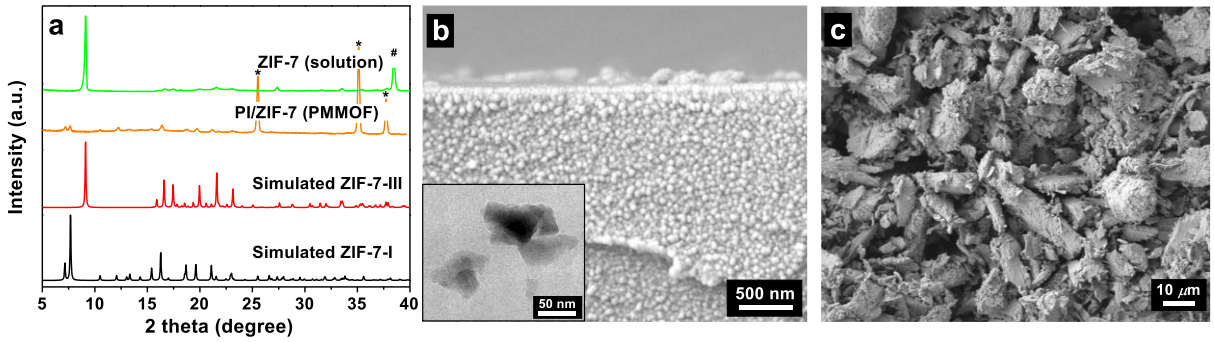

Figure 4.1. (a) XRD patterns and (b) cross-sectional SEM images of as-prepared PI/ZIF-7-I by PMMOF. The insert is the TEM image of *in-situ* formed ZIF-7-I in the polymer. (c) SEM image of ZIF-7-III (solution).

In PMMOF process, crystallization happens in confined spaces inside the polymer (i.e., free volumes),[192-193] thereby affecting the diffusion of precursor species inside the polymer film as well as interactions of reacting species. In other words, ZIF-7 crystallization inside a PAA-Zn film proceeds in a different environment than in a bulk solution. To confirm this, ZIF-7 was synthesized in a solution under the same reaction condition as PMMOF. The obtained ZIF-7 powders exhibited ZIF-7-III (dense layered structure) phase with several microns in size (Figure 4.1a and c). Formation of a different ZIF-7 crystal phase in a bulk solution vs. in PMMOF strongly suggests that the actual reaction conditions are very different. On the other hand, the much smaller particles of *in-situ* grown ZIF-7-I by PMMOF can be attributed mainly to the unique confined environments inside the polymer. It was, therefore, hypothesized that the concentrations and ratios of both absorbed Zn and bIm precursors inside the polymer film can be an important parameter to determine the ZIF-7 crystal phase.

4.3.2. ZIF-7 crystal phase diagram and PMMOF reaction conditions

To confirm our hypothesis on the effect of precursor concentrations and ratios inside the polymer film on ZIF-7 crystal phase, a ZIF-7 crystal phase diagram was established by varying the concentrations and ratios of Zn ions and bIm ligands using bulk solution reaction. The acquired ZIF-7 particles were characterized by SEM and XRD to investigate their crystal phases (Figure 4.2 and 3.3). Four distinctive regions were identified in the crystal phase diagram (see Figure 4.4a): 1) ZIF-7-I phase (marked with red spots), 2) ZIF-7-mix mixed-phase containing both ZIF-7-I and ZIF-7-III phases (marked with yellow spots), 3) ZIF-7-III phase (marked with green spots), and 4) undefinable region due to the lack of precipitations (marked with a dashed line). Representative SEM images and XRD patterns for the three distinctive ZIF-7-I, ZIF-7-mix, and ZIF-7-III samples collected from bulk solutions were displayed in Figure 4.2 and 3.3, respectively. The SEM images presented a spherical shape of ZIF-7-I with sub-micron in size and a planer shape for ZIF-7-mix and ZIF-7-III with microns in size (Figure 4.2). ZIF-7-III showed a smooth surface. In the case of ZIF-7-mix, however, ZIF-7-III seemed covered with debris of ZIF-7-I, suggesting that the two different crystal phases including ZIF-7-I and ZIF-7-III were seemingly physically mixed (Figure 4.2).

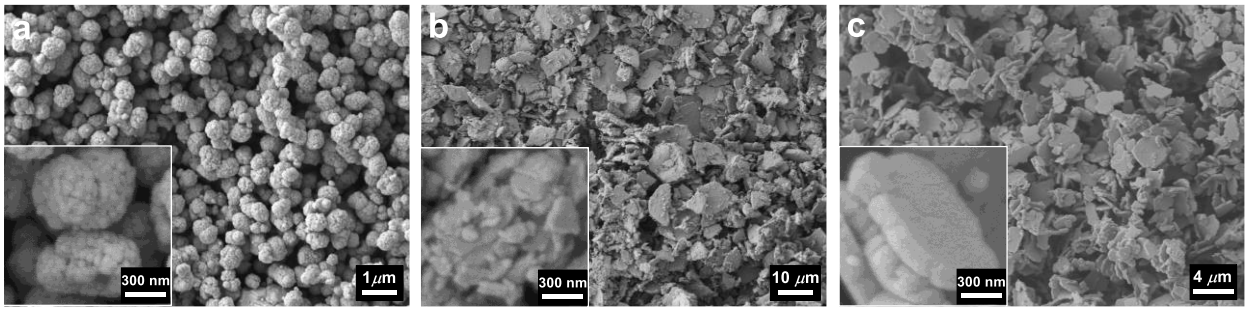

Figure 4.2. SEM images of ZIF-7 particles prepared using solution reaction. (a) ZIF-7-I, (b) ZIF-7-mix, and (c) ZIF-7-III (the inset images exhibited surface of particles).

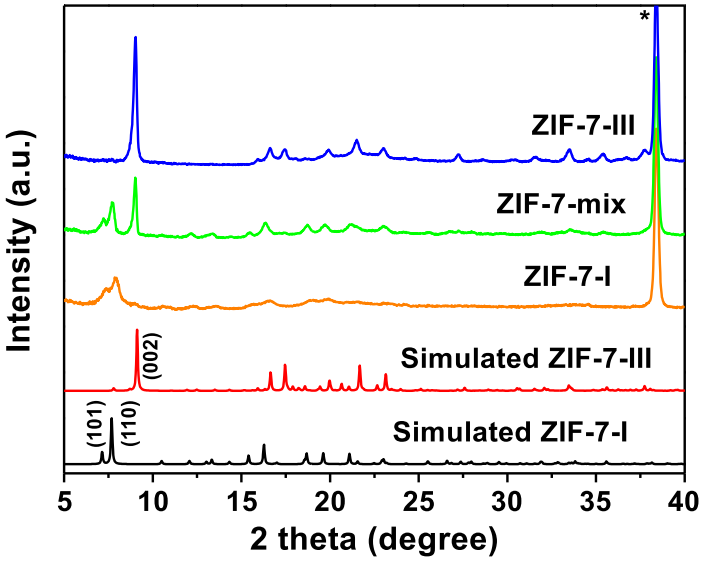

Figure 4.3. XRD patterns of ZIF-7 (solution).

Based on the ZIF-7 crystal phase diagram, the reaction conditions of *in-situ* synthesis of ZIF-7 in the polymer by PMMOF were evaluated by tracking precursor concentrations at three stages: (1) when a PAA film was immersed in the zinc solution, (2) when the polymer film was saturated with Zn ions, (3) when a PAA/ZIF-7 was formed after ligand treatment. The concentration of Zn ions was determined by the amount of evaporated solvents and zinc oxide residues formed by thermal oxidization of dried samples. It is noted that the determined amounts of zinc sources are based on mobile Zn ions rather than immobile Zn ions coordinated to the polymer as mentioned in Chapter 2. This is because

the mobile zinc sources mainly contribute to form ZIF inside the polymer.[124, 193] Initially, as indicated at the point (1) in Figure 4.4a, the concentration of Zn ions in the mother solution was 0.42 mol kg^{-1}. By immersing a PAA film in the zinc solution, Zn ions were absorbed into the polymer free volume (Figure 4.4b (1)). When the polymer was fully saturated with the Zn ions, as shown in Figure 4.4b (2), the total concentration of Zn ions in the PAA film was 1.51 ± 0.08 mol $kg^{-1,}$ and the concentration of mobile Zn ions was 0.89 ± 0.05 mol kg^{-1} (see the point (2) in Figure 4.4a). The Zn ion concentration in the polymer (i.e., 0.89 ± 0.05 mol kg^{-1}) was two times higher than that of the mother solution (i.e., 0.42 mol kg^{-1}). This relatively high zinc concentration inside the PAA film can be explained by the fact that Zn ions were thermodynamically preferred inside the film while solvent molecules were preferred in solution, probably due to 1) the electrostatic interaction of Zn ions with charged polymer and 2) the much smaller size of Zn ions as compared to ethanol (i.e., 0.74 Å of zinc ionic radius vs. 4.5 Å of ethanol critical diameter).[194] After the ligand treatment using the bIm solution with the bIm concentration of 1.05 mol kg^{-1}, the concentration of mobile Zn ions was reduced to 0.053 ± 0.012 mol kg^{-1} (See the point (3) in Figure 4.4a). As depicted in Figure 4.4b (3), the majority of Zn ions were drained from a PAA free volume and bIm ligands were absorbed into the polymer upon the ligand treatment possibly due to the applied electric potential gradient of the precursors inside and outside the polymer.[195] The remaining Zn ions inside the polymer free volume were simultaneously reacted with the absorbed bIm ions upon solvothermal ligand treatment, resulting in the nucleation and growth of ZIF-7 nanocrystals in the PAA free volume (Figure 4.4b (3)). At the final mobile Zn ion concentration (i.e., 0.053 ± 0.012 mol kg^{-1}), it was found that ZIF-7-I phases were presented in the very narrow bIm concentrations

ranging from 0.65 mol kg^{-1} to 1.05 mol kg^{-1} in the ZIF-7 phase diagram (Figure 4.4a). Since PI/ZIF-7 by PMMOF exhibited ZIF-7-I phase (Figure 4.1a), the synthesis conditions (i.e., concentrations of Zn ions and bIm ligands) for ZIF-7 by PMMOF was estimated in the region (3) in Figure 4.4a.

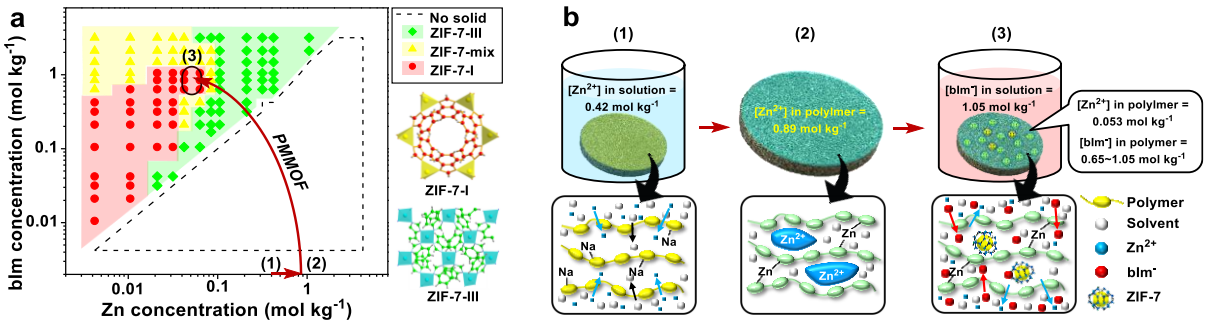

Figure 4.4. (a) ZIF-7 crystal phase diagram as a function of concentrations of zinc and bIm. (b) Illustration of the ZIF-7 systhesis stages and the corresponding conditions upon PMMOF process.

4.3.3. Engineering of ZIF-7 crystal phase of PI/ZIF-7 MMM

The performances of ZIF-7-containing MMMs are expected to be greatly affected by the ZIF-7 phase *in-situ* formed by PMMOF. As such, we attempted to test if the ZIF-7 phase diagram and the evaluated PMMOF reaction conditions can be used to control the formation of not only ZIF-7-I but also the other phases (i.e., ZIF-7-mix and ZIF-7-III). As discussed above, PI/ZIF-7-I MMMs were formed when the zinc concentration in a mother solution is 0.42 mol kg^{-1} (see the α region in Figure 4.5). As the zinc concentration in an ion exchange solution increased to 1.05 mol kg^{-1}, ZIF-7-mix mixed-phase was acquired (see the β region in Figure 4.5) with the crystal phase composition of ZIF-7-I (51 %) and

ZIF-7-III (49 %) (Figure 4.6). It is noted that the percentages of each ZIF-7 phase were calculated by integrating the intensive XRD peaks of (101) and (110) for ZIF-7-I and (002) for ZIF-7-III. When the zinc concentration in an ion exchange solution further increased to 2.11 mol kg^{-1}, ZIF-7-III phase was formed (see the γ region in Figure 4.5), confirmed by the absence of (101) and (110) peaks in the XRD pattern (Figure 4.6). ZIF-7 phases present in MMMs by PMMOF well corresponded to those estimated in the phase diagram. This indicates that the phase diagram and the estimated reaction conditions inside the polymer free volume can give a reasonable guideline to control the ZIF-7 phase in PI/ZIF-7 MMMs by PMMOF.

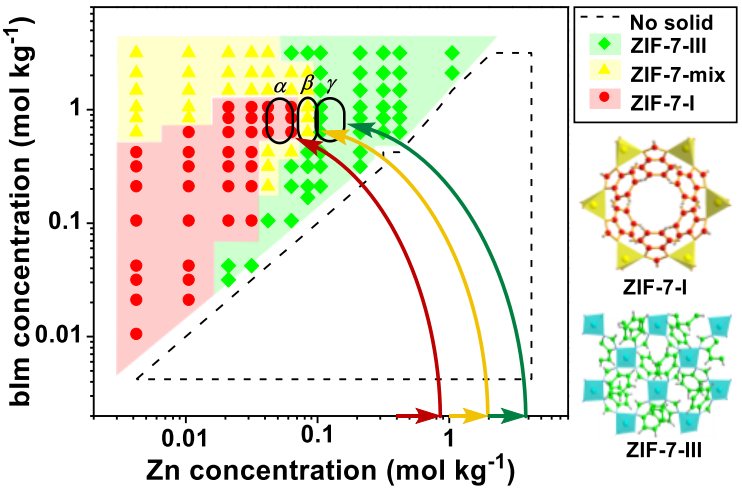

Figure 4.5. ZIF-7 crystal phase diagram and the traced PMMOF reaction conditions at different zinc concentrations in ion exchange solutions.

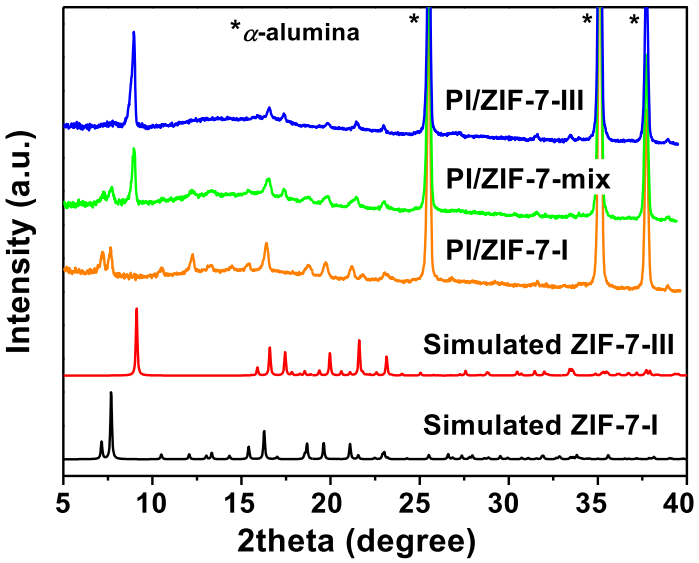

Figure 4.6. XRD patterns of PI/ZIF-7 MMMs by PMMOF with three different ZIF-7 crystal phases.

Interestingly, both PI/ZIF-7-mix and PI/ZIF-7-III MMMs exhibited almost identical cross-sectional morphology as PI/ZIF-7-I (Figure 4.7). Regardless of the crystal phase, the size of *in-situ* grown ZIF-7 nanoparticles was seemed to be significantly smaller than those crystals synthesized by the solution reaction (i.e., > 1 μm) (Figure 4.2). Suppression of micro-sized particle formation was attributed to confined growth inside polymer (i.e., free volume). It is highly desirable to have nano-sized fillers for ultra-thin MMM layers, in particular, asymmetric mixed-matrix hollow fiber membranes.[142] In addition, it was found that total ZIF-7 loading in MMMs could increase with changing ZIF-7 phases from ZIF-7-I to ZIF-7-III (Table 4.1). ZIF-7 loadings in PI/ZIF-7 MMMs by PMMOF were determined using TGA analysis, which is described in Chapter 2. ZIF-7-I content in a PI/ZIF-7-I MMM was estimated at 2.78 wt%. With an increase in Zn concentration relative to that for PI/ZIF-

7-I, 7.00 wt% for ZIF-7-mix in PI/ZIF-7-mix and 9.96 wt% for ZIF-7-III in PI/ZIF-7-III were formed (Table 4.1).

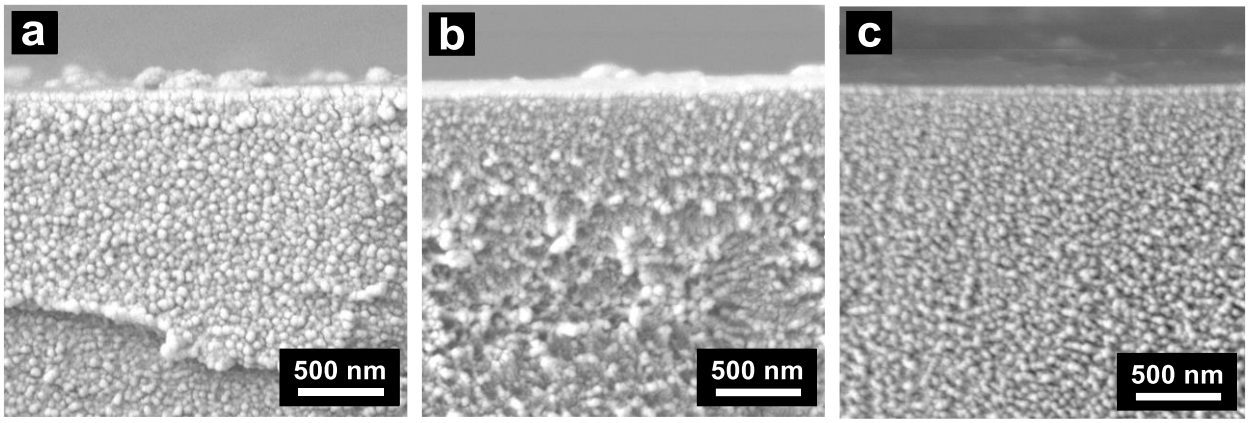

Figure 4.7. SEM images of PI/ZIF-7 MMMs with different crystal phases: (a) PI/ZIF-7-I, (b) PI/ZIF-7-mix, and (c) PI/ZIF-7-III.

Table 4.1. Weight percentages of ZnO induced by thermal oxidization and that of calculated ZIF-7 in a polymer.

Sample	Total ZnO wt%	ZIF-7 derived ZnO wt%	ZIF-7-I wt%	ZIF-7-III wt%	Total ZIF-7 wt%
Washed PAA-Zn	1.38	0.00	0.00	0.00	0.00
ZIF-7-I	25.5	25.5	100	0.00	100
ZIF-7-III	26.3	26.3	0.00	100	100
PI/ZIF-7-I	2.09	0.71	2.78	0.00	2.78
PI/ZIF-7-mix	3.19	1.81	3.63	3.37	7.00
PI/ZIF-7-III	4.00	2.62	0.00	9.96	9.96

4.3.4. Gas transport properties of PI/ZIF-7 MMMs by PMMOF

The single gas permeation of a pristine 6FDA-DAM polymer membrane exhibited similar properties to the reported results for H_2, CO_2, N_2, and CH_4 (Figure 4.8 and Table 4.2).[141, 196] When compared with pristine 6FDA-DAM polymers, PI/ZIF-7-I MMMs by PMMOF showed increased permeabilities for non-condensable gases (i.e., H_2 and N_2) and decreased permeabilities for condensable gas molecules (i.e., CO_2 and CH_4) (Figure 4.8a and Table 4.2). This result can be ascribed to the presence of microporous ZIF-7-I which allows a fast diffusion for non-condensable gases and a retarded diffusion of condensable gases via relatively strong sorption.[197-198] The ideal selectivities of H_2/CO_2, H_2/N_2, and H_2/CH_4 pairs of MMMs increased from 1.36, 30.62, and 40.23 to 2.26, 36.12, and 67.42, respectively. In contrast, there was a slight decrease in the ideal selectivity of CO_2/N_2 (22.54 → 15.97) (Figure 4.8b and Table 4.2). The increased ideal selectivities of H_2/CO_2, H_2/N_2, and H_2/CH_4 pairs are likely due to the molecular sieving effect of ZIF-7-I, whose crystallographically-defined aperture size is ~ 3.0 Å,[199] given the kinetic diameter of hydrogen (2.89 Å). Since the kinetic diameters of both CO_2 and N_2 are 3.3 Å and 3.64 Å, respectively, both molecules can be excluded by ZIF-7-I (Figure 4.8b and Table 4.2). As such, the decreased CO_2/N_2 selectivity can be primarily due to the fact that CO_2 and N_2 interact with ZIF-7-I differently (i.e., CO_2 interacts more strongly than N_2).

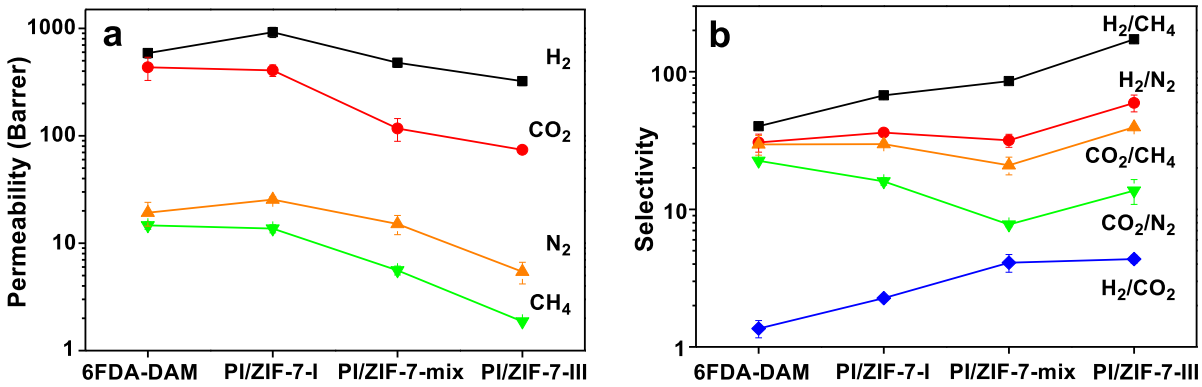

Figure 4.8. Single gas transport results of PI/ZIF-7 MMMs by PMMOF. (a) Permeability, (b) selectivity of 6FDA-DAM and PI/ZIF-7 MMMs with the different ZIF-7 phases.

Table 4.2. Summary of single gas permeation results at 1 atm and room temperature.

Sample	Permeability (Barrer)				Selectivity				
	H_2	CO_2	N_2	CH_4	H_2/CO_2	H_2/N_2	H_2/CH_4	CO_2/N_2	CO_2/CH_4
6FDA-DAM	589.17 ± 59.05	433.63 ± 105.38	19.24 ± 4.81	14.65 ± 1.18	1.36 ± 0.19	30.62 ± 4.59	40.23 ± 0.80	22.54 ± 0.16	29.61 ± 4.82
PI/ZIF-7-I	921.44 ± 100.46	407.41 ± 50.05	25.51 ± 1.57	13.67 ± 1.20	2.26 ± 0.03	36.12 ± 1.72	67.42 ± 1.45	15.97 ± 0.98	29.81 ± 1.05
PI/ZIF-7-mix	478.27 ± 44.76	116.83 ± 28.09	15.08 ± 3.06	5.59 ± 0.52	4.09 ± 0.60	31.71 ± 3.46	85.54 ± 0.01	7.75 ± 0.29	20.90 ± 3.06
PI/ZIF-7-III	322.01 ± 28.66	74.08 ± 1.73	5.42 ± 1.24	1.87 ± 0.07	4.35 ± 0.29	59.45 ± 8.27	172.24 ± 8.50	13.68 ± 2.80	39.63 ± 0.65

As discussed above, ZIF-7 loading increased in the following order: PI/ZIF-7-I < PI/ZIF-7-mix < PI/ZIF-7-III (Table 4.1). Nevertheless, the gas permeabilities increased in the opposite order for all gases tested: PI/ZIF-7-I > PI/ZIF-7-mix > PI/ZIF-7-III (Figure 4.8a). This decreasing trend of gas permeability with an increase in ZIF-7 filler loading can be most likely due to the presence of less permeable ZIF-7-III phase in MMMs (i.e., ZIF-7-III works as a gas barrier).[186] Nevertheless, the ideal gas selectivities of the PI/ZIF-7-III except for CO_2/N_2 were higher than those of the ZIF-7-I MMM (Figure 4.8b). This can be explained that ZIF-7-III nanoparticles *in-situ* grown in the polymer free volume might be loosely stacked, thereby showing possible molecular sieving effect of ZIF-7-III. Furthermore, polymer matrices in PI/ZIF-7 MMMs might become less permeable as ZIF-7 loadings increase since ZIF-7 crystals were formed in polymer free volumes, resulting in the reduction of PI free volume.[124]

For mixed gas separations, three representative gas pairs (CO_2/N_2, H_2/CO_2, and H_2/CH_4) were tested for 6FDA-DAM and PI/ZIF-7-I MMMs. As compared with the single gas separation, the mixed gas separation factors were depressed except for H_2/CH_4 likely due to the competition between two different gas molecules (Figure 4.9).[200] In particular, the substantial decrease in CO_2/N_2 separation factor (~ 60 %) was observed as shown in Figure 4.9a. For H_2/CO_2 binary gas mixture, 6FDA-DAM showed relatively higher H_2 permeability than that for single gas (Figure 4.9b). Meanwhile, the PI/ZIF-7-I MMMs exhibited lower H_2 permeability in binary gas permeation than in single gas permeation (Figure 4.9b). As such, the H_2/CO_2 separation factor of 6FDA-DAM showed slightly lower in binary gas (Figure 4.9b). In contrast, the PI/ZIF-7-I MMMs showed lower separation factor in binary gas (Figure 4.9b), possibly resulting from stronger sorption competition

between H_2 and CO_2 in PI/ZIF-7-I than that in 6FDA-DAM.[201] Similarly, although both 6FDA-DAM and PI/ZIF-7-I showed an increase in the binary H_2/CH_4 separation factor, 6FDA-DAM exhibited a larger increment than that shown by PI/ZIF-7 (Figure 4.9c)

.

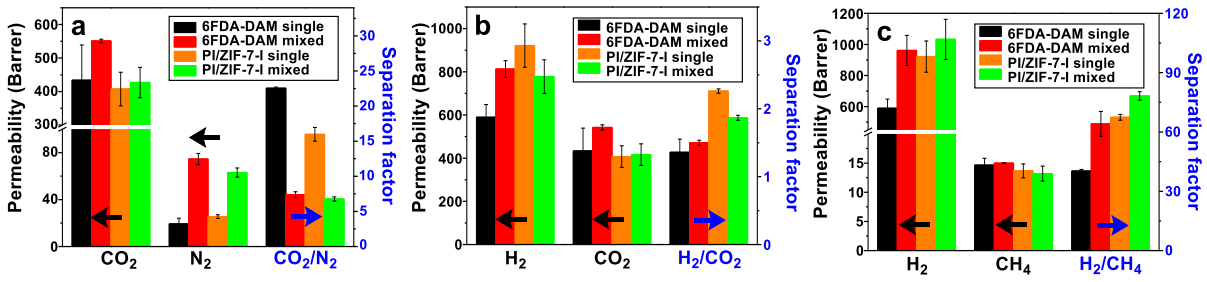

Figure 4.9. Mixed gas separation results of 6FDA-DAM and PI/ZIF-7-I for binary gas mixtures of (a) CO_2/N_2, (b) H_2/CO_2, and (c) H_2/CH_4.

Since the filler content has a great effect on the gas transport properties of MMMs, it is important to compare the transport properties of MMMs with the same filler content in order to discern the effects of fillers. Due to the nature of PMMOF, it is, however, not straight forward to fabricate PI/ZIF-7 MMMs made of three different ZIF-7 phases with the same filler contents. To examine the filler effects, PI/ZIF-7-III MMMs were prepared by a post-phase-transformation from ZIF-7-I containing MMMs using the hydrolysis process in water at 150 ^oC for 3 h. Initially, we attempted to perform hydrolysis on PI/ZIF-7-I. Unfortunately, 6FDA-DAM is hydrophobic, impeding sufficient water adsorption in MMMs, resulted in incomplete hydrolysis regardless of the reaction time.[29] Meanwhile, relatively more hydrophilic PAA/ZIF-7-I, where PAA (i.e., poly(amic acid)) is deimidized PI, resulted in complete hydrolysis, leading to transformation of ZIF-7-I to ZIF-7-III in the polymer. This phase transformation was confirmed by XRD (Figure 4.10).[30] PAA/ZIF-7-

III was then imidized to obtain PI/ZIF-7-III, which is denoted as PI/ZIF-7-III* to distinguish from PI/ZIF-7-III, whose ZIF-7-III is *in-situ* formed via PMMOF.

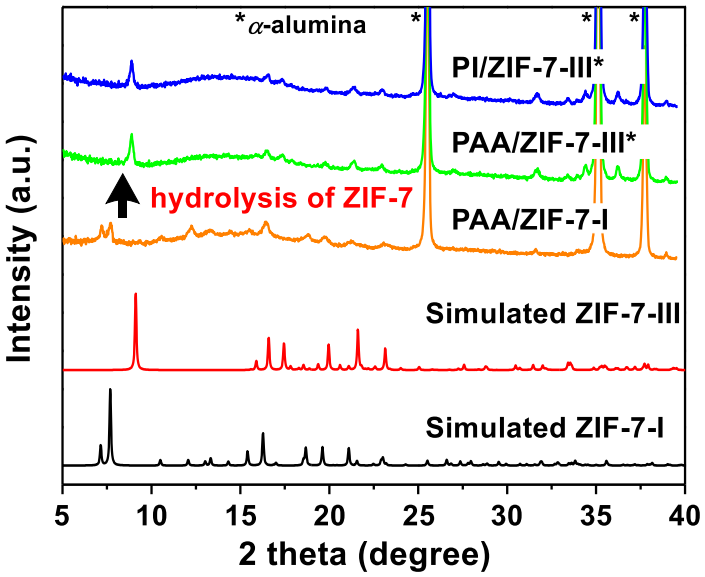

Figure 4.10. XRD patterns of PAA/ZIF-7-I, PAA/ZIF-7-III*, and PI/ZIF-7-III*.

Gas permeation properties of PI/ZIF-7-III* MMMs were tested and compared with those of PI/ZIF-7-I. As presented in Figure 4.11, PI/ZIF-7-III* MMMs showed higher H_2 permeability with similar CO_2 permeability, which is ascribed to the intrinsic property of ZIF-7-III. Peng *et al.*[202] showed that the disorderly stacked exfoliated ZIF-7-III nanosheets showed the exceptionally high H_2/CO_2 separation performance. They claimed that the four-membered rings of ZIF-7-III nanosheets consisting of flexible organic linkers allowed high H_2 permeation while excluding larger CO_2.[202] Hence, PI/ZIF-7-III* showed greater H_2/CO_2 selectivity by ~ 70 % than PI/ZIF-7-I, which can be attributed to better molecular sieving effect of ZIF-7-III than ZIF-7-I for H_2/CO_2 separation.[199, 202]

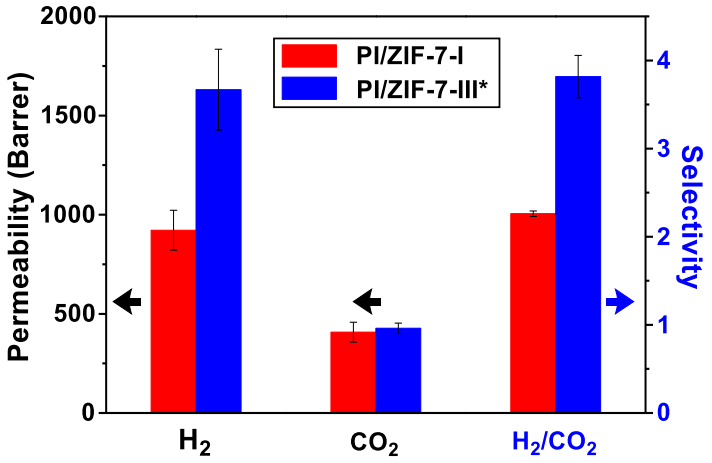

Figure 4.11. Comparison of H_2/CO_2 separation properties of PI/ZIF-7-I and PI/ZIF-7-III*

When compared with other reported MMMs, the PI/ZIF-7 MMMs by PMMOF showed high H_2 permeability and H_2/CO_2 ideal selectivity, effectively surpassing the polymeric upper bound (Figure 4.12).[3, 189, 203-218] While most of the reported MMMs showed mediocre H_2/CO_2 ideal selectivity improvement from their corresponding pristine polymers, the PI/ZIF-7 MMMs by PMMOF exhibited up to ~ 220 % enhancement in the H_2/CO_2 ideal selectivity (Table 4.3). Those enhancements are quite surprising considering the relatively low filler loadings (i.e., ~ 10 wt%), indicating the exceptionally high filler efficiency (Table 4.3). In particular, the PBI/ZIF-7 MMMs prepared by conventional physical blending method, even with 50 wt% ZIF-7-I loading, showed improvement in the H_2/CO_2 ideal selectivity from 8.7 to 14.9 (~ 70 % improvement).[189] On the contrary, the PI/ZIF-7 MMMs by PMMOF with 2.78 wt% ZIF-7 loadings exhibited ~ 66 % and ~ 180 % improvement for ZIF-7-I and ZIF-7-III*, respectively, (Table 4.3). However, the separation performance of other gas pairs rarely exceeded the corresponding upper bounds (Figure 4.13).

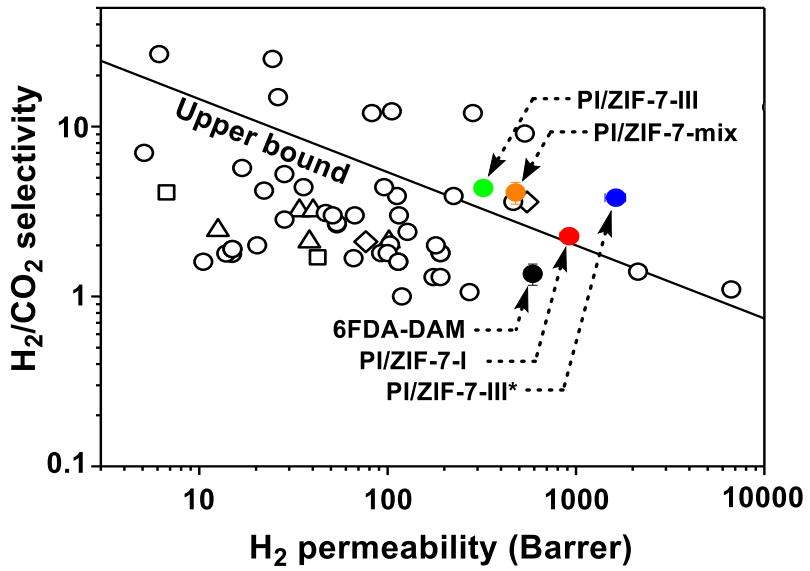

Figure 4.12. H_2/CO_2 separation performance of PI/ZIF-7 MMMs by PMMOF (●) in comparison with those of the MOF-based (○), zeolite-based (△), carbon-based (□), and silica-based (◇) MMMs reported.[20,36-73]

Table 4.3. H_2/CO_2 separation performances of the reported MMMs.

Polymer	Filler	Wt% of filler	H_2 permeability	H_2/CO_2 selectivity	Ref.
Matrimid®5218	C-MOF-5	30	53.8 (120.5 %)	2.66 (-1.8 %)	203
PES	SAPO-34	20	12.57 (82.2 %)	2.45 (2.1 %)	204
Matrimid®5218	hollow silicalite-1	8	38.4 (26.3 %)	2.1 (46.2 %)	205
PBI	ZIF-7	50	26.2 (608.1 %)	14.9 (71.3 %)	189
Matrimid®9725	Zeolite 4A	30	101.60 (464 %)	2.10 (-16 %)	206
6FDA:DSDA/4MPD:4,4′-SDA	NH2-MIL-101	10	114 (26.7 %)	1.6 (3.3 %)	207
6FDA-durene	ZIF-8	15	2136.6 (312.1 %)	1.4 (27.3 %)	208
X-linked 6FDA-durene	ZIF-8	33.3	283.5 (444.1 %)	12.0 (-90.8 %)	

Polymer	Filler	Wt% of filler	H_2 permeability	H_2/CO_2 selectivity	Ref.
PEI	C-MOF-5	25	28.32 (181.2 %)	5.25 (-12.4 %)	209
PPO	Silica	10	548.7 (567.8 %)	3.6 (111.9 %)	211
Matrimid®5218	MIL-53-ht	37.5	103.0 (300.8 %)	2.02 (-34.2 %)	210
Matrimid®5218	MIL-53-as	37.5	66.0 (156.8 %)	1.68 (-45.3 %)	
VTEC™	NH2-MIL-53	20	5.1 (13.3 %)	7.0 (16.7 %)	213
6FDA-DAM	ZIF-11	20	272.45 (1173.1 %)	1.06 (2.9 %)	212
PI	MWCNT@GONRs	2	42.5 (42 %)	1.7 (-15 %)	214
Matrimid®5218	ZIF-11	40	28.36 (63.6 %)	2.84 (-31.2 %)	218
CA	C-MOF-5	12	14.95 (247.7 %)	1.78 (61.8 %)	215
CA	T-MOF-5	12	13.90 (223.3 %)	1.79 (62.7 %)	
6FDA-TTM	Si-H	10	76.5 (86.1 %)	2.1 (40.0 %)	216
P84	Nanodiamond	1	6.7 (-16.3 %)	4.1 (13.8 %)	217
PAI	MOF-1	30	191 (141.2 %)	1.8 (5.9 %)	219
PSf	HKUST-1	10	15.0 (53.1 %)	1.9 (18.8 %)	220
PSf	Mn(HCOO)2	10	10.5 (7.1 %)	1.6 (0.0 %)	
Matrimids5218	Cu-BPY-HFS	30	20.3 (16.0 %)	2.0 (-16.7 %)	221
Matrimids5218	MOF-5	20	114.9 (247.1 %)	3.0 (-9.1 %)	
Ultems1000	MOF-5	20	16.9 (50.9 %)	5.7 (0.0 %)	222
Matrimids5218	HKUST-1	30	66.9 (102.1 %)	3.0 (-9.1 %)	
Matrimids	MOF-5	30	53.8 (120.5 %)	2.7 (0.0 %)	223
Matrimids	ZIF-8	60	35.8 (23.9 %)	4.4 (41.9 %)	35
PPEEs	ZIF-8	30	92.3 (1068 %)	1.8 (28.6 %)	224

Polymer	Filler	Wt% of filler	H_2 permeability	H_2/CO_2 selectivity	Ref.
Matrimids	ZIF-8	30	112.1 (242.8 %)	3.9 (-2.5 %)	225
PBI	ZIF-8	30	105.4 (2749 %)	12.3 (43.0 %)	226
PBI	ZIF-8	30	82.5 (1912 %)	12.0 (34.8 %)	227
PIM-1	ZIF-8	43	6680 (309.8 %)	1.1 (450.0 %)	228
PBI	ZIF-90	45	24.5 (497.6 %)	25 (180.9 %)	229
PPO	HKUST-1	40	119 (58.7 %)	1.0 (-9.1 %)	230
6FDA:DSDA-4MPD:4,4'-SDA (1:1)	NH2-MIL-53(Al)	15	100 (11.0 %)	1.8 (12.5 %)	40
	NH2-MIL-101(Al)	10	114 (26.5 %)	1.6 (0.0 %)	
6FDA-4MPD:4,4'-SDA (1:1)	NH2-MIL-53(Al)	10	175 (3.6 %)	1.3 (0.0 %)	
	NH2-MIL-101(Al)	10	191 (13.0 %)	1.3 (0.0 %)	
PMMA	NH2-CAU-1	15	11 000 (120.0 %)	13 (333.3 %)	231
PSf	Silica-ZIF-8 core–shell	32	224.1 (540.3 %)	3.9 (14.7 %)	232
PBI-BuI	ZIF-8	30	22.1 (256.5 %)	4.2 (55.6 %)	233
DMPBI-BuI	ZIF-8	30	127.5 (896.1 %)	2.4 (-29.4 %)	
DBzPBI-BuI	ZIF-8	20	180.3 (193.6 %)	2.0 (-16.7 %)	
PBI	ZIF-11	39.5	464.7 (2602 %)	3.6 (-28.0 %)	234
Matrimid®5218	Silicalite	10	34.0 (12.2 %)	3.2 (0.0 %)	235
	SAPO-34	10	40.2 (32.7 %)	3.2 (0.0 %)	
	ZIF-8	10	51.1 (68.6 %)	3.0 (-6.3 %)	
Matrimid®5218	ZIF-11	25	95.9 (335.9 %)	4.4 (41.9 %)	236
		10	535 (52.9 %)	9.1 (13.8 %)	
PBI	$Cu_2(ndc)_2(dabco)$	20	6.13 (152.0 %)	26.7 (181.1 %)	237

Polymer	Filler	Wt% of filler	H_2 permeability	H_2/CO_2 selectivity	Ref.
6FDA-DAM	ZIF-7-I	2.78	921.44 (56.4 %)	2.26 (66.2 %)	This work
	ZIF-7-mix	7.00	478.27 (-18.8 %)	4.09 (200.7 %)	
	ZIF-7-III	9.96	322.01 (-45.4 %)	4.35 (219.9 %)	
	ZIF-7-III*	2.78	1630.44 (176.7 %)	3.82 (180.9 %)	

Note: the unit of permeability is Barrer (i.e., 1 Barrer = 10^{-10} cm^3(STP) cm cm^{-2} $cmHg^{-1}$ sec^{-1}). The percentages in the round bracket of H_2 permeability and H_2/CO_2 selectivity indicate the changing percentages of MMMs from its corresponding polymer.

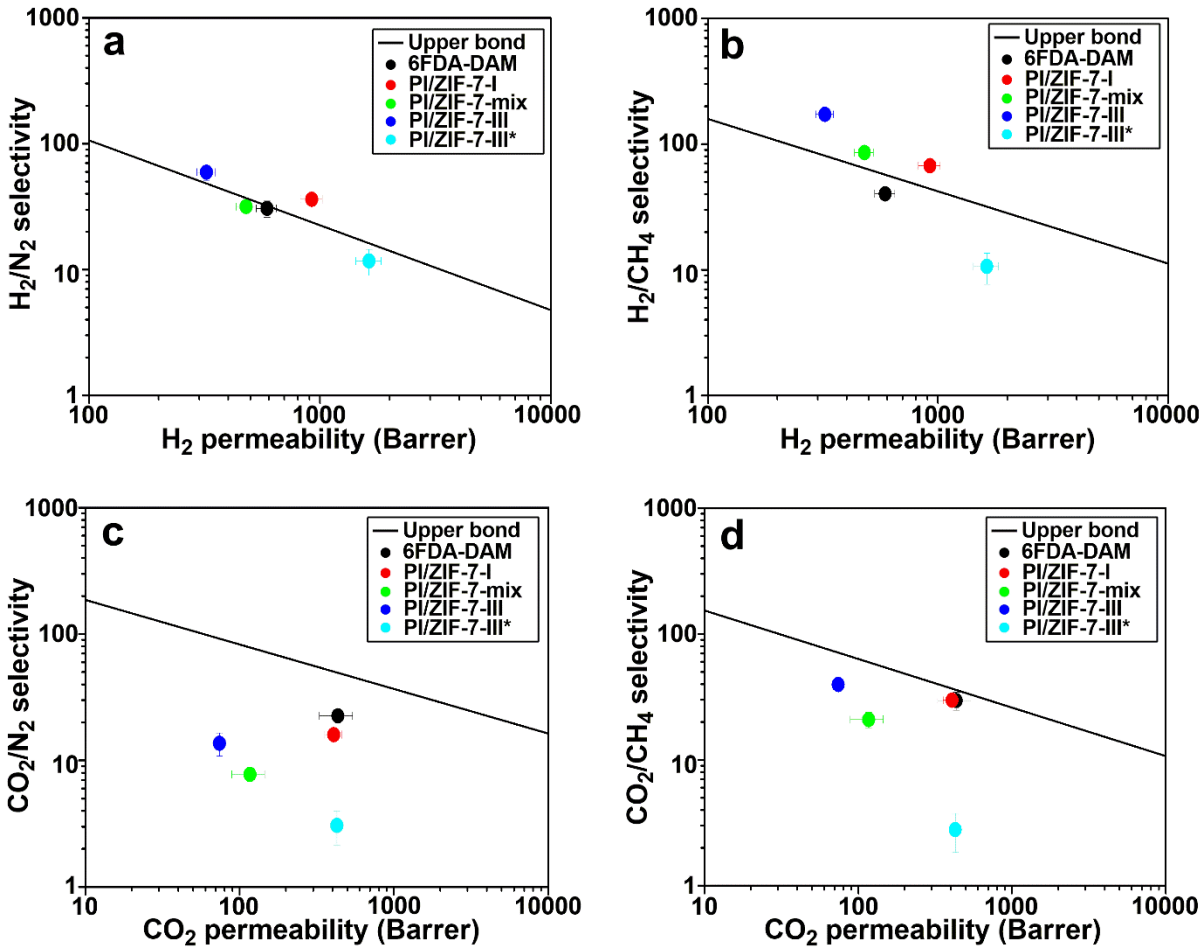

Figure 4.13. Upper bound plot of 6FDA-DAM and PI/ZIF-7 MMMs. (a) H_2/N_2 separation, (b) H_2/CH_4 separation, (c) CO_2/N_2 separation, and (d) CO_2/CH_4 separation.[3]

4.4. Conclusion

In conclusion, we prepared 6FDA-DAM/ZIF-7 MMMs using PMMOF by *in-situ* growing ZIF-7 nanoparticles inside the polymer. To understand the different synthesis conditions between confined and bulk synthesis, a ZIF-7 phase diagram was constructed based on bulk solution synthesis. The ZIF-7 phase diagram was utilized to estimate and design 6FDA-DAM/ZIF-7 MMMs by PMMOF, resulting in controlled synthesis of three different ZIF-7 phases (i.e., ZIF-7-I, ZIF-7-mix, and ZIF-7-III. Among the MMMs, the ZIF-7-III*-based MMM where ZIF-7-III* was transformed from ZIF-7-I, even with 2.78 wt% filler loading, showed the best H_2/CO_2 separation performances, exhibiting the dramatic improvements. The PI/ZIF-7-III* MMMs exhibited improved H_2 permeability and enhanced H_2/CO_2 selectivity by ~ 176 % and ~ 180 %, respectively, as compared with 6FDA-DAM and by ~ 77 % and ~ 69 %, respectively, as compared to PI/ZIF-7-I with the same filler loading. This enhancement was likely due to the more efficient molecular sieving property of ZIF-7-III than that of ZIF-7-I. The current findings are expected an important stepping stone for further development of PMMOF process for *in-situ* formed MOF-based MMM and scalable MMMs.

CHAPTER V

IN-SITU LINKER DOPING AS AN EFFECTIVE MEANS TO TUNE ZIF-8 FILLERS IN MIXED-MATRIX MEMBRANES FOR PROPYLENE/PROPANE SEPARATION

5.1. Introduction

Propylene/propane (C_3H_6/C_3H_8) separation is one of the most energy-intensive processes in the petrochemical industry.[128] Membrane-based C_3H_6/C_3H_8 separation requires only ~ 10 % energy of the conventional thermally-driven distillation process.[238] In particular, mixed-matrix membranes (MMMs), consisting of a continuous polymer phase and a dispersed molecular sieve phase, have been considered as a promising next-generation membrane concept by combining the advantages of both polymer and molecular sieve membranes.[151]

Among several promising fillers for propylene-selective MMMs, zeolitic-imidazole framework-8 (ZIF-8) is one of the most promising and investigated fillers due to its effective aperture size (i.e., 4.0 ~ 4.2 Å).[141] ZIF-8 consists of Zn^{2+} nodes bridged by flexible 2-methylimidazole (mIm) linkers, forming sodalite (SOD) topology. Among a number of ZIF-8 containing MMMs, however, there are only a handful of MMMs reported for C_3H_6/C_3H_8 separation. Koros et al.[1, 142] successfully demonstrated the applicability of MMMs for C_3H_6/C_3H_8 separation by preparing 4,4′-(hexafluoroisopropylidene) diphthalic anhydride-2,4,6-trimethyl-1,3-diaminobenzene (6FDA-DAM)/ZIF-8 MMMs in the form of both flat sheet membranes and hollow fiber membranes. The MMMs showed improved C_3H_6/C_3H_8 separation performances attributed to the well-matching of the polymer and ZIF-8.[151] Nevertheless, even with ZIF-8 loading

*Modified and reprinted with permission from "In-situ linker doping as an effective means to tune ZIF-8 fillers in mixed-matrix membranes for propylene/propane separation" by Sunghwan Park and Hae-Kwon Jeong, *Journal of Membrane Science*, 2020, 596, 117689-117696, Copyright 2020, Elsevier

as high as 48 wt%, the 6FDA-DAM/ZIF-8 MMMs fell short of meeting the commercial viability criteria (i.e., minimum C_3H_6 permeability of 1 Barrer and selectivity of 35).[239] It is noted that the intrinsic propylene and propane permeabilities of ZIF-8 are reported ~ 210 and ~ 2.5 Barrer, respectively.[141] As such, the minimum ZIF-8 loading in 6FDA-DAM required to meet the commercial viability criteria is estimated ~ 60 wt% based on Maxwell model. This strongly suggests the need to find better molecular sieving fillers and/or to further improve composite microstructures by developing better processing methods.

In general, it is quite time-consuming, expensive, and often impossible to find or synthesize more propylene-selective molecular sieving fillers including new ZIFs than ZIF-8.[240] A more rational strategy is to fine-tune the effective aperture size of ZIF-8 by introducing additional metal centers and/or linkers (known as hybrid ZIFs).[241-242] For example, Jeong et al.[242] showed mixed-metal CoZn-ZIF-8 membranes exhibited enhanced C_3H_6/C_3H_8 separation performance than mono-metallic ZIF-8 membranes. Computational studies by Krokidas et al.[243-244] revealed that mixing cobalt and zinc metal centers led to shortening of the metal-linker bond length and to increasing of the bond stiffness between metal centers and mIm linkers, consequently reducing the effective aperture size of ZIF-8 framework. Nair et al.[241, 245] first reported mixed-linker ZIFs, ZIF-8-90 and ZIF-7-8, via *de novo* synthesis and showed continuous control of effective aperture size and polarity [245] and drastic enhancement of their molecular sieving properties for light gas separations.[246-249] Very recently, Jeong et al.[250] reported doped-linker ZIF-8 showing tunable molecular sieving properties. Unlike mixed-linker ZIF-8 where both linkers are capable of forming isostructures of SOD-ZIF-8, doped-linker ZIF-8 has an additional linker (i.e., dopant linker) which alone is not capable of forming SOD-ZIF-8 structures. ZIF-8 particles doped with 2-

ethylimidazolate (eIm) showed restricted metal-linker flexibility, implying reduced effective aperture size.

Besides, microstructures of MMMs (i.e., interfacial structures and filler dispersion) play critical roles for their gas separation performances.[61, 251-252] Conventional physical blending methods for MMM preparation pose several challenges that often lead to poor microstructures including interfacial void formation and agglomeration of filler nanoparticles.[253] Recently, we reported the polymer-modification-enabled *in-situ* metal-organic framework formation (PMMOF) process as a scalable MMM fabrication strategy.[193] Since MOF filler nanoparticles formed *in-situ* inside a modified polyimide, the PMMOF was found highly effective in addressing some of the challenges of conventional MMM processing. The resulting 6FDA-DAM/ZIF-8 MMMs showed much higher C_3H_6/C_3H_8 separation than conventionally-prepared MMMs due to the better adhesion and dispersion of ZIF-8 as well as polymer densification. Moreover, the PMMOF decouples membrane fabrication from filler incorporation process, thereby rendering it commercially more attractive.

Here, we report eIm-doped ZIF-8-containing MMMs prepared by *in-situ* forming doped ZIF-8 fillers inside 6FDA-DAM polymer by PMMOF. *In-situ* grown eIm-doped ZIF-8 nanoparticles inside the polymer were characterized and compared with corresponding eIm-doped ZIF-8 particles that were solution precipitated. Binary propylene/propane separation performance of the 6FDA-DAM/eIm-doped ZIF-8 MMMs was measured and compared with that of conventionally prepared MMMs. Lastly, eIm-doped ZIF-8-based mixed-matrix hollow fiber membranes were prepared by PMMOF and their C_3H_6/C_3H_8 separation performance was examined.

5.2. Experimental

5.2.1. Materials

6FDA-DAM (Mw: 148 k, PDI: 2.14) was purchased from Akron Polymer Systems Inc. Sodium formate (HCOONa, ≥ 99 %, Sigma Aldrich), zinc nitrate hexahydrate ($Zn(NO_3)_2 \cdot 6H_2O$, 98 %, Sigma Aldrich), 2-methyimidazole (mIm) (C4H6N2, ≥ 98 %, Sigma Aldrich), and 2-ethylimidaole (eIm) ($C_5H_8N_2$, ≥ 98 %, Sigma Aldrich) were used. N,N-dimethylformamide (DMF) (C_3H_7NO, > 99.8 %, Alfa Aesar), ethyl acetate (EtOAc) ($C_4H_8O_2$, ≥ 99.5 %, VWR International), and methanol (CH_3OH, > 99.8 %, Alfa Aesar) were used as a solvent. All chemicals were used as received.

5.2.2. Synthesis of eIm-doped ZIF-8 particles by solution precipitation

A metal solution and a ligand solution were prepared separatly. The metal solution was prepared by dissolving 2.5 mmol of zinc nitrate hexahydrate in 15 ml methanol. The ligand solution was made by dissolving total 25 mmol of ligands in 15 ml methanol. The ligand solution was added to the metal solution and mixed for about 1 min. The ligand composition of each linker solution was as follows; 1) 25 mmol of mIm, 2) 20 mmol of mIm and 5 mmol of eIm, 3) 15 mmol of mIm and 10 mmol of eIm, 4) 10 mmol of mIm and 15 mmol of eIm, 5) 5 mmol of mIm and 25 mmol of eIm. The crystallization was carried out at 40 ^oC for 2 h in a Teflon-lined stainless-steel autoclave. It is noted that the autoclave was used for consistency since the crystallization temperature was varied and optimized. The powder samples were collected by centrifugation with 8000 RPM for 20 min. The samples were re-dispersed in methanol by sonication for 30 min and then centrifuged again at the same conditions. The purification steps were repeated two more times to achieve high purity particles. After the purification, the powders were dried at 60 ^oC for

overnight. The samples were denoted as eImx-ZIF-8 where the subscript represents the eIm fraction of the total linkers present in a linker treatment solution, ranging from 0.2 ~ 0.8.

5.2.3. Preparation of 6FDA-DAM/eIm-doped ZIF-8 MMMs by PMMOF

Thin 6FDA-DAM polymer films were prepared on porous α-alumina disks (diameter of 2.2 cm) made according to a previous recipe described elsewhere.[246] In a typical preparation, a polymer solution was prepared by dissolving 0.25 g of 6FDA-DAM in 12.25 g of DMF. 2.4 ml of the polymer solution was slowly dropped onto the polished side of a porous α-alumina disk. Immediately, the sample was placed in a vacuum oven pre-heated at 150 ^{o}C and dried for 1 day, forming a polymer film with a thickness of 8.0 ± 1.5 μm on the α-alumina disk. PMMOF process was then applied to the polymer film as detailed in our recent report.[193] The hydrolysis of the polymer film was carried out in a sodium formate solution (100 mmol of sodium formate in 30 ml of D.I. water). The polymer film was vertically located in a custom-made Teflon holder and then placed in a Teflon-lined autoclave containing the sodium formate solution. The hydrolysis was conducted at 120 ^{o}C for 5 h. After washed with deionized (DI) water overnight using a lab shaker, the sample was subjected to an ion exchange by immersing it in an ion exchange solution (20 mmol of zinc nitrate hexahydrate in 30 ml of DI water) for 3 h. After briefly washed with methanol, the ion-exchanged sample was put into a ligand solution prepared by dissolving 25 mmol of linker mixtures in total in 30 ml of methanol with varying eIm compositions; 0%, 20%, 40%, 60%, and 80%. A ligand treatment was executed in a Teflon-lined autoclave at 40 ^{o}C for 2 h, followed by washing with methanol overnight. Lastly, the sample was thermally imidized at 220 ^{o}C for 3 h in a pre-heated convection oven. Hereafter, the eIm-doped ZIF-8 containing MMMs were named as PI/eImx-ZIF-8 (x = 0.2, 0.4, 0.6, or 0.8) where the subscript represents the eIm fraction of total linkers in the linker treatment solution.

5.2.4. Preparation of PI/eIm-doped ZIF-8 MMMs by physical blending

For comparison, MMMs were also prepared on porous α-alumina disks using conventional physical blending. Preformed eIm-doped ZIF-8 particles of proper amounts (i.e., 4.8 mg of ZIF-8, 4.6 mg of $eIm_{0.2}$-ZIF-8, 3.9 mg of $eIm_{0.4}$-ZIF-8, 2.8 mg of $eIm_{0.6}$-ZIF-8, 1.2 mg of $eIm_{0.8}$-ZIF-8) were fully dispersed in 0.98 g of DMF under sonication for 30 min. 20 mg of 6FDA-DAM was then added to an eIm-doped ZIF-8 suspension, followed by further sonication for 30 min. 2.4 ml of the prepared polymer/filler solution was slowly dropped onto an α-alumina disk. Immediately after, the sample was placed in a pre-heated oven at 150 ^{o}C and dried for 1 day at the same temperature under vacuum.

5.2.5. Coating of 6FDA-DAM on polymer hollow fibers

Polyethersulfone (PES) microfiltration hollow fibers (surface pore size of ~ 200 nm, Repligen Co.) were coated with thin 6FDA-DAM layers by dip-coating inside a glove bag saturated with EtOAc. A 6FDA-DAM solution was prepared by dissolving 0.50 g of 6FDA-DAM in 12.0 g of EtOAc. An as-purchased PES hollow fiber was dipped in the prepared polymer dope solution. Immediately after, the fiber was taken out and dried vertically in the glove bag for 7 h. The resulting 6FDA-DAM coated PES hollow fiber was dried at room temperature for 1 h and then at 60 ^{o}C overnight in a convection oven.

5.2.6. Characterizations

Scanning electron microscope (SEM) images were taken using a JEOL JSM-7500F at an acceleration voltage of 5 keV with 15 mm working distance. Transmission electron microscope (TEM) images were collected using a FEI Tecnai FE-TEM under cryogenic conditions using

microtomed samples. Powder X-ray diffraction (PXRD) was collected using a Rigaku Miniflex II at a 2 θ range of 5 – 40 ° with Cu-Kα radiation (λ = 1.5406 Å). Nitrogen adsorption isotherms were obtained using ASAP 2010 (Micromeritics) at 77 K after degassing samples at 150 °C under vacuum for 24 h. Solution proton nuclear magnetic resonance (1H-NMR) spectra were obtained using a Bruker Avance III (500 MHz system). Solution NMR samples were prepared by dissolving ZIF samples in 550 μL of deuterated acetic acid-d4. Fourier transform infrared (FT-IR) spectra were measured by a Nicolet iS5 spectrophotometer (Thermo Scientific) equipped with an attenuated total reflectance (ATR, iD7) accessory. X-ray photoelectron spectroscopy (XPS) was performed using an Omicron ESCA+ with Mg X-ray source at 300W. Thermogravimetric analysis (TGA, Q50 TA instruments) was carried out at a temperature range from 25 °C to 700 °C at heating rate of 10°C/min.

5.2.7. Gas permeation measurements

Gas permeation characteristics of membranes were measured by the Wicke-Kallenbach technique using equimolar binary C_3H_6 and C_3H_8 gas mixture at room temperature under atmospheric pressure. Feed gas was provided at 20 cm3 min-1, while the permeate side was swept by argon gas with the flow rate of 20 cm3 min-1. A steady-state of gas permeation was declared when the deviation of measured gas permeance was less than 1 % with 30 min interval. The permeated gas compositions were determined using a gas chromatography (GC 7890A, Agilent) equipped with a flame ionized detector (FID) and a HP-plot Q column.

5.3. Results and discussion

5.3.1. Characterizations of MMMs containing 2-ethylimidazole (eIm)-doped ZIF-8

MMMs containing 2-ethylimidazole (eIm)-doped ZIF-8 (i.e., $Zn(mIm)_{2-x}(eIm)_x$) were prepared by *in-situ* growth of ZIFs in 6FDA-DAM polyimide (PI) using PMMOF. As discussed in Chapter 2, PMMOF includes four steps: hydrolysis of PI, ion exchange, ligand treatment, and imidization. As detailed in our recent report,[193] each step was described and characterization results were presented in Chapter 2. Figure 5.1a presents the XRD patterns of the resulting PI/eIm-doped ZIF-8 MMMs, showing SOD-ZIF-8 phases regardless of the eIm percentages.[250] As shown in the scanning electron micrographs of MMMs in Figure 5.1b-f, many particles were found on the surface. The substantial fractions of ZIF crystals *in-situ* formed inside the polymer were confirmed by conducting surface acid treatment.

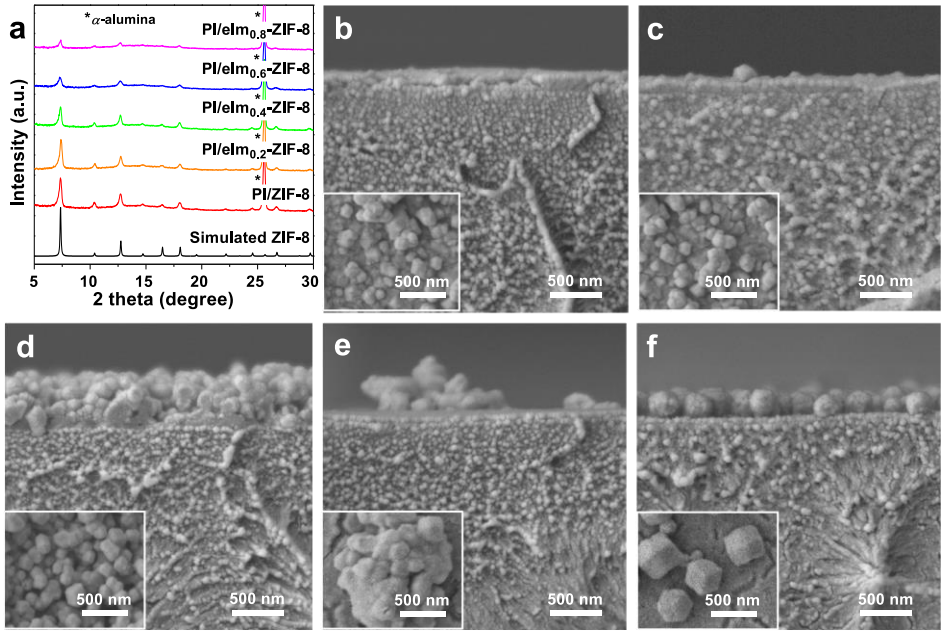

Figure 5.1. (a) XRD patterns of as-prepared PI/ZIF-8 and PI/eIm-doped ZIF-8 MMMs by PMMOF. SEM images of as-prepared MMMs by PMMOF; PI/ZIF-8 (b), $PI/eim_{0.2}$-ZIF-8 (c), $PI/eim_{0.4}$-ZIF-

8 (d), PI/eim$_{0.6}$-ZIF-8 (e), and PI/eim$_{0.8}$-ZIF-8 (f). The inset images on the bottom left are top views of the corresponding samples.

As the eIm content increased, the crystal size of surface-bounded eIm-doped ZIF-8 increased from ~ 100 nm to ~ 500 nm (Figure 5.1b-f), following the same trend as solvothermally synthesized eIm-doped ZIF-8.[250] Since the pKa value of eIm (8.00) is higher than that of mIm (7.86),[254] the higher pKa might decrease the crystal growth rate, forming larger crystals.[183] In stark contrast, the size of eIm-doped ZIF-8 grown inside the polymer seemed to be not affected by changing eIm-doping compositions. Figure 5.2 presents cross-sectional transmission electron micrographs and electron diffraction patters of the membranes. As indicated by arrows in Figure 5.2 a1-d1, spherical shaped eIm-doped ZIF-8 particles of sub-100 nm in size were observed. Interestingly, a poorly defined phase was observed as well (Figure 5.2 a1-d1). Considering its morphology, the unknown phase seems lacking crystallinity, which might be similar to the so called not well-crystallized ZIF deposit formed in confined spaces reported by Ma and Tsapatsis et al.[255] This is possibly due to the *in-situ* nucleation and growth of eIm-doped ZIF-8 crystals in confined spaces (i.e., polymer free volume).[193] It is reminded that a larger filler size fundamentally limits the preparation of ultra-thin active layers (i.e., < 1 μm) in MMMs.[142] However, the sub-100 nm size of *in-situ* formed eIm-doped ZIF-8 fillers, independent of eIm-doping compositions, is highly desirable to achieve ultra-thin active layers.

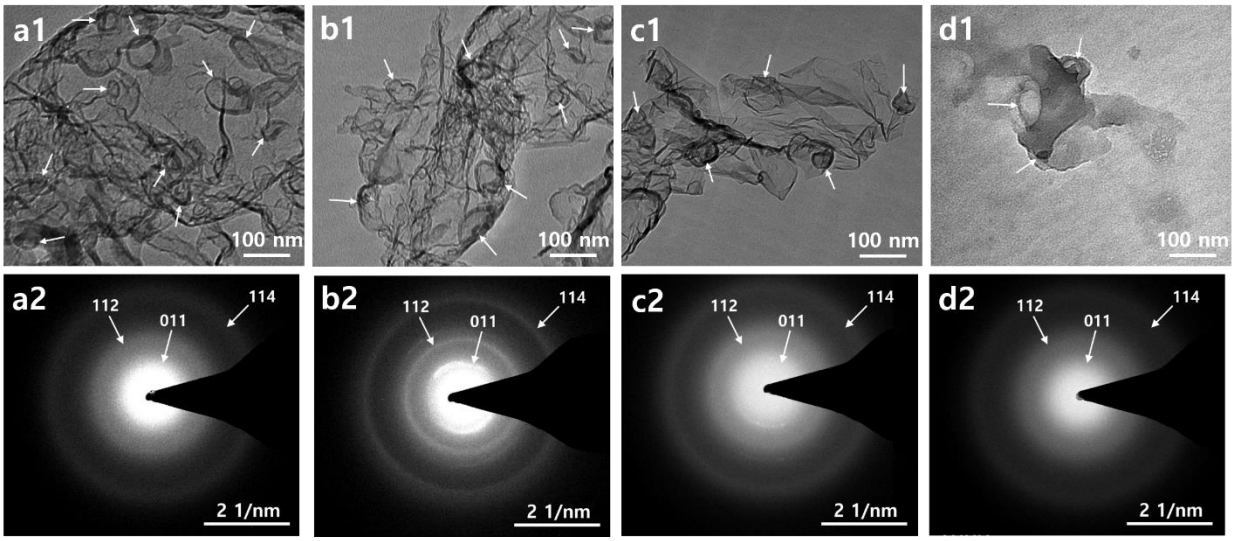

Figure 5.2. (a1-d1) TEM images of PI/eIm-doped ZIF-8 MMMs (left column) and (a2-d2) their corresponding SAED patterns (right column). PI/eIm$_{0.2}$-ZIF-8 (a). PI/eIm$_{0.4}$-ZIF-8 (b). PI/eIm$_{0.6}$-ZIF-8 (c). PI/eIm$_{0.8}$-ZIF-8 (d).

^{1}H-NMR analysis was performed to determine the actual compositions of eIm linkers doped in ZIF-8 fillers inside the polymer. Surface-bound crystals were completely removed from the samples in order to measure only those embedded inside the polymer. Figure 5.3 shows ^{1}H-NMR spectra of the samples with various eIm percentages in the ligand treatment solutions. Based on the NMR analysis, the percentages of eIm linkers actually doped in ZIF-8 were estimated approximately 7, 16, 31, and 48 mol% with 20, 40, 60, and 80 mol% in the linker treatment solutions, respectively. At first, the lower eIm content in ZIF-8 than in precursor solutions was attributed due to the different diffusion rates of linkers in the polymer, which can be varied by size, solvent, affinity with polymer, and others. The eIm compositions in doped-ZIF-8 were, however, comparable with those of solution precipitated ones; approximately 6, 15, 28, and 48 mol%. This strongly indicates that the doping of eIm was not significantly affected by diffusion of linkers

under the current conditions. Instead, the doping was likely determined by the fact that mIm was more favorably incorporated to ZIF-8 than the bulkier eIm.[250] Nevertheless, the more eIm present in the precursor solutions, the more eIm doped in ZIF-8 frameworks.

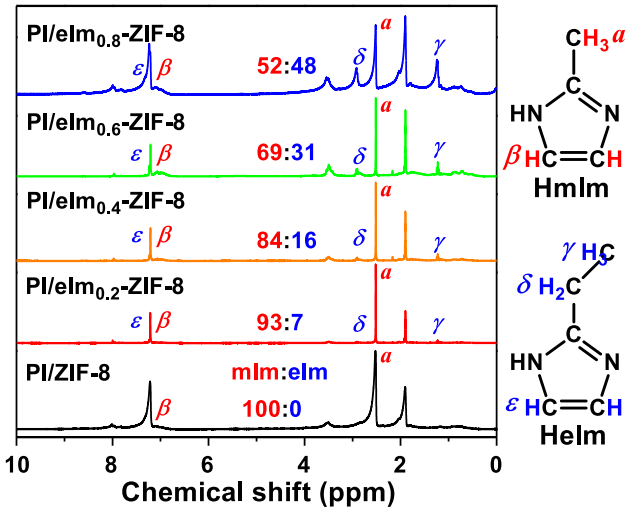

Figure 5.3. ^{1}H-NMR spectra of PI/ZIF-8 and PI/eIm-doped ZIF-8 MMMs by PMMOF. The ratios between mIm and eIm incorporated in the frameworks were noted and determined based on the following formula: eIm% = $(A_{\gamma}/3)/[(A_{\beta} + A_{\varepsilon})/2]$ where A represents peak area.

It is important to quantify the filler loadings in MMMs to investigate the effect of fillers on gas separations.[1, 151] The loadings of ZIF-8 and eIm-doped ZIF-8 in MMMs were determined by thermal oxidization after eliminating surface-bound ZIFs by the acid treatment (Table 5.1). Interestingly, the filler content in MMMs gradually decreased as the content of eIm dopants increased (Figure 5.4). This is further confirmed by a gradual decrease in the XRD intensity of MMMs as the eIm content increased regardless of the presence of surface-bound eIm-doped ZIF-8 crystals (Figure 5.1a). The decrease in eIm-doped ZIF-8 loadings with increasing eIm fractions

appeared following the same trend as the yields of doped ZIF-8 synthesized in solutions (Figure 5.4), strongly suggesting the presence of a close correlation between the filler contents in MMMs and the yield of solution-precipitated doped crystals. In other words, the filler contents in MMMs by PMMOF can be deduced by the yield of solution-precipitated doped fillers.

Table 5.1. Quantification of eIm-doped ZIF-8 in MMMs.

Sample	ZnO of MMMs (wt%)	ZnO of ZIFs (wt%)	ZIF loading in MMMs (wt%)
PI/ ZIF-8	8.3 (6.9)	35.9	19.3
PI/eIm$_{0.2}$-ZIF-8	8.1 (6.7)	35.8	18.8
PI/eIm$_{0.4}$-ZIF-8	7.2 (5.8)	35.2	16.3
PI/eIm$_{0.6}$-ZIF-8	5.6 (4.2)	34.6	12.3
PI/eIm$_{0.8}$-ZIF-8	3.3 (1.9)	33.8	5.7

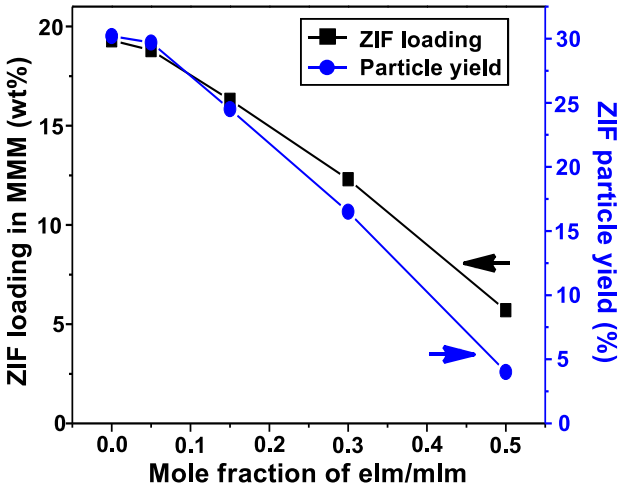

Figure 5.4. Comparison of eIm-doped ZIF-8 loadings in MMMs by PMMOF and yields of solution-precipitated eIm-doped ZIF-8 crystals.

5.3.2. Propylene/propane separation performance of eIm-doped ZIF-8-based MMMs

The C_3H_6/C_3H_8 separation performances of the PI/eIm-doped ZIF-8 MMMs are presented in Figure 5.5 and Table 5.2. Despite the relatively lower loadings of eIm-doped ZIF-8 (12.3 - 18.8 wt%) in MMMs than that of ZIF-8 (19.3 wt%), the PI/eIm-doped ZIF-8 MMMs exhibited improved C_3H_6/C_3H_8 separation performances as compared to the PI/ZIF-8 (Figure 5.5). The MMMs containing eIm-doped ZIF-8 fillers with the relatively low eIm- dopant content (i.e., PI/eIm$_{0.2}$-ZIF-8) exhibited the C_3H_6 permeability ~ 62 % higher than the PI/ZIF-8 with a similar separation factor (Figure 5.5). On the contrast, the PI/eIm$_{0.6}$-ZIF-8 showed the opposite trend that there was a slight decrease in the C_3H_6 permeability by ~ 18 % with a significantly enhanced separation factor (~ 111 %), meeting the so called commercially-viable performance criteria.[129, 239] (Figure 5.5). It is noted that most of the previous studies on MMMs for C_3H_6/C_3H_8 separation failed to significantly improve separation factors except a few.[1, 135, 138, 256-262] In the case of the PI/eIm$_{0.4}$-ZIF-8, the C_3H_6/C_3H_8 separation performance was in between those of the PI/eIm$_{0.2}$-ZIF-8 and the PI/eIm$_{0.6}$-ZIF-8; both the C_3H_6 permeability (~ 16 %) and the C_3H_6/C_3H_8 separation factor (~ 75 %) were higher than those of the PI/ZIF-8 (Figure 5.5). The PI/eIm$_{0.8}$-ZIF-8 showed the separation performance lower than the PI/ZIF-8 possibly due to the ~ 3-fold lower ZIF contents in polymer (5.7 wt%). In light of this, the higher loading of eIm-doped ZIF-8 in the polymer would lead to further improved C_3H_6/C_3H_8 separation performances of MMMs as drawn in the arrows in Figure 5.5.

Interestingly, the enhanced separation factor of PI/eIm-doped ZIF-8 MMMs with increasing eIm-dopant contents seems to deviate from eIm-doped ZIF-8 polycrystalline membranes recently reported by our group.[250] For the polycrystalline membranes, a systematic increase in the permeance and a decrease in the separation factors were observed as the eIm dopant content

increased. This opposite trend might be attributed to the relatively low eIm doping (up to 2.5 % eIm in the framework) in the case of the polycrystalline membranes,[250] since there exists a threshold concentration of doped linker for tuning of effective aperture size.[263] More importantly, unlike eIm-doped ZIF-8 polycrystalline membranes, the flexibility of ligands is likely restricted by a strong interaction with the surrounding polymer, thereby reducing the flip-flopping motion of eIm-doped ZIF-8 in MMMs.[264]

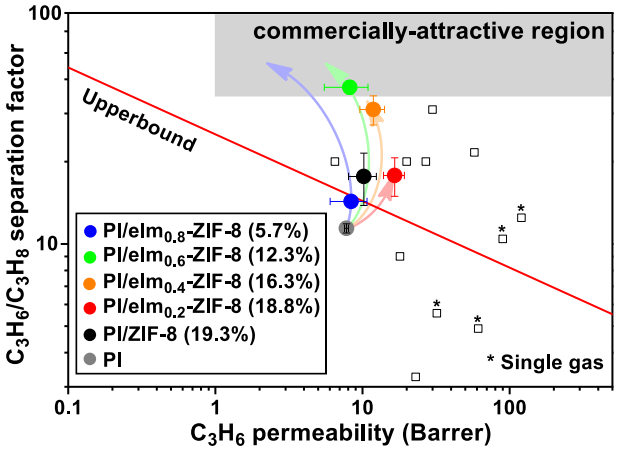

Figure 5.5. C_3H_6/C_3H_8 upper bound plot of PI/ZIF-8 and PI/eIm-doped ZIF-8 MMMs prepared by PMMOF (solid circle) and the MMM data in literatures (open rectangular).[5, 28-36] Note: the arrows are arbitrarily drawn for illustration purpose to indicate the hypothetical separation performance improvement of PI/eIm-doped ZIF-8 MMMs when eIm-doped ZIF-8 loading increases up to ~20 wt%.

Table 5.2. Propylene/propane separation performances of PI, PI/ZIF-8 and PI/eIm-doped ZIF-8 MMMs prepared by PMMOF as well as physical blending.

MMM fabrication method	Sample	ZIF loading (wt%)	Propylene permeability (Barrer)	Propane permeability (Barrer)	Propylene/propane separation factor
-	PI	-	7.79 ± 0.24	0.68 ± 0.05	11.4 ± 0.4
PMMOF	PI/ZIF-8	19.3	10.23 ± 2.19	0.58 ± 0.25	17.7 ± 3.8
	PI/eIm$_{0.2}$-ZIF-8	18.8	16.57 ± 2.68	0.93 ± 0.30	17.8 ± 2.9
	PI/eIm$_{0.4}$-ZIF-8	16.3	11.87 ± 2.27	0.38 ± 0.12	31.0 ± 3.8
	PI/eIm$_{0.6}$-ZIF-8	12.3	8.21 ± 2.70	0.22 ± 0.06	37.4 ± 2.1
	PI/eIm$_{0.8}$-ZIF-8	5.7	8.38 ± 2.35	0.59 ± 0.18	14.3 ± 0.4
Blending	PI/ZIF-8	19.3	21.88 ± 1.20	1.32 ± 0.11	16.5 ± 0.5
	PI/eIm$_{0.2}$-ZIF-8	18.8	42.94 ± 1.98	2.92 ± 0.21	14.7 ± 0.4
	PI/eIm$_{0.4}$-ZIF-8	16.3	28.51 ± 1.25	1.67 ± 0.02	17.1 ± 0.5
	PI/eIm$_{0.6}$-ZIF-8	12.3	22.99 ± 0.35	1.21 ± 0.01	19.1 ± 0.1
	PI/eIm$_{0.8}$-ZIF-8	5.7	12.68 ± 0.23	0.90 ± 0.06	14.0 ± 0.6

As such, we attributed the systematic enhancement in the C_3H_6/C_3H_8 separation performances of eIm-doped ZIF-8 containing MMMs to the effective tuning of ZIF-8 apertures resulting from relatively high eIm doping [250] and restricted flip-flopping motion of linkers.[264] To further investigate, N_2 adsorption studies were conducted on eIm-doped ZIF-8 crystals that were solvothermally synthesized (Figure 5.6). Table 5.3 summarizes the surface areas and the pore volumes of the eIm-doped ZIF-8 particles, which are consistent with the previous report.[250] As shown in Figure 5.6, there were two threshold pressures of sudden increases in N_2 adsorption, known as "gate-opening".[265] The second gate-opening pressure moved to the higher relative pressure with increasing eIm contents and eventually disappeared for the doped ZIF-8 with eIm content greater than 31 mol% (eIm$_{0.6}$-ZIF-8). Since the gate-opening of ZIFs is caused by the reorientation of flexible organic linkers,[248, 265] this shift in the gate-opening pressure toward higher relative pressure strongly suggests that the flexibility of ZIF-8 was restricted by incorporation of eIm linkers. Furthermore, the ATR-FTIR spectra shown in Figure 5.7 clearly exhibit blue-shifts of the Zn-N vibration of eIm-doped ZIF-8 at ~ 420 cm^{-1}, meaning the enhanced stiffness of Zn-N

bonds upon eIm doping, i.e., restricted flexibility of ZIF-8.[130, 250] Since the ethyl group in eIm exhibits greater electron donating ability than the methyl group in mIm, the Zn-N bond distance with eIm is expected shorter and mechanically stiffer than that with mIm. The restricted flip-flopping motion of eIm-doped ZIF-8 with incorporation of eIm linkers is expected to reduce the effective aperture size of eIm-doped ZIF-8.[130] On the other hand, as shown in Figure 5.6, the first gate-opening pressure decreased with higher eIm contents, indicating that eIm-doped ZIF-8 might possess more open micropore structure of eIm-doped ZIF-8 and/or more favorable interaction with adsorbates than ZIF-8.[265] The more open micropore is likely due to the reconfiguration of the aperture structure resulting from the presence of bulkier eIm linkers while the more favorable interaction with adsorbates might be owing to the bulkier ethyl groups. The slight increase in the C_3H_6 permeability of the PI/eIm$_{0.2}$-ZIF-8 compared to that of the PI/ZIF-8 might be attributed mostly to the change in the microstructure, not much to do with eIm doping since the actual dopant concentration (~ 7%) is much less than a percolation threshold.[263] As the dopant concentration further increases as in the case of the PI/eIm$_{0.4}$-ZIF-8 and PI/eIm$_{0.6}$-ZIF-8, the significantly enhanced C_3H_6/C_3H_8 separation factors of the PI/eIm-doped ZIF-8 MMMs were observed, which were attributed likely to the reduced effective aperture size of the eIm-doped ZIF-8.

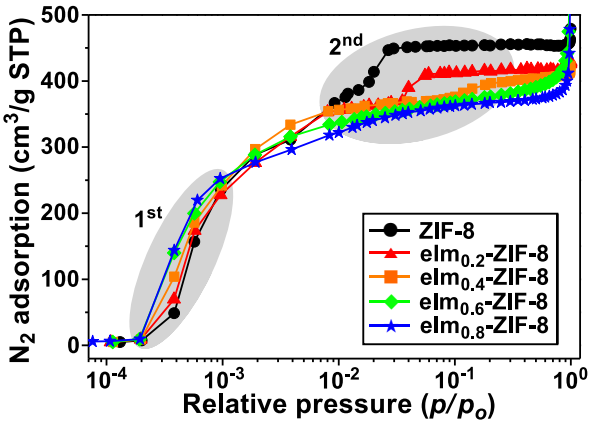

Figure 5.6. N_2 adsorption isotherms of ZIF-8 and eIm-doped ZIF-8 at 77K with log scale abscissa plot.

Table 5.3. Micropore volume, and Brunauer-Emmet-Teller (BET) and Langmuir surface areas of ZIF-8 and eIm-doped ZIF-8 particles.

Sample	Micropore volume ($cm^3\ g^{-1}$)	BET surface area ($m^2\ g^{-1}$)	Langmuir surface area ($m^2\ g^{-1}$)
ZIF-8	0.693	1764.1	1985.8
$eIm_{0.2}$-ZIF-8	0.615	1606.2	1823.1
$eIm_{0.4}$-ZIF-8	0.524	1593.5	1793.5
$eIm_{0.6}$-ZIF-8	0.508	1513.6	1696.4
$eIm_{0.8}$-ZIF-8	0.449	1458.6	1624.9

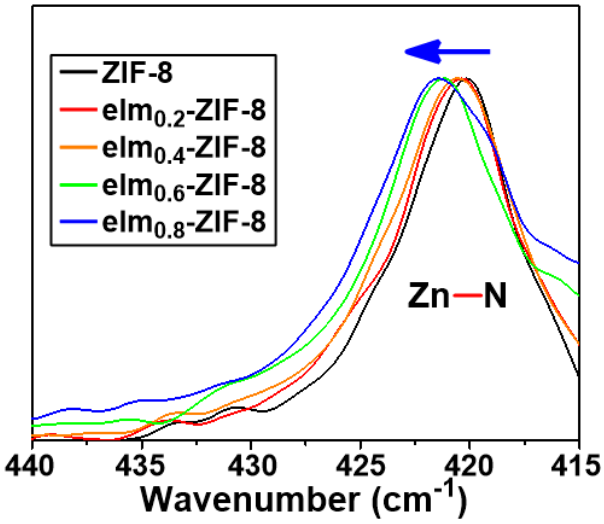

Figure 5.7. ATR-FTIR spectra of Zn-N bonds of ZIF-8 and eIm-doped ZIF-8 particles.

As comparison, we prepared PI/eIm-doped ZIF-8 MMMs using conventional physical blending method. Figure 5.8 and Table 5.2 compare their C_3H_6/C_3H_8 separation performances with those by PMMOF. Comparing with the MMMs by PMMOF, the PI/eIm-doped ZIF-8 MMMs

prepared by blending method showed higher permeabilities and lower C_3H_6/C_3H_8 separation factors, which might come from the relatively poor adhesion between polymer and filler (Figure 5.9). The poor adhesion between eIm-doped ZIF-8 and polymer matrix possibly might be owing to the eIm concentration as well as the increased particle size with increasing eIm contents. This denotes that the PMMOF is more effective in obtaining enhanced MMM microstructures (i.e., interfacial structures, filler dispersion, etc.). The PI/ZIF-8 by PMMOF exhibited decreased propylene permeability than the PI/ZIF-8 prepared by blending method, likely due to the densification of polymer upon PMMOF (i.e., reduced polymer free volume upon *in-situ* growing ZIF fillers).[193] The densification of polymer upon PMMOF might also play a role in enhancing the separation factors.

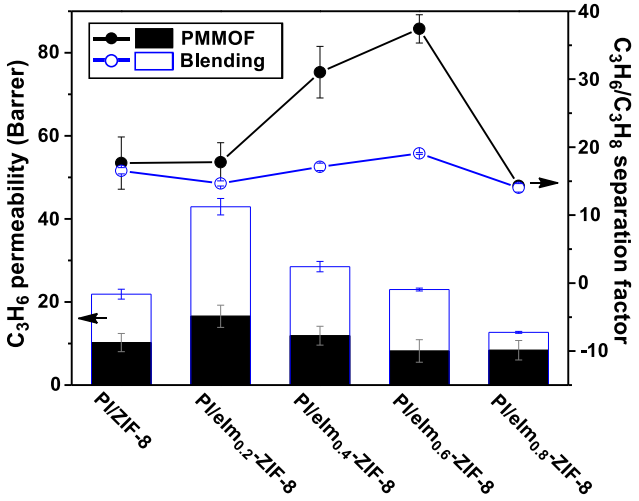

Figure 5.8. Comparison of C_3H_6/C_3H_8 separation performance of PI/eIm-doped ZIF-8 MMMs prepared by PMMOF and a conventional blending method.

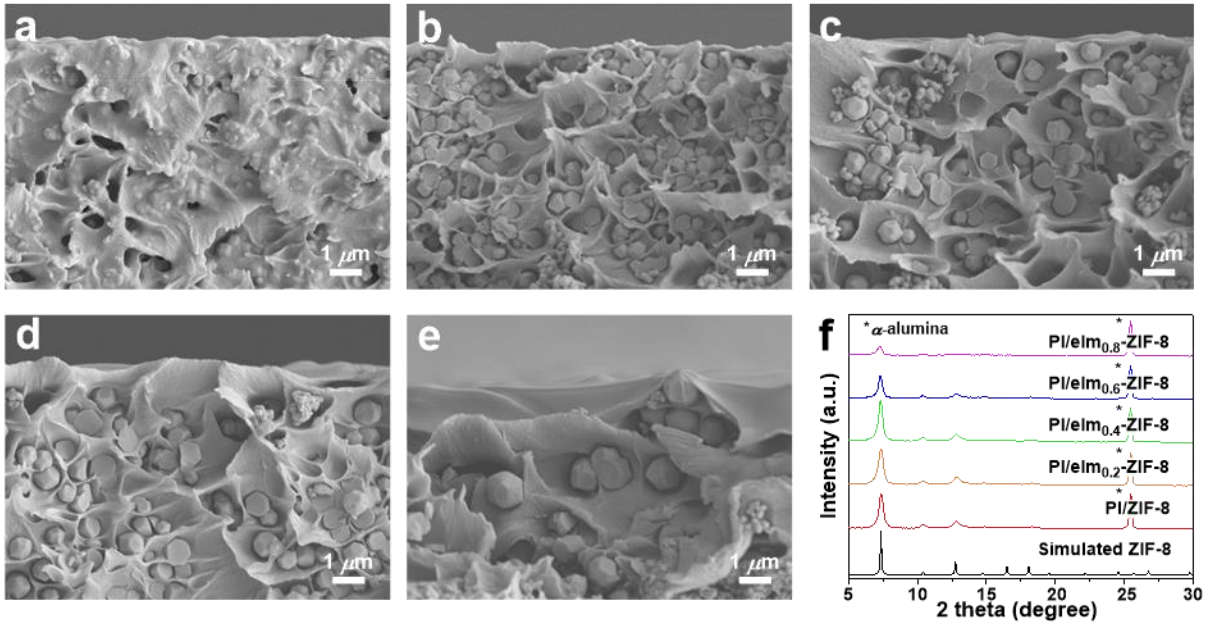

Figure 5.9. SEM images of PI/eIm-ZIF-8 MMMs prepared by physical blending. PI/ZIF-8 (a), PI/eIm$_{0.2}$-ZIF-8 (b), PI/eIm$_{0.4}$-ZIF-8 (c), PI/eIm$_{0.6}$-ZIF-8 (d), PI/eIm$_{0.8}$-ZIF-8 (e), XRD diffraction patterns of PI/ZIF-8 and PI/eIm-ZIF-8 MMMs prepared by physical blending (f).

5.3.3. eIm-doped ZIF-8-based mixed-matrix hollow fiber membranes

For large-scale commercial gas separation applications, hollow fiber membranes are preferred than flat sheet membranes.[142, 266] As a proof-of-concept, the eIm-doping strategy combined with PMMOF was applied on scalable hollow fiber membranes (HFMs). Thin and selective 6FDA-DAM layers were coated with thicknesses of ~ 1 μm on porous PES hollow fibers (Figure 5.10a). The PI coating layers were transformed to PI/ZIF-8 (Figure 5.10b) or PI/eIm$_{0.6}$-ZIF-8 (Figure 5.10c) layers while maintaining membrane thickness. The formation of ZIF-8 and eIm-doped ZIF-8 was confirmed by X-ray diffraction (Figure 5.10d). Comparing with the PI/ZIF-8 mixed-matrix hollow fiber membranes (MMHFMs), the PI/eIm-doped ZIF-8 MMHFMs showed the improved

C_3H_6/C_3H_8 separation factor and comparable C_3H_6 permeance (Figure 5.10e), which is consistent with the results of flat membranes.

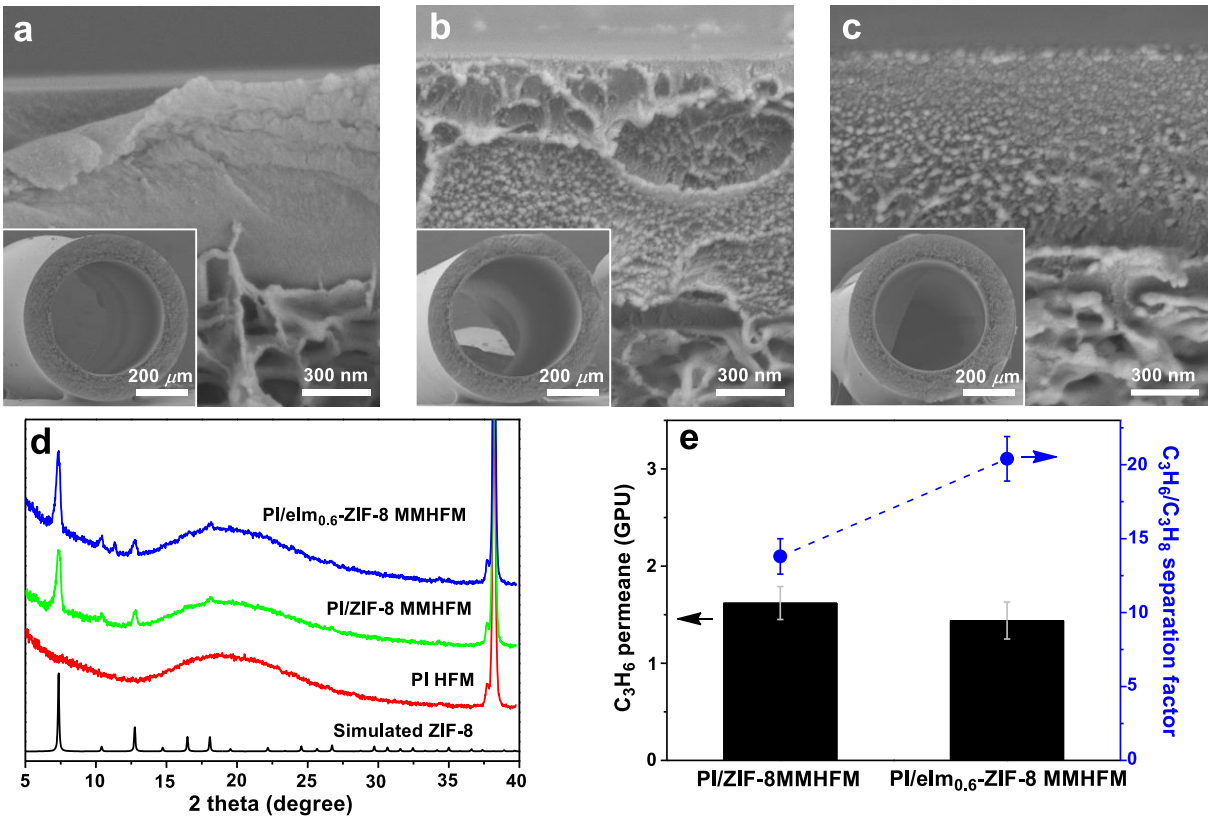

Figure 5.10. SEM images of PI HFM (a), PI/ZIF-8 MMHFM (b), and PI/eIm$_{0.6}$-ZIF-8 MMHFM (c). (d) XRD diffraction patterns of PI HFM and PI/ZIF MMHFMs. (e) C_3H_6/C_3H_8 separation performance of PI/ZIF-8 and PI/eIm$_{0.6}$-ZIF-8 MMHFMs.

5.4. Conclusion

Here, we reported, for the first time, a linker doping strategy as a novel means to improve gas separation performances of MMMs. 2-ethylimidazole (eIm) was used as a dopant ligand to tune the effective aperture size of ZIF-8 filler in MMMs. eIm-doped ZIF-8 fillers with the dopant

content as high as 50 mol% were successfully formed *in-situ* in MMMs using the PMMOF process. The eIm-doped ZIF-8 containing MMMs with a relatively low eIm content (7 mol%) enlarged the pore structure of ZIF-8, enhancing C_3H_6 permeability (~ 62 %) while maintaining C_3H_6/C_3H_8 separation factor as compared with ZIF-8 containing MMMs. On the contrary, at the relatively high eIm content (~ 31 mol%), the eIm-doped ZIF-8 in MMMs dramatically improved the C_3H_6/C_3H_8 separation factor (~ 111 %) with a small decrease in the propylene permeability despite the slightly low filler contents. The improvement in the C_3H_6/C_3H_8 separation factor was attributed to the restricted flip-flopping motion of ZIF-8, thereby reduced the effective aperture size of ZIF-8 owing to the presence of bulkier eIm in the framework. Finally, the linker doping strategy along with the *in-situ* MOF formation based MMM fabrication strategy (PMMOF) was successfully applied to prepare eIm-doped ZIF-8-containing mixed-marix hollow fiber membranes, showing enhanced C_3H_6/C_3H_8 separation factor as compared with those MMMs containing undoped ZIF-8. The ability to tune the molecular sieving properties of ZIF-8 fillers in MMMs combined with the capability of producing MMHFMs with sub-micron thick selective layers is expected a major step toward the scalable applications of high-performance MMMs for gas separations.

CHAPTER VI

CONTROLLING PROPYLENE/PROPANE SEPARATION PERFORMANCES FOR MIXED-MATRIX MEMBRANES DERIVED FROM IN-ISTU FORMATION OF ZIF-8 BY CROSSLINKING

6.1. Introduction

For gas separation, mixed-matrix membranes (MMMs) are promising alternatives to the current polymer membranes whose performances are limited by the trade-off between permeability and selectivity.[3] A number of studies demonstrated that incorporating highly permeable and/or selective molecular sieve fillers in polymer matrices led to the improved gas separation performances of polymer membranes, overcoming their intrinsic limitations.[43, 48, 105]

Despite their potentials, there have been only a few reports on MMMs in more scalable geometries such as hollow fiber forms (i.e., mixed-matrix hollow fiber membranes with submicron selective skin layers) for large-scale applications.[45] This is probably due to several challenges of applying established hollow fiber spinning processes to mixed-matrix hollow fiber membrane (HFMMM) fabrication, often leading to poor interface between polymer matrix and fillers,[267] filler agglomeration,[60] several micron-thick selective skin layers,[268] and others. It turns out extremely difficult to address the above-mentioned challenges when fillers need to be incorporated in submicron selective skin layers of HFMMMs.[268]

Recently, we reported a novel MMM fabrication technique namely polymer-modification enabled *in-situ* metal-organic framework formation (PMMOF) to address the above-mentioned issues associated with scalable MMM formation.[124-125, 269] The PMMOF decouples a polymer membrane fabrication step from a filler incorporation step by growing MOF fillers *in-situ* in a

modified-polyimide film. The resulting MMMs exhibited excellent C3 separation as compared to those MMMs prepared by the conventional blending method. Furthermore, we demonstrated the first MMM module containing multi-stranded mixed-matrix hollow fiber membranes with submicron-thick selective skin layers by transforming a preformed module with PI-coated polyethersulfone hollow fibers using the PMMOF.[270]

Unfortunately, the PMMOF led to a significant decrease in the gas permeability.[124, 269] The low permeability was attributed possibly to polymer densification/rigidification upon the *in-situ* formation of fillers.[124] It is known that the gas permeability in polymer decreases due to reduced polymer free volume and/or restricted chain mobility.[271] Polymer rigidification is expected more pronounced in the MMMs prepared by the PMMOF than in those conventional MMMs. This is because *in-situ* filler formation during the PMMOF results in fillers with much smaller in size (< 100 nm) and enhanced compatibility with polymer, thereby providing larger and more compatible polymer/filler interfaces, consequently more restricted polymer chain mobility.[272] Therefore, we hypothesize that polymers with more rigid structures and higher free volumes may reduce further rigidification/densification upon the PMMOF, thereby mitigating the permeability decrease.

Cross-linking polymer chains is an effective means to get a more rigid polymer structure. Cross-linking has been widely used in polymer gas separation membranes to enhance their resistance of plasticization under aggressive condensable gas conditions such as CO_2, CH_4, and C_3H_6.[273-274] As a derivative of 4,4′-(Hexafluoroisopropylidene)diphthalic anhydride (6FDA)-base polyimides, 4,4'-(hexafluoroisopropylidene) diphthalic anhydride- diaminobenzoic acid 2,4,6-trimethyl-1,3-phenylenediamine (6FDA-DAM:DABA) is a thermally cross-linkable polymer and has been extensively studied for gas separations.[275-278] Sub-T_g cross-linking of 6FDA-

DAM:DABA (3:2) led to excellent plasticization resistance.[275, 277] Furthermore, the nano-scale chain rearrangement upon cross-linking enhanced the gas permeabilities of the polymer several times.[275]

In this study, we prepared ZIF-8-containing MMMs by the PMMOF using cross-linked 6FDA-DAM:DABA (3:2) polymer films. The polymer films were cross-linked at different temperatures, resulting in different degrees of cross-linking. We investigated the effect of degree of cross-linking on the *in-situ* formation of ZIF-8 filler particles in the cross-linked polymers and tested the C_3H_6/C_3H_8 separation performances of the MMMs. The results indicated that the degree of cross-linking played a key role in mitigating the C_3H_6 permeability and controlling the C_3H_6/C_3H_8 separation performances.

6.2 Experimental

6.2.1. Materials

4,4'-(hexafluoroisopropylidene) diphthalic anhydride- diaminobenzoic acid 2,4,6-trimethyl-1,3-phenylenediamine (6FDA-DAM:DABA) (3:2) with Mw of 223k and PDI of 2.37 was purchased from Akron Polymer Systems Inc. Polymer of intrinsic microporosity-1 (PIM-1) was kindly provided from Hanyang University in Korea. Sodium formate (HCOONa, ≥ 99 %), zinc nitrate hexahydrate ($Zn(NO_3)_2 \cdot 6H_2O$, 98 %), and 2-methylimidazole (HmIm) ($C_4H_6N_2$, 99 %) were provided from Sigma-Aldrich. Methanol (CH_3OH, > 99.8 %), chloroform ($CHCl_3$, > 99.8 %), and N,N-dimethylformamide (DMF) (C_3H_7NO, > 99.8 %) were obtained from Alfa Aesar. All chemicals were used as-received without further purification.

6.2.2. Preparation of polymer membranes

Polymer films were prepared by a drop casting method on porous α-alumina disks. The preparation of α-alumina disks is described elsewhere.[279] 6FDA-DAM:DABA (3:2) was dissolved in DMF with a polymer concentration of 2 wt%. 0.24 ml of the polymer solution was slowly dropped onto an α-alumina disk. Immediately after, the sample was placed in a vacuum oven pre-heated at 150 ^{o}C and dried for 1 day. For a reference, PIM-1 polymer films were prepared. 2 wt% of a PIM-1 polymer solution prepared by dissolving the polymer in $CHCl_3$ was casted onto an α-alumina disk in a solvent-saturated glove bag. For both samples, the polymer layers on α-alumina disks were ~ 8 μm thick.

6.2.3. Heat-treatment of polymer membranes

The film samples of 6FDA-DAM:DABA (hereafter, PI) were thermally cross-linked at 370 ^{o}C and 420 ^{o}C, denoted as X-PI(370) and X-PI(420), respectively, for 120 min with a ramp rate of 10 ^{o}C min^{-1} under the argon flow of 200 cm^3 min^{-1} in a tube furnace (Thermo Scientific, USA). Before heating, the reactor was purged with UHP argon for at least 1 h at room temperature. The gas flow rate was controlled by a mechanical flowmeter (Cole Palmer).

6.2.4. Preparation of MMMs by PMMOF

The PMMOF process involves hydrolysis, ion exchange, ligand treatment, and imidization.[124] The cross-linked polymer films were hydrolyzed at different conditions depending on the degree of cross-linking. 0.67 M and 3.33 M sodium formate solutions were prepared by dissolving 20 mmol and 100 mmol of sodium formate in 30 ml of D.I. water, respectively. X-PI(370) was hydrothermally hydrolyzed at 120 ^{o}C for 3 h in a Teflon-lined

autoclave containing the 0.67 M sodium formate solution with the film vertically placed in a custom-made Teflon holder. X-PI(420) was similarly hydrolyzed in the 3.33 M sodium formate solution at at 120 ^{o}C for 5 h. It is noted that the hydrolysis conditions were chosen to achieve similar degree of hydrolysis (i.e., degree of deimidization) for both X-PIs to avoid the sample disintegration upon the hydrolysis step. For ion exchange, the hydrolyzed films were saturated with zinc solutions of varying concentrations (20 mmol, 40 mmol, and 60 mmol of zinc nitrate hexahydrate in 40 ml of DI water) for 2 h. After briefly washing with methanol, the films were then immersed into a ligand solution (25 mmol of HmIm in 30 ml of methanol) and the reaction was carried out at 40 ^{o}C for 2 h. Afterward, the films were washed in flash methanol for 1 day at room temperature using a lab shaker. Finally, the thermal imidization was performed at 250 ^{o}C for 3 h in a pre-heated convection oven. For comparison, PIM-1/ZIF-8 MMMs were prepared by slightly modifying the PMMOF process. The prepared PIM-1 films were immersed into the ion exchange solutions with the zinc concentration of 20 mmol and 40 mmol. Followed by the brief washing step with methanol, the ligand treatment was conducted using the ligand solution prepared by dissolving 25 mmol of HmIm in 30 ml of methanol at 40 ^{o}C for 2 h. After washing the samples with methanol at room temperature overnight, those are dried at 120 ^{o}C for 1 h.

6.2.5. Characterizations

Thermogravimetric analysis (TGA, Q50 TA instruments) was carried out at a temperature range from 25 ^{o}C to 700 ^{o}C with a heating rate of 10 ^{o}C/min under air or argon flow of 50 cm^3 min^{-1}. Differential scanning calorimetry (DSC, Q20 TA instruments) was performed by ramping the temperature from 25 ^{o}C to 420 ^{o}C with a rate of 5 ^{o}C/min under 100 cm^3 min^{-1} of argon flow using Tzero aluminum hermetic pans. All DSC results were taken from 1st scan to avoid polymer

thermal hysteresis. Electron micrographs were taken using a scanning electron microscope (SEM, JEOL JSM-7500F) operated at an acceleration voltage of 5 keV with a working distance of 15 mm. Powder X-ray diffraction (PXRD, Rigaku Miniflex II) patterns were taken using Cu-Kα radiation (λ = 1.5406 Å) at a 2 θ range of 5 – 40 °. Fourier transform infrared (FT-IR) spectra were taken using a spectrometer (Nicolet iS5 Thermo Scientific) equipped with an attenuated total reflectance (ATR, iD7) accessory in a wavenumber range of 4000 – 400 cm^{-1} with a resolution of 4 cm^{-1} and 16 scans.

6.2.6. Gas permeation measurements

C3 gas permeation tests were conducted by the Wicke-Kallenbach technique using equimolar binary C_3H_6 and C_3H_8 gas mixture at room temperature under 1 atm. Both feed and argon sweep gases were supplied at a flow rate of 20 cm^3 min^{-1}. The permeation performances of membranes were measured at steady-states. Steady states were declared when the variation of the gas permeance reached at less than 1% with 30 min intervals. The gas compositions on the permeate side were determined using a gas chromatography (GC 7890A, Agilent) equipped with a flame ionized detector (FID) and a HP-plot Q column.

6.3. Results and discussion

6.3.1. Fabrication of cross-linked-PI/ZIF-8 MMMs by the PMMOF

Figure 6.1 shows two different approaches to prepare MMMs consisting of ZIF-8 fillers embedded in cross-linked 6FDA-DAM:DABA (3:2) polymer (X-PI). The first approach seems feasible with either the conventional blending methods or the PMMOF process. It involves the incorporation of ZIF-8 fillers in an uncross-linked polymer (PI) followed by the cross-linking of

MMMs at temperature below the decomposition temperature of ZIF-8 (i.e., T_d of ZIF-8 ~ 300 °C and ~ 500 °C under air and inert gas, respectively).[280] However, this approach poises a critical challenge that ZIF-8 structure can be compromised not only by thermal treatment at high temperature of above 330 °C but also by the presence of acidic DABA moieties (i.e., carboxyl groups).[163, 275] Furthermore, Lively et al.[163] reported the gelation of ZIF-8-containing 6FDA-DAM:DABA (4:1) dope solutions upon sonication, thereby fabricating 6FDA-DAM:DABA (4:1)/ZIF-8 MMMs with extra cautions.[163] Considering these challenges, we take the second approach where the polymer is first cross-linked, followed by the *in-situ* formation of ZIF-8 fillers inside the cross-linked polymer via the PMMOF process as illustrated in Figure 6.1. Since cross-linked polymers are not easily dissolved in common organic solvents,[275, 281] the PMMOF is expected much more effective in fabricating X-PI/ZIF-8 MMMs than the conventional blending methods.

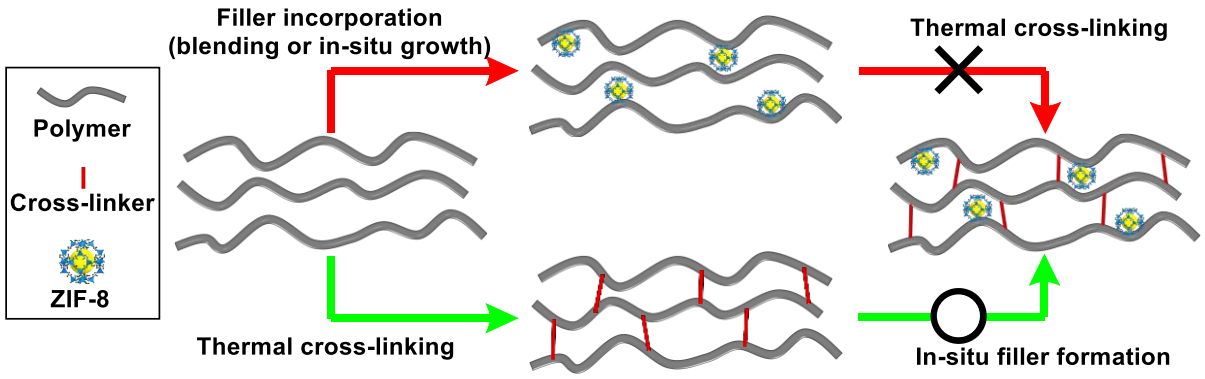

Figure 6.1. Schematic illustration of preparing cross-linked PI polymer/ZIF-8 MMMs with two different routes: filler incorporation followed by cross-linking (red) vs. cross-linking followed by filler formation (green).

6.3.2. Thermal cross-linking of polymer

Figure 6.2a presents the thermal decomposition behaviors of PI and X-PI at two different heat-treatment temperatures of 370 °C and 420 °C, which are below and above of T_g reported (~ 387 °C), respectively.[275, 278] For the PI, a minor weight loss was observed in the temperature span of ca. 400 ~ ca. 465 °C with weight change of ~ 3.3 wt% (Figure 6.2a). This minor weight loss is attributed to the thermal decarboxylation and subsequent generation of phenyl radicals, consequently leading to a decarboxylation-induced polymer cross-linking (Figure 6.2b).[275, 282] Following the minor weight loss, there was a major weight loss resulting from degradation of polymer chain backbones in the temperature range of ca. 465 °C ~ 800 °C with the additional weight loss of ~ 46 wt% (Figure 6.2a). The X-PI samples treated at 370 °C (hereafter, X-PI (370)) and at 420 °C (hereafter, X-PI (420)) showed ~ 2.9 wt% and ~ 0.4 wt% loss in the range of ca. 400 ~ ca. 465 °C, respectively (Figure 6.2a). This indicates a partial loss of the carboxyl groups of the X-PI (370) and almost complete removal of the carboxyl groups of the X-PI (420).

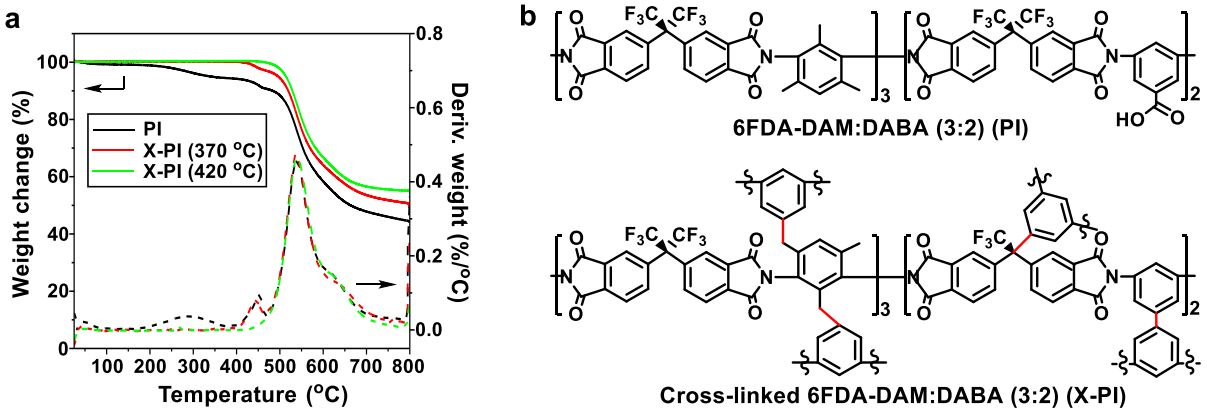

Figure 6.2. (a) TGA thermograms of free-standing 6FDA-DAM:DABA (3:2) (PI), X-PI (370), and X-PI (420) and (b) a possible chemical structure of the cross-linked PI in comparison with the chemical structure of the PI.

To confirm cross-linking, the solubilities of free-standing X-PI films were tested by immersing 10 mg of the samples in 2 ml of DMF at room temperature. As expected, the pristine PI films were immediately dissolved in DMF, whereas the X-PI films were swollen but preserved for at least one day, confirming a decrease in their solubilities upon cross-linking (Figure 6.3). The X-PI(370) was swollen more intensely and rapidly than the X-PI(420) likely due to its lower degree of cross-linking.[283] Figure 6.4 presents the X-ray diffraction patterns of the X-PI samples in comparison of that of the PI sample. As shown in the figure, the PI sample shows two broad peaks at 2θ of ~ 13.4 º and ~ 15.5 º, suggesting the presence of two inter-chain distances, ~ 6.6 Å and ~ 5.7 Å. Upon cross-linking, the intensity of the peak at ~ 13.4 º increased while that of the peak at ~15.5 º decreased. This result is consistent with the previous report that the average inter-chain distance was enlarged upon cross-linking (i.e., the portion of the inter-chain distance of ~ 6.6 Å was increased relative to that of ~ 5.7 Å), suggesting an increase in the polymer free-volume.[275] Furthermore, the T_g of the X-PI samples increased from ~ 367 ºC to ~ 381 ºC and ~ 415 ºC upon cross-linking at 370 ºC and 420 ºC, respectively (see Figure 6.5), indicating significantly restricted polymer chain flexibility with the increase in the degree of cross-linking.

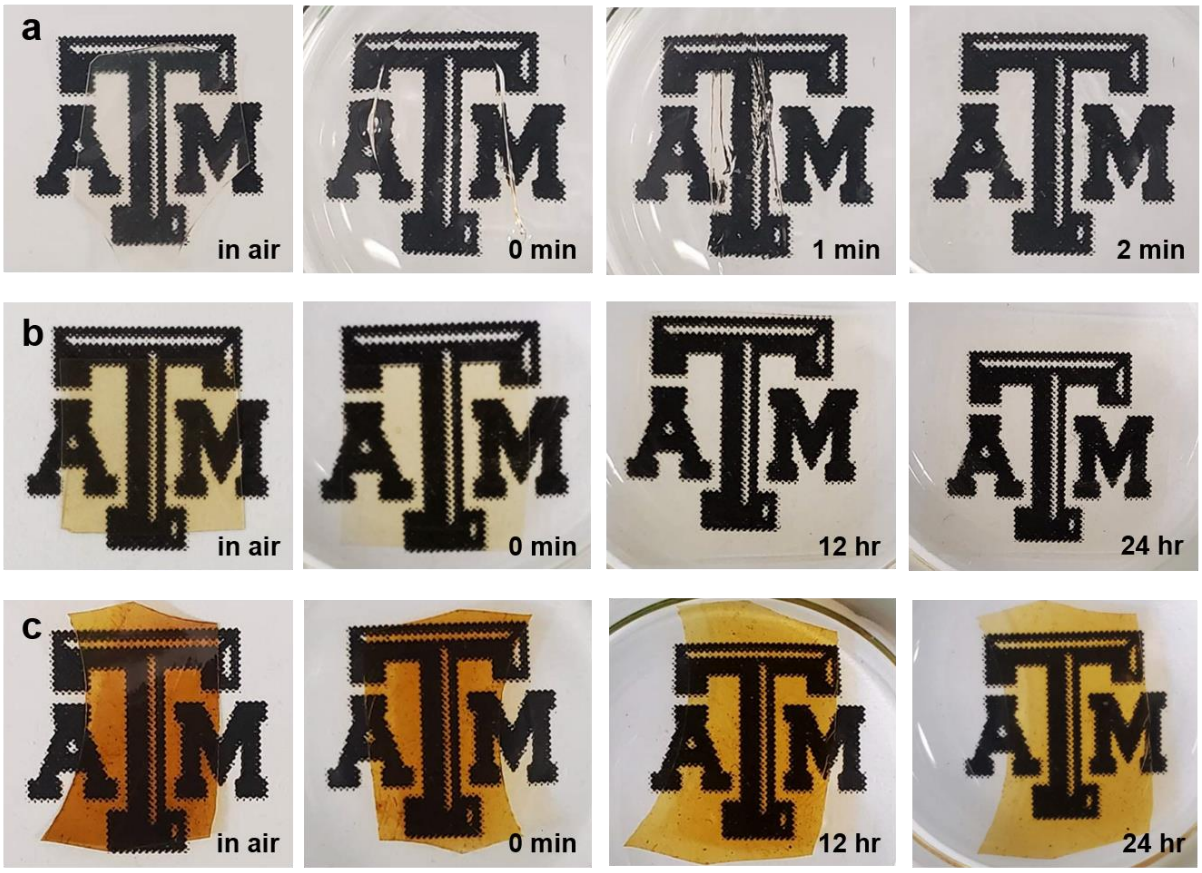

Figure 6.3. Photographic images of PI (a), X-PI(370) (b), and X-PI(420) (c) in air and DMF.

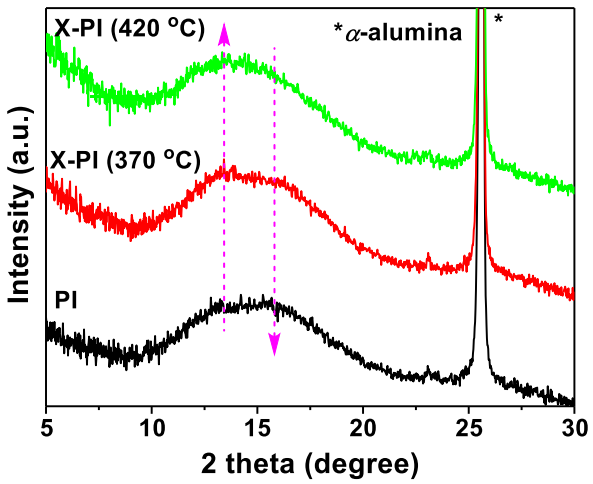

Figure 6.4. XRD patterns of PI and X-PIs coated on α-alumina supports.

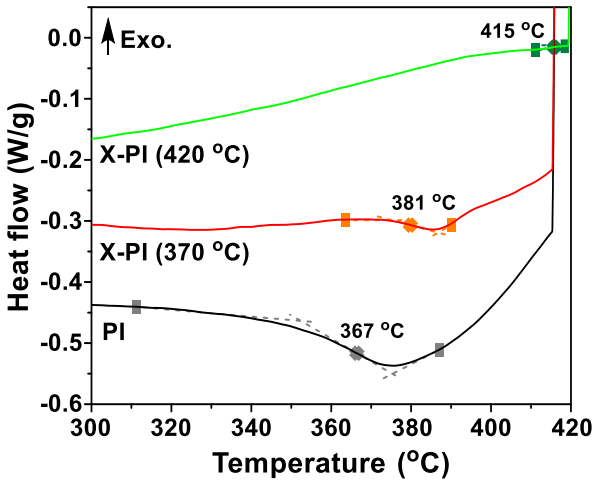

Figure 6.5. DSC thermogram of PI and X-PIs.

6.3.3. *In-situ* ZIF-8 formation in cross-linked polymers

The *in-situ* formation of ZIF-8 in X-PIs was performed by the PMMOF which involves four steps: hydrolysis, ion exchange, ligand treatment, and imidization.[124] First, the imide rings of a X-PI(420) were cleaved via hydrolysis, turning it into a cross-linked poly(amic acid) (X-PAA). It was confirmed that the intensities of the asymmetric C=O stretching (~ 1722 cm^{-1}) and C-N stretching (1355 ~ 1359 cm^{-1}) of imide rings decreased as compared with that of the C-C stretching of benzene rings (~ 1486 cm^{-1}) upon hydrolysis (Figure 6.6 and Figure 6.7). Based on the ratio of the C-N and C-C stretching intensities, the degree of imidization (DI) of the X-PAA was estimated at ~ 70 %.[124] It is noted that the less cross-linked X-PI(370) samples were more prone to hydrolysis than the more cross-linked X-PI(420), requiring milder hydrolysis to achieve the similar DI. Due to the similar degree of hydrolysis, the X-PI (370) showed similar FT-IR spectra (see Figure 6.7). Once ZIF-8 was *in-situ* formed, the X-PAA/ZIF-8 was imidized, resulting in the increase in the normalized intensities of the asymmetric C=O and C-N stretching by that of the C-C stretching of the X-PAA/ZIF-8 (Figure 6.6 and Figure 6.7). It indicated imide

ring formation from the carboxylic salts of the X-PAA/ZIF-8, thereby forming an X-PI/ZIF-8. The degree of imidization of the X-PI/ZIF-8 increased to ~ 90 % from ~ 60 % of the X-PAA/ZIF-8, which is comparable with that reported in our previous work.[124]

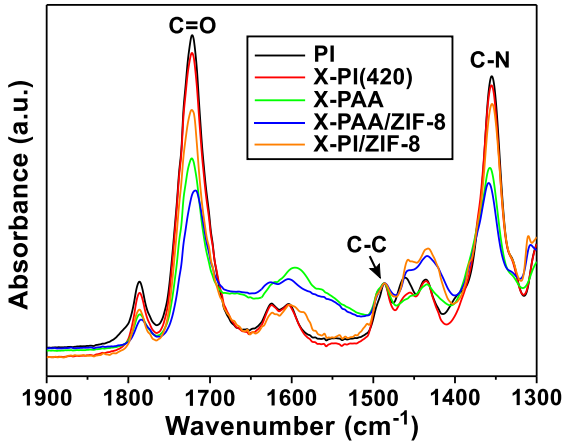

Figure 6.6. FT-IR spectra of the X-PI(420) sample at each polymer modification step in comparison with that of the pristine PI.

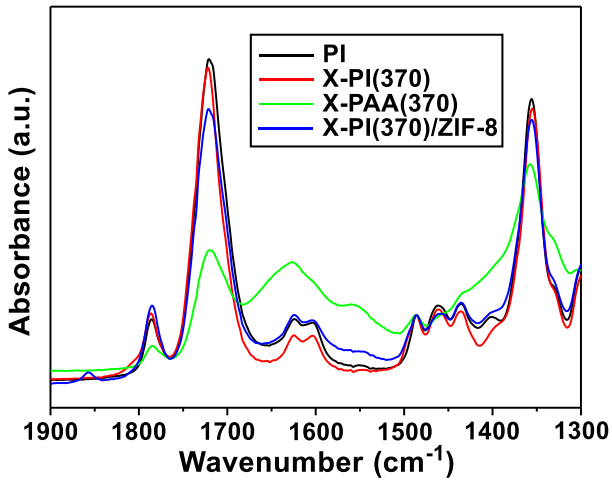

Figure 6.7. FT-IR spectra of the X-PI(370) sample at each polymer modification step in comparison with that of the pristine PI.

To confirm the presence of *in-situ* formed ZIF-8 inside the X-PIs, all surface-bound ZIF-8 particles were removed by gently wiping the top sample surface with a Kimwipe soaked with a diluted acid solution (i.e., 0.1 M of H_2NO_3). As shown in Figure 6.8, the XRD intensities of both X-PI/ZIF-8 samples were decreased after the acid treatment. The corresponding SEM images showed that surface-bound ZIF-8 clusters were eliminated by the acid treatment (Figure 6.9). Nevertheless, there remained ZIF-8 diffraction patterns (Figure 6.8), indicating that ZIF-8 particles were formed inside the X-PI films by the PMMOF. In addition, the XRD showed that the (011) peak of the X-PI(370)/ZIF-8 is stronger than that of the X-PI(420)/ZIF-8, indicating that more ZIF-8 filler particles formed inside the X-PI(370) than the X-PI(420). On the other hand, the broader and very small (011) peak of the PI/ZIF-8 along with unidentified peaks strongly suggested the crystallinity of ZIF-8 formed *in-situ* inside the uncross-linked PI was compromised likely due to the decomposition by the acidic DABA moieties of the polymer (Figure 6.8).

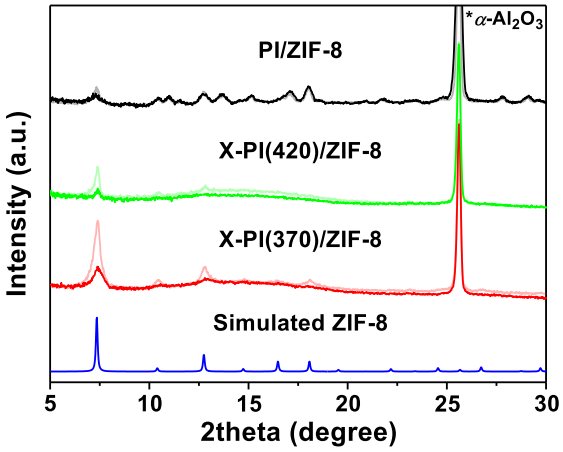

Figure 6.8. XRD patterns of X-PI(370)/ZIF-8, X-PI(420)/ZIF-8, and PI/ZIF-8. The overlapped lines in lighter colors are the diffraction patterns of the samples before acid treatments for the comparison.

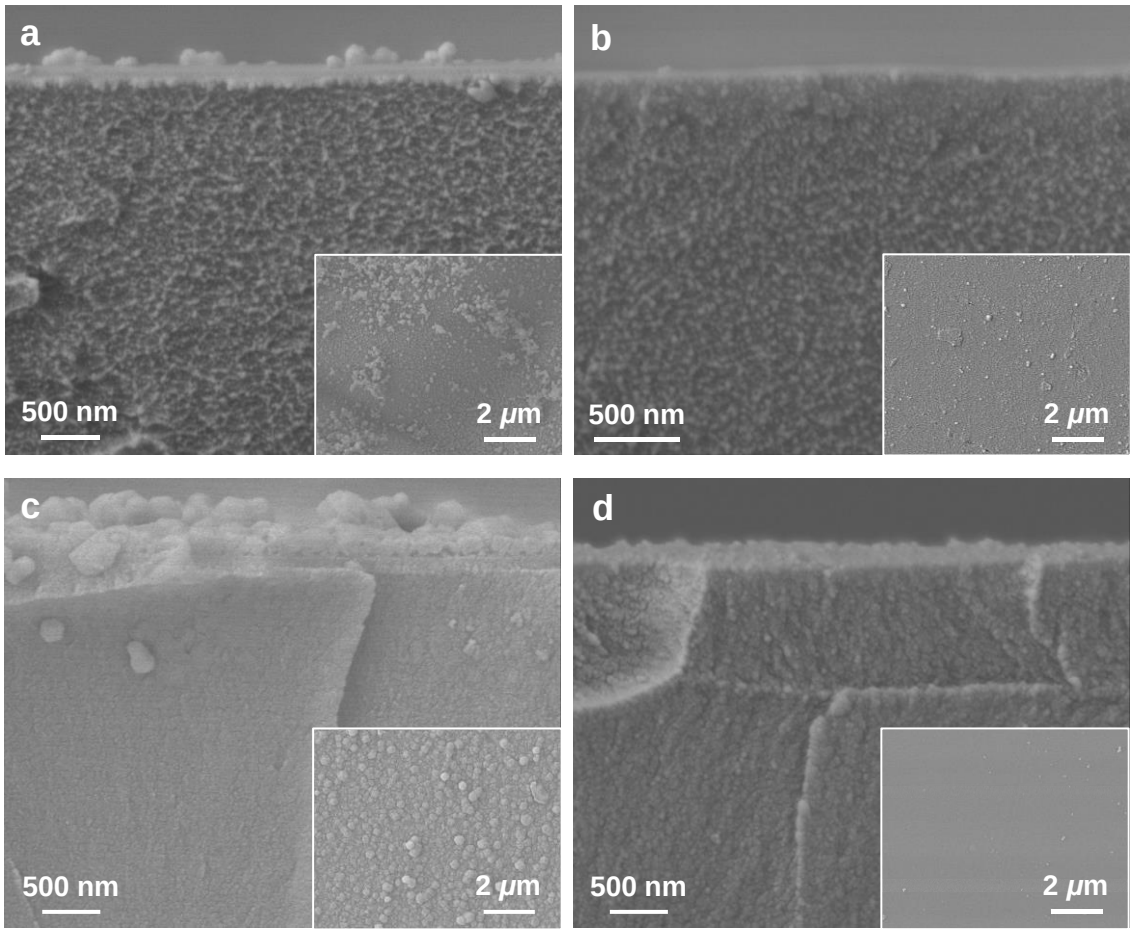

Figure 6.9. Cross-sectional SEM images of (a) as-prepared and (b) acid-treated X-PI(370)/ZIF-8 and (c) as-prepared and (d) acid-treated X-PI(420)/ZIF-8. The inset images are the corresponding top views.

As seen in Figure 6.9a and b, the X-PI(370)/ZIF-8 showed a rough cross-sectional surface, which was consistent with the previous observation made in uncross-linked 6FDA-DAM/ZIF-8 MMMs.[124] In stark contrast, the X-PI(420)/ZIF-8 showed a smooth cross-sectional surface (Figure 6.9c and d), which might be attributed to the suppressed formation of ZIF-8 as observed in the XRD. The high degree of cross-linking likely impeded zinc uptakes in the free volume by obstructing a swelling of the polymer,[284] thereby leading to the smaller amount of ZIF particles forming than in the X-PI(370)/ZIF-8. Under the same ion exchange conditions (i.e., 0.5 M zinc solution), the ZIF-8 loadings in the X-PI(370)/ZIF-8 and the X-PI(420)/ZIF-8 were estimated at ~ 8 wt% and ~ 3 wt%, respectively(the detailed analysis on ZIF-8 loadings is presented in the paragraph below). As such, it was surmised that the rough cross-sectional surface of the X-PI stemmed likely from an *in-situ* formation of ZIF-8 particles in the swollen polymer.

As the zinc concentration of the ion exchange solution increased from 0.5 M to 1.0 M to 1.5 M, the ZIF-8 loading in the X-PI increased continuously (Figure 6.10 and Table 6.1).[124] The ZIF-8 loading was determined based on the residual weight of the corresponding free-standing MMM sample upon thermal oxidation (Figure 6.11). As shown in Figure 6.10, the X-PI(370)/ZIF-8 samples showed not only significantly more ZIF-8 loadings but also much sharper increase than the X-PI(420)/ZIF-8. This is likely due to the favorable formation of ZIF-8 particles resulting from the lower degree of cross-linking of the X-PI(370).

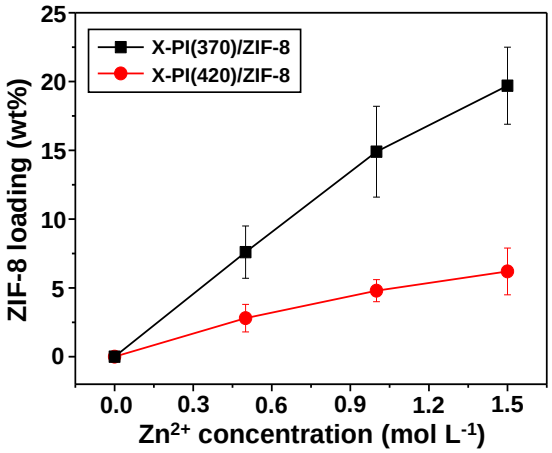

Figure 6.10. ZIF-8 loadings in X-PI/ZIF-8 MMMs as a function of the zinc concentrations of ion exchange solutions.

Table 6.1. Loading percentages of ZIF-8 *in-situ* formed in cross-linked polymers.

Sample	Zinc concentration in ion exchange solution		
	0.5 M	1.0 M	1.5 M
X-PI(370)/ZIF-8	7.6 ± 1.9 wt%	14.9 ± 3.3 wt%	19.7 ± 2.8 wt%
X-PI(420)/ZIF-8	2.8 ± 1.0 wt%	4.8 ± 0.8 wt%	6.2 ± 1.7 wt%

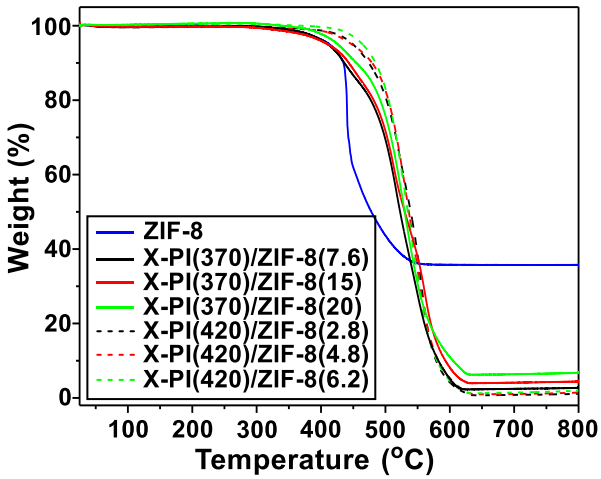

Figure 6.11. TGA thermogram of ZIF-8 and MMMs under air flow. The numbers in a bracket are the concentrations of zinc in ion exchange solutions with a unit of molarity.

To check the chain flexibility of the X-PI/ZIF-8 MMMs, differential scanning calorimetry (DSC) experiments were performed. As shown in Figure 6.12a, the T_g of the X-PI(370)/ZIF-8 decreased relative to that of the X-PI(370), suggesting the cross-linked polymer became less rigid upon the PMMOF possibly due to the incomplete imidization. Nevertheless, the T_g of the X-PI(370)/ZIF-8 remained unchanged regardless of ZIF-8 loading, indicating no further chain rigidification. In contrast, the T_g of the uncross-linked 6FDA-DAM/ZIF-8 MMMs increased slightly relative to that of the 6FDA-DAM, indicating that the uncross-linked polymer became more rigid upon ZIF-8 incorporation (i.e., chain rigidification) (Figure 6.12b). Upon the *in-situ* formation of ZIF-8 fillers, the uncross-linked polymer underwent the more intensive rigidification than the cross-linked rigid polymer. As seen in Figure 6.12c, the X-PI(470)/ZIF-8 MMMs showed no distinct endothermic peaks in the DSC curves in the tested range of temperatures (up to 420 ^{o}C). Instead, the polymers were decomposed prior to a glass transition owing to their rigid structure (Figure 6.12c).

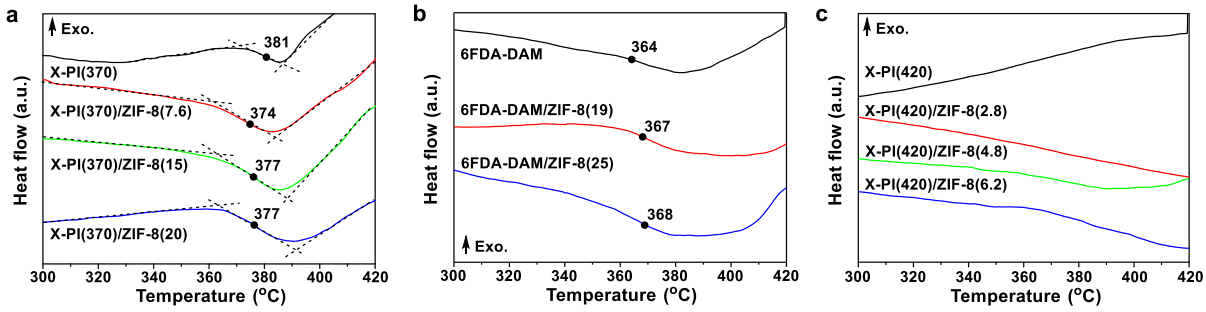

Figure 6.12. DSC thermograms of X-PI(370) and X-PI(370)/ZIF-8 MMMs. The numbers in the brackets are the ZIF-8 loadings.

6.3.4. C_3H_6/C_3H_8 separation performance

Figure 6.13a represents the C_3H_6 permeabilities and C3 separation factors of the X-PI and the X-PI/ZIF-8 MMMs as a function of ZIF-8 loading.[124] Despite the lower ZIF-8 loadings, the X-PI(420)/ZIF-8 MMMs showed a more dramatic decrease in the C_3H_6 permeability than the X-PI(370)/ZIF-8 MMMs (Figure 6.13a and Table 6.2). The X-PI(420)/ZIF-8 showed a sharper increase in the separation factor than the X-PI(370)/ZIF-8 likely due to the more severe polymer densification (Figure 6.13a and Table 6.2). While the both X-PI/ZIF-8 membranes showed a steady increase in the separation factor at the relatively low ZIF-8 fractions, the X-PI(370)/ZIF-8 exhibited a sudden reduction in both separation factor and C_3H_6 permeability when the loading was greater than ~ 15 wt% (Figure 6.13a).

The X-PI/ZIF-8 MMMs, in particular, the X-PI(370)/ZIF-8 MMMs, showed relatively high C3 separation factors with relatively low C_3H_6 permeability in comparison with those MMMs reported recently (Figure 6.13b).[1, 124-125, 138, 140, 256, 258, 260, 262, 285-291] The C3 separation performance of the X-PI(420)/ZIF-8 tended to follow the upper bound with the increased filler loadings (Figure 6.13b). In stark contrast, the X-PI(370)/ZIF-8 MMMs showed significantly increased separation factor (i.e., from ~ 18 to ~ 43) with a small reduction in the permeability (i.e., from ~ 3.1 Barrer to ~ 2.3 Barrer), satisfying the criteria for commercial C3 separation (i.e., C_3H_6 permeability > 1 Barrer and C3 separation factor > 35) (Figure 6.13b).[292] Although the X-PI(420)/ZIF-8 displayed more pronounced permeability reduction than the X-PI(370)/ZIF-8, the X-PI(420)/ZIF-8 MMMs showed higher C_3H_6 permeability than the X-PI(370)/ZIF-8 MMMs due to the high permeability of the neat polymers. It is noted that the neat X-PI(420) showed higher C_3H_6 permeability than the neat X-PI(370) possibly due to the increased free volume by chain rearrangements, similar to thermally-rearranged polymer (TR-polymer).[275, 293]

To investigate the permeability reduction thoroughly, as shown in Figure 6.13c, the C_3H_6 permeabilities of the MMMs using different polymer matrix (i.e., X-PI(370) and X-PI(420), 6FDA-DAM[124], and PIM-1) were normalized based on their neat polymer membranes and compared as a function of ZIF-8 loadings. It is reminded that all MMMs were prepared by the PMMOF except PIM-1. Since there are no imide groups in PIM-1, the PIM-1/MMMs were prepared without hydrolysis and imidization steps. As the ZIF-8 loadings increased, the normalized C_3H_6 permeabilities of all MMMs decreased, showing negative exponential trend curves (Figure 6.13c). It was likely due to the decrease in the polymer free volumes and the restricted chain mobilities as ZIF-8 particles incorporated in the polymer. Therefore, the slopes of trend the curves indicate the extents of change of the polymer properties (i.e., densification and rigidification) resulting from the incorporation of ZIF-8. The slopes increased in the order of X-PI(370) < 6FDA-DAM << X-PI(420) < PIM-1 (Figure 6.13c). We initially supposed that a polymer with a larger free volume and a more rigid structure might mitigate the densification and the rigidification upon ZIF-8 incorporation, thereby suppressing permeability reduction. However, PIM-1/ZIF-8 exhibited the most dramatic permeability reduction although PIM-1 possesses an exceptionally large volume and is one of the most rigid polymers (T_g of above 500 ^oC).[294] Similarly, the more rigid X-PI(420)/ZIF-8 MMMs showed much more dramatic decrease in the permeability than the X-PI(370)/ZIF-8 MMMs.

The considerable permeability reduction of the PIM-1/ZIF-8 and the X-PI(420)/ZIF-8 might be attributed to the negligible polymer swellings and the absence of the subsequent chain rearrangements upon the PMMOF. Both PIM-1 and X-PI(420) were less likely to be swollen during the PMMOF process since PIM-1 did not go through the hydrolysis step and the fully cross-linked X-PI(420) was expected to show high resistance to swelling. On the other hands, the

less rigid X-PI(370)/ZIF-8 and the uncross-linked 6FDA-DAM/ZIF-8 MMMs showed much less permeability reduction. More swellable X-PI(370) and 6FDA-DAM were prone to generate additional free volumes upon the chain rearrangements (Figure 6.13d). As such, the regenerated free volume by the swelling is likely critical to prevent the blockage of gas transport pathway by *in-situ* formed crystals. On the other hand, despite the lower degree of swelling of X-PI(370) than that of 6FDA-DAM due to the partial cross-linking, the X-PI(370) more effectively prevented the permeability decrease compared to the 6FDA-DAM (Figure 6.13c). This was likely attributed to the higher chain rigidity of X-PI(370) than that of 6FDA-DAM, which prevented the rigidification of polymers by fillers, supporting our initial assumption that controlled crosslinking degree enable to suppress the permeability reduction.[295]

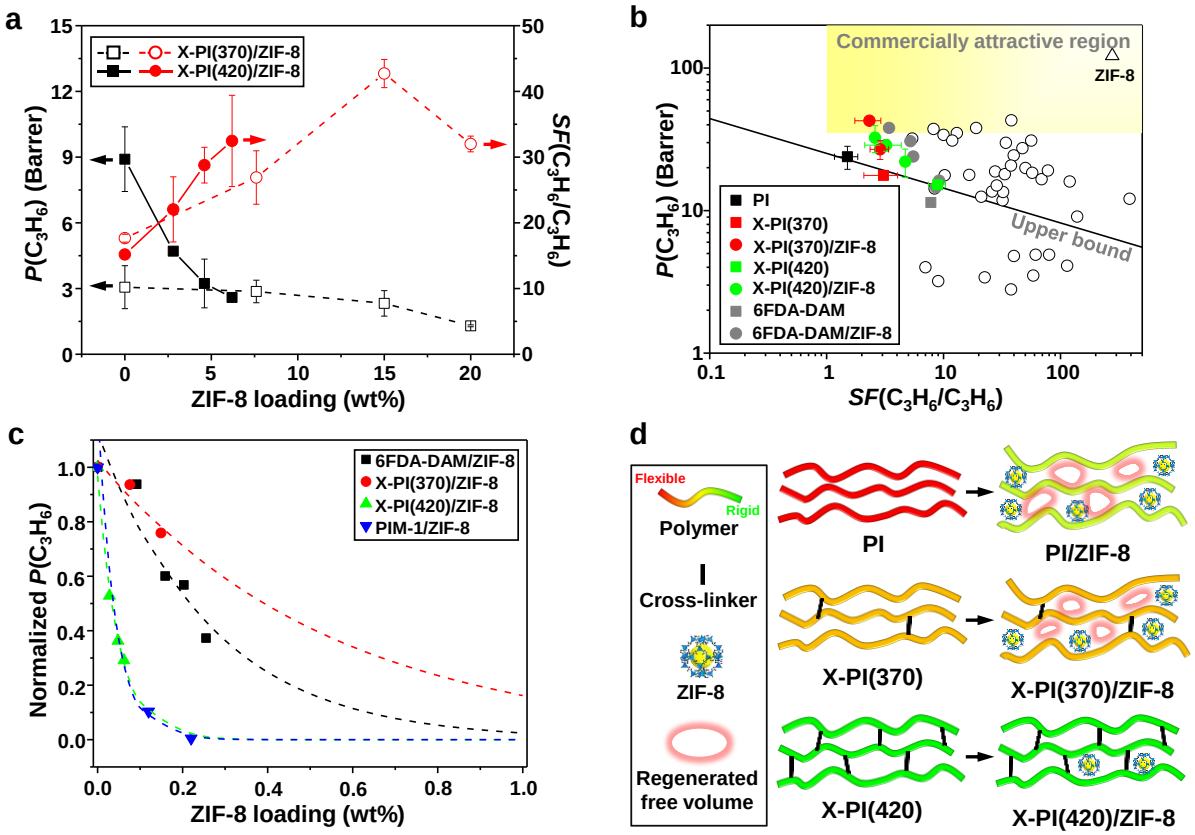

Figure 6.13. (a) C_3H_6 permeability (*P*) and C3 separation factor (*SF*) of the X-PI/ZIF-8 MMMs as a function of ZIF-8 loadings in the MMMs, (b) upper bound plot of the C3 separation performances of the X-PI/ZIF-8 MMMs in comparison with those of reported MMMs (○)[11, 29-42] and ZIF-8 (△)[1], (c) normalized C_3H_6 permeabilities of *in-situ* formed ZIF-8 containing MMMs as a function of ZIF-8 loadings, and (d) schematic illustrations of the free volume and chain flexibility changes before and after the PMMOF process.

Table 6.2. Summary of C_3H_6/C_3H_8 separation performances of polymer membranes and MMMs at ~ 1 atm and room temperature.

Sample	ZIF-8 loading (wt%)	C_3H_6 permeability (Barrer)	C_3H_6/C_3H_8 separation factor
PI	-	1.51 ± 0.34	23.9 ± 4.4
X-PI(370)	-	3.06 ± 0.98	17.7 ± 0.6
X-PI(370)/ZIF-8	7.6	2.87 ± 0.51	26.9 ± 4.1
	14.9	2.32 ± 0.58	42.7 ± 2.1
	19.7	1.30 ± 0.04	32.0 ±1.2
X-PI(420)	-	8.91 ± 1.48	15.2 ± 0.7
X-PI(420)/ZIF-8	2.8	4.71 ± 0.01	22.0 ± 5.0
	4.8	3.23 ± 0.08	28.8 ± 2.7
	6.2	2.59 ± 0.15	32.5 ± 6.9

6.4. Conclusion

In conclusion, we demonstrated a strategy to mitigate the gas permeability reduction of ZIF-8-containing MMMs by the polymer-modification enabled *in-situ* metal-organic framework formation (PMMOF). The strategy is based on controlling a degree of cross-linking of the continuous polymer phases. The cross-linkable polyimide (i.e., 6FDA-DAM:DABA (3:2)) was

thermally cross-linked at the sub-T_g (370 ^oC) and above- T_g (420 ^oC), denoted as X-PI(370) and X-PI(420), respectively. The degree of cross-linking led to variation in the polymer properties (i.e. free volume, chain mobility, swelling resistance, and etc.), thereby considerably affecting the *in-situ* formation of ZIF-8 filler particles. The more cross-linked the polymer the more restricted the *in-situ* formation of ZIF-8 particles. As a consequence, the X-PI(420)/ZIF-8 MMMs showed a considerable decrease in the C_3H_6 permeability and a moderate increase in the C3 separation factor. However, a substantially larger amount of ZIF-8 particles were formed in the less cross-linked polymer (i.e., X-PI(370)) than in the more-crosslinked X-PI(420). Consequently the X-PI(370)/ZIF-8 MMMs showed a significant C3 separation factor improvement (from ~ 18 to ~ 43 at 15wt% of loading) with a minor C_3H_6 permeability reduction (from ~ 3.1 Barrer to ~ 2.3 Barrer), satisfying the commercially attractive C3 separation criteria. Furthermore, the permeability reduction of the MMMs prepared by the PMMOF was investigated by comparing with MMMs made of uncross-linked 6FDA-DAM and rigid PIM-1. The more swellable polymers (i.e., 6FDA-DAM and less cross-linked X-PI(370)) showed much less permeability reductions than the other less swellable polymers (i.e., PIM-1 and more cross-linked X-PI(420)). Besides, the X-PI(370)/ZIF-8 MMMs showed a much smaller permeability reduction than the 6FDA-DAM/ZIF-8 MMMs, suggesting the rigidification by the *in-situ* formed ZIF-8 upon the PMMOF was mitigated with the X-PI(370). In other words, there are two important factors that interplay to suppress permeability reduction in MMMs prepared by the PMMOF: 1) the polymer swelling upon the PMMOF that might regenerate free volume and 2) the rigid polymer structures that are resistant to further rigidification upon the PMMOF.

CHAPTER VII

TRANSFORMING POLYMER HOLLOW FIBER MEMBRANE MODULES TO MIXED-MATRIX HOLLOW FIBER MEMBRANE MODULES FOR POLYLENE/PROPANE SEPARATION

7.1. Introduction

Membrane-based propylene/propane (C3 separation) separation is an energy-efficient alternative to conventional thermally-driven technologies such as distillation.[238] Nevertheless, the efficiency of energy saving depends largely on the separation performance of membranes.[128] The inherent separation performance limitation (i.e., trade-off between permeability and selectivity) of cost-effective and scalable polymeric membranes precludes the polymer membranes from satisfying the commercial-attractive C3 separation performance criteria (i.e., > 1 Barrer of C_3H_6 permeability and > 35 of C3 selectivity).[129, 239] Although polycrystalline molecular sieve membranes such as ZIF-8 membranes showed surprisingly high C3 separation performance,[130, 296-297] they are prohibitively expensive mainly due to the difficulty and complexity of synthesis among others.[298] Thus there have been great research interests in mixed-matrix membranes (MMMs) combining advantages of both processible polymer and molecular sieve membranes by dispersing a molecular sieve phase with a continuous polymer phase.[1, 138, 140, 258]

Despite the impressive advancement over decades, the majority of the reported MMMs were in flat sheet forms. Given the area-to-volume ratio, however, hollow fiber forms are much more

*Modified and reprinted with permission from "Transforming Polymer Hollow Fiber Membrane Modules to Mixed-Matrix Hollow Fiber Membrane Modules for Propylene/Propane Separation" by Sunghwan Park and Hae-Kwon Jeong, *Journal of Membrane Science*, 2020, 612, 118429-118436, Copyright 2020, Elsevier

desirable for large-scale applications.[61, 251, 299-301] The rarity of mixed-matrix hollow fiber membranes (MMHFMs) testifies the engineering challenges associated with spinning high-quality fibers using filler-containing dope solutions.[142, 302] There have been only very few reports on MMHFMs, in particular, for C3 separation which requires much fewer defects than other light gas separations.[142] Koros and his coworkers[142] were the first to successfully demonstrate 6FDA-DAM/ZIF-8 MMHFMs with ZIF-8 loading as high as 30 wt% for C3 separation. Though pioneering, the as-spun MMHFMs showed poor C3 separation performance and the relatively high C3 separation factor (27.5) could be achieved only after multiple additional coating layers were applied.[142] It is noteworthy of mentioning that the presence of the additional coatings would increase the overall thickness of MMM skin layers. In fact, the propylene permeance of the MMHFMs were substantially decreased after the additional coatings. It is, therefore, of critical importance to develop new MMM fabrication methodologies that enable facile and scalable formation of asymmetric MMHFMs with submicron-thick MMM skin layers exhibiting relatively high C3 separation performances without additional coating layers.

It is extremely challenging to form high-quality asymmetric MMHFMs in a scalable manner using conventional physical blending and single-step spinning methods stemming from the difficulty of controlling skin layer defects and polymer/filler interfacial structures.[101, 303-304] Recently we proposed the polymer-modification-enabled *in-situ* metal-organic framework formation (PMMOF) as a scalable MMM fabrication method.[193, 305-306] The PMMOF decouples polymer film deposition and MMM formation steps, thereby enabling scalable formation of MMMs with unprecedentedly thin skin layers.[193, 305] Furthermore, the PMMOF is more likely to produce MMMs with less defects since MOF crystals grow *in-situ* inside polymer, effectively suppressing interfacial void formations and defective particle agglomerations.[193, 305] As a proof-

of-concept, we also reported fabrication of MMHFMs by the PMMOF, showing the propylene/propane separation factors of ~ 20.[193] It is noted that the MMHFMs reported were premade and then assembled into a test module for gas permeation testing.[193, 305] Considering the difficulty of modulation,[307] it would be quite attractive if one can start with off-the-shelf polymer hollow fiber membrane (HFM) modules and transform them to MMHFM modules.

Here, we report 6FDA-DAM/ZIF-8 MMHFM modules by transforming custom-made lab-scale modules preformed with commercially-available polyethersulfone (PES) HFMs coated with 6FDA-DAM using the PMMOF process. Single-strand 6FDA-DAM/ZIF-8 MMHFM modules were fully characterized using a battery of tools. The C3 separation performances of the single-strand MMHFM modules were measured and compared with the previously reported various types of HFMs including MMHFMs. The stability of the individual membrane strands was also investigated with respect to aging and plasticization. Finally, we demonstrated and tested the first MMHFM modules consisting of up to seven strands, exhibiting increased membrane surface area and decent C3 separation performance. To the best of our knowledge, the multi-strand MMHFM modules are the first of its kind.

7.2. Experimental

7.2.1. Materials

6FDA-DAM (4,4′-(hexafluoroisopropylidene) diphthalic anhydride-2,4,6-trimethyl-1,3-diaminobenzene, Mw: 148k, PDI: 2.14) was purchased from Akron Polymer Systems Inc. Polyethersurfone (PES) microfiltration hollow fiber membrane modules (MiniKros Sampler) were purchased from Repligen corporation. Sodium formate (HCOONa, ≥ 99 %), zinc nitrate hexahydrate ($Zn(NO_3)_2 \cdot 6H_2O$, 98 %), 2-methylimidazole (Hmim) ($C_4H_6N_2$, 99 %), and

polydimethylsiloxane (PDMS, Sylgard® 184, Dow Chemical) were obtained from Sigma-Aldrich. Methanol (CH_3OH, > 99.8 %, Alfa Aesar), ethyl acetate ($C_4H_8O_2$, ≥ 99.5 %, VWR International), and hexane (C_6H_{14}, ACS grade, VWR International) were used as solvents. All chemicals were used as-received without further purification.

7.2.2. Polyimide coating on porous hollow fiber supports

Individual polyethersulfone (PES) hollow fiber strands (OD: ~700 μm, ID: ~500 μm and surface pore size: ~0.2 μm) were obtained by disassembling an as-purchased PES module. The hollow fiber strands were cut into smaller strands with ~ 10 cm in length. To coat a thin 6FDA-DAM polyimide (PI) layer on a PES fiber strand, a PI coating solution was prepared by dissolving 4 wt% of 6FDA-DAM in ethyl acetate. The PES hollow fiber membrane was then dip-coated with the coating solution in a glove bag saturated with ethyl acetate vapor. The HFM was taken out and hanged vertically in the glove bag overnight for slow solvent evaporation. The resulting 6FDA-DAM coated PES HFM was dried under air for an hour and then further dried at 60 ^oC overnight in a convection oven.

7.2.3. Modulation of hollow fibers

PI-coated HFMs were assembled into a laboratory-scale HFM module. The module was made of 316 stainless steel tube fittings (Swagelok): one 1/4 in male union cross, four 1/4 in nuts and four 1/4 in ferrule sets. Ferrule sets were connected to 1/4 in Teflon tubing cut into 3 cm and two of them were connected to the union cross at opposite sides using nuts. 1 ~ 7 fiber strands were put into the connected fitting. Both ends of the Teflon tubing were then sealed with epoxy resin (3M Scotch-Weld DP110 flexible temperature resistant gray epoxy) using a syringe. After

curing the epoxy, each end of the epoxy sealed Teflon tubing was cut to open both ends of the HFM module. The nuts and ferrule sets were connected to the ends of the module. The module was ~ 10 cm long with the effective HFM length of ~ 6 cm. Figure 7.2 presents the photographs of the prepared HFM module.

7.2.4. Preparation of mixed-matrix hollow fiber membranes using the PMMOF

The PMMOF proceeded with the following steps: 1) hydrolysis, 2) ion-exchange, 3) ligand treatment, and 4) imidization.[193] All of the steps proceeded by filling the solutions from the shell side of a module loaded with a PI-coated PES hollow fiber membrane. The hydrolysis of the PI-coated PES HFM was carried out in an aqueous sodium formate solution (20 mmol of sodium formate dissolved in 30 ml D.I. water) at 120 ^{o}C for two hours. After cooling down, the HFMs were washed with water overnight at room temperature. Na ions coordinated to the hydrolyzed PI layer were then exchanged with Zn ions. The ion-exchange was performed by treating the hydrolyzed HFM in a zinc nitrate hexahydrate solution with a various zinc content (20, 40, and 60 mmol) in 30 ml of water at room temperature for 3 hours. After the ion-exchange solution was drained from the HFM module, a ligand treatment solution (25 mmol of 2-methylimidazole dissolved in 30 ml methanol) was filled into the HFM module. The HFM module containing the ligand treatment solution was then placed into a convection oven pre-heated at 40 ^{o}C for 2 hours. Afterwards, the module was taken out and kept at room temperature for additional 2 hours. The HFM were then washed with methanol overnight at room temperature. Finally, the HFMs were dried at room temperature for an hour and then thermally imidized at 210 ^{o}C for 3 hours. It is noted that when the HFM module was filled with solutions, both ends of the module were sealed with plugs.

7.2.5. PDMS coating on hollow fiber membranes

For the confirmation of the absence of major defects on MMHFMs, PDMS coating was applied to the HFM modules. 2wt% solution of Sylgard® was prepared in hexane at 75 ^{o}C for 1 hours with stirring. The HFM modules were filled with the PDMS solution and the modules were shaken for 5 min. The solution was drained out of the modules. Soaking HFMs with the PDMS solution was repeated 2 more times. Finally, the module was placed in a vacuum oven and the PDMS was cured at 75 ^{o}C for 2 hours under vacuum.

7.2.6. Characterizations

Scanning electron microscope (SEM) images were taken using a JEOL JSM-7500F at 5 keV acceleration voltage and 15 mm working distance. SEM samples were prepared by freeze fracturing in liquid nitrogen followed by Pt coating with thickness of 5 nm. Transmission electron microscopy (TEM) analysis was conducted using a FEI Tecnai FE-TEM under cryogenic conditions. TEM samples were prepared by microtoming to ~ 60 nm in thickness using a Leica UC7 ultramicrotome at room temperature. X-ray diffraction (XRD) patterns were taken using a Miniflex II (Rigaku) with Cu-Kα radiation (λ = 1.5406 Å) in the 2 θ range of 5 – 40 ^{o}. Attenuated total reflectance Fourier transform infrared (ATR-FTIR) spectra were obtained using a Nicolet iS5 spectrophotometer (Thermo Scientific) equipped with iD7 ATR with a resolution of 2 cm^{-1} and 16 scans in the wavenumber range of 4000 – 400 cm^{-1}. Thermogravimetric analysis (TGA) was conducted using a Q50 (TA instruments) at the temperature range of 25 – 800 ^{o}C with the heating rate of 10 ^{o}C min^{-1} under the air flow of 60 cm^{3} min^{-1}.

7.2.7. Gas permeation measurements

The equimolar binary C_3H_6/C_3H_8 gas separation properties of prepared HFMs were measured using the Wicke-Kallenbach technique at room temperature under atmospheric feed pressure. The feed gas was supplied at 20 cm^3 min^{-1} while the argon sweeping gas was flowed at 20 cm^3 min^{-1} on the permeate side. Steady-states were declared when the difference in the measured C_3H_6 permeance of a sample was less than 1 % in a 30 min interval. Composition of the permeated gases was determined by gas chromatography (GC 7890A, Agilent) equipped with a flame ionized detector (FID) and a HP-plot Q column. C_3H_6 single gas was used to determine the effect of the feed pressure on the permeation property of HFMs. The feed pressure was controlled using a back-pressure regulator located at the end of HFM modules.

7.3. Results and discussion

7.3.1. Transforming polymer HFM modules to PI/ZIF-8 MMFHM module by the PMMOF

The PMMOF enables transformation of a polymer hollow fiber membrane (HFM) module to a mixed-matrix hollow fiber membrane (MMHFM) module.[193] To perform the PMMOF, a thin 6FDA-DAM polyimide (PI) layer was dip-coated on a commercial polyethersulfone (PES) hollow fiber membrane, several of which were then assembled into a module with both of the ends open (see Figure 7.1 and 7.2). PES HFMs were selected as supports due to their low material cost (~ 20 USD/kg), mechanical,[308] chemical (mostly inert to the PMMOF),[309] and thermal stability (T_g of ~ 220 ^oC)[310] as well as their compatibility with fluorinated polyimides.[311] Ethyl acetate was carefully chosen as a solvent since it dissolves 6FDA-DAM while PES HFMs

were intact in ethyl acetate (Figure 7.3). The PI-coated HFMs were assembled into a module by sealing both ends with epoxy (Figure 7.2).

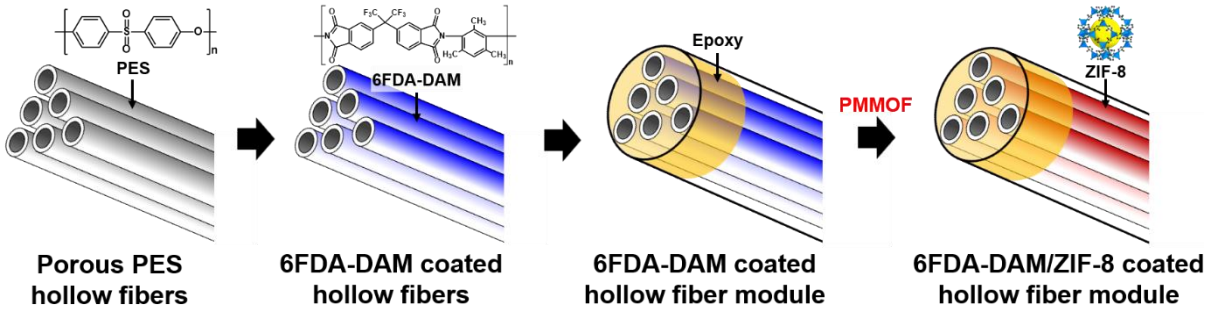

Figure 7.1. Schematic illustration of evolution of commercial polymer (PES) HFMs to PI-coated polymer HFMs to a PI-coated HFM module to a PI/ZIF-8 MMHFM module.

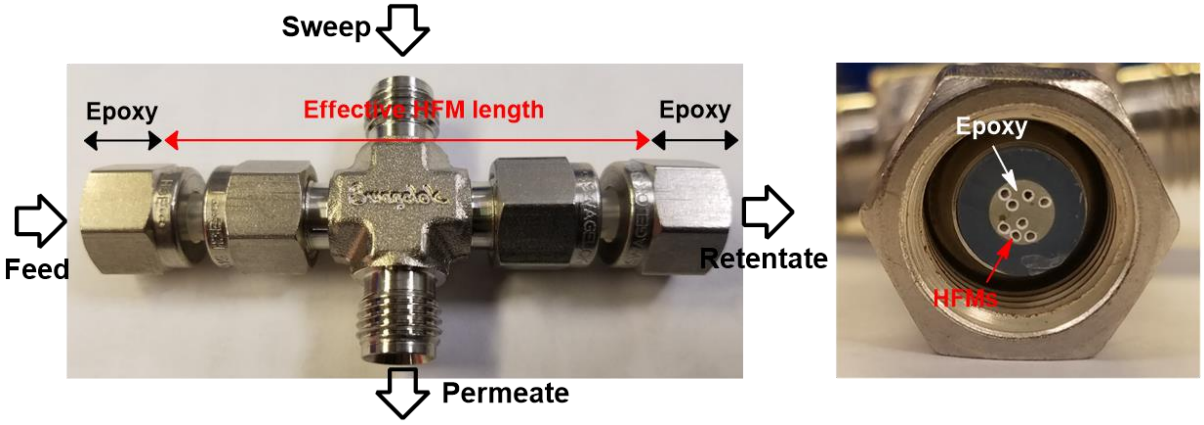

Figure 7.2. Photographs of a polymer hollow fiber membrane module.

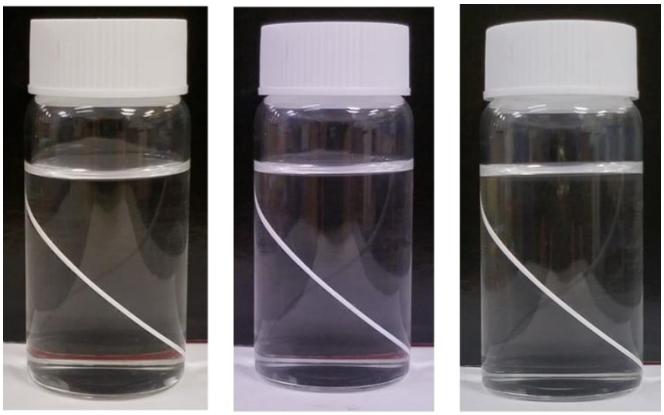

Figure 7.3. Commercial PES hollow fiber membranes immersing in ethyl acetate.

The PMMOF process involves four steps: hydrolysis, ion exchange, ligand treatment, and imidization (Figure 3.1). We demonstrated the potential of the PMMOF to transform flat polymer membranes or single polymer hollow fiber membranes into high-quality MMMs in Chapter 3. There were, however, several processing issues that should be addressed in order to apply the PMMOF to HFM modules. One such issue has to do with properly controlling hydrolysis reaction. Hydrolysis reaction partially deimidized a PI layer to form a poly(amic acid) sodium salt (PAA-Na) layer (Figure 3.1). This hydrolysis step is essential to provide environments inside polymer, enabling accommodation of MOF precursors and eventually *in-situ* MOF formation inside polymer.[193, 312] Since the PI coating layer on a PES HFM was much thinner (~ 0.75 μm) than that on a flat alumina disk (~ 7 μm),[193] the hydrolysis under the same conditions as in our previous work (i.e., in a sodium formate solution (3.33 M) at 120 ^{o}C for 5 hours) severely damaged the PI coating layer on a HFM (Figure 7.4a). As such, the hydrolysis time was reduced from 5 hours to less than 3 hours, thereby substantially suppressing damages to the coating layer upon the hydrolysis (Figure 7.4b and 7.4c). Another challenge was to ensure sufficient soaking of a zinc solution during the ion-exchange step.[193] Due to the nature of the

module, air bubbles were trapped in the module, thereby limiting saturation of the solution. As such, air bubbles were removed by evacuating one side of the HFM module under vacuum while solutions were supplied to the other side. During the ligand treatment step where ZIF-8 forms in polymer free volume (PAA/ZIF-8),[193] the polymer HFMs were most swelled, thereby causing damages to the skin layers in the limited space of the module (Figure 7.5). It was possible to alleviate these damages by maintaining the packing density of the hollow fiber module at < 30 %. The last step was to thermally imidize the PAA to the PI, stabilizing the gas separation performance of the membrane.[193] During this thermal imidization step, an epoxy with high thermal resistance was used to minimize the thermal expansion and degradation of epoxy (Figure 7.6).

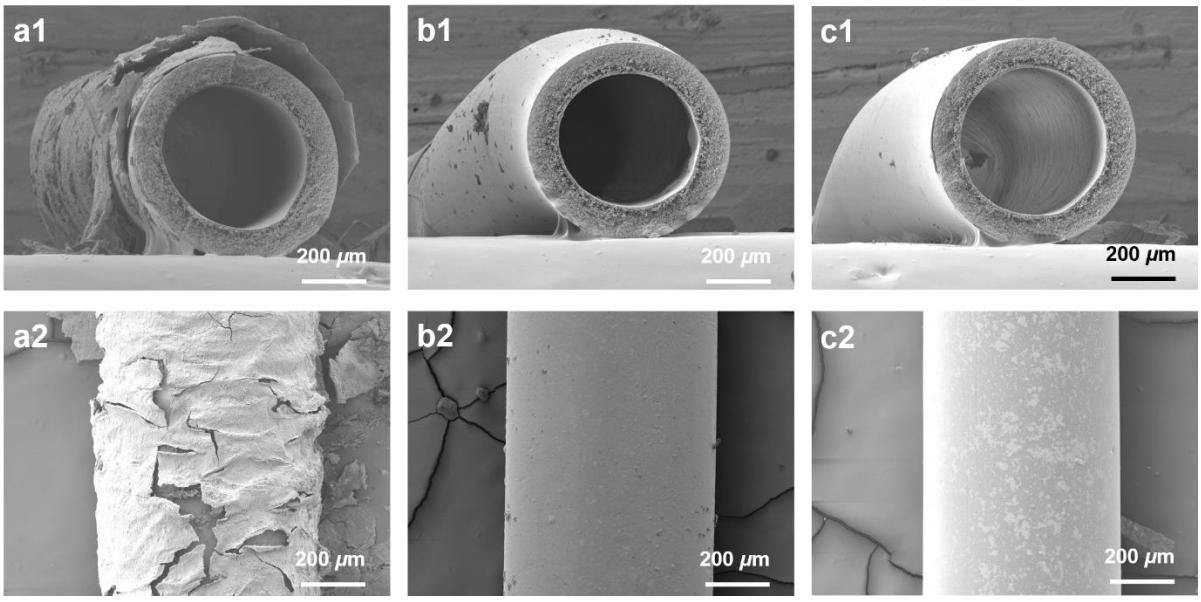

Figure 7.4. SEM images of PI/ZIF-8 MMHFMs prepared under normal hydrolysis times: (a) 5h, (b) 3h, and (c) 2h. (a1-c1) cross-section and (a2-c2) top view.

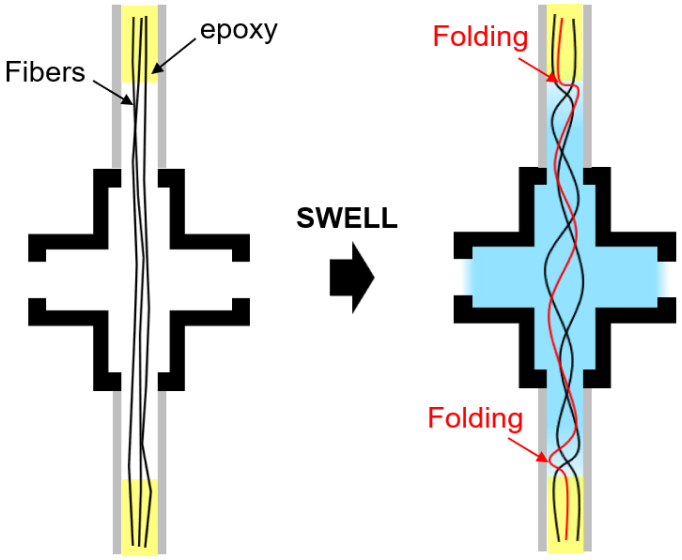

Figure 7.5. Illustration of swelling of HFMs in a module upon the ligand treatment.

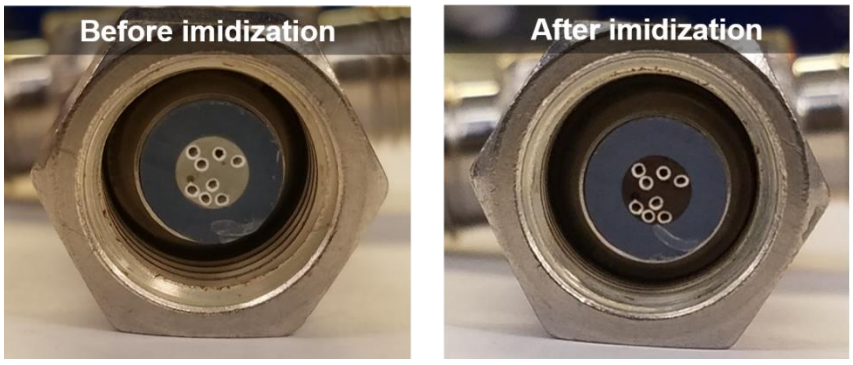

Figure 7.6. Photographs of an HFM module before and after imidization.

7.3.2. Characterizations of PI/ZIF-8 MMFHMs by the PMMOF

FI-IR spectra were taken to monitor the chemical modifications of the PI layer by the PMMOF (see Figure 7.7). As shown in the Figure 7.7, there were two strong peaks of the PI at 1723 and 1356 cm^{-1} which assigned to C=O and C-N in imide ring, respectively.[313] It is noted that these peaks related to the imide ring of the PI were not overlapped with that of the PES

support. However, the C-C stretching bands of the benzene rings of the PI and the PES were overlapped at 1485 cm^{-1}.[313] Since the hydrolysis reaction during the PMMOF did not affect benzene rings, the intensity of the C-C peaks of the PI and PES overlapped was preserved upon the PMMOF. As such, the C-C peak was regarded as an internal standard. The intensities of the C=O and C-N peaks were reduced relatively comparing with that of the C-C peak upon the hydrolysis. This is because the imide ring of the PI was turned into the carboxyl group of the PAA (Figure 7.7). The deimidization was quantitatively evaluated based on the changes of the ratio between the intensities of the C=O and C-C peaks. As the PI turned into the PAA-Na, the ratio decreased from 2.96 to 2.43, indicating ~ 18 % of deimidization. This was less than that of the flat membranes (~ 35 %)[193] due to the milder hydrolysis conditions which were necessary in order to preserve the integrity of the PI skin layer. It is worthy of mentioning that the basic Hmim solution also partially deimidized the polymer (Figure 7.7). The final thermal imdization step again increased the ratio, attaining 95 % of imidization (i.e., 5 % of deimidization) (Figure 7.7).

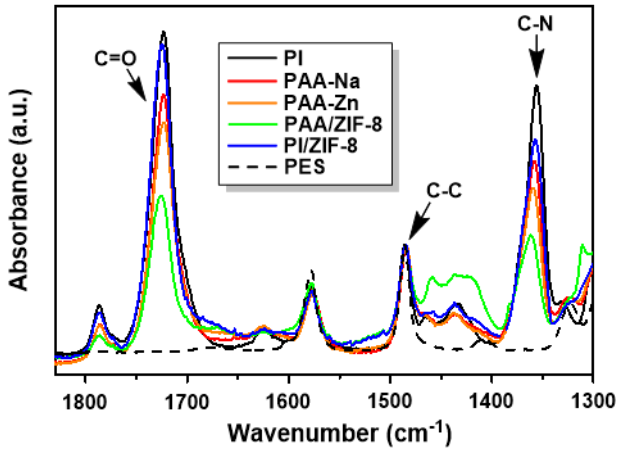

Figure 7.7. Evolution of the FT-IR spectrum of a sample during the PMMOF process.

The dimensions and morphology of the HFMs were determined by SEM images. The commercial PES microfiltration HFMs used in this study possess the outer diameter of ~ 700 μm and the inner diameter of ~ 500 μm (Figure 7.8a1). They were symmetrically porous with the surface pore size of ~ 200 nm (Figure 7.8a2).[314] When the shell sides of the PES HMFs were coated with PI, the porous surfaces of the PES HFMs were completely covered with PI coating layers of ~ 750 nm thickness (Figure 7.8b). The thickness of the PI coating was controlled by varying the polymer concentration in a dope solution. It was found that the thickness of the skin layer was linearly correlated with the polymer concentration in a dope solution (Figure 7.9). Importantly, the submicron thickness of the PI coating layer was well-preserved throughout the PMMOF steps (Figure 7.8c1). There was no delamination possibly due to the proper affinity between the two polymers and the similar expansion/shrinking rates.[311]

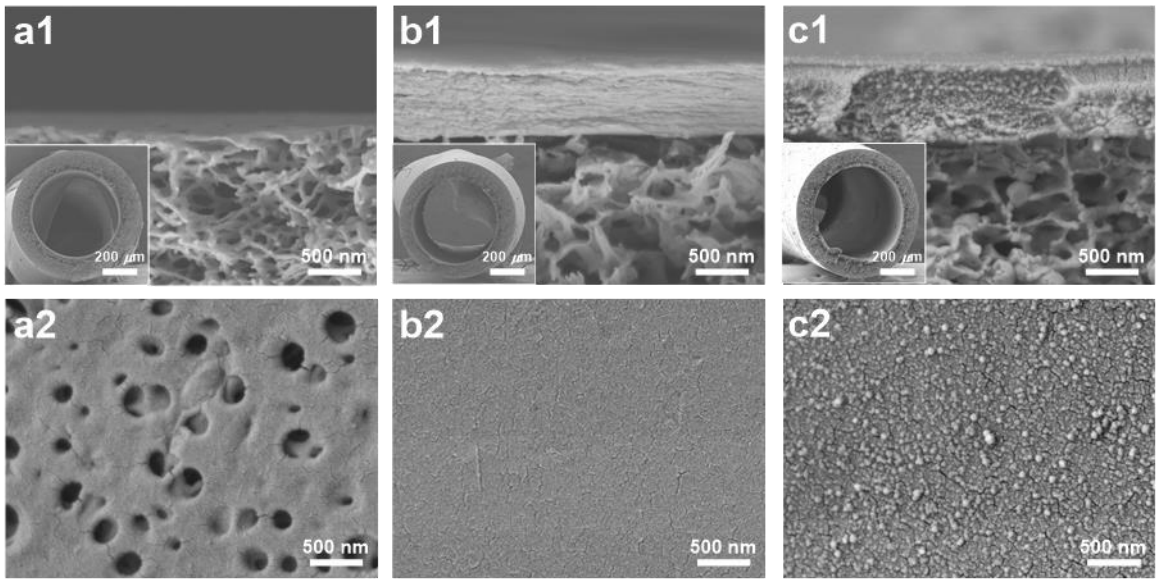

Figure 7.8. SEM images of the shell sides of (a) pristine PES HFM, (b) PI-coated HFM, and (c) PI/ZIF-8 MMHFM: cross-sectional view (a1, b1, and c1) and top view (a2, b2, and c2). Inset images in a1-c1 represent low magnification images of cross-sections of HFMs.

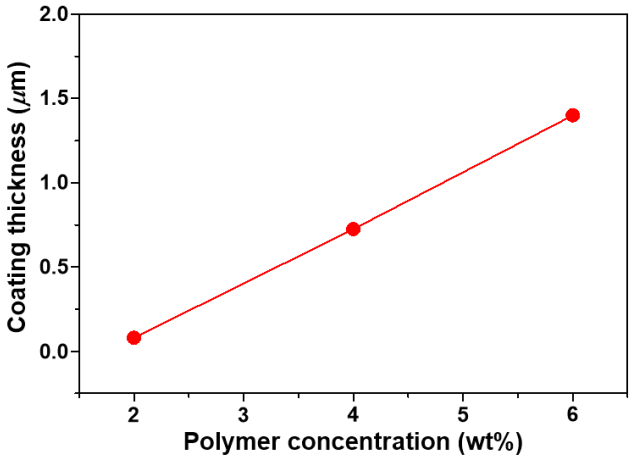

Figure 7.9. Thickness of coating as a function of polymer concentration in a coating solution

The *in-situ* formation of ZIF-8 in the polymer HFMs was investigated by XRD patterns. After the PMMOF, there appeared a strong (110) diffraction peak at 7.3 ° of 2θ and a relatively low intensity of (112) peak at 12.8 ° of 2θ along with the broad amorphous hump from polymer (Figure 7.10). The peaks were well-matched with those of simulated ZIF-8 diffraction patterns, indicating the formation of ZIF-8 (Figure 7.10). As shown in Figure 7.8c and Figure 7.11a, however, ZIF-8 particles of ~ 100 nm and ~ 200 nm in size were founded on the membrane surface as well as inside the porous support, respectively. It is noted that the ZIF-8 precursor solutions were likely percolated from the shell side of HFMs and filled in pores on the lumen side of HFMs, forming ZIF-8 crystals on the support layer. These ZIF-8 particles were removed by flowing a nitric acid solution (0.1 M) through the bore (Figure 7.11b) followed by dropping the acid solution on the surface (Figure 7.11c). After the sequential acid treatments, there was the notable intensity reduction of the PI/ZIF-8 MMHFM. Nevertheless, it showed the relatively strong intensity of the diffraction pattern, strongly indicating the presence of a substantial amount of *in-situ* formed ZIF-8 particles inside the skin layer (Figure 7.10).

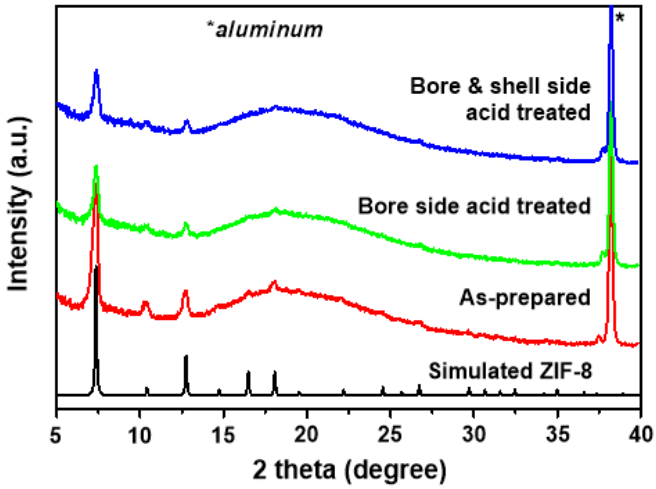

Figure 7.10. XRD patterns of as-prepared PI/ZIF-8 MMHFMs along with PI/ZIF-8 MMHFMs acid-treated on bore side and acid-treated both bore and shell sides with a nitric acid solution.

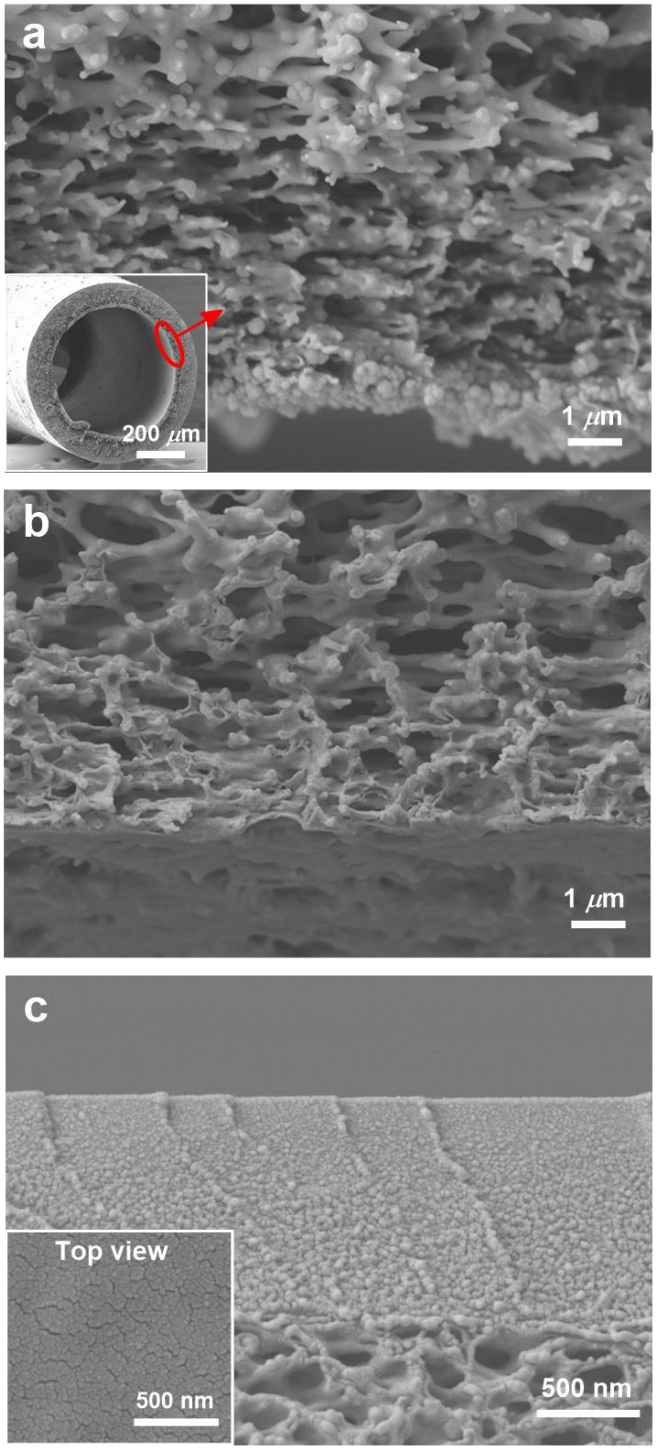

Figure 7.11. Cross-sectional SEM images of (a) as-prepared PI/ZIF-8 MMHFMs (bore side), (b) the one after a nitric acid solution was flowed through the bore (bore side), and (c) the one after a nitric acid solution was flowed to both of the bore and the shell (shell side).

To further confirm the presence of *in-situ* formed ZIF-8 particles inside the PI layer, TEM analysis was performed. Figure 7.12 presents the TEM images and the corresponding selected area electron diffraction (SAED) patterns. It is noted that the TEM analysis was carried out on the acid-treated sample to exclude ZIF-8 grown outside the polymer layer. The SAED pattern (Figure 7.12a) was well-matched with that of ZIF-8 in literatures,[315] confirming that the darker regions in the TEM images (Figure 7.12b-c) were randomly oriented *in-situ* grown ZIF-8 crystals inside the PI layer. As shown in Figure 7.12b-c, the *in-situ* formed ZIF-8 in the skin layer represented unique morphologies as observed in our previous reports.[193, 305]. ZIF-8 agglomerates show ring-like and rod-like shapes, likely resulting from the confined growth of ZIF-8 inside the polymer free volume. When the PI is hydrolyzed (i.e., deimidized), the free volume of the resulting polymer (i.e., PAA-Na) is drastically increased, providing enlarged spaces for ZIF-8 formation.[193] Further studies are required to understand the *in-situ* formation of uniquely-shaped ZIF-8 particles inside polymer by the PMMOF.

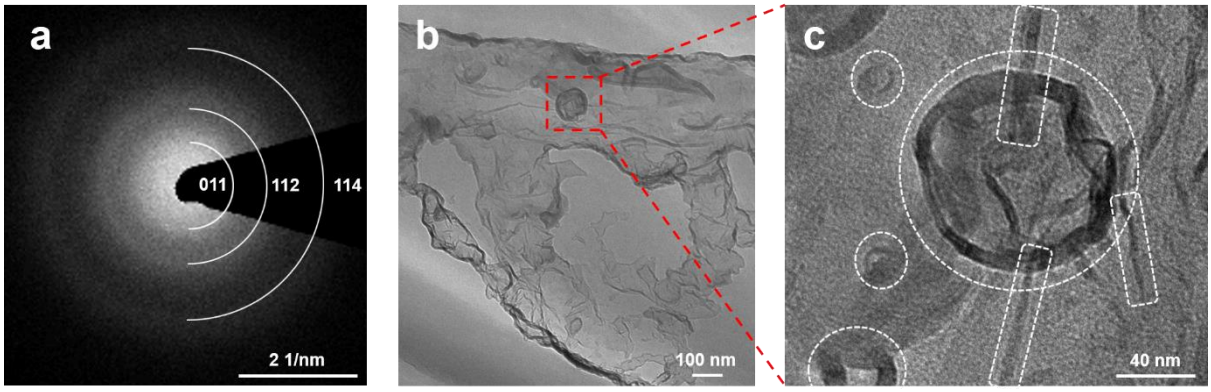

Figure 7.12. TEM analysis of *in-situ* grown ZIF-8 in the PI skin layer: (a) selected area electron diffraction (SAED) pattern, (b) low magnification TEM image, (c) high magnification TEM image. Note that the SAED was taken from the sample area of (c).

The maximum loading percentages of ZIF-8 fillers in the polymer were estimated to 14.5, 19.6, and 29.6 wt% (Table 7.1). In our previous work,[193] a similar observation was made in that ZIF-8 content in a polymer was increased as the zinc concentration in ion exchange solutions increased. The percentages of ZIF-8 loading were calculated based on the contents of ZnO residue formed upon thermal decomposition under air flow (Figure 7.13). The loading percentages of ZIF-8 in overall HFM were estimated as follows:

$$ZIF\text{-}8\ wt\% = \frac{W_{ZnO\ from\ PI/ZIF\text{-}8\ MMHFM} - W_{ZnO\ from\ PAA\text{-}Zn\ HFM}}{W_{ZnO\ from\ pure\ ZIF\text{-}8}} \times 100(\%). \qquad (7.1)$$

where W is a residual weight percentage of thermal decomposition. The residue (i.e., ZnO) wt% of PI/ZIF-8 MMHFMs were subtracted from that of PAA-Zn by considering the zinc ions coordinated to polymer, which are negligibly participate to form ZIF-8.[124] By dividing the subtracted wt% of PI/ZIF-8 by the residue wt% of ZIF-8, the loading percentages of ZIF-8 in overall HFMs were calculated (third column of Table 7.1). It was supposed that the residue of PI/ZIF-8 are consist with ZnO mainly due to the almost complete thermal decomposition of organic parts under air condition.[1] In addition, the calculation of ZIF-8 loading percentages in the PI layer was as follows;

The wt% of PI coating layer was 29.1 ± 2.8 wt%.

$$\frac{m_{PI}}{m_{PI}+m_{PES}} = 0.291 \qquad (7.2)$$

By rearranging the expression,

$$2.43 m_{PI} = m_{PES}.$$

m_{PES} can be replaced to $2.43m_{PI}$ in the following equation to get a relation between m_{PI} and m_{ZIF-8}.

$$\frac{m_{ZIF-8}}{m_{PI}+m_{PES}+m_{ZIF-8}} = 0.1092\ for\ PI/ZIF-8(30) \quad (7.3)$$

$$\frac{m_{ZIF-8}}{3.43m_{PI}+m_{ZIF-8}} = 0.1092 \quad (7.4)$$

$$m_{PI} = 2.38m_{ZIF-8} \quad (7.5)$$

ZIF-8 loading percentages in the PI layer is as follow;.

$$\frac{m_{ZIF-8}}{m_{PI}+m_{ZIF-8}} = \frac{m_{ZIF-8}}{2.38m_{ZIF-8}+m_{ZIF-8}} = 0.296 \quad (7.6)$$

The estimated ZIF-8 wt% in the PI layer was represented in the fourth column of Table 7.1. For clarification, PI/ZIF-8 MMHFM samples with different ZIF-8 loading were named with loading (wt%) in bracket (i. e., PI/ZIF-8 (15) is a PI/ZIF-8 MMFHM with 15wt% loading).

Table 7.1. Loading percentages of ZIF-8 in PI/ZIF-8 MMHFMs by the PMMOF.

Sample	Residue (wt%)	ZIF-8 in overall HFM (wt%)	ZIF-8 in PI (wt%)
PAA-Zn	0.44	n/a	n/a
PI/ZIF-8 (15)	2.12	4.70	14.5
PI/ZIF-8 (20)	2.81	6.65	19.6
PI/ZIF-8 (30)	4.34	10.92	29.6
ZIF-8	35.69	n/a	n/a

Note: To avoid the overestimation of ZIF-8 loading percentages, ZIF-8 bonded on the surface and in the support for PI/ZIF-8 MMHFMs was simply removed by flowing 0.1 M HNO_3 solution.

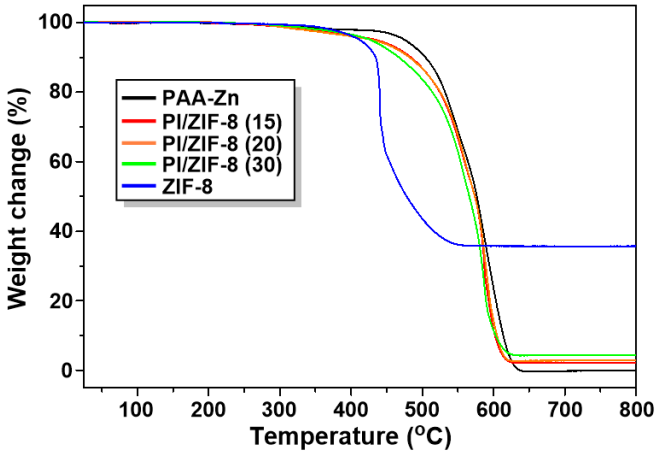

Figure 7.13. TGA thermograms of samples under air.

7.3.3. Gas permeation of PI/ZIF-8 MMFHMs by the PMMOF

7.3.3.1 C_3H_6/C_3H_8 separation performance

The C3 separation performances of the PI/ZIF-8 MMHFM modules were comparable with those of the corresponding previously reported single-fiber MMHFMs.[193] For example, the C_3H_6 permeances of the PI/ZIF-8 (20) MMHFM modules were ~ 2.17 GPU (single fiber) and ~2.55 GPU (module).[193] Besides, the separation factors were ~ 20 (single fiber) and ~ 19.3 (module).[193] This strongly suggests that the PMMOF could be applied to hollow fibers whether they are in a module or individual fibers.

We investigated the effect of ZIF-8 contents on C3 separation performance. When the loading percentages of ZIF-8 in the PI/ZIF-8 MMHFMs increased, the C3 separation factor increased because of the molecular sieving effect of ZIF-8 (Figure 7.14a and Table 7.2).[141] ZIF-8 loading had a little effect on the C_3H_6 permeances of the PI/ZIF-8 MMHFMs. It is likely due to the interplay between the permeability increase by microporous ZIF-8 [9, 11] and the permeability decrease by the reduced free volume of polymer upon the PMMOF process.[23]

Upon the PMMOF, the C_3H_6 permeance was significantly reduced (about five-fold) (Figure 7.14a and Table 7.2). This noticeable permeance reduction was likely because of the polymer densification upon the PMMOF.[193, 316] Nevertheless, the separation factor of the PI/ZIF-8 MMHFMs was significantly increased at the higher ZIF-8 loadings.

The C3 separation performances of the single-strand PI/ZIF-8 MMHFM modules were compared with previously reported other hollow fiber membranes including polymer,[317-321] CMS,[322-324] ZIF-8,[266, 296, 325-326] and PI/ZIF-8 MMHFMs prepared by conventional blending methods.[142] Despite the potential of MMHFMs, to best of our knowledge, there has been only one report on MMHFMs for C3 separation so far. Even though the PI/ZIF-8 MMHFMs prepared by a blending method showed C3 separation capability, the separation factor of the as-spun MMHFMs was lower than that of the polymer HFMs due to defects (Figure 7.14b).[142] Therefore, additional coating steps were necessary to improve the separation factor, significantly sacrificing propylene permeance (Figure 7.14b). The defects on MMHFMs were generally formed upon spinning process due to the complicated parameters associated with spinning a filler suspended dope solution.[134] Unlike the PI/ZIF-8 MMHFMs made by conventional blending, the MMHFMs by the PMMOF showed more improved C3 separation performances even without additional coatings (Figure 7.14b). When additional PDMS coating was applied to the PI/ZIF-8 MMHFMs prepared by the PMMOF, there were no further improvements of the C3 separation factor, indicating the absence of major defects. It is surmised that decoupling of spinning step and MMM formation step in the PMMOF effectively suppressed defect formations.

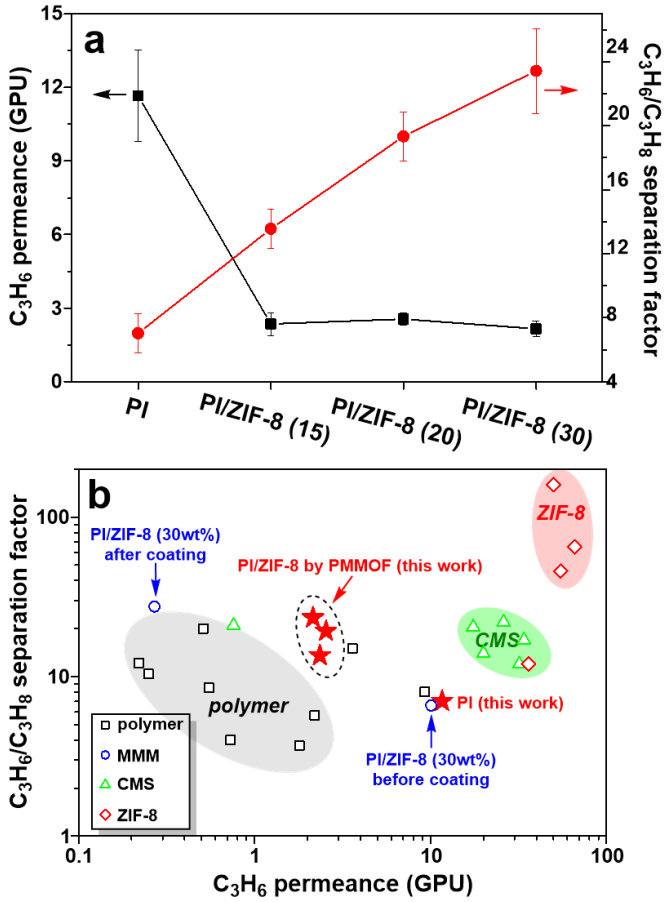

Figure 7.14. (a) Effect of ZIF-8 loading on C3 separation performance and (b) C_3H_6 permeance and C3 separation factor of single-strand PI/ZIF-8 MMHFM modules in comparison with those of the HFMs previously reported.[142, 266, 296, 317-326]

Table 7.2. C_3H_6/C_3H_8 separation performances of PI HFMs and PI/ZIF-8 MMHFMs with different ZIF-8 loadings.

Sample	C_3H_6 permeance (GPU)	C_3H_8 permeance (GPU)	C_3H_6/C_3H_8 separation factor
PI	11.66 ± 1.86	1.66 ± 0.55	7.0 ± 1.2
PI/ZIF-8 (15)	2.35 ± 0.47	0.17 ± 0.05	13.6 ± 1.2
PI/ZIF-8 (20)	2.55 ± 0.25	0.13 ± 0.02	19.3 ± 1.5
PI/ZIF-8 (30)	2.15 ± 0.32	0.09 ± 0.02	23.4 ± 2.7

7.3.3.2 Stability of the C_3H_6/C_3H_8 separation performances

It is of great practical interest to investigate the time-dependent and pressure-dependent separation performances.[276, 327] First, the time-dependent separation performances of the PI HFM and PI/ZIF-8 (30) MMHFM were monitored for 25 days with 5 days intervals. A PI HFM showed gradual decrease in the C_3H_6 permeance during the period of the test (Figure 7.15a), which was likely due to the aging effect of the PI. Due to its inherently high fractional free volume (FFV), the PI (i.e., 6FDA-DAM) is known to be susceptible to aging, significantly affecting its long-term gas separation.[327] In a stark contrast, a PI/ZIF-8 (30) MMHFM showed unexpectedly stable C_3H_6 permeance and C3 separation factor with time (Figure 7.15a). This stable performance might be attributed to the improved adhesion between PI and ZIF-8 as well as the free volume reduction by *in-situ* growth of ZIF-8 in the polymer. Similarly, MMMs without interfacial voids showed stable gas separation performances due to a partial anti-aging effect in the presence of fillers.[328-329]

The stability of C3 separation performance under the high pressure is of critical importance since condensable C_3H_6 and C_3H_8 gas molecules can be strongly absorbed into the polymer, resulting in plasticization of the polymer at high pressure.[274] In this regard, the prepared HFMs were tested under the feed pressure up to 6 bar of C_3H_6 single gas. As the feed pressure increased to 2 bar, the C_3H_6 permeance of the PI HFMs decreased (Figure 7.15b) which can be explained based on the dual-mode gas sorption model of glass polymer.[330-331] When the feed pressure raised over 3 bar, the C_3H_6 permeance increased (Figure 7.15b) due to the plasticization. In contrast, the PI/ZIF-8 MMHFMs showed the plasticization pressure shifted above 6 bar, continuously decreasing C_3H_6 permeance over the pressure range (Figure 7.15b). There were similar observations that plasticization was alleviated by fillers.[139, 332-333] It was likely that the

fillers effectively rigidified polymer chain, thereby suppressing plasticization of polymer. Furthermore, the decrease in the permeance with increasing feed pressure further supported that the prepared PI/ZIF-8 MMHFMs were defect-free.[334]

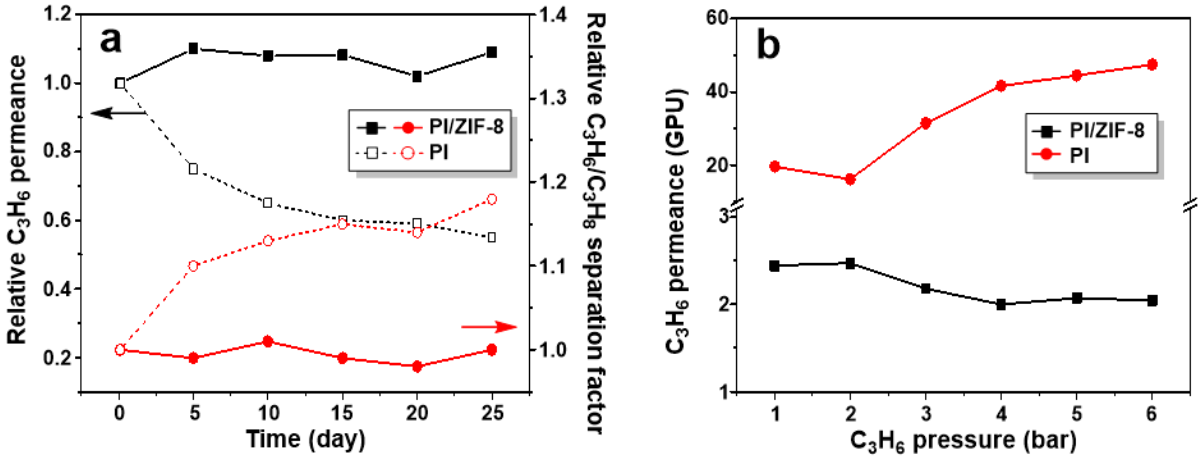

Figure 7.15. C3 separation performances of a PI HFM and a PI/ZIF-8 (30) MMHFM: (a) long-term stability and (b) pressure dependent C_3H_6 permeance.

7.3.3.3 Scale-up of the MMHFMs by the PMMOF

To show scalable fabrication of MMHFMs by the PMMOF, the membrane surface area of the PI/ZIF-8 (30) was increased by increasing the number of fibers packed in a HFM module (i.e., increasing the packing density). As the membrane surface area increased from 1.23 to 6.15 cm^2 (increasing packing density from 5 to 24 %), the C_3H_6 flow rate increased linearly and the C3 separation factor of the PI/ZIF-8 MMHFM modules remained relatively constant (Figure 7.16). When the membrane surface area further increased to 8.61 cm^2, the separation factor was sharply decreased while the C_3H_6 flow rate increased exponentially (Figure 7.16). This is likely due to the facts that the fibers could be damaged by folding upon swelling in the limited space of the module. Obviously, it becomes more difficult to control defects as the membrane surface area

increases. Further optimization of the PMMOF is required to suppress defect formation as number of fibers increases.

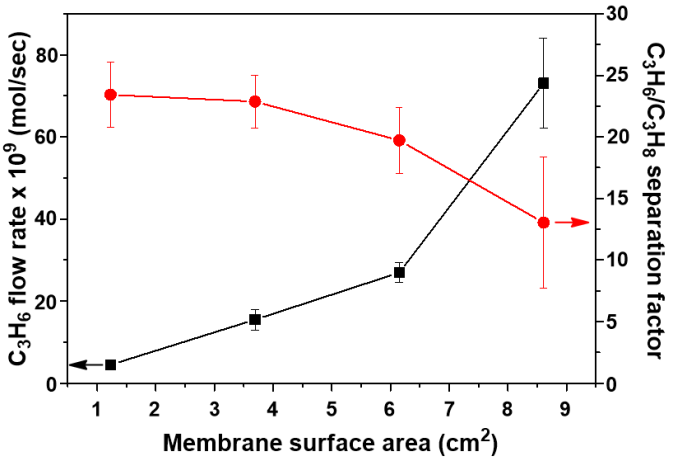

Figure 7.16. C3 separation performance of PI/ZIF-8 (30) MMHFMs as a function of membrane surface area.

7.4. Conclusion

We successfully demonstrated fabrication of 6FDA-DAM/ZIF-8 MMHFM modules by transforming modules premade of commercial polymer HFMs using the PMMOF. The PMMOF enabled *in-situ* growth of ZIF-8 inside the ultrathin 6FDA-DAM skin layer (~750 nm) coated on the porous PES hollow fiber, leading to facile transformation of polymer HFM to MMHFM in a module. To the best of our knowledge, the prepared asymmetric MMHFM exhibited the thinnest MMM skin layer (i.e., ~750 nm) among the MMHFMs reported. The *in-situ* formed ZIF-8 exhibited unique morphologies likely due to confined growth in polymer free volume. Up to ~30 wt% of ZIF-8 loading in the skin layer was achieved. As the ZIF-8 loading increased, C3 separation factor increased with the small changes in C_3H_6 permeance. Compared to the MMHFM prepared by the conventional method, the MMHFM by the PMMOF showed improved

C_3H_6/C_3H_8 separation performances even with no additional coatings (i.e., C_3H_6 permeance ~ 2.2 GPU of and C3 separation factor ~ 23.4). The MMHFM showed negligible aging effect on its C3 separation performance (up to 25 days) and little plasticization effect (up to 6 bar of C_3H_6). Finally, MMHFM modules containing up to 7 fiber strands were successfully demonstrated and their C3 separation performance was measured. Although the PMMOF process needs to be further optimized for practical large-scale applications, it is expected that the multi-strand MMHFM modules presented here would be one important step toward commercial MMHFMs.

CHAPTER VIII

CONCLUSIONS AND FUTURE DIRECTIONS

8.1. Conclusions

Polymer/MOF MMMs, in particular ZIF-8-containing MMMs, showed a great potential for propylene/propane separation. Despite tremendous efforts, there have been no MMMs applied for industrial applications mainly due to the moderate separation performances and several fundamentally challenging processing issues. In Chapter III, we propose a new paradigm of MMM fabrication based on *in-situ* formation of ZIF-8 nanocrystals in 6FDA-DAM polyimide. Our PMMOF strategy was able to 1) eliminate interfacial voids formation between polymer and filler and 2) achieve well-dispersed ZIF-8 nanocrystals with less than ~100 nm in size. Most importantly, PMMOF enables decoupling of MOF incorporation step from polymer hollow fiber membrane (HFM) processing step (i.e., spinning), overcoming one of the major engineering challenges facing the current physical-blending-based method, which is to spin filler-containing dough solutions. The resulting 6FDA-DAM/ZIF-8 MMMs prepared by PMMOF showed much improved prolylene/propane separation factor compared to the 6FDA-DAM/ZIF-8 MMMs prepared by the covonventional method, satisfying the commercial propylene/propane separation performance criteria. General applicability of PMMOF was demonstrated, enabling a myriad combinations of high quality polyimide/MOF composites. Finally, as a proof-of-concept, asymmetric mixed-matrix hollow fiber membranes with ~ 750 nm were prepared by PMMOF, showing promising C_3H_6/C_3H_8 separation performance.

PMMOF is potentially a paradigm-shifting polymer/MOF-based MMMs preparation technique. However, exploring actual synthesis condition of MOF inside polymer phase has been

yet reported and it is quite challenging due to the nature of in-situ growth of MOF in confined spaces. In Chapter IV, a systematic approach to performing an investigation of actual reaction conditions of in-situ MOF formation in polymer phase was conducted using ZIF-7 and 6FDA-DAM polyimide. First, the difference of crystal phases of ZIF-7 synthesized in a bulk solution (dense layered ZIF-7, ZIF-7(L)) and in a polymer (narrow-open pore structured ZIF-7, ZIF-7(lp)) at the same apparent reaction conditions was observed. Using the ZIF-7 crystal phase diagram determined by varying ZIF-7 precursors concentrations, the actual reaction conditions of ZIF-7 in the polymer free volume were able to be tracked. The understanding of reaction conditions of in-situ formed ZIF-7 in polymer allowed to control the crystal phases of ZIF-7, fabricating mixed-matrix membranes (MMMs) containing ZIF-7 with three different crystal phases (i.e., ZIF-7(lp), ZIF-7(L), and ZIF-7(lp-L)). Lastly, the gas separation performances of the fabricated PI/ZIF-7 MMMs were investigated. Among them, PI/ZIF-7(L) MMMs prepared by a post phase-transition from ZIF-7(lp) containing MMMs showed the significantly improved H_2/CO_2 separation performance, successfully overcoming the polymeric membrane upper bound.

Zeolitic-Imidazole Framework-8 (ZIF-8) has attracted numerous research attentions due to their well-fitting effective aperture size for propylene/propane (C3) separation. To date, there have been many reports for polymer/ZIF-8 MMMs showing promising C3 separation performances. However, the reported ZIF-8-based MMMs have rarely met the commercially attractive C3 performance criteria, which is minimum propylene permeability of 1 Barrer and selectivity of 35. In Chapter V, we reported a new strategy to in-situ tune the aperture size of ZIF-8 fillers in polymer to improve C3 separation performance of MMMs. Our method is based on doping of 2-ethylimidazole (eIm) linkers on ZIF-8 filler via in-situ formation of the fillers in the polymer. The eIm linker doping on ZIF-8 in the polymer was achieved up to ~ 50 mol%,

which was a lot more than in solution precipitation. The C3 separation performance of the resulting eIm-doped ZIF-8 containing MMMs showed dramatically improved C3 separation factor, meeting the commercially attractive criteria at the eIm-doping of ~ 30 mol% with only ~ 12 wt% of filler loading. Also, we demonstrated formation of mixed-matrix hollow fiber membranes, which is a significant step toward practical applications.

PMMOF has been developed to fabricate scalable MMMs for the commercial applications by decoupling polymer membrane processing step and filler incorporation step using in-situ formation of fillers in a polymer. However, despite the substantially enhanced separation factors, especially for propylene/propane separation by ZIF-8, the in-situ formed fillers led to densify and rigidify a polymer matrix, decreasing in the permeability with increasing filler loadings. In Chapter VI, to address this issue, we used the cross-linkable polyimide (i.e., 4,4'-(hexafluoroisopropylidene) diphthalic anhydride- diaminobenzoic acid 2,4,6-trimethyl-1,3-phenylenediamine (6FDA-DAM:DABA) (3:2)). By carefully controlling the degree of cross-linking, the propylene permeability reduction by the in-situ formed ZIF-8 fillers was effectively mitigated. We found that the inherent rigidity of polymer as well as the swelling of the polymer followed by chain rearrangement were critical to prevent the severe permeation reduction. These findings would be a valuable stepping stone for the development of the PMMOF process aiming for commercial scale MMM fabrications.

Lastly, in Chapter VII, we showed the potential of the PMMOF to produce high-quality MMHFM modules in a scalable manner by converting preformed modules made of commercial-available polyethersulfone (PES) HFMs coated with a 6FDA-DAM skin layer to 6FDA-DAM/ZIF-8 MMHFM modules. The resulting MMHFM module showed a promising propylene/propane separation performance without additional polymer coating steps, suggesting

the superiority of the PMMOF as compared to conventional spinning processes. In addition, the MMHFM prepared by the PMMOF showed relatively high resistances to aging and plasticization. Finally, we prepared and tested multi-strand MMHFM modules consisting of up to 7 fiber strands, which is, to the best of our knowledge, the first of its kind. Demonstration of multi-strand MMHFM modules presented here is expected an important step toward commercial application of MMHFMs.

8.2. Future Directions

By decoupling polymer membrane fabrications and filler incorporations using in-situ filler formations, the scalable high performance MMMs were successfully prepared by suppressing the issues of conventional blending-based MMMs fundamentally. However, the PMMOF process involves multiple steps, making the processes to be complicated and likely less economical. A new one-step scalable MMMs fabrication strategy is highly desired.

The primary key to fabricate MMMs by the one-step is the simultaneity of dry-jet/wet-quenching induced polymer phase inversion and in-situ synthesis of ZIF-8 crystals. The 6FDA-DAM polyimide (PI) solution is prepared by adding proper amounts of Zn sources (Fig. 8.1). The polymer solution is cast on a porous filter paper with a casting knife and then evaporates volatile components for a short time (dry-jet) to generate a thin and dense skin layer on the top surface (Fig. 8.1). As the casted polymer solution is immersed into the coagulation bath containing HmIm ligands, the liquid (solvent) - liquid (non-solvent) demixing occurs (wet-quenching) (Fig. 8.1). As shown in Fig. 1, the spaces occupied with solvents are filled with the infused non-solvent, which leads to entanglements of dissolved polymer chains, vitrifying the polymer with asymmetric structures. At the same time, the in-situ nucleation and growth of ZIF-8 crystals arise by the

counter-diffusion of Zn ions in the polymer solution and mIm ligand ions in the coagulation bath instantly by rapid reactions (Fig. 8.1). As a result, the asymmetric PI/ZIF-8 MMMs, which are namely in-sync MMMs, are fabricated (Fig. 8.1).

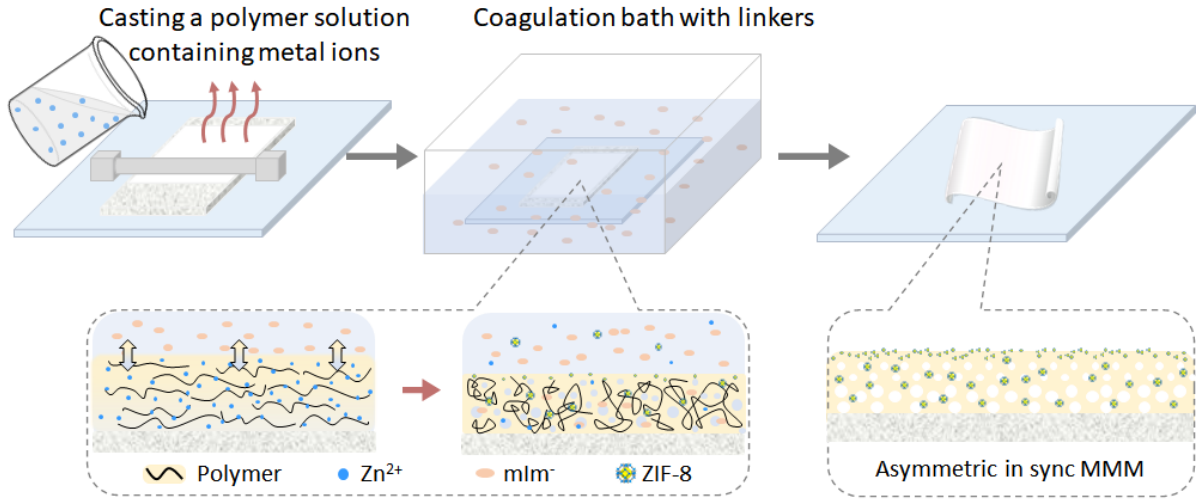

Figure 8.1. Schematic illustration of in-sync MMM fabrication.

REFERENCES

(1) Zhang, C.; Dai, Y.; Johnson, J. R.; Karvan, O.; Koros, W. J. High performance ZIF-8/6FDA-DAM mixed matrix membrane for propylene/propane separations. *Journal of Membrane Science* **2012,** *389*, 34-42.

(2) Spillman, R. Chapter 13 Economics of gas separation membrane processes. In *Membrane Science and Technology*; Noble, R. D.; Stern, S. A., Eds.; Elsevier: 1995; pp 589-667.

(3) Robeson, L. M. The upper bound revisited. *Journal of Membrane Science* **2008,** *320* (1-2), 390-400.

(4) Freeman, B. D. Basis of permeability/selectivity tradeoff relations in polymeric gas separation membranes. *Macromolecules* **1999,** *32* (2), 375-380.

(5) Vanherck, K.; Koeckelberghs, G.; Vankelecom, I. F. J. Crosslinking polyimides for membrane applications: A review. *Progress in Polymer Science* **2013,** *38* (6), 874-896.

(6) Carreon, M. A.; Li, S. G.; Falconer, J. L.; Noble, R. D. Alumina-supported SAPO-34 membranes for CO2/CH4 separation. *Journal of the American Chemical Society* **2008,** *130* (16), 5412.

(7) Jeon, M. Y.; Kim, D.; Kumar, P.; Lee, P. S.; Rangnekar, N.; Bai, P.; Shete, M.; Elyassi, B.; Lee, H. S.; Narasimharao, K.; Basahel, S. N.; Al-Thabaiti, S.; Xu, W. Q.; Cho, H. J.; Fetisov, E. O.; Thyagarajan, R.; DeJaco, R. F.; Fan, W.; Mkhoyan, K. A.; Siepmann, J. I.; Tsapatsis, M. Ultra-selective high-flux membranes from directly synthesized zeolite nanosheets. *Nature* **2017,** *543* (7647), 690-+.

(8) Koros, W. J.; Mahajan, R. Pushing the limits on possibilities for large scale gas separation: which strategies? *Journal of Membrane Science* **2000,** *175* (2), 181-196.

(9) Nandi, B. K.; Uppaluri, R.; Purkait, M. K. Preparation and characterization of low cost ceramic membranes for micro-filtration applications. *Applied Clay Science* **2008,** *42* (1-2), 102-110.

(10) Vinh-Thang, H.; Kaliaguine, S. A comprehensive computational strategy for fitting experimental permeation data of mixed matrix membranes. *Journal of Membrane Science* **2014,** *452*, 271-276.

(11) Anjum, M. W.; Bueken, B.; De Vos, D.; Vankelecom, I. F. J. MIL-125(Ti) based mixed matrix

membranes for CO2 separation from CH4 and N-2. *Journal of Membrane Science* **2016,** *502*, 21-28.

(12) Dong, G.; Li, H.; Chen, V. Challenges and opportunities for mixed-matrix membranes for gas separation. *Journal of Materials Chemistry A* **2013,** *1* (15), 4610-4630.

(13) Guo, X.; Qiao, Z.; Liu, D.; Zhong, C. Mixed-matrix membranes for CO2 separation: role of the third component. *Journal of Materials Chemistry A* **2019,** *7* (43), 24738-24759.

(14) Gao, L.; Li, C.; Huang, W.; Mei, S.; Lin, H.; Ou, Q.; Zhang, Y.; Guo, J.; Zhang, F.; Xu, S.; Zhang, H. MXene/Polymer Membranes: Synthesis, Properties, and Emerging Applications. *Chemistry of Materials* **2020,** *32* (5), 1703-1747.

(15) Guan, W.; Dai, Y.; Dong, C.; Yang, X.; Xi, Y. Zeolite imidazolate framework (ZIF)-based mixed matrix membranes for CO2 separation: A review. *Journal of Applied Polymer Science* **2020,** *137* (33), 48968.

(16) Lin, R.; Villacorta Hernandez, B.; Ge, L.; Zhu, Z. Metal organic framework based mixed matrix membranes: an overview on filler/polymer interfaces. *Journal of Materials Chemistry A* **2018,** *6* (2), 293-312.

(17) Vinh-Thang, H.; Kaliaguine, S. Predictive Models for Mixed-Matrix Membrane Performance: A Review. *Chemical Reviews* **2013,** *113* (7), 4980-5028.

(18) Kulprathipanja, S. Mixed matrix membrane development. *Membrane Technology* **2002,** *2002* (4), 9-12.

(19) Neubert, J. K. Das Verhalten von Kautschuk zu Kohlensäure. *Zeitschrift für Chemie und Industrie der Kolloide* **1912,** *11* (3), 136-136.

(20) Christen, G. F., A.; Faure, A. Membrane Hétérogène Pour le Fractionnement de Mélanges Fluides, et Son Emploi. 2,079,460 (A5), 1971.

(21) Kemp, D. R.; Paul, D. R. Gas sorption in polymer membranes containing adsorptive fillers. *Journal of Polymer Science: Polymer Physics Edition* **1974,** *12* (3), 485-500.

(22) Li, S. K. W. N. N. Separation of fluids by means of mixed matrix membranes. US4740219A, 1988.

(23) Robeson, L. M. Correlation of separation factor versus permeability for polymeric membranes.

Journal of Membrane Science **1991,** *62* (2), 165-185.

(24) Robeson, L. M. The upper bound revisited. *Journal of Membrane Science* **2008,** *320* (1), 390-400.

(25) Jia, M.; Peinemann, K.-V.; Behling, R.-D. Molecular sieving effect of the zeolite-filled silicone rubber membranes in gas permeation. *Journal of Membrane Science* **1991,** *57* (2), 289-292.

(26) Duval, J.-M.; Kemperman, A. J. B.; Folkers, B.; Mulder, M. H. V.; Desgrandchamps, G.; Smolders, C. A. Preparation of zeolite filled glassy polymer membranes. *Journal of Applied Polymer Science* **1994,** *54* (4), 409-418.

(27) Bouma, R. H. B.; Checchetti, A.; Chidichimo, G.; Drioli, E. Permeation through a heterogeneous membrane: the effect of the dispersed phase. *Journal of Membrane Science* **1997,** *128* (2), 141-149.

(28) Mahajan, R.; Koros, W. J. Factors Controlling Successful Formation of Mixed-Matrix Gas Separation Materials. *Industrial & Engineering Chemistry Research* **2000,** *39* (8), 2692-2696.

(29) David Richard Corbin, H. C. F., Mark Brandon Shiflett Mixed matrix nanoporous carbon membranes. WO2001097956A1, 2001.

(30) Okan Max Ekiner, S. S. K. Process for making hollow fiber mixed matrix membranes. US6663805B1, 2003.

(31) Yehia, H.; Pisklak, T. J.; Ferraris, J.; Balkus, K.; Musselman, I. H. Methane Facilitated Transport Using Copper(II) Biphenyl Dicarboxylatetriethylenediamine/Poly(3-Acetoxyethylthiophene) Mixed Matrix Membranes. *Polym. Prepr.* **2004,** *45*, 35-36.

(32) Jeong, H.-K.; Krych, W.; Ramanan, H.; Nair, S.; Marand, E.; Tsapatsis, M. Fabrication of Polymer/Selective-Flake Nanocomposite Membranes and Their Use in Gas Separation. *Chemistry of Materials* **2004,** *16* (20), 3838-3845.

(33) Takahashi, S.; Paul, D. R. Gas permeation in poly(ether imide) nanocomposite membranes based on surface-treated silica. Part 1: Without chemical coupling to matrix. *Polymer* **2006,** *47* (21), 7519-7534.

(34) Shu; Husain, S.; Koros, W. J. Formation of Nanostructured Zeolite Particle Surfaces via a Halide/Grignard Route. *Chemistry of Materials* **2007,** *19* (16), 4000-4006.

(35) Ordoñez, M. J. C.; Balkus, K. J.; Ferraris, J. P.; Musselman, I. H. Molecular sieving realized with ZIF-8/Matrimid® mixed-matrix membranes. *Journal of Membrane Science* **2010,** *361* (1), 28-37.

(36) Bae, T.-H.; Lee, J. S.; Qiu, W.; Koros, W. J.; Jones, C. W.; Nair, S. A High-Performance Gas-Separation Membrane Containing Submicrometer-Sized Metal–Organic Framework Crystals. *Angew Chem Int Ed* **2010,** *49* (51), 9863-9866.

(37) Park, K. S.; Ni, Z.; Côté, A. P.; Choi, J. Y.; Huang, R.; Uribe-Romo, F. J.; Chae, H. K.; O'Keeffe, M.; Yaghi, O. M. Exceptional chemical and thermal stability of zeolitic imidazolate frameworks. *Proceedings of National Academy of Sciences of the United States of America* **2006,** *103* (27), 10186-10191.

(38) Ahn, J.; Chung, W.-J.; Pinnau, I.; Song, J.; Du, N.; Robertson, G. P.; Guiver, M. D. Gas transport behavior of mixed-matrix membranes composed of silica nanoparticles in a polymer of intrinsic microporosity (PIM-1). *Journal of Membrane Science* **2010,** *346* (2), 280-287.

(39) Yu, X.; Wang, Z.; Zhao, J.; Yuan, F.; Li, S.; Wang, J.; Wang, S. An Effective Method to Improve the Performance of Fixed Carrier Membrane via Incorporation of CO2-selective Adsorptive Silica Nanoparticles. *Chinese Journal of Chemical Engineering* **2011,** *19* (5), 821-832.

(40) Seoane, B.; Sebastián, V.; Téllez, C.; Coronas, J. Crystallization in THF: the possibility of one-pot synthesis of mixed matrix membranes containing MOF MIL-68(Al). *CrystEngComm* **2013,** *15* (45), 9483-9490.

(41) Mari, V.; Bhagiyalakshmi, M.; Alqaheem, Y.; Alomair, A.; Pérez, A.; Rana, M. Recent Progress of Fillers in Mixed Matrix Membranes for CO 2 Separation: A Review. *Separation and Purification Technology* **2017,** *188*, 431-450.

(42) Goh, P. S.; Ismail, A. F.; Sanip, S. M.; Ng, B. C.; Aziz, M. Recent advances of inorganic fillers in mixed matrix membrane for gas separation. *Separation and Purification Technology* **2011,** *81* (3), 243-264.

(43) Galizia, M.; Chi, W. S.; Smith, Z. P.; Merkel, T. C.; Baker, R. W.; Freeman, B. D. 50th Anniversary Perspective: Polymers and Mixed Matrix Membranes for Gas and Vapor Separation: A Review and Prospective Opportunities. *Macromolecules* **2017,** *50* (20), 7809-7843.

(44) Li, W.; Pan, F.; Song, Y.; Wang, M.; Wang, H.; Walker, S.; Wu, H.; Jiang, Z. Construction of molecule-selective mixed matrix membranes with confined mass transfer structure. *Chinese Journal of Chemical Engineering* **2017,** *25* (11), 1563-1580.

(45) Hamid, M. R. A.; Jeong, H.-K. Recent advances on mixed-matrix membranes for gas separation: Opportunities and engineering challenges. *Korean Journal of Chemical Engineering* **2018,** *35* (8), 1577-1600.

(46) Kim, W.-g.; Nair, S. Membranes from nanoporous 1D and 2D materials: A review of opportunities, developments, and challenges. *Chemical Engineering Science* **2013,** *104*, 908-924.

(47) Park, H. B.; Kamcev, J.; Robeson, L. M.; Elimelech, M.; Freeman, B. D. Maximizing the right stuff: The trade-off between membrane permeability and selectivity. *Science* **2017,** *356* (6343), eaab0530.

(48) Ebadi Amooghin, A.; Mashhadikhan, S.; Sanaeepur, H.; Moghadassi, A.; Matsuura, T.; Ramakrishna, S. Substantial breakthroughs on function-led design of advanced materials used in mixed matrix membranes (MMMs): A new horizon for efficient CO2 separation. *Progress in Materials Science* **2019,** *102*, 222-295.

(49) Li, X.; Cheng, Y.; Zhang, H.; Wang, S.; Jiang, Z.; Guo, R.; Wu, H. Efficient CO2 Capture by Functionalized Graphene Oxide Nanosheets as Fillers To Fabricate Multi-Permselective Mixed Matrix Membranes. *Acs Applied Materials & Interfaces* **2015,** *7* (9), 5528-5537.

(50) Kang, Z.; Peng, Y.; Qian, Y.; Yuan, D.; Addicoat, M. A.; Heine, T.; Hu, Z.; Tee, L.; Guo, Z.; Zhao, D. Mixed Matrix Membranes (MMMs) Comprising Exfoliated 2D Covalent Organic Frameworks (COFs) for Efficient CO2 Separation. *Chemistry of Materials* **2016,** *28* (5), 1277-1285.

(51) Mubashir, M.; Fong, Y. Y.; Leng, C. T.; Keong, L. K. Issues and Current Trends of Hollow-Fiber Mixed-Matrix Membranes for CO2 Separation from N2 and CH4. **2018,** *41* (2), 235-252.

(52) Aroon, M. A.; Ismail, A. F.; Montazer-Rahmati, M. M.; Matsuura, T. Effect of chitosan as a functionalization agent on the performance and separation properties of polyimide/multi-walled carbon nanotubes mixed matrix flat sheet membranes. *Journal of Membrane Science* **2010,** *364* (1), 309-317.

(53) Nafisi, V.; Hägg, M.-B. Development of dual layer of ZIF-8/PEBAX-2533 mixed matrix membrane for CO2 capture. *Journal of Membrane Science* **2014,** *459*, 244-255.

(54) Zulhairun, A. K.; Ismail, A. F.; Matsuura, T.; Abdullah, M. S.; Mustafa, A. Asymmetric mixed matrix membrane incorporating organically modified clay particle for gas separation. *Chemical Engineering Journal* **2014,** *241*, 495-503.

(55) Sun, J.; Li, Q.; Chen, G.; Duan, J.; Liu, G.; Jin, W. MOF-801 incorporated PEBA mixed-matrix composite membranes for CO2 capture. *Separation and Purification Technology* **2019,** *217*, 229-239.

(56) Hua, Y.; Wang, H.; Li, Q.; Chen, G.; Liu, G.; Duan, J.; Jin, W. Highly efficient CH4 purification by LaBTB PCP-based mixed matrix membranes. *Journal of Materials Chemistry A* **2018,** *6* (2), 599-606.

(57) Md. Nordin, N. A. H.; Ismail, A. F.; Mustafa, A.; Murali, R. S.; Matsuura, T. Utilizing low ZIF-8 loading for an asymmetric PSf/ZIF-8 mixed matrix membrane for CO2/CH4 separation. *Rsc Advances* **2015,** *5* (38), 30206-30215.

(58) Zahri, K.; Wong, K. C.; Goh, P. S.; Ismail, A. F. Graphene oxide/polysulfone hollow fiber mixed matrix membranes for gas separation. *Rsc Advances* **2016,** *6* (92), 89130-89139.

(59) Liu, G.; Chernikova, V.; Liu, Y.; Zhang, K.; Belmabkhout, Y.; Shekhah, O.; Zhang, C.; Yi, S.; Eddaoudi, M.; Koros, W. J. Mixed matrix formulations with MOF molecular sieving for key energy-intensive separations. *Nature Materials* **2018,** *17* (3), 283-289.

(60) Dong, G. X.; Li, H. Y.; Chen, V. K. Challenges and opportunities for mixed-matrix membranes for gas separation. *Journal of Materials Chemistry A* **2013,** *1* (15), 4610-4630.

(61) Hamid, M. R. A.; Jeong, H. K. Recent advances on mixed-matrix membranes for gas separation: Opportunities and engineering challenges. *Korean Journal of Chemical Engineering* **2018,** *35* (8), 1577-1600.

(62) Aroon, M. A.; Ismail, A. F.; Matsuura, T.; Montazer-Rahmati, M. M. Performance studies of mixed matrix membranes for gas separation: A review. *Separation and Purification Technology* **2010,** *75* (3), 229-242.

(63) Perez, E. V.; Karunaweera, C.; Musselman, I. H.; Balkus, K. J.; Ferraris, J. P. J. P. Origins and evolution of inorganic-based and MOF-based mixed-matrix membranes for gas separations. **2016,** *4* (3), 32.

(64) Ryan Adams, J. R. J., Chen Zhang, Ryan Lively, Ying Dai, Omoyen Esekhile, Junqiang Liu, William J. Koros. Mixed-Matrix Membranes. In *Encyclopedia of Membrane Science and Technology*; E.M. Hoek, V. V. T., Ed.; 2013; pp 1-34.

(65) Park, S.; Kang, W. R.; Kwon, H. T.; Kim, S.; Seo, M.; Bang, J.; Lee, S. h.; Jeong, H. K.; Lee, J. S. The polymeric upper bound for N2/NF3 separation and beyond; ZIF-8 containing mixed matrix membranes. *Journal of Membrane Science* **2015,** *486*, 29-39.

(66) Thompson, J. A.; Chapman, K. W.; Koros, W. J.; Jones, C. W.; Nair, S. Sonication-induced Ostwald ripening of ZIF-8 nanoparticles and formation of ZIF-8/polymer composite membranes. *Microporous and Mesoporous Materials* **2012,** *158*, 292-299.

(67) Xie, K.; Fu, Q.; Qiao, G. G.; Webley, P. A. Recent progress on fabrication methods of polymeric thin film gas separation membranes for CO2 capture. *Journal of Membrane Science* **2019,** *572*, 38-60.

(68) Duval, J.-M.; Kemperman, A. J. B.; Folkers, B.; Mulder, M. H. V.; Desgrandchamps, G.; Smolders, C. A. Preparation of zeolite filled glassy polymer membranes. **1994,** *54* (4), 409-418.

(69) Roh, D. K.; Kim, S. J.; Jeon, H.; Kim, J. H. Nanocomposites with Graft Copolymer-Templated Mesoporous MgTiO3 Perovskite for CO2 Capture Applications. *Acs Applied Materials & Interfaces* **2013,** *5* (14), 6615-6621.

(70) Yang, K.; Dai, Y.; Ruan, X.; Zheng, W.; Yang, X.; Ding, R.; He, G. Stretched ZIF-8@GO flake-like fillers via pre-Zn(II)-doping strategy to enhance CO2 permeation in mixed matrix membranes. *Journal of Membrane Science* **2020,** *601*, 117934.

(71) Burmann, P.; Zornoza, B.; Téllez, C.; Coronas, J. Mixed matrix membranes comprising MOFs and porous silicate fillers prepared via spin coating for gas separation. *Chemical Engineering Science* **2014,** *107*, 66-75.

(72) Fauzan, N. A. B.; Mannan, H. A.; Nasir, R.; Mohshim, D. F. B.; Mukhtar, H. Various Techniques for Preparation of Thin-Film Composite Mixed-Matrix Membranes for CO2 Separation. *Chemical Engineering & Technology* **2019,** *42* (12), 2608-2620.

(73) Chaki, S. H.; Mahato, K. S.; Malek, T. J.; Deshpande, M. P. CuAlS2 thin films – Dip coating deposition and characterization. *Journal of Science: Advanced Materials and Devices* **2017,** *2* (2), 215-224.

(74) Fan, H.; Shi, Q.; Yan, H.; Ji, S.; Dong, J.; Zhang, G. Simultaneous Spray Self-Assembly of Highly Loaded ZIF-8–PDMS Nanohybrid Membranes Exhibiting Exceptionally High Biobutanol-Permselective Pervaporation. *Angew Chem Int Ed* **2014,** *53* (22), 5578-5582.

(75) Mohammed Rasool Qtaishat, S. A. Novel techniques for preparing multi-layer polymeric and mixed matrix membranes and a device for membrane distillation. WO2014111889A2, 2014.

(76) Weigelt, F.; Georgopanos, P.; Shishatskiy, S.; Filiz, V.; Brinkmann, T.; Abetz, V. Development and Characterization of Defect-Free Matrimid(®) Mixed-Matrix Membranes Containing Activated Carbon Particles for Gas Separation. *Polymers* **2018,** *10* (1), 51.

(77) Nasir, R.; Mukhtar, H.; Man, Z.; Mohshim, D. F. Material Advancements in Fabrication of Mixed-Matrix Membranes. *Chemical Engineering & Technology* **2013,** *36* (5), 717-727.

(78) Liu, J.; Bae, T.-H.; Qiu, W.; Husain, S.; Nair, S.; Jones, C. W.; Chance, R. R.; Koros, W. J. Butane isomer transport properties of 6FDA–DAM and MFI–6FDA–DAM mixed matrix membranes. *Journal of Membrane Science* **2009,** *343* (1), 157-163.

(79) Askari, M.; Chung, T.-S. Natural gas purification and olefin/paraffin separation using thermal cross-linkable co-polyimide/ZIF-8 mixed matrix membranes. *Journal of Membrane Science* **2013,** *444*, 173-183.

(80) Francis, L. F. Chapter 3 - Melt Processes. In *Materials Processing*; Francis, L. F., Ed.; Academic Press: Boston, 2016; pp 105-249.

(81) Kim, J.-J.; Jang, T.-S.; Kwon, Y.-D.; Kim, U. Y.; Kim, S. S. Structural study of microporous polypropylene hollow fiber membranes made by the melt-spinning and cold-stretching method. *Journal of Membrane Science* **1994,** *93* (3), 209-215.

(82) Wei, F. J.; Shao, H. J.; Wu, B.; Zhang, K. Z.; Luo, D. J.; Qin, S. H.; Hao, Z. Effect of Spin-Draw Rate and Stretching Ratio on Polypropylene Hollow Fiber Membrane Made by Melt-Spinning and Stretching Method. *International Polymer Processing* **2018,** *33* (1), 13-19.

(83) Shahidi, K.; Rodrigue, D. Production of Composite Membranes by Coupling Coating and Melt Extrusion/Salt Leaching. *Industrial & Engineering Chemistry Research* **2017,** *56* (5), 1306-1315.

(84) Razzaz, Z.; Rodrigue, D. Hollow Fiber Porous Nanocomposite Membranes Produced via Continuous Extrusion: Morphology and Gas Transport Properties. *Materials (Basel,*

Switzerland) **2018,** *11* (11), 2311.

(85) Covarrubias, C.; Quijada, R. Preparation of aluminophosphate/polyethylene nanocomposite membranes and their gas permeation properties. *Journal of Membrane Science* **2010,** *358* (1), 33-42.

(86) Kathuria, A.; Abiad, M. G.; Auras, R. Deterioration of metal–organic framework crystal structure during fabrication of poly(l-lactic acid) mixed-matrix membranes. *Polymer International* **2013,** *62* (8), 1144-1151.

(87) Kim, H.; Abdala, A. A.; Macosko, C. W. Graphene/Polymer Nanocomposites. *Macromolecules* **2010,** *43* (16), 6515-6530.

(88) Sinha Ray, S.; Okamoto, M. Polymer/layered silicate nanocomposites: a review from preparation to processing. *Progress in Polymer Science* **2003,** *28* (11), 1539-1641.

(89) Adak, B.; Joshi, M.; Butola, B. S. Polyurethane/clay nanocomposites with improved helium gas barrier and mechanical properties: Direct versus master-batch melt mixing route. *Journal of Applied Polymer Science* **2018,** *135* (27), 46422.

(90) Fasihi, M.; Abolghasemi, M. R. Oxygen barrier and mechanical properties of masterbatch-based PA6/nanoclay composite films. *Journal of Applied Polymer Science* **2012,** *125* (S1), E2-E8.

(91) Zhu, A.; Cai, A.; Zhang, J.; Jia, H.; Wang, J. PMMA-grafted-silica/PVC nanocomposites: Mechanical performance and barrier properties. *Journal of Applied Polymer Science* **2008,** *108* (4), 2189-2196.

(92) Kim, H.; Macosko, C. W. Morphology and Properties of Polyester/Exfoliated Graphite Nanocomposites. *Macromolecules* **2008,** *41* (9), 3317-3327.

(93) Kim, H.; Macosko, C. W. Processing-property relationships of polycarbonate/graphene composites. *Polymer* **2009,** *50* (15), 3797-3809.

(94) Jin, J.; Rafiq, R.; Gill, Y. Q.; Song, M. Preparation and characterization of high performance of graphene/nylon nanocomposites. *European Polymer Journal* **2013,** *49* (9), 2617-2626.

(95) Cui, Y.; Kundalwal, S. I.; Kumar, S. Gas barrier performance of graphene/polymer nanocomposites. *Carbon* **2016,** *98*, 313-333.

(96) Maiti, P.; Yamada, K.; Okamoto, M.; Ueda, K.; Okamoto, K. New Polylactide/Layered Silicate Nanocomposites: Role of Organoclays. *Chemistry of Materials* **2002,** *14* (11), 4654-4661.

(97) Sinha Ray, S.; Yamada, K.; Okamoto, M.; Ogami, A.; Ueda, K. New Polylactide/Layered Silicate Nanocomposites. 3. High-Performance Biodegradable Materials. *Chemistry of Materials* **2003,** *15* (7), 1456-1465.

(98) Rigotti, D.; Checchetto, R.; Tarter, S.; Caretti, D.; Rizzuto, M.; Fambri, L.; Pegoretti, A. Polylactic acid-lauryl functionalized nanocellulose nanocomposites: Microstructural, thermo-mechanical and gas transport properties. *Express Polymer Letters* **2019,** *13*, 858-876.

(99) Han, J.; Lee, W.; Choi, J. M.; Patel, R.; Min, B.-R. Characterization of polyethersulfone/polyimide blend membranes prepared by a dry/wet phase inversion: Precipitation kinetics, morphology and gas separation. *Journal of Membrane Science* **2010,** *351* (1), 141-148.

(100) Husain, S.; Koros, W. J. Mixed matrix hollow fiber membranes made with modified HSSZ-13 zeolite in polyetherimide polymer matrix for gas separation. *Journal of Membrane Science* **2007,** *288* (1), 195-207.

(101) Jiang, L. Y.; Chung, T. S.; Cao, C.; Huang, Z.; Kulprathipanja, S. Fundamental understanding of nano-sized zeolite distribution in the formation of the mixed matrix single- and dual-layer asymmetric hollow fiber membranes. *Journal of Membrane Science* **2005,** *252* (1), 89-100.

(102) Widjojo, N.; Chung, T.-S. Thickness and Air Gap Dependence of Macrovoid Evolution in Phase-Inversion Asymmetric Hollow Fiber Membranes. *Industrial & Engineering Chemistry Research* **2006,** *45* (22), 7618-7626.

(103) Li, Y.; Chung, T.-S.; Huang, Z.; Kulprathipanja, S. Dual-layer polyethersulfone (PES)/BTDA-TDI/MDI co-polyimide (P84) hollow fiber membranes with a submicron PES–zeolite beta mixed matrix dense-selective layer for gas separation. *Journal of Membrane Science* **2006,** *277* (1), 28-37.

(104) Zhu, H.; Jie, X.; Wang, L.; Kang, G.; Liu, D.; Cao, Y. Effect of MIL-53 on phase inversion and gas separation performance of mixed matrix hollow fiber membranes. *Rsc Advances* **2016,** *6* (73), 69124-69134.

(105) Wang, Y.; Wang, X.; Guan, J.; Yang, L.; Ren, Y.; Nasir, N.; Wu, H.; Chen, Z.; Jiang, Z. 110th Anniversary: Mixed Matrix Membranes with Fillers of Intrinsic Nanopores for Gas

Separation. *Industrial & Engineering Chemistry Research* **2019,** *58* (19), 7706-7724.

(106) Sun, H.; Wang, T.; Xu, Y.; Gao, W.; Li, P.; Niu, Q. J. Fabrication of polyimide and functionalized multi-walled carbon nanotubes mixed matrix membranes by in-situ polymerization for CO2 separation. *Separation and Purification Technology* **2017,** *177*, 327-336.

(107) Ma, L.; Svec, F.; Tan, T.; Lv, Y. Mixed Matrix Membrane Based on Cross-Linked Poly[(ethylene glycol) methacrylate] and Metal–Organic Framework for Efficient Separation of Carbon Dioxide and Methane. *Acs Applied Nano Materials* **2018,** *1* (6), 2808-2818.

(108) Molavi, H.; Shojaei, A.; Mousavi, S. A. Improving mixed-matrix membrane performance via PMMA grafting from functionalized NH2–UiO-66. *Journal of Materials Chemistry A* **2018,** *6* (6), 2775-2791.

(109) Lin, R.; Ge, L.; Hou, L.; Strounina, E.; Rudolph, V.; Zhu, Z. Mixed Matrix Membranes with Strengthened MOFs/Polymer Interfacial Interaction and Improved Membrane Performance. *Acs Applied Materials & Interfaces* **2014,** *6* (8), 5609-5618.

(110) Tien-Binh, N.; Rodrigue, D.; Kaliaguine, S. In-situ cross interface linking of PIM-1 polymer and UiO-66-NH2 for outstanding gas separation and physical aging control. *Journal of Membrane Science* **2018,** *548*, 429-438.

(111) Zhang, Y.; Feng, X.; Li, H.; Chen, Y.; Zhao, J.; Wang, S.; Wang, L.; Wang, B. Photoinduced postsynthetic polymerization of a metal-organic framework toward a flexible stand-alone membrane. *Angew Chem Int Ed Engl* **2015,** *54* (14), 4259-4263.

(112) Zhang, S.; Zhang, J.; Zhang, Y.; Deng, Y. Nanoconfined Ionic Liquids. *Chemical Reviews* **2017,** *117* (10), 6755-6833.

(113) Yao, B.-J.; Ding, L.-G.; Li, F.; Li, J.-T.; Fu, Q.-J.; Ban, Y.; Guo, A.; Dong, Y.-B. Chemically Cross-Linked MOF Membrane Generated from Imidazolium-Based Ionic Liquid-Decorated UiO-66 Type NMOF and Its Application toward CO2 Separation and Conversion. *Acs Applied Materials & Interfaces* **2017,** *9* (44), 38919-38930.

(114) Lau, W. J.; Ismail, A. F.; Misdan, N.; Kassim, M. A. A recent progress in thin film composite membrane: A review. *Desalination* **2012,** *287*, 190-199.

(115) Wong, K. C.; Goh, P. S.; Ismail, A. F. Thin film nanocomposite: the next generation selective

membrane for CO2 removal. *Journal of Materials Chemistry A* **2016,** *4* (41), 15726-15748.

(116) Yu, S.; Li, S.; Huang, S.; Zeng, Z.; Cui, S.; Liu, Y. Covalently bonded zeolitic imidazolate frameworks and polymers with enhanced compatibility in thin film nanocomposite membranes for gas separation. *Journal of Membrane Science* **2017,** *540*, 155-164.

(117) Wong, K. C.; Goh, P. S.; Ng, B. C.; Ismail, A. F. Thin film nanocomposite embedded with polymethyl methacrylate modified multi-walled carbon nanotubes for CO2 removal. *Rsc Advances* **2015,** *5* (40), 31683-31690.

(118) Awad, A.; Aljundi, I. H. Layer-by-layer assembly of carbide derived carbon-polyamide membrane for CO2 separation from natural gas. *Energy* **2018,** *157*, 188-199.

(119) Sánchez-Laínez, J.; Paseta, L.; Navarro, M.; Zornoza, B.; Téllez, C.; Coronas, J. Ultrapermeable Thin Film ZIF-8/Polyamide Membrane for H2/CO2 Separation at High Temperature without Using Sweep Gas. *Advanced Materials Interfaces* **2018,** *5* (19), 1800647.

(120) Kim, J. H.; Lee, Y. M. Gas permeation properties of poly(amide-6-b-ethylene oxide)–silica hybrid membranes. *Journal of Membrane Science* **2001,** *193* (2), 209-225.

(121) Gomes, D.; Nunes, S. P.; Peinemann, K.-V. Membranes for gas separation based on poly(1-trimethylsilyl-1-propyne)–silica nanocomposites. *Journal of Membrane Science* **2005,** *246* (1), 13-25.

(122) Marti, A. M.; Venna, S. R.; Roth, E. A.; Culp, J. T.; Hopkinson, D. P. Simple Fabrication Method for Mixed Matrix Membranes with in Situ MOF Growth for Gas Separation. *Acs Applied Materials & Interfaces* **2018,** *10* (29), 24784-24790.

(123) Ma, L.; Svec, F.; Lv, Y.; Tan, T. In situ bottom–up growth of metal–organic frameworks in a crosslinked poly(ethylene oxide) layer with ultrahigh loading and superior uniform distribution. *Journal of Materials Chemistry A* **2019,** *7* (35), 20293-20301.

(124) Park, S.; Abdul Hamid, M. R.; Jeong, H.-K. Highly Propylene-Selective Mixed-Matrix Membranes by in Situ Metal–Organic Framework Formation Using a Polymer-Modification Strategy. *Acs Applied Materials & Interfaces* **2019,** *11* (29), 25949-25957.

(125) Park, S.; Jeong, H.-K. In-situ linker doping as an effective means to tune zeolitic-imidazolate framework-8 (ZIF-8) fillers in mixed-matrix membranes for propylene/propane separation. *Journal of Membrane Science* **2020,** *596*, 117689.

(126) Sanders, D. E.; Smith, Z. P.; Guo, R. L.; Robeson, L. M.; McGrath, J. E.; Paul, D. R.; Freeman, B. D. Energy-efficient polymeric gas separation membranes for a sustainable future: A review. *Polymer* **2013,** *54* (18), 4729-4761.

(127) Ghosh, T. K.; Lin, H. D.; Hines, A. L. Hybrid Adsorption Distillation Process for Separating Propane and Propylene. *Industrial & Engineering Chemistry Research* **1993,** *32* (10), 2390-2399.

(128) Amedi, H. R.; Aghajani, M. Economic Estimation of Various Membranes and Distillation for Propylene and Propane Separation. *Industrial & Engineering Chemistry Research* **2018,** *57* (12), 4366-4376.

(129) Burns, R. L.; Koros, W. J. Defining the challenges for C3H6/C3H8 separation using polymeric membranes. *Journal of Membrane Science* **2003,** *211* (2), 299-309.

(130) Kwon, H. T.; Jeong, H. K.; Lee, A. S.; An, H. S.; Lee, J. S. Heteroepitaxially Grown Zeolitic Imidazolate Framework Membranes with Unprecedented Propylene/Propane Separation Performances. *Journal of the American Chemical Society* **2015,** *137* (38), 12304-12311.

(131) Lee, M. J.; Kwon, H. T.; Jeong, H. K. High-Flux Zeolitic Imidazolate Framework Membranes for Propylene/Propane Separation by Postsynthetic Linker Exchange. *Angewandte Chemie-International Edition* **2018,** *57* (1), 156-161.

(132) Pimentel, B. R.; Parulkar, A.; Zhou, E. K.; Brunelli, N. A.; Lively, R. P. Zeolitic Imidazolate Frameworks: Next-Generation Materials for Energy-Efficient Gas Separations. *Chemsuschem* **2014,** *7* (12), 3202-3240.

(133) Vinoba, M.; Bhagiyalakshmi, M.; Alqaheem, Y.; Alomair, A. A.; Perez, A.; Rana, M. S. Recent progress of fillers in mixed matrix membranes for CO2 separation: A review. *Separation and Purification Technology* **2017,** *188*, 431-450.

(134) Lin, R. J.; Hernandez, B. V.; Ge, L.; Zhu, Z. H. Metal organic framework based mixed matrix membranes: an overview on filler/polymer interfaces. *Journal of Materials Chemistry A* **2018,** *6* (2), 293-312.

(135) Yang, F.; Mu, H.; Wang, C. Q.; Xiang, L.; Yao, K. X.; Liu, L. M.; Yang, Y.; Han, Y.; Li, Y. S.; Pan, Y. C. Morphological Map of ZIF-8 Crystals with Five Distinctive Shapes: Feature of Filler in Mixed-Matrix Membranes on C3H6/C3H8 Separation. *Chemistry of Materials* **2018,** *30* (10), 3467-3473.

(136) Ordonez, M. J. C.; Balkus, K. J.; Ferraris, J. P.; Musselman, I. H. Molecular sieving realized with ZIF-8/Matrimid (R) mixed-matrix membranes. *Journal of Membrane Science* **2010,** *361* (1-2), 28-37.

(137) Song, Q. L.; Nataraj, S. K.; Roussenova, M. V.; Tan, J. C.; Hughes, D. J.; Li, W.; Bourgoin, P.; Alam, M. A.; Cheetham, A. K.; Al-Muhtaseb, S. A.; Sivaniah, E. Zeolitic imidazolate framework (ZIF-8) based polymer nanocomposite membranes for gas separation. *Energy & Environmental Science* **2012,** *5* (8), 8359-8369.

(138) Lin, R. J.; Ge, L.; Diao, H.; Rudolph, V.; Zhu, Z. H. Propylene/propane selective mixed matrix membranes with grape-branched MOF/CNT filler. *Journal of Materials Chemistry A* **2016,** *4* (16), 6084-6090.

(139) Yu, J.; Wang, C. Q.; Xiang, L.; Xu, Y. Z.; Pan, Y. C. Enhanced C3H6/C3H8 separation performance in poly(vinyl acetate) membrane blended with ZIF-8 nanocrystals. *Chemical Engineering Science* **2018,** *179*, 1-12.

(140) Liu, D. H.; Xiang, L.; Chang, H.; Chen, K.; Wang, C. Q.; Pan, Y. C.; Li, Y. S.; Jiang, Z. Y. Rational matching between MOFs and polymers in mixed matrix membranes for propylene/propane separation. *Chemical Engineering Science* **2019,** *204*, 151-160.

(141) Zhang, C.; Lively, R. P.; Zhang, K.; Johnson, J. R.; Karvan, O.; Koros, W. J. Unexpected Molecular Sieving Properties of Zeolitic Imidazolate Framework-8. *Journal of Physical Chemistry Letters* **2012,** *3* (16), 2130-2134.

(142) Zhang, C.; Zhang, K.; Xu, L. R.; Labreche, Y.; Kraftschik, B.; Koros, W. J. Highly scalable ZIF-based mixed-matrix hollow fiber membranes for advanced hydrocarbon separations. *Aiche Journal* **2014,** *60* (7), 2625-2635.

(143) Zhang, C.; Koros, W. J. Zeolitic lmidazolate Framework-Enabled Membranes: Challenges and Opportunities. *Journal of Physical Chemistry Letters* **2015,** *6* (19), 3841-3849.

(144) Zhu, H. T.; Jie, X. M.; Cao, Y. M. Fabrication of Functionalized MOFs Incorporated Mixed Matrix Hollow Fiber Membrane for Gas Separation. *Journal of Chemistry* **2017**,

(145) Abdul Hamid, M. R.; Kim, S.; Kim, J. S.; Lee, Y. M.; Jeong, H.-K. In-Situ Formation of Zeolitic-Imidazolate Framework Thin Films and Composites Using Modified Polymer Substrates. *Journal of Materials Chemistry A* **2019**,

(146) Chen, Z. W.; Holmberg, B.; Li, W. Z.; Wang, X.; Deng, W. Q.; Munoz, R.; Yan, Y. S. Nafion/zeolite nanocomposite membrane by in situ crystallization for a direct methanol fuel cell. *Chemistry of Materials* **2006,** *18* (24), 5669-5675.

(147) Clausi, D. T.; Koros, W. J. A rapid feedback characterization technique for polymeric hollow fiber membranes using disperse dyes. *Journal of Membrane Science* **1997,** *129* (2), 237-242.

(148) Kim, S. I.; Pyo, S. M.; Ree, M. Investigation of glass transition behaviors in poly(amic acid) precursors of semiflexible polyimides by oscillating differential scanning calorimetry. *Macromolecules* **1997,** *30* (25), 7890-7897.

(149) Chugunova, N. F.; Startsev, V. M.; Bartenev, G. M.; Bardyshev, I. I.; Skvortsov, A. G. Kinetics of Change of Free-Volume of Films during Thermal Imidization of Polyamic Acid. *Vysokomolekulyarnye Soedineniya Seriya A* **1984,** *26* (9), 1944-1948.

(150) Ioan, S.; Cosutchi, A. I.; Hulubei, C.; Macocinschi, D.; Ioanid, G. Surface and interfacial properties of poly(amic acid)s and polyimides. *Polymer Engineering and Science* **2007,** *47* (4), 381-389.

(151) Koros, W. J.; Zhang, C. Materials for next-generation molecularly selective synthetic membranes. *Nature Materials* **2017,** *16* (3), 289-297.

(152) Yu, H. C.; Jung, J. W.; Choi, J. Y.; Chung, C. M. Kinetic Study of Low-Temperature Imidization of Poly(amic acid)s and Preparation of Colorless, Transparent Polyimide Films. *Journal of Polymer Science Part a-Polymer Chemistry* **2016,** *54* (11), 1593-1602.

(153) Xu, Y.; Zhao, A. L.; Wang, X. L.; Xue, H.; Liu, F. L. Influence of Curing Accelerators on the Imidization of Polyamic Acids and Properties of Polyimide Films. *Journal of Wuhan University of Technology-Materials Science Edition* **2016,** *31* (5), 1137-1143.

(154) Kim, G. H.; Dong, W.; Yoon, C. S.; Kim, Y. H. Synthesis of duplex nanoparticles in polyimide by the reaction of polyamic acid with Cu-Zn alloy films. *Colloids and Surfaces a-Physicochemical and Engineering Aspects* **2008,** *321* (1-3), 292-296.

(155) Wang, M. S.; Jiang, L. X.; Kim, E. J.; Hahn, S. H. Electronic structure and optical properties of Zn(OH)(2): LDA+U calculations and intense yellow luminescence. *Rsc Advances* **2015,** *5* (106), 87496-87503.

(156) Pradhan, D.; Sindhwani, S.; Leung, K. T. Template-Free Electrochemical Growth of Single-Crystalline Zinc Nanowires at an Anomalously Low Temperature. *Journal of Physical*

Chemistry C **2009,** *113* (36), 15788-15791.

(157) Wind, J. D.; Staudt-Bickel, C.; Paul, D. R.; Koros, W. J. The effects of crosslinking chemistry on CO2 plasticization of polyimide gas separation membranes. *Industrial & Engineering Chemistry Research* **2002,** *41* (24), 6139-6148.

(158) Ba, C. Y.; Economy, J. Preparation of PMDA/ODA polyimide membrane for use as substrate in a thermally stable composite reverse osmosis membrane. *Journal of Membrane Science* **2010,** *363* (1-2), 140-148.

(159) Taubert, A.; Wind, J. D.; Paul, D. R.; Koros, W. J.; Winey, K. I. Novel polyimide ionomers: CO2 plasticization, morphology, and ion distribution. *Polymer* **2003,** *44* (6), 1881-1892.

(160) Liu, H.; Guo, P.; Regueira, T.; Wang, Z. H.; Du, J. F.; Chen, G. J. Irreversible Change of the Pore Structure of ZIF-8 in Carbon Dioxide Capture with Water Coexistence. *Journal of Physical Chemistry C* **2016,** *120* (24), 13287-13294.

(161) Dong, W. G.; Kim, G. H.; Choi, J. Y.; Ybon, J. R.; Kim, Y. H. A study of the curing behavior of polyamic acid coated on a Cu or Zn layer. *Colloids and Surfaces a-Physicochemical and Engineering Aspects* **2008,** *324* (1-3), 122-125.

(162) Wu, Z. P.; Wu, D. Z.; Yang, W. T.; Jin, R. G. Preparation of highly reflective and conductive metallized polyimide films through surface modification: processing, morphology and properties. *Journal of Materials Chemistry* **2006,** *16* (3), 310-316.

(163) Lively, R. P.; Dose, M. E.; Xu, L. R.; Vaughn, J. T.; Johnson, J. R.; Thompson, J. A.; Zhang, K.; Lydon, M. E.; Lee, J. S.; Liu, L.; Hu, Z. S.; Karvan, O.; Realff, M. J.; Koros, W. J. A high-flux polyimide hollow fiber membrane to minimize footprint and energy penalty for CO2 recovery from flue gas. *Journal of Membrane Science* **2012,** *423*, 302-313.

(164) Hou, C. T.; Xu, Q.; Peng, J. Y.; Ji, Z. P.; Hu, X. Y. (110)-Oriented ZIF-8 Thin Films on ITO with Controllable Thickness. *Chemphyschem* **2013,** *14* (1), 140-144.

(165) Qiu, W. L.; Chen, C. C.; Kincer, M. R.; Koros, W. J. Thermal analysis and its application in evaluation of fluorinated polyimide membranes for gas separation. *Polymer* **2011,** *52* (18), 4073-4082.

(166) James, J. B.; Lin, Y. S. Kinetics of ZIF-8 Thermal Decomposition in Inert, Oxidizing, and Reducing Environments. *Journal of Physical Chemistry C* **2016,** *120* (26), 14015-14026.

(167) Pal, R. Permeation models for mixed matrix membranes. *Journal of Colloid and Interface Science* **2008,** *317* (1), 191-198.

(168) Craig Colling, G. H., John Bartels Processes using solid perm-selective membranes in multiple groups for simultaneous recovery of specified products from a fluid mixture. 2002.

(169) Semino, R.; Moreton, J. C.; Ramsahye, N. A.; Cohen, S. M.; Maurin, G. Understanding the origins of metal–organic framework/polymer compatibility. *Chemical Science* **2018,** *9* (2), 315-324.

(170) Ahmed, I.; Jhung, S. H. Composites of metal–organic frameworks: Preparation and application in adsorption. *Materials Today* **2014,** *17* (3), 136-146.

(171) Sachdeva, S.; Soccol, D.; Gravesteijn, D. J.; Kapteijn, F.; Sudhölter, E. J. R.; Gascon, J.; de Smet, L. C. P. M. Polymer–Metal Organic Framework Composite Films as Affinity Layer for Capacitive Sensor Devices. *ACS Sensors* **2016,** *1* (10), 1188-1192.

(172) Liang, X.; Zhang, F.; Feng, W.; Zou, X.; Zhao, C.; Na, H.; Liu, C.; Sun, F.; Zhu, G. From metal–organic framework (MOF) to MOF–polymer composite membrane: enhancement of low-humidity proton conductivity. *Chemical Science* **2013,** *4* (3), 983-992.

(173) Li, H.; Eddaoudi, M.; O'Keeffe, M.; Yaghi, O. M. Design and synthesis of an exceptionally stable and highly porous metal-organic framework. *Nature* **1999,** *402* (6759), 276-279.

(174) Park, K. S.; Ni, Z.; Cote, A. P.; Choi, J. Y.; Huang, R. D.; Uribe-Romo, F. J.; Chae, H. K.; O'Keeffe, M.; Yaghi, O. M. Exceptional chemical and thermal stability of zeolitic imidazolate frameworks. *Proceedings of the National Academy of Sciences of the United States of America* **2006,** *103* (27), 10186-10191.

(175) Wu, M.-X.; Yang, Y.-W. Metal–Organic Framework (MOF)-Based Drug/Cargo Delivery and Cancer Therapy. **2017,** *29* (23), 1606134.

(176) Cui, Y. J.; Yue, Y. F.; Qian, G. D.; Chen, B. L. Luminescent Functional Metal-Organic Frameworks. *Chemical Reviews* **2012,** *112* (2), 1126-1162.

(177) Yoon, M.; Srirambalaji, R.; Kim, K. Homochiral Metal–Organic Frameworks for Asymmetric Heterogeneous Catalysis. *Chemical Reviews* **2012,** *112* (2), 1196-1231.

(178) Li, J. R.; Sculley, J.; Zhou, H. C. Metal-Organic Frameworks for Separations. *Chemical Reviews* **2012,** *112* (2), 869-932.

(179) Li, J. R.; Kuppler, R. J.; Zhou, H. C. Selective gas adsorption and separation in metal-organic frameworks. *Chemical Society Reviews* **2009,** *38* (5), 1477-1504.

(180) Zornoza, B.; Tellez, C.; Coronas, J.; Gascon, J.; Kapteijn, F. Metal organic framework based mixed matrix membranes: An increasingly important field of research with a large application potential. *Microporous and Mesoporous Materials* **2013,** *166*, 67-78.

(181) Jeazet, H. B. T.; Staudt, C.; Janiak, C. Metal-organic frameworks in mixed-matrix membranes for gas separation. *Dalton Transactions* **2012,** *41* (46), 14003-14027.

(182) Schejn, A.; Balan, L.; Falk, V.; Aranda, L.; Medjahdi, G.; Schneider, R. Controlling ZIF-8 nano- and microcrystal formation and reactivity through zinc salt variations. *Crystengcomm* **2014,** *16* (21), 4493-4500.

(183) Cravillon, J.; Nayuk, R.; Springer, S.; Feldhoff, A.; Huber, K.; Wiebcke, M. Controlling Zeolitic Imidazolate Framework Nano- and Microcrystal Formation: Insight into Crystal Growth by Time-Resolved In Situ Static Light Scattering. *Chemistry of Materials* **2011,** *23* (8), 2130-2141.

(184) Aguado, S.; Bergeret, G.; Titus, M. P.; Moizan, V.; Nieto-Draghi, C.; Bats, N.; Farrusseng, D. Guest-induced gate-opening of a zeolite imidazolate framework. *New Journal of Chemistry* **2011,** *35* (3), 546-550.

(185) Li, Y. S.; Liang, F. Y.; Bux, H.; Feldhoff, A.; Yang, W. S.; Caro, J. Molecular Sieve Membrane: Supported Metal-Organic Framework with High Hydrogen Selectivity. *Angewandte Chemie-International Edition* **2010,** *49* (3), 548-551.

(186) Zhao, P.; Lampronti, G. I.; Lloyd, G. O.; Wharmby, M. T.; Facq, S.; Cheetham, A. K.; Redfern, S. A. T. Phase Transitions in Zeolitic Imidazolate Framework 7: The Importance of Framework Flexibility and Guest-Induced Instability. *Chemistry of Materials* **2014,** *26* (5), 1767-1769.

(187) He, M.; Yao, J. F.; Li, L. X.; Wang, K.; Chen, F. Y.; Wang, H. T. Synthesis of Zeolitic Imidazolate Framework-7 in a Water/Ethanol Mixture and Its Ethanol-Induced Reversible Phase Transition. *Chempluschem* **2013,** *78* (10), 1222-1225.

(188) Li, T.; Pan, Y. C.; Peinemann, K. V.; Lai, Z. P. Carbon dioxide selective mixed matrix composite membrane containing ZIF-7 nano-fillers. *Journal of Membrane Science* **2013,** *425*, 235-242.

(189) Yang, T. X.; Xiao, Y. C.; Chung, T. S. Poly-/metal-benzimidazole nano-composite membranes for hydrogen purification. *Energy & Environmental Science* **2011,** *4* (10), 4171-4180.

(190) Xiang, L.; Sheng, L. Q.; Wang, C. Q.; Zhang, L. X.; Pan, Y. C.; Li, Y. S. Amino-Functionalized ZIF-7 Nanocrystals: Improved Intrinsic Separation Ability and Interfacial Compatibility in Mixed-Matrix Membranes for CO2/CH4 Separation. *Advanced Materials* **2017,** *29* (32),

(191) Al-Maythalony, B. A.; Alloush, A. M.; Faizan, M.; Dafallah, H.; Elgzoly, M. A. A.; Seliman, A. A. A.; Al-Ahmed, A.; Yamani, Z. H.; Habib, M. A. M.; Cordova, K. E.; Yaghi, O. M. Tuning the Interplay between Selectivity and Permeability of ZIF-7 Mixed Matrix Membranes. *Acs Applied Materials & Interfaces* **2017,** *9* (39), 33401-33407.

(192) Park, S.; Hamid, M. R. A.; Jeong, H. K. Highly Propylene-Selective Mixed-Matrix Membranes by in Situ Metal Organic Framework Formation Using a Polymer-Modification Strategy. *Acs Applied Materials & Interfaces* **2019,** *11* (29), 25949-25957.

(193) Hamid, M. R. A.; Park, S.; Kim, J. S.; Lee, Y. M.; Jeong, H. K. In situ formation of zeolitic-imidazolate framework thin films and composites using modified polymer substrates. *Journal of Materials Chemistry A* **2019,** *7* (16), 9680-9689.

(194) Song, Z.; Huang, Y.; Xu, W. L.; Wang, L.; Bao, Y.; Li, S.; Yu, M. Continuously Adjustable, Molecular-Sieving “Gate” on 5A Zeolite for Distinguishing Small Organic Molecules by Size. *Scientific Reports* **2015,** *5*, 13981.

(195) Al-Amshawee, S.; Yunus, M. Y. B.; Azoddein, A. A. M.; Hassell, D. G.; Dakhil, I. H.; Abu Hasan, H. Electrodialysis desalination for water and wastewater: A review. *Chemical Engineering Journal* **2020,** *380*,

(196) Do, Y. S.; Lee, W. H.; Seong, J. G.; Kim, J. S.; Wang, H. H.; Doherty, C. M.; Hill, A. J.; Lee, Y. M. Thermally rearranged (TR) bismaleimide-based network polymers for gas separation membranes. *Chemical Communications* **2016,** *52* (93), 13556-13559.

(197) Morris, W.; He, N.; Ray, K. G.; Klonowski, P.; Furukawa, H.; Daniels, I. N.; Houndonougbo, Y. A.; Asta, M.; Yaghi, O. M.; Laird, B. B. A Combined Experimental-Computational Study on the Effect of Topology on Carbon Dioxide Adsorption in Zeolitic Imidazolate Frameworks. *Journal of Physical Chemistry C* **2012,** *116* (45), 24084-24090.

(198) Park, S.; Jang, E.; An, H.; Choi, W.; Kim, J. H.; Lee, J. H.; Choi, J.; Lee, J. S. The Lifshitz-van der Waals acid-base theory assisted fabrication of MFI-containing mixed matrix membranes for gas separations. *Microporous and Mesoporous Materials* **2018,** *264*, 60-69.

(199) Li, Y.-S.; Liang, F.-Y.; Bux, H.; Feldhoff, A.; Yang, W.-S.; Caro, J. Molecular Sieve Membrane: Supported Metal–Organic Framework with High Hydrogen Selectivity. **2010,** *49* (3), 548-551.

(200) Park, S.; Lee, A. S.; Do, Y. S.; Kim, J. F.; Hwang, S. S.; Lee, Y. M.; Lee, J. H.; Lee, J. S. Side-chain engineering of ladder-structured polysilsesquioxane membranes for gas separations. *Journal of Membrane Science* **2016,** *516*, 202-214.

(201) Bachman, J. E.; Long, J. R. Plasticization-resistant Ni2(dobdc)/polyimide composite membranes for the removal of CO2 from natural gas. *Energy & Environmental Science* **2016,** *9* (6), 2031-2036.

(202) Peng, Y.; Li, Y.; Ban, Y.; Jin, H.; Jiao, W.; Liu, X.; Yang, W. Metal-organic framework nanosheets as building blocks for molecular sieving membranes. **2014,** *346* (6215), 1356-1359.

(203) Perez, E. V.; Balkus, K. J.; Ferraris, J. P.; Musselman, I. H. Mixed-matrix membranes containing MOF-5 for gas separations. *Journal of Membrane Science* **2009,** *328* (1-2), 165-173.

(204) Karatay, E.; Kalipcilar, H.; Yilmaz, L. Preparation and performance assessment of binary and ternary PES-SAPO 34-HMA based gas separation membranes. *Journal of Membrane Science* **2010,** *364* (1-2), 75-81.

(205) Zornoza, B.; Esekhile, O.; Koros, W. J.; Tellez, C.; Coronas, J. Hollow silicalite-1 sphere-polymer mixed matrix membranes for gas separation. *Separation and Purification Technology* **2011,** *77* (1), 137-145.

(206) Ahmad, J.; Hagg, M. B. Development of matrimid/zeolite 4A mixed matrix membranes using low boiling point solvent. *Separation and Purification Technology* **2013,** *115*, 190-197.

(207) Seoane, B.; Tellez, C.; Coronas, J.; Staudt, C. NH2-MIL-53(Al) and NH2-MIL-101(Al) in sulfur-containing copolyimide mixed matrix membranes for gas separation. *Separation and Purification Technology* **2013,** *111*, 72-81.

(208) Wijenayake, S. N.; Panapitiya, N. P.; Versteeg, S. H.; Nguyen, C. N.; Goel, S.; Balkus, K. J.;

Musselman, I. H.; Ferraris, J. P. Surface Cross-Linking of ZIF-8/Polyimide Mixed Matrix Membranes (MMMs) for Gas Separation. *Industrial & Engineering Chemistry Research* **2013,** *52* (21), 6991-7001.

(209) Arjmandi, M.; Pakizeh, M. Mixed matrix membranes incorporated with cubic-MOF-5 for improved polyetherimide gas separation membranes: Theory and experiment. *Journal of Industrial and Engineering Chemistry* **2014,** *20* (5), 3857-3868.

(210) Hsieh, J. O.; Balkus, K. J.; Ferraris, J. P.; Musselman, I. H. MIL-53 frameworks in mixed-matrix membranes. *Microporous and Mesoporous Materials* **2014,** *196*, 165-174.

(211) Zhuang, G. L.; Tseng, H. H.; Wey, M. Y. Preparation of PPO-silica mixed matrix membranes by in-situ sol-gel method for H-2/CO2 separation. *International Journal of Hydrogen Energy* **2014,** *39* (30), 17178-17190.

(212) Boroglu, M. S.; Yumru, A. B. Gas separation performance of 6FDA-DAM-ZIF-11 mixed-matrix membranes for H-2/CH4 and CO2/CH4 separation. *Separation and Purification Technology* **2017,** *173*, 269-279.

(213) Perez, E. V.; Kalaw, G. J. D.; Ferraris, J. P.; Balkus, K. J.; Musselman, I. H. Amine-functionalized (Al) MIL-53/VTEC™ mixed-matrix membranes for H2/CO2 mixture separations at high pressure and high temperature. *Journal of Membrane Science* **2017,** *530*, 201-212.

(214) Xue, Q. Z.; Pan, X. L.; Li, X. F.; Zhang, J. Q.; Guo, Q. K. Effective enhancement of gas separation performance in mixed matrix membranes using core/shell structured multi-walled carbon nanotube/graphene oxide nanoribbons. *Nanotechnology* **2017,** *28* (6),

(215) Arjmandi, M.; Pakizeh, M.; Saghi, M.; Arjmandi, A. J. P. C. Study of Separation Behavior of Activated and Non-Activated MOF-5 as Filler on MOF-based Mixed-Matrix Membranes in H2/CO2 Separation. **2018,** *58* (4), 317-329.

(216) Lanč, M.; Sysel, P.; Šoltys, M.; Štěpánek, F.; Fónod, K.; Klepić, M.; Vopička, O.; Lhotka, M.; Ulbrich, P.; Friess, K. Synthesis, preparation and characterization of novel hyperbranched 6FDA-TTM based polyimide membranes for effective CO2 separation: Effect of embedded mesoporous silica particles and siloxane linkages. *Polymer* **2018,** *144*, 33-42.

(217) Pulyalina, A.; Polotskaya, G.; Rostovtseva, V.; Pientka, Z.; Toikka, A. Improved Hydrogen Separation Using Hybrid Membrane Composed of Nanodiamonds and P84 Copolyimide.

Polymers **2018,** *10* (8),

(218) Yumru, A. B.; Safak Boroglu, M.; Boz, I. ZIF-11/Matrimid® mixed matrix membranes for efficient CO2, CH4, and H2 separations. **2018,** *8* (3), 529-541.

(219) Detlev Fritsch, K.-V. P., Dominique De Figueiredo Gomes Composite material, in particular composite membrane, and process for the production of the same. US7658784B2, 2010.

(220) Car, A.; Stropnik, C.; Peinemann, K.-V. Hybrid membrane materials with different metal–organic frameworks (MOFs) for gas separation. *Desalination* **2006,** *200* (1), 424-426.

(221) Zhang, Y.; Musselman, I. H.; Ferraris, J. P.; Balkus, K. J. Gas permeability properties of Matrimid® membranes containing the metal-organic framework Cu–BPY–HFS. *Journal of Membrane Science* **2008,** *313* (1), 170-181.

(222) Chunqing Liu, B. M., Stephen T. Wilson, Annabelle I. Benin, Mark E. Schott Metal organic framework—polymer mixed matrix membranes. US7637983B1, 2009.

(223) Perez, E. V.; Balkus, K. J.; Ferraris, J. P.; Musselman, I. H. Mixed-matrix membranes containing MOF-5 for gas separations. *Journal of Membrane Science* **2009,** *328* (1), 165-173.

(224) Díaz, K.; López-González, M.; del Castillo, L. F.; Riande, E. Effect of zeolitic imidazolate frameworks on the gas transport performance of ZIF8-poly(1,4-phenylene ether-ether-sulfone) hybrid membranes. *Journal of Membrane Science* **2011,** *383* (1), 206-213.

(225) Song, Q.; Nataraj, S. K.; Roussenova, M. V.; Tan, J. C.; Hughes, D. J.; Li, W.; Bourgoin, P.; Alam, M. A.; Cheetham, A. K.; Al-Muhtaseb, S. A.; Sivaniah, E. Zeolitic imidazolate framework (ZIF-8) based polymer nanocomposite membranes for gas separation. *Energy & Environmental Science* **2012,** *5* (8), 8359-8369.

(226) Yang, T.; Shi, G. M.; Chung, T.-S. Symmetric and Asymmetric Zeolitic Imidazolate Frameworks (ZIFs)/Polybenzimidazole (PBI) Nanocomposite Membranes for Hydrogen Purification at High Temperatures. **2012,** *2* (11), 1358-1367.

(227) Yang, T.; Chung, T.-S. High performance ZIF-8/PBI nano-composite membranes for high temperature hydrogen separation consisting of carbon monoxide and water vapor. *International Journal of Hydrogen Energy* **2013,** *38* (1), 229-239.

(228) Bushell, A. F.; Attfield, M. P.; Mason, C. R.; Budd, P. M.; Yampolskii, Y.; Starannikova, L.;

Rebrov, A.; Bazzarelli, F.; Bernardo, P.; Carolus Jansen, J.; Lanč, M.; Friess, K.; Shantarovich, V.; Gustov, V.; Isaeva, V. Gas permeation parameters of mixed matrix membranes based on the polymer of intrinsic microporosity PIM-1 and the zeolitic imidazolate framework ZIF-8. *Journal of Membrane Science* **2013,** *427*, 48-62.

(229) Yang, T.; Chung, T.-S. Room-temperature synthesis of ZIF-90 nanocrystals and the derived nano-composite membranes for hydrogen separation. *Journal of Materials Chemistry A* **2013,** *1* (19), 6081-6090.

(230) Ge, L.; Zhou, W.; Rudolph, V.; Zhu, Z. Mixed matrix membranes incorporated with size-reduced Cu-BTC for improved gas separation. *Journal of Materials Chemistry A* **2013,** *1* (21), 6350-6358.

(231) Cao, L.; Tao, K.; Huang, A.; Kong, C.; Chen, L. A highly permeable mixed matrix membrane containing CAU-1-NH2 for H2 and CO2 separation. *Chemical Communications* **2013,** *49* (76), 8513-8515.

(232) Sorribas, S.; Zornoza, B.; Téllez, C.; Coronas, J. Mixed matrix membranes comprising silica-(ZIF-8) core–shell spheres with ordered meso–microporosity for natural- and bio-gas upgrading. *Journal of Membrane Science* **2014,** *452*, 184-192.

(233) Bhaskar, A.; Banerjee, R.; Kharul, U. ZIF-8@PBI-BuI composite membranes: elegant effects of PBI structural variations on gas permeation performance. *Journal of Materials Chemistry A* **2014,** *2* (32), 12962-12967.

(234) Li, L.; Yao, J.; Wang, X.; Cheng, Y.-B.; Wang, H. ZIF-11/Polybenzimidazole composite membrane with improved hydrogen separation performance. **2014,** *131* (22),

(235) Carter, D.; Tezel, F. H.; Kruczek, B.; Kalipcilar, H. Investigation and comparison of mixed matrix membranes composed of polyimide matrimid with ZIF – 8, silicalite, and SAPO – 34. *Journal of Membrane Science* **2017,** *544*, 35-46.

(236) Sánchez-Laínez, J.; Zornoza, B.; Mayoral, Á.; Berenguer-Murcia, Á.; Cazorla-Amorós, D.; Téllez, C.; Coronas, J. Beyond the H2/CO2 upper bound: one-step crystallization and separation of nano-sized ZIF-11 by centrifugation and its application in mixed matrix membranes. *Journal of Materials Chemistry A* **2015,** *3* (12), 6549-6556.

(237) Kang, Z.; Peng, Y.; Hu, Z.; Qian, Y.; Chi, C.; Yeo, L. Y.; Tee, L.; Zhao, D. Mixed matrix membranes composed of two-dimensional metal–organic framework nanosheets for pre-combustion CO2 capture: a relationship study of filler morphology versus membrane

performance. *Journal of Materials Chemistry A* **2015,** *3* (41), 20801-20810.

(238) Sholl, D. S.; Lively, R. P. Seven chemical separations to change the world. *Nature* **2016,** *532* (7600), 435-437.

(239) Craig W. Colling, G. A. H., John V. Bartels PROCESSES USING SOLID PERM-SELECTIVE MEMBRANES IN MULTIPLE GROUPS FOR SIMULTANEOUS RECOVERY OF SPECIFIED PRODUCTS FROM A FLUID MIXTURE. 0004040 A1, 2004.

(240) Phan, A.; Doonan, C. J.; Uribe-Romo, F. J.; Knobler, C. B.; O'Keeffe, M.; Yaghi, O. M. Synthesis, Structure, and Carbon Dioxide Capture Properties of Zeolitic Imidazolate Frameworks. *Accounts of Chemical Research* **2010,** *43* (1), 58-67.

(241) Thompson, J. A.; Blad, C. R.; Brunelli, N. A.; Lydon, M. E.; Lively, R. P.; Jones, C. W.; Nair, S. Hybrid Zeolitic Imidazolate Frameworks: Controlling Framework Porosity and Functionality by Mixed-Linker Synthesis. *Chemistry of Materials* **2012,** *24* (10), 1930-1936.

(242) Hillman, F.; Zimmerman, J. M.; Paek, S. M.; Hamid, M. R. A.; Lim, W. T.; Jeong, H. K. Rapid microwave-assisted synthesis of hybrid zeolitic-imidazolate frameworks with mixed metals and mixed linkers. *Journal of Materials Chemistry A* **2017,** *5* (13), 6090-6099.

(243) Krokidas, P.; Castier, M.; Moncho, S.; Sredojevic, D. N.; Brothers, E. N.; Kwon, H. T.; Jeong, H. K.; Lee, J. S.; Economou, I. G. ZIF-67 Framework: A Promising New Candidate for Propylene/Propane Separation. Experimental Data and Molecular Simulations. *Journal of Physical Chemistry C* **2016,** *120* (15), 8116-8124.

(244) Krokidas, P.; Moncho, S.; Brothers, E. N.; Castier, M.; Economou, I. G. Tailoring the gas separation efficiency of metal organic framework ZIF-8 through metal substitution: a computational study. *Physical Chemistry Chemical Physics* **2018,** *20* (7), 4879-4892.

(245) Eum, K.; Jayachandrababu, K. C.; Rashidi, F.; Zhang, K.; Leisen, J.; Graham, S.; Lively, R. P.; Chance, R. R.; Sholl, D. S.; Jones, C. W.; Nair, S. Highly Tunable Molecular Sieving and Adsorption Properties of Mixed-Linker Zeolitic Imidazolate Frameworks. *Journal of the American Chemical Society* **2015,** *137* (12), 4191-4197.

(246) Hillman, F.; Brito, J.; Jeong, H. K. Rapid One-Pot Microwave Synthesis of Mixed-Linker Hybrid Zeolitic-Imidazolate Framework Membranes for Tunable Gas Separations. *Acs Applied Materials & Interfaces* **2018,** *10* (6), 5586-5593.

(247) Sanchez-Lainez, J.; Veiga, A.; Zornoza, B.; Balestra, S. R. G.; Hamad, S.; Ruiz-Salvador, A. R.; Calero, S.; Tellez, C.; Coronas, J. Tuning the separation properties of zeolitic imidazolate framework core-shell structures via post-synthetic modification. *Journal of Materials Chemistry A* **2017,** *5* (48), 25601-25608.

(248) Krokidas, P.; Moncho, S.; Brothers, E. N.; Castier, M.; Jeong, H. K.; Economou, I. G. On the Efficient Separation of Gas Mixtures with the Mixed-Linker Zeolitic-Imidazolate Framework-7-8. *Acs Applied Materials & Interfaces* **2018,** *10* (46), 39631-39644.

(249) Hou, Q. Q.; Wu, Y.; Zhou, S.; Wei, Y. Y.; Caro, J.; Wang, H. H. Ultra-Tuning of the Aperture Size in Stiffened ZIF-8_Cm Frameworks with Mixed-Linker Strategy for Enhanced CO2/CH4 Separation. *Angewandte Chemie-International Edition* **2019,** *58* (1), 327-331.

(250) Hillman, F.; Jeong, H. K. Linker-Doped Zeolitic Imidazolate Frameworks (ZIFs) and Their Ultrathin Membranes for Tunable Gas Separations. *Acs Applied Materials & Interfaces* **2019,** *11* (20), 18377-18385.

(251) Chung, T. S.; Jiang, L. Y.; Li, Y.; Kulprathipanja, S. Mixed matrix membranes (MMMs) comprising organic polymers with dispersed inorganic fillers for gas separation. *Progress in Polymer Science* **2007,** *32* (4), 483-507.

(252) Liu, C.; Kulprathipanja, S.; M. W. Hillock, A.; Husain, S.; Koros, W. Recent Progress in Mixed-Matrix Membranes. 2008; pp 787-819.

(253) Thompson, J. A.; Vaughn, J. T.; Brunelli, N. A.; Koros, W. J.; Jones, C. W.; Nair, S. Mixed-linker zeolitic imidazolate framework mixed-matrix membranes for aggressive CO2 separation from natural gas. *Microporous and Mesoporous Materials* **2014,** *192*, 43-51.

(254) Zhang, S. M. A reliable and efficient first principles-based method for predicting pKa values. 4. organic bases. *Journal of Computational Chemistry* **2012,** *33* (31), 2469-2482.

(255) Ma, X. L.; Kumar, P.; Mittal, N.; Khlyustova, A.; Daoutidis, P.; Mkhoyan, K. A.; Tsapatsis, M. Zeolitic imidazolate framework membranes made by ligand-induced permselectivation. *Science* **2018,** *361* (6406), 1008-1011.

(256) Sun, H. X.; Ma, C.; Wang, T.; Xu, Y. Y.; Yuan, B. B.; Li, P.; Kong, Y. Preparation and Characterization of C60-Filled Ethyl Cellulose Mixed-Matrix Membranes for Gas Separation of Propylene/Propane. *Chemical Engineering & Technology* **2014,** *37* (4), 611-619.

(257) Yuan, B. B.; Sun, H. X.; Wang, T.; Xu, Y. Y.; Li, P.; Kong, Y.; Niu, Q. J. Propylene/propane permeation properties of ethyl cellulose (EC) mixed matrix membranes fabricated by incorporation of nanoporous graphene nanosheets. *Scientific Reports* **2016,** *6*,

(258) An, H.; Park, S.; Kwon, H. T.; Jeong, H. K.; Lee, J. S. A new superior competitor for exceptional propylene/propane separations: ZIF-67 containing mixed matrix membranes. *Journal of Membrane Science* **2017,** *526*, 367-376.

(259) Amedi, H. R.; Aghajani, M. Modified zeolitic-midazolate framework 8/poly(ether-block-amide) mixed-matrix membrane for propylene and propane separation. *Journal of Applied Polymer Science* **2018,** *135* (21),

(260) Ma, X. H.; Swaidan, R. J.; Wang, Y. G.; Hsiung, C. E.; Han, Y.; Pinnau, I. Highly Compatible Hydroxyl-Functionalized Microporous Polyimide-ZIF-8 Mixed Matrix Membranes for Energy Efficient Propylene/Propane Separation. *Acs Applied Nano Materials* **2018,** *1* (7), 3541-3547.

(261) Kunjattu, S. H.; Ashok, V.; Bhaskar, A.; Pandare, K.; Banerjee, R.; Kharul, U. K. ZIF-8@DBzPBI-BuI composite membranes for olefin/paraffin separation. *Journal of Membrane Science* **2018,** *549*, 38-45.

(262) Liu, Y.; Chen, Z. J.; Liu, G. P.; Belmabkhout, Y.; Adil, K.; Eddaoudi, M.; Koros, W. Conformation-Controlled Molecular Sieving Effects for Membrane-Based Propylene/Propane Separation. *Advanced Materials* **2019,** *31* (14),

(263) Verploegh, R. J.; Wu, Y.; Sholl, D. S. Lattice-Gas Modeling of Adsorbate Diffusion in Mixed-Linker Zeolitic Imidazolate Frameworks: Effect of Local Imidazolate Ordering. *Langmuir* **2017,** *33* (26), 6481-6491.

(264) Diestel, L.; Wang, N. Y.; Schwiedland, B.; Steinbach, F.; Giese, U.; Caro, J. MOF based MMMs with enhanced selectivity due to hindered linker distortion. *Journal of Membrane Science* **2015,** *492*, 181-186.

(265) Fairen-Jimenez, D.; Moggach, S. A.; Wharmby, M. T.; Wright, P. A.; Parsons, S.; Duren, T. Opening the Gate: Framework Flexibility in ZIF-8 Explored by Experiments and Simulations. *Journal of the American Chemical Society* **2011,** *133* (23), 8900-8902.

(266) Lee, M. J.; Hamid, M. R. A.; Lee, J.; Kim, J. S.; Lee, Y. M.; Jeong, H. K. Ultrathin zeolitic-imidazolate framework ZIF-8 membranes on polymeric hollow fibers for propylene/propane separation. *Journal of Membrane Science* **2018,** *559*, 28-34.

(267) Mahajan, R.; Koros, W. J. Mixed matrix membrane materials with glassy polymers. Part 1. *Polymer Engineering and Science* **2002,** *42* (7), 1420-1431.

(268) Zhang, C.; Zhang, K.; Xu, L.; Labreche, Y.; Kraftschik, B.; Koros, W. J. Highly scalable ZIF-based mixed-matrix hollow fiber membranes for advanced hydrocarbon separations. *Aiche Journal* **2014,** *60* (7), 2625-2635.

(269) Park, S.; Cho, K. Y.; Jeong, H. K. Polyimide/ZIF-7 mixed-matrix membranes: understanding thein situconfined formation of the ZIF-7 phases inside a polymer and their effects on gas separations. *Journal of Materials Chemistry A* **2020,** *8* (22), 11210-11217.

(270) Park, S.; Jeong, H. K. Transforming polymer hollow fiber membrane modules to mixed-matrix hollow fiber membrane modules for propylene/propane separation. *Journal of Membrane Science* **2020,** *612*,

(271) Ghosal, K.; Freeman, B. D. Gas separation using polymer membranes: an overview. **1994,** *5* (11), 673-697.

(272) Monsalve-Bravo, G. M.; Dutta, R. C.; Bhatia, S. K. Multiscale simulation of gas transport in mixed-matrix membranes with interfacial polymer rigidification. *Microporous and Mesoporous Materials* **2020,** *296*,

(273) Chen, C. C.; Qiu, W. L.; Miller, S. J.; Koros, W. J. Plasticization-resistant hollow fiber membranes for CO2/CH4 separation based on a thermally crosslinkable polyimide. *Journal of Membrane Science* **2011,** *382* (1-2), 212-221.

(274) Velioglu, S.; Ahunbay, M. G.; Tantekin-Ersolmaz, S. B. Propylene/propane plasticization in polyimide membranes. *Journal of Membrane Science* **2016,** *501*, 179-190.

(275) Qiu, W.; Chen, C.-C.; Xu, L.; Cui, L.; Paul, D. R.; Koros, W. J. Sub-Tg Cross-Linking of a Polyimide Membrane for Enhanced CO2 Plasticization Resistance for Natural Gas Separation. *Macromolecules* **2011,** *44* (15), 6046-6056.

(276) Cui, L. L.; Qiu, W. L.; Paul, D. R.; Koros, W. J. Responses of 6FDA-based polyimide thin membranes to CO2 exposure and physical aging as monitored by gas permeability. *Polymer* **2011,** *52* (24), 5528-5537.

(277) Hillock, A. M. W.; Koros, W. J. Cross-linkable polyimide membrane for natural gas purification and carbon dioxide plasticization reduction. *Macromolecules* **2007,** *40* (3), 583-

587.

(278) Qiu, W. L.; Xu, L. R.; Chen, C. C.; Paul, D. R.; Koros, W. J. Gas separation performance of 6FDA-based polyimides with different chemical structures. *Polymer* **2013,** *54* (22), 6226-6235.

(279) Kwon, H. T.; Jeong, H.-K. Highly propylene-selective supported zeolite-imidazolate framework (ZIF-8) membranes synthesized by rapid microwave-assisted seeding and secondary growth. *Chemical Communications* **2013,** *49* (37), 3854-3856.

(280) Yin, H.; Kim, H.; Choi, J.; Yip, A. C. K. Thermal stability of ZIF-8 under oxidative and inert environments: A practical perspective on using ZIF-8 as a catalyst support. *Chemical Engineering Journal* **2015,** *278*, 293-300.

(281) Eguchi, H.; Kim, D. J.; Koros, W. J. Chemically cross-linkable polyimide membranes for improved transport plasticization resistance for natural gas separation. *Polymer* **2015,** *58*, 121-129.

(282) Kratochvil, A. M.; Koros, W. J. Decarboxylation-Induced Cross-Linking of a Polyimide for Enhanced CO2 Plasticization Resistance. *Macromolecules* **2008,** *41* (21), 7920-7927.

(283) Tarleton, E. S.; Robinson, J. P.; Salman, M. Solvent-induced swelling of membranes - Measurements and influence in nanofiltration. *Journal of Membrane Science* **2006,** *280* (1-2), 442-451.

(284) Mahkam, M.; Doostie, L. The relation between swelling properties and cross-linking of hydrogels designed for colon-specific drug delivery. *Drug Delivery* **2005,** *12* (6), 343-347.

(285) Yu, J.; Wang, C.; Xiang, L.; Xu, Y.; Pan, Y. Enhanced C3H6/C3H8 separation performance in poly(vinyl acetate) membrane blended with ZIF-8 nanocrystals. *Chemical Engineering Science* **2018,** *179*, 1-12.

(286) Chi, W. S.; Kim, S. J.; Lee, S. J.; Bae, Y. S.; Kim, J. H. Enhanced Performance of Mixed-Matrix Membranes through a Graft Copolymer-Directed Interface and Interaction Tuning Approach. *ChemSusChem* **2015,** *8* (4), 650-658.

(287) Japip, S.; Wang, H.; Xiao, Y. C.; Chung, T. S. Highly permeable zeolitic imidazolate framework (ZIF)-71 nano-particles enhanced polyimide membranes for gas separation. *Journal of Membrane Science* **2014,** *467*, 162-174.

(288) Oh, J. W.; Cho, K. Y.; Kan, M. Y.; Yu, H. J.; Kang, D. Y.; Lee, J. S. High-flux mixed matrix membranes containing bimetallic zeolitic imidazole framework-8 for C3H6/C3H8 separation. *Journal of Membrane Science* **2020,** *596*,

(289) Shen, Q.; Cong, S. Z.; He, R. R.; Wang, Z.; Jin, Y. H.; Li, H.; Cao, X. Z.; Wang, J.; Van der Bruggen, B.; Zhang, Y. T. SIFSIX-3-Zn/PIM-1 mixed matrix membranes with enhanced permeability for propylene/propane separation. *Journal of Membrane Science* **2019,** *588*,

(290) Askari, M.; Chung, T. S. Natural gas purification and olefin/paraffin separation using thermal cross-linkable co-polyimide/ZIF-8 mixed matrix membranes. *Journal of Membrane Science* **2013,** *444*, 173-183.

(291) Zhang, Q.; Li, H. B.; Chen, S.; Duan, J. G.; Jin, W. Q. Mixed-matrix membranes with soluble porous organic molecular cage for highly efficient C3H6/C3H8 separation. *Journal of Membrane Science* **2020,** *611*,

(292) Craig Colling, G. H., John Bartels Processes using solid perm-selective membranes in multiple groups for simultaneous recovery of specified products from a fluid mixture. US20040004040A1, 2002.

(293) Park, H. B.; Jung, C. H.; Lee, Y. M.; Hill, A. J.; Pas, S. J.; Mudie, S. T.; Van Wagner, E.; Freeman, B. D.; Cookson, D. J. Polymers with cavities tuned for fast selective transport of small molecules and ions. *Science* **2007,** *318* (5848), 254-258.

(294) Du, N. Y.; Robertson, G. P.; Pinnau, I.; Guiver, M. D. Polymers of Intrinsic Microporosity with Dinaphthyl and Thianthrene Segments. *Macromolecules* **2010,** *43* (20), 8580-8587.

(295) Nguyen, T. B.; Hoang, V. T.; Chen, X. Y.; Rodrigue, D.; Kaliaguine, S. Crosslinked MOF-polymer to enhance gas separation of mixed matrix membranes. *Journal of Membrane Science* **2016,** *520*, 941-950.

(296) Eum, K.; Ma, C.; Rownaghi, A.; Jones, C. W.; Nair, S. ZIF-8 Membranes via Interfacial Microfluidic Processing in Polymeric Hollow Fibers: Efficient Propylene Separation at Elevated Pressures. *Acs Applied Materials & Interfaces* **2016,** *8* (38), 25337-25342.

(297) Zhou, S.; Wei, Y. Y.; Li, L. B.; Duan, Y. F.; Hou, Q. Q.; Zhang, L. L.; Ding, L. X.; Xue, J.; Wang, H. H.; Caro, J. Paralyzed membrane: Current-driven synthesis of a metal-organic framework with sharpened propene/propane separation. *Science Advances* **2018,** *4* (10),

(298) Tsapatsis, M. Toward High-Throughput Zeolite Membranes. *Science* **2011,** *334* (6057), 767-

768.

(299) Bastani, D.; Esmaeili, N.; Asadollahi, M. Polymeric mixed matrix membranes containing zeolites as a filler for gas separation applications: A review. *Journal of Industrial and Engineering Chemistry* **2013,** *19* (2), 375-393.

(300) Jusoh, N.; Yeong, Y. F.; Chew, T. L.; Lau, K. K.; Shariff, A. M. Current Development and Challenges of Mixed Matrix Membranes for CO2/CH4 Separation. *Separation and Purification Reviews* **2016,** *45* (4), 321-344.

(301) Park, H. B.; Kamcev, J.; Robeson, L. M.; Elimelech, M.; Freeman, B. D. Maximizing the right stuff: The trade-off between membrane permeability and selectivity. *Science* **2017,** *356* (6343),

(302) Moore, T. T.; Koros, W. J. Non-ideal effects in organic-inorganic materials for gas separation membranes. *Journal of Molecular Structure* **2005,** *739* (1-3), 87-98.

(303) Clausi, D. T.; Koros, W. J. Formation of defect-free polyimide hollow fiber membranes for gas separations. *Journal of Membrane Science* **2000,** *167* (1), 79-89.

(304) Ahmad, A. L.; Otitoju, T. A.; Ooi, B. S. Hollow fiber (HF) membrane fabrication: A review on the effects of solution spinning conditions on morphology and performance. *Journal of Industrial and Engineering Chemistry* **2019,** *70*, 35-50.

(305) Park, S.; Jeong, H. K. In-situ linker doping as an effective means to tune zeolitic-imidazolate framework-8 (ZIF-8) fillers in mixed-matrix membranes for propylene/propane separation. *Journal of Membrane Science* **2020,** *596*,

(306) Park, S.; Cho, K. Y.; Jeong, H.-K. Polyimide/ZIF-7 mixed-matrix membranes: understanding the in situ confined formation of the ZIF-7 phases inside a polymer and their effects on gas separations. *Journal of Materials Chemistry A* **2020**,

(307) Li, D. F.; Wang, R.; Chung, T. S. Fabrication of lab-scale hollow fiber membrane modules with high packing density. *Separation and Purification Technology* **2004,** *40* (1), 15-30.

(308) Chung, T. S.; Qin, J. J.; Gu, J. Effect of shear rate within the spinneret on morphology, separation performance and mechanical properties of ultrafiltration polyethersulfone hollow fiber membranes. *Chemical Engineering Science* **2000,** *55* (6), 1077-1091.

(309) Arahman, N.; Nursidik; Mukramah; Maulidayanti, S.; Putri, A. O. The stability of Poly(ether

sulfone) membranes treated in hot water and hypochlorite solution. *International Symposium on Applied Chemistry 2015* **2015,** *16*, 709-715.

(310) Righetti, M. C.; Boggioni, A.; Laus, M.; Antonioli, D.; Sparnacci, K.; Boarino, L. Thermal and mechanical properties of PES/PTFE composites and nanocomposites. *Journal of Applied Polymer Science* **2013,** *130* (5), 3624-3633.

(311) Li, D. F.; Chung, T. S.; Wang, R.; Liu, Y. Fabrication of fluoropolyimide/polyethersulfone (PES) dual-layer asymmetric hollow fiber membranes for gas separation. *Journal of Membrane Science* **2002,** *198* (2), 211-223.

(312) Tsuruoka, T.; Kumano, M.; Mantani, K.; Matsuyama, T.; Miyanaga, A.; Ohhashi, T.; Takashima, Y.; Minami, H.; Suzuki, T.; Imagawa, K.; Akamatsu, K. Interfacial Synthetic Approach for Constructing Metal-Organic Framework Crystals Using Metal Ion-Doped Polymer Substrate. *Crystal Growth & Design* **2016,** *16* (5), 2472-2476.

(313) Kim, H. T.; Kim, S. K.; Park, J. K. Development of in-plane orientation in pyromellitic dianhydride-oxydianiline polyimide film on substrate during thermal imidization. *Polymer Journal* **1999,** *31* (2), 154-159.

(314) Pendergast, M. M.; Hoek, E. M. V. A review of water treatment membrane nanotechnologies. *Energy & Environmental Science* **2011,** *4* (6), 1946-1971.

(315) Gai, P. B.; Zhang, H. J.; Zhang, Y. S.; Liu, W.; Zhu, G. B.; Zhang, X. H.; Chen, J. H. Simultaneous electrochemical detection of ascorbic acid, dopamine and uric acid based on nitrogen doped porous carbon nanopolyhedra. *Journal of Materials Chemistry B* **2013,** *1* (21), 2742-2749.

(316) Hsu, T. C. J.; Liu, Z. L. Solvent Effect on the Curing of Polyimide Resins. *Journal of Applied Polymer Science* **1992,** *46* (10), 1821-1833.

(317) Krol, J. J.; Boerrigter, M.; Koops, G. H. Polyimide hollow fiber gas separation membranes: preparation and the suppression of plasticization in propane/propylene environments. *Journal of Membrane Science* **2001,** *184* (2), 275-286.

(318) Visser, T.; Wessling, A. Auto and mutual plasticization in single and mixed gas C-3 transport through Matrimid-based hollow fiber membranes. *Journal of Membrane Science* **2008,** *312* (1-2), 84-96.

(319) Ito, A.; Hwang, S. T. Permeation of Propane and Propylene through Cellulosic Polymer

Membranes. *Journal of Applied Polymer Science* **1989,** *38* (3), 483-490.

(320) Yoshino, M.; Nakamura, S.; Kita, H.; Okamoto, K.; Tanihara, N.; Kusuki, Y. Olefin/paraffin separation performance of asymmetric hollow fiber membrane of 6FDA/BPDA-DDBT copolyimide. *Journal of Membrane Science* **2003,** *212* (1-2), 13-27.

(321) Okamoto, K.; Yoshino, M.; Noborio, K.; Maeda, H.; Tanaka, K.; Kita, H. Preparation of carbon molecular sieve membranes and their gas separation properties. *Membrane Formation and Modification* **2000,** *744*, 314-329.

(322) Xu, L. R.; Rungta, M.; Brayden, M. K.; Martinez, M. V.; Stears, B. A.; Barbay, G. A.; Koros, W. J. Olefins-selective asymmetric carbon molecular sieve hollow fiber membranes for hybrid membrane-distillation processes for olefin/paraffin separations. *Journal of Membrane Science* **2012,** *423*, 314-323.

(323) Okamoto, K.; Kawamura, S.; Yoshino, M.; Kita, H.; Hirayama, Y.; Tanihara, N.; Kusuki, Y. Olefin/paraffin separation through carbonized membranes derived from an asymmetric polyimide hollow fiber membrane. *Industrial & Engineering Chemistry Research* **1999,** *38* (11), 4424-4432.

(324) Yoshino, M.; Nakamura, S.; Kita, H.; Okamoto, K.; Tanihara, N.; Kusuki, Y. Olefin/paraffin separation performance of carbonized membranes derived from an asymmetric hollow fiber membrane of 6FDA/BPDA-DDBT copolyimide. *Journal of Membrane Science* **2003,** *215* (1-2), 169-183.

(325) Eum, K.; Rownaghi, A.; Choi, D.; Bhave, R. R.; Jones, C. W.; Nair, S. Fluidic Processing of High-Performance ZIF-8 Membranes on Polymeric Hollow Fibers: Mechanistic Insights and Microstructure Control. *Advanced Functional Materials* **2016,** *26* (28), 5011-5018.

(326) Brown, A. J.; Brunelli, N. A.; Eum, K.; Rashidi, F.; Johnson, J. R.; Koros, W. J.; Jones, C. W.; Nair, S. Interfacial microfluidic processing of metal-organic framework hollow fiber membranes. *Science* **2014,** *345* (6192), 72-75.

(327) Cui, L. L.; Qiu, W. L.; Paul, D. R.; Koros, W. J. Physical aging of 6FDA-based polyimide membranes monitored by gas permeability. *Polymer* **2011,** *52* (15), 3374-3380.

(328) Gao, Z. C.; Li, L. Q.; Li, H. L.; Chen, R. F.; Wang, S.; Wang, Y. G. A hybrid zeolitic imidazolate framework Co-IM-mIM membrane for gas separation. *Journal of Central South University* **2017,** *24* (8), 1727-1735.

(329) Smith, S. J. D.; Lau, C. H.; Mardel, J. I.; Kitchin, M.; Konstas, K.; Ladewig, B. P.; Hill, M. R. Physical aging in glassy mixed matrix membranes; tuning particle interaction for mechanically robust nanocomposite films. *Journal of Materials Chemistry A* **2016,** *4* (27), 10627-10634.

(330) Paul, D. R. Gas Sorption and Transport in Glassy-Polymers. *Berichte Der Bunsen-Gesellschaft-Physical Chemistry Chemical Physics* **1979,** *83* (4), 294-302.

(331) Stannett, V. The transport of gases in synthetic polymeric membranes — an historic perspective. *Journal of Membrane Science* **1978,** *3* (2), 97-115.

(332) Shahid, S.; Nijmeijer, K. Performance and plasticization behavior of polymer-MOF membranes for gas separation at elevated pressures. *Journal of Membrane Science* **2014,** *470*, 166-177.

(333) Bachman, J. E.; Smith, Z. P.; Li, T.; Xu, T.; Long, J. R. Enhanced ethylene separation and plasticization resistance in polymer membranes incorporating metal-organic framework nanocrystals. *Nature Materials* **2016,** *15* (8), 845-+.

(334) Kosuri, M. R.; Koros, W. J. Defect-free asymmetric hollow fiber membranes from Torlon®, a polyamide–imide polymer, for high-pressure CO2 separations. *Journal of Membrane Science* **2008,** *320* (1), 65-72.